Università degli Studi di Ferrara

DOTTORATO DI RICERCA IN SCIENZE DELLA TERRA

CICLO XXIX

SETTORE SCIENTIFICO DISCIPLINARE GEO/06

COORDINATORE DEL CORSO DI DOTTORATO: Prof. MASSIMO COLTORTI

TITOLO

ADSORPTION AND DESORPTION OF FUEL-BASED COMPOUNDS FROM WATER THROUGH SYNTHETIC ZEOLITE ZSM-5

Dottoranda

Elisa Rodeghero

Tutori

Prof. Giuseppe Cruciani

Prof.ssa Annalisa Martucci

ANNI

2014-2016

Questo lavoro è dedicato a tre amici

che sono stati molto importanti

in questi ultimi dieci anni:

Annalisa "fragolona", Salvatore Pepi e Salvatore Cavaleri.

Grazie

“πάντα ῥεῖ ὡς ποταμός”

“Non si può discendere due volte nel medesimo fiume

e non si può toccare due volte una sostanza mortale nel medesimo stato,

ma a causa dell’impetuosità e della velocità del mutamento

essa si disperde e si raccoglie, viene e va.”

Eraclito

Acknowledgements

I would like to thank the Italian Ministry for University and Research (MIUR) and the Research Centre for Unconventional Energies, Istituto ENI G. Donegani Environmental Technologies (San Donato Milanese (MI), Italy) for funding this PhD research.

I would like to acknowledge the European Synchrotron Radiation Facility (ESRF, Grenoble) for providing beamtime for proposal CH-3510 "In situ XRD study of structural modifications and desorption kinetics of zeolites used for removal of non-polar organic compounds from contaminated water".

I would like to express my gratitude to Prof. Giuseppe Cruciani and Prof. Annalisa Martucci, my research supervisors, for the skills and the professionalism they have passed down to me.

Assistance in chemistry provided by Prof. Luisa Pasti and her research group has been greatly appreciated. Their support has been fundamental for succeeding in this work.

I am also grateful to the referees Roberto Millini, Vice President of R&D Program Energy Transition - CO_2 Capture and Utilization at eni s.p.a., and Prof. Mojgan Zendehdel, from the Department of Chemistry at Arak University (Iran), for giving suggestions on how to improve this dissertation.

I would like to extend my thanks to my colleagues Dr. Matteo Ardit and Giada Beltrami (PhD student) for their patience and support. I also wish to thank my English teacher Elena Tomiolo, who helped me to pronounce English properly before every oral comunication, and all my friends, who are always fundamental in my life.

Finally, a special mention goes to my family, in particular Lilly, Lilla, mum, dad and Duccio.

Contents

Figure captions

List of tables

List of equations

Abbreviations used in the text

1,1-DCA: 1,1-dichloroethane

1,2-DCE: 1,2-dichloroethane

10MR: 10 member ring

111-TCA: 1,1,1-trichloroethane

ACs: activated carbons

AOPs: Advanced Oxidation Processes

Bio-PRBs: Bioaugumented Permeable Reactive Barriers

BTEX: Benzene, TOL, Ethylbenzene, and Xylenes

C.F.A.: Crystallographic Free Area

CA: caffeic acid

CB: chlorobenzene

CBLM: bi- Langmuir model

CECs: contaminants of emerging concern

CLM: classical competitive Langmuir model

Cl-VOCs: Chlorinated volatile organic compounds

CNTs: carbon nanotubes

DTA: differential thermal analysis

DTG: differential thermogravimetric analysis

EC: European Commission

ESRF: European Synchrotron Radiation Facility

GACs: granular activated carbons

GC–FID: Gas Chromatography–Flame Ionization Detector

GSAS: General Structure Analysis System

HS-GC-MS: Head Space Gas Chromatography coupled to Mass Spectrometry

HS-SPME: Head Space-Solid Phase Micro Extraction

HT: high-temperature

IARC: International Agency for Research on Cancer

IAST: ideal adsorbed solution theory

LACs: low-cost adsorbents

MEP: Ministry of Environmental Protection of China

MTBE: methyl-tert-butyl-ether

NTE: negative thermal expansion

n-ZVI: nano zero-valent iron

P&T: pump and treat

p.u.c.: per unit cell

PACs: powder activated carbons

PAHs: Poly-Aromatic Hydrocarbons

PBU: Primary Building Units

PCE: tetrachloroethene

PACs: powder activated carbons

PAHs: Poly-Aromatic Hydrocarbons

PBU: Primary Building Units

PCE: tetrachloroethene

PerBU: Periodic Building Units

PFO: Lagergren's pseudo-first-order kinetics

p-HBA: p-hydroxybenzaldehyde

PRBs: Permeable Reactive Barriers

PSO: Lagergren's pseudo second order kinetics

SBUs: Secondary Building Units

SC: Straight Channel

SC-A: Straight Channel ring A

SC-B: Straight Channel ring B

SSUs: Secondary Structural Units

TCE: 1,1,2-trichloroethene

TG: thermogravimetric analysis

TOL: toluene or methyl-benzene

US EPA: United States Environmental Protection Agency

US EPA: United States Environmental Protection Agency

SC-B:

SSUs: Secondary Structural Units

TCE: 1,1,2-trichloroethene

TG: thermogravimetric analysis

TOL: toluene or methyl-benzene

US EPA: United States Environmental Protection Agency

USGS: United States Geological Survey

WHO: World Health Organisation

XRPD: X-ray powder diffraction

ZVI: Zero-Valent Iron

ZZ: Sinusoidal Channel

ZZ-A: Sinusoidal Channel ring A

ZZ-B: Sinusoidal Channel ring B

Abstract

This dissertation is conceived as a comprehensive report of the results obtained during the three years of doctorate study within a project on the adsorption/desorption of VOCs from aqueous solutions by means of a zeolite ZSM-5. This work is part of a wider project co-funded by the Italian Ministry for University and Research (MIUR; PRIN project "SoWaZe", prot. 2010EARRRZ 009) which started from a previous scientific collaboration with the Research Center for Non-Conventional Energy – Istituto Eni Donegani Environmental Technologies.

The drawback of the strong and rapid development of the chemical and agrochemical industries is a release of a large number of pollutants in the environment. The aquatic ecosystem is vulnerable because it is frequently a recipient of these toxic compounds. Indeed, water reserves represented by groundwater are seriously compromised in many industrial areas, in particular in districts hosting petrochemical activities and oil industry. For this reason, the occurrence of fuel-based pollutants in the aquatic environment has been recognized as one of the global emerging issues. The growing interest in the pollutants removal from natural water derives from their harmful effects on the environment and on the biotic communities even at very low concentrations. In light of this, a big challenge is to look for eco-friendly adsorbent materials, having a good performance/price ratio. As a matter of fact, some of these materials have been already employed in technologies with low environmental impact and high efficiency to overthrow the pollution of hydrocarbon cycle. As in the case of PRBs for water treatment, it has been demonstrated that adsorption technologies are an efficient removal process for several solutes.

Hydrophobic zeolites are environmentally compatible materials, which have been employed as adsorbents for the removal of contaminants from water bodies. Due to their chemical-physical and structural features, zeolites represent fundamental adsorbents for the recovery of groundwater polluted by organic contaminants, such as chlorinated compounds and hydrocarbons. This exciting context is further enriched by the fact that, once the saturation is reached, these materials can be easily regenerated by thermal processes without changing their initial features and they can be re-used several times.

On the basis of the above statements, the combination of chromatographic, diffractometric and thermogravimetric techniques has been employed to investigate the adsorptive-desorptive properties of hydrophobic synthetic zeolite as well as the temperature dependence of the desorption processes.

Finally, the understanding of the competitive behaviour of adsorbed pollutants in binary mixture and/or in presence of humic acids and the adsorption capacity of the regenerated zeolites have been tested. Specifically, *in situ* HT synchrotron XRPD (time-resolved) was used as a tool to understand the features of organophilic ZSM-5 zeolite (SiO_2/Al_2O_3 ~ 280) when 1,2-DCE, TOL, and MTBE (both as single component as well as binary mixtures) are adsorbed and desorbed. The structural modifications of ZSM-5 zeolite are monitored through thermal treatment from room temperature to 600°C. The results achieved by means of Rietveld refinements of the investigated compounds highlight the "out-of-equilibrium effects" that govern the adsorption/desorption dynamic conditions in ZSM-5 powders. In addition, the whole process takes advantage from the complementary use of both *in situ* XRPD and gas-chromatography experimental techniques.

Riassunto

Il presente elaborato riporta in modo esteso i risultati ottenuti nel corso del dottorato di ricerca riguardo il processo di adsorbimento/desorbimento di VOCs, disciolti in soluzione acquosa, operato da campioni di zeolite ZSM-5. Questo lavoro fa parte di un progetto più ampio co-finanziato dal Ministero Italiano per l'Università e la Ricerca (MIUR; PRIN project "SoWaZe", prot. 2010EARRRZ 009) e derivante da un'attività di collaborazione scientifica pregressa con i laboratori del Research Center for Non-Conventional Energy – Istituto Eni Donegani Environmental Technologies.

La forte e rapida crescita delle industrie chimiche ed agrochimiche ha avuto un impatto negativo dovuto al rilascio nell'ambiente di ingenti quantitativi di inquinanti. In particolare, il sistema acquatico risulta essere molto vulnerabile in quanto spesso recettore primario di questi contaminanti tossici. Infatti la qualità delle riserve d'acqua, costituite dalle acque di falda, è seriamente compromessa soprattutto nelle zone su cui sorgono e si sviluppano industre petrolifere e petrolchimiche. Per questa ragione, la presenza di contaminanti organici nelle acque è stata riconosciuta come una delle problematiche globali emergenti e la rimozione di questi inquinanti una questione di grande interesse. Essi infatti, anche in piccole concentrazioni, hanno effetti negativi sull'ambiente e sulle comunità biotiche. Alla luce di quanto detto, la sfida attuale è quella di ricercare un materiale adsorbente eco-compatibile che mostri un buon rapporto efficacia/prezzo da utilizzare in tecnologie di environmental remediation, al fine di ridurre l'inquinamento da idrocarburi. Nel trattamento delle acque, le tecnologie di adsorbimento, quali le PRBs, sono risultate efficienti nel processo di rimozione di alcuni soluti. In particolare, le zeoliti a carattere idrofobico vengono impiegate nella rimozione di contaminanti disciolti nei corpi idrici. Grazie alle loro proprietà chimico-fisiche e strutturali, le zeoliti sono materiali di importanza strategica quando utilizzate nella rimozione di composti organici quali ad esempio clorurati e idrocarburi. Uno degli aspetti che ha suscitato maggiore interesse in ambito scientifico ed industriale è la rigenerazione di questi materiali mediante trattamento termico. Tale trattamento non altera o compromette le proprietà strutturali preesistenti e quindi le zeoliti si prestano ad un possibile riutilizzo in processi di adsorbimento successivi.

Sulla base di quanto riportato, grazie all'utilizzo combinato di diverse tecniche quali la cromatografia, la diffrazione da polveri e le analisi termogravimetriche ci si propone di capire in modo dettagliato quali siano le capacità e le proprietà di adsorbimento/desorbimento di zeoliti sintetiche a carattere idrofobico ed organofilico. Altro obiettivo è la determinazione, a livello atomistico, degli effetti indotti dal trattamento termico su questi materiali. Inoltre, lo studio dell'adsorbimento di miscele di inquinanti fornisce informazioni specifiche sia sui possibili comportamenti di tipo competitivo sia sulla selettività della zeolite in presenza di acidi umici, nella soluzione acquosa. L'ultimo punto prevede sarà anche di testare la capacità di adsorbimento di alcuni campioni rigenerati. L'analisi *in situ* HT XRPD e le analisi cromatografiche sono tecniche fra di loro complementari e si integrano nel supportare i risultati ottenuti.

In particolare, la tecnica HT-XRPD effettuata *in situ* mediante luce di sincrotrone è usata in questo lavoro come chiave di lettura per comprendere il processo di adsorbimento/desorbimento nella zeolite ZSM-5 (SiO_2/Al_2O_3 ~ 280) di 1,2-DCE, TOL ed MTBE adsorbiti da soluzione acquosa sia singolarmente sia come miscele binarie. Allo stesso modo questa tecnica permette di monitorare le modificazioni strutturali che intervengono nei campioni di zeolite durante il trattamento termico, in un intervallo di temperatura compreso tra i 25 e i 600°C. I risultati, ottenuti dall'analisi strutturale Rietveld dei dati raccolti in rampa, permettono di evidenziare gli effetti "lontano dall'equilibrio" dei processi di adsorbimento/desorbimento nei campioni di ZSM-5 in condizioni dinamiche.

1. Hydrocarbon pollution: water global emergency

1.1 Introduction to the issue

Water contamination is soaring from the end of 20th century due to a very fast development of industries, a badly conceived urbanization, as well as of agricultural practices. In fact, if from one side this development gives rise to a general improvement of the standard of living, the flip side is an increasing of the environment pollution by CECs [1]. Being frequently a recipient for these contaminants, the aquatic ecosystem and the water quality are seriously deteriorated and sometime hopelessly compromised. Today, less than 3% of water is truly usable for the human practices [2]. Often, recycled water and treated wastewater effluents deriving by malfunctioned wastewater treatment plants is discharged into the environment. This determines not only the contamination of surface water (lakes and rivers), but also of groundwater aquifers. For this reason, surface and groundwater pollution is considered a global emergency and the removal of hazardous organic compounds from the water bodies becomes a common objective. In particular, the presence of these chemicals at ultra-trace levels might cause the development of sub-lethal toxic effects in aquatic organisms (i.e., reproductive and immune dysfunctions, neurological disorders) and in human health [3]. Nevertheless, the traditional wastewater treatments (vaporization, dilution, decomposition, and reactions to sunlight action) designed to degrade or remove organic compounds or reduce the levels of their concentrations are not completely effective. In the recent years, new technologies which employ different types of materials were developed to support the traditional methods. In particular, adsorption technologies (based on the physic-adsorption process) and adsorbent materials have been shown to be an effective and eco-friendly alternative to remove chemicals from water.

The following sections will give an overview of the contaminants of emerging concern as well as of the most recent technologies and materials employed to clean up contaminated waters. Particular attention will be given to organics, methods and materials selected for the present work.

1.2 The main contaminants of emerging concern dissolved in water

The USGS gives a general definition of the contaminants of CECs, namely any substance (natural or synthetic) which is present in the environment beyond ultra-trace levels and that could cause adverse ecological and human health effects.

Kept in many things of everyday usage and resistant to natural degradation processes, CECs are continuously released into the environment where they can accumulate and persist over time provoking negative effects [1,4]. The main sources of CECs are the following: treated sewage sludge, industrial wastewater effluents, untreated wastewater from manufacturing facilities, landfill leachate, effluents from poultry farms, veterinary antibiotics and agricultural runoff containing pesticides [1,4–7]. Emerging contaminants are normally divided into categories that describe their main characteristics (features). For example, the most common categories are pharmaceuticals, pesticides, personal care products and PAHs. Each of these categories have many different potential health impacts on humans and other biological species.

Among CECs, great attention has been paid on the removal of compounds, which fall under the VOCs category mostly derived from oil and gas exploration and production [1,8–11].

The US EPA adopts the general definition of VOCs as "*organic chemical compounds of carbon whose composition makes it possible for them to evaporate under normal indoor atmospheric conditions of temperature and pressure".* These compounds can be also classified in relation to their boiling point which is in general less than (or equal to) 250°C, measured at atmospheric pressure. For example, in its definition of VOCs, the European Union uses the boiling point rather than the volatility [3]. As reported by USGS, the most common detected VOCs in groundwater are: MTBE, PCE, TCE, TOL, 111-TCA, benzene, 1,2-DCE, 1,1-DCA, and CB [12]. In general VOCs are divided into two main groups: aliphatic hydrocarbons (alkanes, alkenes), and aromatic hydrocarbons [13]. In the first group, alkanes are hydrocarbon molecules (linear, branched or cyclic) with carbon-carbon single bonds only. If they contain at least a Cl atom, the molecules are defined as chlorinated alkanes (such as 1,2-DCE). Instead, in the case of alkenes, the hydrocarbon molecules contain at least a carbon-carbon double bond. If one of more H are replaced by chlorine atoms, the molecules are defined chlorinated alkenes (e.g., 1,1-dichloroethene). On the other hand, aromatic compound can be described as organic molecule that contains one or more benzene or equivalent heterocyclic rings. In particular,

the aromatic properties follow the Hückel's rule: the molecule has 4n+2 π electrons (n=0 or any positive integer); is cyclic (a ring of atoms), is planar (all atoms in the molecule lie in the same plane); is fully conjugated (p orbitals at every atom in the ring). Organic compounds that not show aromatic properties are classified as aliphatic compounds and they are typically less stable than aromatic chemicals.

In general, Cl-VOCs, that include chlorinated alkanes, chlorinated alkenes, and chlorinated aromatics, constitute an important ubiquitous class of pollutants widely revealed in environmental matrices [9,14,15]. In the past, Cl-VOCs have been extensively used for many industrial and domestic applications. In particular, these organic compounds were employed as solvents, pharmaceuticals, pesticides, products for water disinfection, adhesives and refrigerants. Leaks, spills, and wrong disposal practices have led to widespread contamination of groundwater by Cl-VOCs [9,14,16]. Because of their diffusion in the environment, their human toxicity, and the tendency to persist in groundwater [4,9], these contaminants are of particular concern for human health. As a matter of fact, it is easily possible assume Cl-VOCs by inhalation or ingestion during daily activities such as drinking, eating, swimming, bathing and showering. As suggested by recent studies, there is a linkage between the assumption of these hazardous organics and the increasing of cancers and adverse reproductive outcomes [17–19]. For this reason, the removal of Cl-VOCs is considered a priority by the main authorities of several countries: the MEP of China, US EPA and EC.

One of these potential carcinogens chemicals is 1,2-DCE which is a chlorinated alkane belonging to the B2 (or 2B) principal organic contaminant class (*i.e.*, possibly carcinogenic to humans) by US EPA and IARC, respectively. 1,2-DCE is also known as ethylene dichloride, and is a colorless liquid slightly soluble in water (0.87 g/100 ml). The worldwide annual production (considering the available data for Europe, United States, and Japan) of this chemical is around 15,868,000 tones [20]. Since the evidences obtained by National Cancer Institute of multiple tumor types in two mammalian species after 1,2-DCE exposure, the maximum value for this oncogenic chemical in order to maintained the water quality and protect humans health is fixed to 0,6 μg/L [21]. Nowadays, the research is devoted to clarify the mechanism of cancer formation as well as the development of efficient technologies to solved the widespread contamination of this Cl-VOCs in water matrix.

Another important organic frequently presents in the contaminated water is CB which is a chlorinated aromatic compound. It belongs to the “principal organic contaminant class”

(iii): *i.e.*, "*Halobenzenes and substituted halobenzenes: derivatives of benzene which have at least one halogen atom attached to the ring and which may or may not have straight or branched chain hydrocarbon, nitrogen or oxygen substituent"* [22]. On the base of the National Toxicology Program, the US EPA declares evidences of chlorobenzene's carcinogenicity, but the obtained results are not very clear. As a matter of fact, CB was resulted inactive in most short-term analyses, suggesting a potential oncogenic activity. In general, the exposition to growing levels of CB induces neoplastic nodules or benign tumors (hepatocellular adenomas). In the case of this chemical, the most stringent threshold value for the quality of water is fixed to 5 μg/L [22].

With reference to the aromatic hydrocarbons group, an important "subgroup" must be taken into exam. Specifically, BTEX constitute one of the main marine environment pollutants due to accidental spills or leaks [9]. Due to release of petroleum products (gasoline, diesel, fuel, lubricating oil) and from leaking oil tanks, BTEX are also commonly present in urban and industrial areas [23,24]. These chemicals are hydrophobic and hence have a very low solubility in water (benzene: ~ 1700 ppm; TOL and ethylbenzene ~ 500-550 ppm; xylenes: ~ 130-180 ppm). For this reason BTEX tend to persist in groundwater and they can be transported several kilometers away from the pollution plume. BTEX compounds can cause adverse health effects on humans, including central nervous system impairments, respiratory problems and liver and kidney damages [10,25,26]. According to what reported above, the US EPA and the WHO have classified BTEX as priority pollutants that must be removed from water and they have fixed their maximum concentration levels in order to guarantee the water quality and human health protection. The maximum permissible concentration of benzene, TOL, and xylene in drinking water is 1, 5, 5 μg/L, respectively (in the case of xylene the maximum concentration is applied to each of its isomers) [27–29].

Among those belonging to the BTEX group, this work is mainly focused on TOL. TOL is a chemical in which one hydrogen atom of benzene molecule is replaced by a methyl group (CH_3). This mono-substituted benzene derivative is a liquid (at ambient temperature) colorless aromatic hydrocarbon compound with low solubility in water and relatively low boiling point (~111°C). TOL is less volatile than benzene, however, it produces flammable vapors. In general, this chemical is employed as solvent oils, resins, natural and synthetic rubber, and, due to its antiknock properties, it is mainly used in the formulation of fuels for car and airplane. The toxic effects of TOL have been extensively documented.

In humans [30], TOL mainly affects the central and peripheral nervous system as well as it induces cardiac arrhythmias, hematological and hepatic changes. In animals, chronic inhalation of TOL is resulted in renal, hepatic, hematological and neurological effects [28,30]. On the basis of the these studies, US EPA has imposed the maximum concentration of this organic contaminant in groundwater to 5 μg/L.

From the environmental point of view, another important VOC is MTBE. MTBE is a volatile ether derived from the catalytic reaction of methanol and isobutene. It is volatile and colorless liquid at room temperature with low boiling point of 55.2°C. This chemical is one of the main constituents of petroleum fuel and enter in the surrounding environment through car emissions, evaporative losses from gasoline stations and vehicles, storage tank releases, pipeline leaks and accidental spills, and refinery stock releases. MTBE is relative soluble in water (0.42 g/100 ml) and it rapidly moves into ground water and resists to the biodegradation for long time [31]. As reported by F. Hamed [10], the total worldwide production in 1998 of this compound was 6.6 billion gallons and the World Health Organisation estimated that MTBE is one of the top 50 chemicals produced. About the human health protection, the US EPA defined that the threshold value of this chemical in water matrix must be 10 μg/L [32]. As a matter of fact, MTBE is defined as a compound with oncogenic effects. Furthermore, MTBE possesses non-oncogenic effects, such as: appearance of liver and adrenal weight as well as secondary lesions of hyperplasia of the parathyroid and mineralization of tissue were associated with nephropathy.

In light of what stated above, it emerges the need of tools to remove or reduce the concentration of VOCs in the environmental matrices. The technologies and the materials that have been developed and used for this purpose will be described in the following paragraphs.

1.3 Overview of the main technologies and methods to clean up contaminated waters

Among the objectives of the world's leading institutions, one of the main priority is the decontamination of both waters and groundwaters from dissolved organic compounds by means of a large number of methods and techniques. These techniques include both ex-situ and *in situ* methods. In particular, the major ex-situ treatments consist in the P&T approach, while the *in situ* methods consist of applying biological and chemical or physical methods [2,33,34].

The P&T technique consists in three main treatment phases. Firstly, polluted groundwater is pumped from the aquifers to the surface treatment facilities in which (second step) the polluted water are clean-up. The last step is the re-injection of the depurated water in the aquifer [2].

In situ techniques: Chemicals dissolved in groundwaters can be treated in two main ways, *i.e.*, converted into non-hazard compounds or adsorbed by adsorbent materials.
Nowadays, to reduce hazardous substances in non-harmful compounds for the environment and human health, biological and chemical methods are routine approaches. However, by a practical point of view those kind of approaches have shown several limits.
The main biological techniques are founded on the use of bacteria and fungi which with their metabolic activity decompose the organic compounds [34,35]. Although many studies report promising results at the "laboratory-scale", they are not so effective at the "production-scale". As a matter of fact, the degradation through the biological approach is negatively affected by the wide presence of several species of organics. For this reason, the biological approach results more suitable in presence of low contaminants concentration or when a little range of contaminant species are involved. Recent studies highlight that good performances are obtained in pilot plants which combine biodegradation with the adsorption process [36–39]. However, biological methods cannot resolve the problem of the organics removal from water and more suitable techniques need to be evaluated.
Among the chemical methods, photodegradation, photocatalysis, and AOPs as ozonation and photo-Fenton treatments are the most commonly studied and used techniques in water treatments. In particular, photodegradation consists in the degradation of chlorinated and aromatic hydrocarbon by direct or indirect photolysis. This method shows good performance to destroy chemicals dissolved in water at mild condition without rising secondary harmful compounds. On the other hand, photocatalytic and oxidation treatments showed several problems [40–44]. In particular, the compounds degradation can be

influenced by the environmental conditions (*e.g.*, temperature and pH), and the presence of other species dissolved in water. For example, in some cases it was observed the formation of byproducts more toxic than the pollutant itself. For these reasons, it is essential to test the effectiveness of these methods in real water systems.

Recently, an alternative combined method to reclaim polluted water was also considered. In particular, AOPs were associated with the bioremediation treatments to remove aliphatic and aromatic hydrocarbons from industrial wastewaters [35]. These combined techniques would expand the efficiency of the treatment in presence of contaminants characterized by high chemical stability and low biodegradability. This technique mainly works in two directions: the AOPs pre-treatment reduces the recalcitrant compounds into more biodegradable intermediate compounds, and then the biological method reduces them into non-toxic compounds. Clearly, in order to find the optimal operating conditions, the use of this combined technique must be connected to a deep knowledge on the chemical and biological characteristics of wastewater. In particular, the biodegradability assessment is not only necessary in the pre-treated water, but also during the AOPs processes. Recent studies from literature show that ozonation or Fenton processes joint with mixed bacterial cultures or activated-sludge biosystems are used to remove polycyclic aromatic hydrocarbons and dimethylsulphoxide (CH3)2S=O [45–47]. However, many gaps need to be filled in order to achieve similar results during operation procedures and to limit the treatment costs. As a matter of fact, no studies consider the competitive aspect between the organic pollutants and the natural organic matter present in real waters. Moreover, high concentration of compounds may inhibit biodegradation. It is important to remind that, during both the treatment planning and the plant design, oxidant chemicals and biological cultures should not interact with each other [35].

To summarize, biological and chemical methods or the combination of them show several problems both as replicability from laboratory to real-scale as well as for the interferences that occur in the real environmental conditions.

The physical methods are an alternative way to compensate for the shortcomings of chemical and biological treatments. Adsorption based treatment technology offers several advantages, such as low operation costs and reduced waste generation [2,9–11]. In particular, the adsorption process associated with the capacity of several materials to remove dissolved organic substances from water give back a fundamental method in the physicochemical treatment of wastewater treatment and water reclamation [37,48–51].

The term "adsorption" was proposed by Du Bois-Reymond and used for the first time in literature by Kayser [5,52]. In general the adsorption phenomenon can be defined as a process that produces an enrichment of adsorbates on the surface of an adsorbent. On the contrary the term "absorption" indicates a transfer of a substance from one bulk phase to another bulk phase [53]. When adsorption and absorption occur simultaneously, or it is not possible to distinguish between them, the correct term is the more general "sorption" [5]. Adsorption process can show or physical or chemical character. In the case of physical adsorption dipole-dipole interaction, hydrogen bonding and Van der Waal's force are involved. On the other hand, chemical adsorption or chemisorption is characterized by an electrostatic chemical bonding between adsorbate and adsorbent. In relation to the type of involved phases, adsorption process can take place in four types of systems: liquid-gas, liquid-liquid, solid-liquid, solid-gas. Changing the boundary conditions of the system (*e.g.*, temperature, pH or pressure) it is possible to desorb the adsorbed species. In particular, in this dissertation the organic molecules desorption process is induced by changing the temperature through a thermal treatment.

From an analytical point of view, adsorption equilibrium, adsorption kinetics and adsorption dynamics are the main features of adsorption process. In particular adsorption equilibrium is the basis of all adsorption model and is related to the variation of three parameters: adsorbed amount, adsorbate concentration, and temperature. The equilibrium is expressed by a formula which is defined as "adsorption isotherm" and that describes the relation of the amount of solute adsorbed per unit weight of adsorbent as function of the concentration of solute remaining in solution, at constant temperature. There are four main different types of adsorption isotherms: Langmuir isotherm (based on the theory of monolayer molecular adsorption; is an isotherm model for ideal adsorption on homogeneous surface), Freundlich isotherm (*i.e.*, adsorption of polar compounds on polar inhomogeneous surface in low or medium polarity solvents). The combination of these models give rise to the third kind of adsorption isotherm, the so called Langmuir-Freundlich isotherm that is an empirical isotherm used to study the adsorption behaviour on heterogeneous surfaces. Finally, Brunauer, Emmett and Teller developed in 1938 the BET isotherm based on the theory of multilayered molecules adsorption. Considering the multilayered adsorption, the solute molecules can be adsorbed from the solution before the formation of an upper layer.

As mentioned above, the other feature of the adsorption process is the adsorption kinetics that describes how the solute concentration changes in function of the time. This concept is

valid also for the desorption process: both processes are time-dependent. When the space parameter is also considered (spatial-dependent process) information on the adsorption dynamics can be obtained.

In case of multi-solute adsorption, the parameters that must be taken into account for the theoretical description of the phenomenon are much more than in case of single component [5]. For instance, the adsorption of more than one type of molecule can be characterized through the competition of the available adsorption sites within the adsorbent materials. In particular, multi-component adsorption from a dilute aqueous solution involves solvent–adsorbate interactions, and competitive adsorption of water on the adsorbent materials other than adsorbate–adsorbate and adsorbate–adsorbent interactions; hence, the complexity of the process increases for aqueous mixture with respect to gas phase systems [54–56]. In the adsorption of mixtures, single sorbate interactions with a sorbent can be altered (*i.e.*, competition occurs) by the presence and quantity of other sorbates, and by the solvent. In general, at low concentrations competitive interactions are not expected to play a significant role in the adsorption process [56]. In case of high concentrations or during the life time of the adsorbent used in adsorption technologies, a full understanding of the competitive interactions among adsorbates would be necessary to predict adsorbent behaviour [56].

Currently, the main adsorption based technologies (mainly developed by Eni S.p.A.) are the PRBs and the En-Z-Lite^{TM} technology. PRBs represent an efficient technology for several contaminants that it has been employed in USA, Europe, Australia, and Japan for a total of 80 PRBs apparatuses. Besides, PRBs technology is more economically sustainable than other *in situ* technologies [37,57–59]. As reported by Perego et al. [2], the best performances of PRBs are obtained in a sandy soil and groundwater with constant water flow. Moreover, this technology shows many advantages such as no superficial facilities (for storage, treatment and transport of water), and minimal maintenance costs. Especially, this technology does not consume energy because it exploits natural flow of groundwater.

Some works reported the results obtained for the removal of several hydrocarbons though the use of PRBs combined with biological techniques (Bio-PRBs) [37,60–63]. The Bio-PRBs have been shown contradictory outcomes in the removal of organic compounds, but in general this technique is suitable in case of low concentrations of contaminates. Although not completely effective, Bio-PRBs remains an interesting up-grade of PRBs because it operates rapidly without a cost increase, and without engendering secondary toxic compounds.

At the same time, En-Z-Lite™ technology adopts the drain and gate scheme combining PRBs and P&T technologies. This system consists of a sequence of layers named "packed bed" in which the adsorbent materials find place. In particular, in order to remove as much of dissolved pollutants as possible, these materials are mainly constituted by different types of zeolites. At full-scale a plant that works in this condition can successfully treat about 360 m^3/day of polluted groundwater for several years [2].

A further alternative is represented by membranes technology. This is based on the diffusion and physi-sorption processes which sort the materials that are present in the water in relation to their size. In general, the thin films of adsorbent materials that constitute membranes operate three main “size separation”: microfiltration, ultrafiltration, and finally nano-filtration [64–66]. In general, this technology employs polymeric adsorbent materials, but also zeolite membranes are recently employed. In particular, these zeolite membranes satisfy two very important requirements: high selectivity and high permeate flux. Moreover these membranes show a very high resistance to harsh conditions.

As explained thus far, adsorption-based technologies turned out to be the best fit between laboratory-scale and real-scale results. For these reasons, adsorption process is the most used method among all the water treatment techniques. In these technologies adsorbent materials play an important role in order to satisfy the removal of the large types of chemicals. The following sections briefly describe the main adsorbent materials used in adsorption technologies. In particular, more attention will be given to zeolites in order to better describe the material selected for this dissertation.

1.4 The main adsorbent materials involved in the adsorption-based technologies

As discussed above, there are many methods and technologies to clean up polluted waters by organic compounds. In spite of all these possibilities, the real challenge is to find and employ materials that may satisfy several requirements and that may be efficient in real conditions [2]. First of all, it is essential that adsorbents behave as eco-friendly materials. In other words, they should not be potentially toxic or generate harmful byproducts to the environment and human health. It also means that they are safe materials: they must be easily handled without health risks. Besides, other two essential characteristics in the choice of these materials should be taken into account: reactivity and stability. In order to use them for a long period, adsorbent materials should possess high reaction rates and high stability. Finally, adsorbent materials should be easily available and cost-effective.

Adsorbent materials can be sorted by their origin within three principal categories: minerals, organics and biological materials. The most known and used adsorbents are: activated carbons, zeolites, clays, silica beads, LACs such as agricultural wastes and biomass, and polymeric materials such as organic polymeric resins and the alternative biopolymers [34,67]. Most of these materials are synthetic products: in this way it is possible to obtain an "ideal" material that exhibits the required behaviour.

However, an excellent adsorption performance is often accompanied by very expensive production processes. At variance with synthetic materials, natural adsorbents are lower-cost materials but they can be exclusively used in specific applications due to their heterogeneous composition. Clay minerals are the main category (class) of these natural materials.

Clay minerals are layered materials which constitute the most abundant available natural adsorbents. They can be divided into seven groups: kaolinite and serpentine, micas, vermiculite, smectites, pyrophyllite and talc, chlorite and finally the palygorskite and sepiolite group [68]. Clay minerals are characterized by large surface area and high ion-exchange capacity. In particular, due to their negative net charge these materials are widely use to remove positively charged species as heavy metal cations and organic dyes. On the other hand, lower performances are shown in the removal of hydrophobic or non-polar organic pollutants. Clay minerals can be modified introducing cationic surfactant molecules in order to overcome this drawback [34].

In this way, it is possible to modify the surface properties of clays and to improve their organophilic character. Recently, the literature reported several studies about new possibilities in using different materials as adsorbents. The peculiarity of these alternative materials is that they have a lower cost than traditional adsorbents. For this reason they are defined low-cost adsorbents. A recent review of these materials is reported by Gupta and Suhas [69]. LACs cover a wide typology of materials from natural to synthetic ones [6]. In general, they can be classified in relation to their availability or in dependence to their nature (i.e., inorganic or organic materials). Regarding their origin, these adsorbents can be natural materials (as wood, lignin and coal) used as they are or with minor treatments, such as industrial, agricultural and domestic wastes or byproducts (*e.g.*, orange peel, shells, sawdust, straw, fly ash, sludge, palm oil ash and red mud). Finally, also synthesized products are considered part of these alternative materials. In spite of many studies about the application of LACs in wastewater treatments, it is difficult to evaluate their practical importance. For this reason, a combination of methodologies and strategies employing LACs should be encouraged and developed.

Among the organic adsorbents, ACs are widely used as media to the contaminant removal [70–72]. In general, ACs derive by a carbonization process of carbon-containing raw materials like coal, coconut shells, lignite, wood and peat. After carbonization ACs are activated by gas or chemical method. Even if chemical activation is preferable for water treatment applications (*i.e.*, ACs show high micropore volume), the chemicals used for the activation could be released in water causing pollution. Moreover, several studies are devoted to investigate the possibility to develop affinity for specific contaminants by the modification of the physical and chemical characteristics of ACs [71,73–75]. The possible methods to modify activated carbons can be summarized as it follows: chemical modification that includes acid, basic and impregnation treatments, physical modification by heat treatment, and biological modification which means bioadsorption. The most representative water treatment within those reported in the literature is the acidic treatment that seems to be the most suitable to modify ACs [71]. Activated carbons are available in powder (PACs) or granular form (GACs). The range of the particle size is < 40 μm, and from 0.5 to 4 mm, respectively. In the water treatments, GACs is preferable than PACs.

The adsorption capability of activated carbons depends on several factors among which: the pore structure, the physio-chemical characteristics of the organics, and the environmental conditions such as pH and contaminants concentration [72]. Moreover, in

the case of multicomponent systems the interference of natural organic matter (NOM) and the competition between several organic species reduce the ACs adsorption capacity.

An recently developed alternative technology involves the use of CNTs. CNTs is a new type of finite carbon structures consisting of needle-like tubes [76]. Due to their numerous properties (*e.g.*, electronic, optoelectronic, semiconductor, mechanical, chemical and physical), these materials are the focus of many interdisciplinary researches [77–82]. The synthesis of CNTs may be carried out in three main ways: arc-discharge, laser ablation, and chemical vapor deposition (CVD) [77,83]. Based on their structure, CNTs can be classified as single-wall carbon nanotubes (SWCNTs) or as multi-wall carbon nanotubes (MWCNTs) [34,83]. As reported by several works, CNTs have been used as adsorbents to remove volatile organic compounds such as 1,2-diCB and various divalent metal ions from aqueous solution [84–87]. However, the moderate area, their dependence on the pH, and negative effects due to the presence of various organic compounds and organic matter limit their use as adsorbents for clean-up polluted waters [34].

A common reactive material widely used as adsorbent is the ZVI. The effectiveness of this material for water decontamination has been extensively treated in literature. Moreover, recent advances of ZVI in the removal of chlorinated organic compounds are also reported [88–92]. In general, chemicals are degraded into non-toxic or less toxic species by electrons transfer from ZVI to the hazardous compounds. However, this material is not characterized by a high surface area and, as a consequence, the adsorption capability may be reduced. To overcome this problem and improve the adsorption capacity, n-ZVI showing a higher surface area and a higher reactivity have been developed. However, these materials are expensive because of the nature of reagents and the complex synthesis procedures [93]. Many papers in the scientific literature report the encouraging results obtained in the theoretical and practical applications of ZVI. For example, ZVI is often exploited in association with Advanced Oxidation Processes or chemical treatment and also in the PRBs technology. Despite these positive results, more improvements are needed to prepare and utilize ZVI [94].

Polymeric resins are another typology of adsorbents. They derive from the polymerization of styrene or acrylic acid ester and are characterized by high physical and chemical stability as well as high surface area and adsorption capacity [34]. In water treatments, these adsorbents are not fully suitable for several reasons, such as: polymeric resins adsorption capacity is strongly affected by environmental conditions such as pH, temperature and contaminants concentration as well as the physico-chemical

characteristics of organics. Furthermore, the economic aspects are not irrelevant. Indeed, the costs to produce these polymers and to regenerate them make these materials much more expensive than the traditional adsorbents.

In the field of amorphous molecular sieve materials, silica and silica-alumina are widely known. In particular, mesostructured silica-based materials are of considerable interest for the removal of VOCs. Among all, siliceous SBA-15, MCM-41, MCM-48 and KIT-6 are the most representative mesoporous materials [2,95]. These materials are characterized by a wide pore opening with large specific pore volume and high surface area. In particular, the framework of SBA-15 and MCM-41 is characterized by mono-dimensional uniform cylindrical mesopores, while MCM-48 and KIT-6 exhibit a three-dimensional bicontinuous cubic net of mesopores. Moreover, in the case of KIT-6 the adjacent mesopore channels are connected by smaller complementary pores. All these mesostructured materials are characterized by a hydrophobic character and many studies are conducted to verify their adsorption capability of VOCs. The results reported in the scientific literature highlight that SBA-15 and KIT-6 show the greatest affinity for various typologies of volatile compounds. Additionally, MCM-41 shows the lowest VOCs adsorption capacity [96–101]. The good affinity to a very large number of hydrocarbon compounds suggests the use of some mesoporous silica adsorbents in PRBs technology [2]. However, their effectiveness at real-scale has to be still demonstrated.

Zeolites are considered an important family of adsorbent materials complementary to mesoporous silica. Except for natural zeolites, which can be considered as the natural adsorbents described above, hydrophobic and organophilic synthetic zeolites turned out to be effective adsorbent material in the removal of fuel-based compounds dissolved in water. Many studies are focused on the adsorption capacity of these materials because they are a promising alternative to overcome the problems previously arisen for the above described materials. As a matter of fact, zeolites conciliate high resistance to environmental conditions such as pH or chemical and biological stress as well as high adsorption capacity and selectivity. Besides, synthetic high-silica zeolites usually show an excellent thermal stability and this makes easy their regeneration and reuse in the adsorption processes. For all these reasons, zeolites are the materials selected for this dissertation. In particular, a set of ZSM-5 samples have been analyzed. The aim of this study is to investigate not only the adsorption but also the organics desorption and the effects of the regeneration process on the analyzed zeolites. The following sections will give an overview about the characteristics of the investigated material, with particular emphasis to ZSM-5 zeolite.

1.4.1. General notions about zeolites

In 1756, the Swedish mineralogist A. F. Cronsted introduced "*zeolites"* as a new family of minerals after his first discover of stilbite. The term derived from the Cronsted's observation of behaviour on heating (in a borax bead) of these minerals: they showed a sort of tumescence during heating [102]. For this reason he called these minerals "*zeolite*" which is derived from the Greek term "ζέω λίθος", literally "stone that boils". The pioneers in the research and description of the properties of zeolites were Damour in 1840, who discovered the reversibility of hydration-dehydration process [103] and Eichorn, in 1858, who recognized the reversible ion exchange capability of chabazite [104]. The aptitude of dehydrated zeolites to adsorb organic liquids (such as alcohol and benzene) was firstly observed by Friedel in 1896. Upon this observation he developed the concept that zeolites consist of a sort of open spongy framework that was understood as a porous material with properties similar to those of a sponge [105]. The trade of zeolites began starting from 1905, when Gans used them as a water softener in Germany. Unsatisfied by the performance of some zeolites he used, Gans in 1907 synthesized the first zeolite, which was launched on the American market in 1913. Grandjean in 1909 (studying the adsorption of gases) noted that the chabazite adsorbs compounds such as ammonia, air, hydrogen, hydrogen sulfide, iodine and bromine [106]. In 1925, Weigel and Steinhof recognized for the first time the capability of zeolites to separate molecules in relation to their size (molecular sieve capacity). In particular their experiments demonstrated that chabazite zeolite adsorbed water, alcohol and formic acid excluding acetone and benzene. However, they did not understand the reason of this effect and they wrote: *"…because of this difference, it is concluded that there is not chemical reaction involved, but the exact nature of the union is not yet been determined*" [107,108]. Afterwards, this zeolite's feature was defined by McBain with the term "molecular sieve" which indicates porous solid materials that act as sieves on a molecular scale. Regarding that, about twenty years later Barrer has defined zeolites as rigid crystal sponges able to adsorb in their pores a large number of molecules with a specific size and shape, but they are unable to adsorb molecules with "wrong" shape and dimension [109,110]. Besides, Barrer attempted to classify zeolites in different groups in relation to their adsorption capability. In the first group he placed all the zeolites able to adsorb small molecules such as methane and ethane; zeolites able to rapidly adsorb hydrocarbons such as methane and ethane and more slowly molecules are part of the second group; finally the third group is composed of zeolites as mordenite, which are able to adsorb only very small molecules.

The traditional definition of zeolite was proposed by Hey (1930) [111], who concluded that zeolites in general have aluminosilicate frameworks with loosely bonded alkali or alkali-earth cations, or both. Molecules of H_2O occupy extra-framework positions. With intensification of research and the advent of the electron microprobe, a flood of information on compositions has become available, and with automated single-crystal X-ray diffractometers and other developments, many phases have been investigated [112]. As a result of the development of knowledge about these materials it was possible to find out that some minerals that meet the traditional criteria, however, contain P and Be or other elements in tetrahedral sites. On the other hand, several minerals showing zeolitic properties defer from traditional requirements for a zeolite in having a framework interrupted by some (OH) groups. For all these reasons the Hey's definition (1930) [111] is found to be obsolete and restrictive and it had to extend it to a wider range of materials characterized by "zeolitic properties". In 1963 Smith already tried to give a broader definition to avoid the danger of excluding a possible candidate from the group. He gave an explanation based on the crystal structure of the zeolite, which was defined as an "*alumino-silicate with a framework structure enclosing cavities occupied by large ions and water molecules, both of which have considerable freedom of movement, permitting ion-exchange and reversible dehydration"* [113]. Therefore in 1997, the Commission of New Minerals and Mineral Names (CNMMN) adopted the following definition: "*A zeolite mineral is a crystalline substance with a structure characterized by a framework of linked tetrahedra, each consisting of four O atoms surrounding a cation. This framework contains open cavities in the form of channels and cages. These are usually occupied by H_2O molecules and extra-framework cations that are commonly exchangeable. The channels are large enough to allow the passage of guest species. In the hydrated phases, dehydration occurs at temperatures mostly below about 400°C and is largely reversible. The f'ramework may be interrupted by (OH,F) groups; these occupy a tetrahedron apex that is not shared with adjacent tetrahedra*" [112]. As reported by Alberti et al.[112], this definition considers that zeolites in the historical and mineralogical sense are naturally occurring minerals, irrespective of how the term may be applied to synthetic materials.

By a structural point of view, zeolites constitute an important family of microporous materials characterized by: hierarchical structures, selective pore sizes and high external surface area [114]. In particular, zeolite can be defined as a tectosilicate based on corner-sharing TO_4 tetrahedra (PBU) forming a three-dimensional framework with uniformly

sized pores [115]. In general, the term "framework" indicates a corner sharing network of tetrahedrally coordinated atoms, which are mainly represented by Si, Al and P atoms. In some cases also B, Ga, Be and other species [116] can be present in the zeolitic framework. The Database of Zeolite Structure [117] includes today 232 topological distinct tetrahedral TO_4 frameworks. If the PBU is constituted by tetrahedra of silicon (SiO_4) and aluminum (AlO_4), zeolites present an anionic framework. The negative framework's charge is balanced by "*extra-framework"* mobile cationic species located in the zeolite's microporosity. This microporosity is constituted by channels or cages. Besides, in relation on the silicon-aluminum oxides ratio (SiO_4/AlO_4) zeolites show an hydrophilic or hydrophobic character. In particular, when this ratio is low zeolites are an hydrophilic materials and find employment in the removal of cationic species, heavy metals and radioactive elements [34,118–121].

On the other hand, zeolite's hydrophobicity increases as this ratio increases. For instance, high-silica zeolites ($SiO_4/AlO_4 > 10$) that show a marked hydrophobic character are an organophilic materials with high affinity for non-polar organic molecules. Therefore, they are not only potential adsorbents for organic compounds [9,10,15,34,48,53,56,122–126] but can be used also as heterogeneous catalysts or in the separation process [9,127,128].

Finally, zeolite's framework can be conceived as a composition of finite and infinite units (the latter are composed by chains or layers) that describe zeolite's topologies, they are named SBUs [129]. The concept of SBUs is different from that of the Secondary Structural Units (SSUs), which represents only a structural feature. In general, it is possible to assume that framework cannot be made up only by these types of units. In several cases, framework can be constituted by more than one SBUs and the unit cell always contains an integral number of SBUs that composed the framework [129]. In many cases zeolite's framework can be described by the PerBU which are represented by *"[…]smaller units composed of a limited number of T-atoms by applying simple operation(s) to the smaller unit, e.g. translation, rotation"* [129]. As for the SBUs, also the PerBU are infinite (chains, tubes and layers) and finite (4-rings, 6-rings and cages), and they can be used together to build the zeolite framework.

1.4.2. MFI topology: ZSM-5

The PerBU of MFI topology containing (modified) 5-rings and the framework can be described by units of 12 T atoms which consist of two 5-1 PBU (Figure 1). Pentasil-chains are related by a mirror plane perpendicular to *b* and are connected into the PerBU [130,131].

Figure 1. MFI framework.

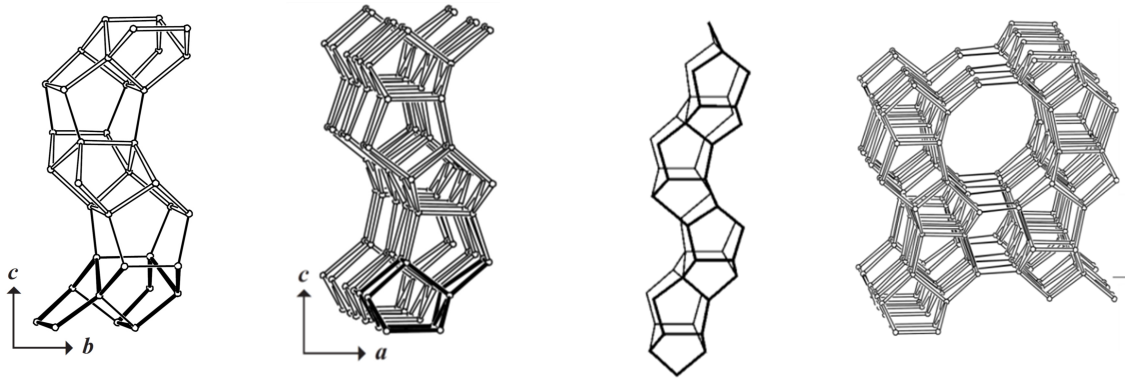

1) MFI framework described by 5-rings and 12 T atoms

2) The PBU 5-1

3) The Pentasil chain

4) Mode connection in MFI topology

Moreover, MFI topology is characterized by cavities formed by the intersections of the two 10-ring channel systems (Figure 2). Below are reported the figures that show the typology of cavities and how they are linked.

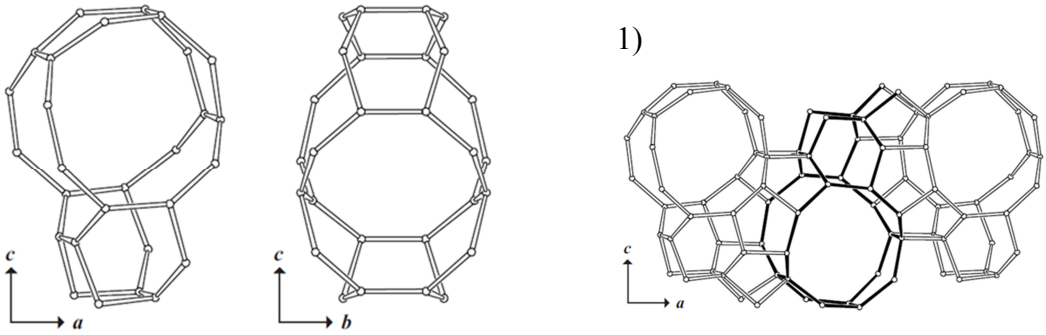

Figure 2. Cavity in MFI topology (along b and a respectively). Linkage of cavities in MFI topology: view of sinusoidal 10-ring channels parallel to a (1); the second view along a axis (2) represent the linkage of the cavities into straight 10-ring channel.

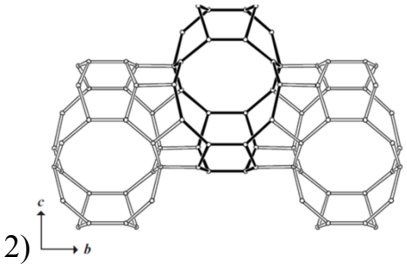

Specifically, ZSM-5 (Zeolite Socony Mobil type 5) is a pentasil medium-pore zeolite widely used as shape-selective catalysts and sorbents due to its shape selectivity, solid acidity, ion exchangeability, pore size and thermal stability. Its framework is characterized by two intersecting sets of tubular channels: a sinusoidal 10MR channel parallel to the [010] direction and a straight 10MR channel parallel to the [100] direction. Their openings are ~ 5.1-5.5 Å and ~ 5.3 - 5.6 Å respectively (Figure 3).

Figure 3. Channels system in ZSM-5.

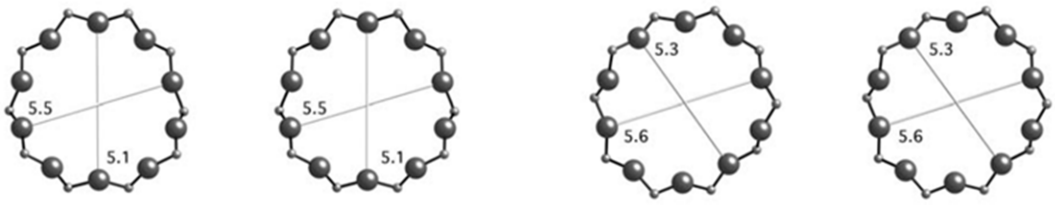

Sinusoidal 10MR channel [100]
opening 5.1-5.5 Å

Straight 10MR channel [010]
opening 5.3-5.6 Å

The topological symmetry is orthorhombic *Pnma*, but its real symmetry strongly depends on the synthesis and post synthesis treatment, SiO_2/Al_2O_3 ratio, structural defects, temperature, nature and amount of sorbate organic molecules [117,129,130,132–136].

2. Materials and experimental techniques

In this work four main techniques are used to obtain the expecting results: adsorption isotherms and gas chromatography, XRPD with conventional and non-conventional radiation, finally thermogravimetric and differential thermal analysis. This paragraph reported the main information about these techniques. In some cases more details are reported in the specific section of the results.

2.1. Materials

The materials use in this work are the following. On regard to organic molecules, TOL (purity 99.9%), MTBE (purity 99.8%), 1,2-DCE (purity 99.8%) and CB (purity 99.9%) caffeic acid (CA) (purity 99.8%) and p-hydroxybenzaldehyde (p-HBA) (purity 99.8%) were obtained from Sigma-Aldrich (Steinheim, Germany).
The zeolite sample used in this study is a hydrophobic ZSM-5 (CBV28014, Zeolyst International) characterized by SiO_2/Al_2O_3 ~280, Na_2O content < 0.05% w/w, NH_4^+ content < 0.1% w/w, and specific surface area of 400 m^2g^{-1}.

2.2. Gas chromatography

The contaminants concentration in the aqueous solutions was determined by GC–FID. Prior to this, the organics were extracted from the water sample by HS-SPME. The head space mode was used to extract organic compounds from 10 ml of solution in 25 ml glass flasks sealed with Teflon screw caps. 2 mL of a 300 $g \cdot L^{-1}$ NaCl solution were added to the sample. Samples were immersed in a thermostatic water bath at 40°C (±0.5°C) and maintained under controlled agitation with a magnetic stirrer (300 rpm) for 10 min to reach equilibrium conditions before SPME insertion. The fiber was inserted into the GC injector for analysis and kept at 250°C. Desorption time was 1 min. The GC used in this work was an HRGC5160 MEGA SERIES Instrument (Carlo Erba, Italy) equipped with a split/splitless injector and an FID detector. A fused-silica capillary column OV-1 (30 m × 0.32 mm I.D., 0.1 μm film thickness; MEGA, MI, I) was used. Helium (99.999%) was used as a carrier gas at 30 kPa constant head pressure. The detector temperature was kept constant at 250°C. The GC oven was programmed as follows (the isothermal times reported in parenthesis): 40°C (5 min), 5°C·min^{-1} to 80°C (5 min), 30°C·min^{-1} to 100°C (5 min).

In the case of binary mixtures, the concentration of contaminants in the aqueous solution was determined by HS-GC-MS. The analysis was carried out using an Agilent GC-MS system (Santa Clara, CA, USA) consisting of a GC 6850 Series II Network coupled to a Pal G6500-CTC injector and a Mass Selective Detector 5973 Network. HS autosampler injector conditions were: incubation oven temperature 80°C, incubation time 50 min, headspace syringe temperature 85°C, agitation speed 250 rpm, agitation on time 30 s, agitation off time 5 s, injection volume 500 µL, fill speed 30 $\mu L \cdot s^{-1}$, syringe pull-up delay 5 s, injection speed 250 $\mu L \cdot s^{-1}$, pre-injection delay 0 s, post injection delay 2 s, syringe flush 30 s with nitrogen. The injected solutions consisted of 100 µL of sample solutions, diluted in 10 mL of an aqueous solution saturated with NaCl, containing 10 µL of 500 $mg \cdot L^{-1}$ of fluorobenzene in methanol as internal standard. A DB-624 UI GC column (L = 20 m, I.D. = 0.18 mm, df = 1.00 µm film thickness, Agilent, Santa Clara, CA, USA) was used. High purity helium was the carrier gas with a constant ow rate of 0.7 $mL \cdot min^{-1}$. The oven temperature gradient started at 40°C for 4 minutes and then ramped to 130°C at 15°C min^{-1}. The injector temperature was kept at 150°C. All samples were injected in split mode (10:1). The mass spectrometer operated in electron impact mode (positive ion, 70 eV). The source temperature and the quadrupole temperature were set to 230°C and 150°C, respectively. The mass spectra were acquired in full scan mode. The electronic scan speed was 1562 $amu \cdot s^{-1}$ in a mass range from 30 to 300 amu. For identification and quantification of the target analyte the SIM (selected ion monitoring) chromatograms were extracted from the acquired signal by selecting the most abundant characteristic fragments at m/z = 62.49 (1,2-DCE), m/z = 73.57 (MTBE) and m/z = 91.92 (TOL). Chromatographic peak of each analyte was identified by comparison of the retention time and the mass spectrum with standard compound and library data; quantitative analysis was performed using calibration curves.

2.3. Adsorption isotherm

The adsorption isotherm was determined using the batch method. Batch experiments were carried out in duplicate in 20 ml crimp top reaction glass flasks sealed with PTFE septa (Supelco, PA, USA). The flasks were filled in order to have minimum head space, a solid/solution 1:4 ($mg \cdot mL^{-1}$) ratio was employed. The solids were separated from the aqueous solution using centrifugation (14,000 rpm for 30 min) after equilibration, for 24 h

at a temperature of 25.3 ± 0.5°C under stirring. Contaminants concentrations in solutions with regenerated samples were read before and after equilibration by HS-SPME-GC-FID in order to determine the adsorbed quantities (q) and the equilibrium concentrations (C_e).

As the binary mixture, adsorption isotherms were determined using the batch method. Batch experiments were carried out in duplicate in 20 mL crimp top reaction glass flasks sealed with PTFE septa (Supelco, PA, USA). The flasks were filled in order to have the minimum headspace. A solid/solution ratio of 1:4 ($mg \cdot mL^{-1}$) was employed. After equilibration for 24 hours at a temperature of 25.3 ±0.5°C under stirring, the solids were separated from the aqueous solution using centrifugation (14,000 rpm for 30 min). To determine adsorbed quantities (q) and equilibrium concentrations (C_e), concentrations of TOL, MTBE, 1,2-DCE and CB were determined in solutions before and after equilibration with the zeolite. The uptake (q) was calculated as follows (Equation 1):

$$q = \frac{(C_0 - C_e)\, V}{m}$$

Equation 1 - Adsorption isotherm

where C_0 is the initial concentrations in solution ($mg \cdot L^{-1}$); V is the solution volume (L); and m is the mass of sorbent (g). All experiments were carried out in duplicates (deviations were within 5%). Experimental isotherm data were fitted to two different models of competitive sorption isotherms. All the model parameters were evaluated by non-linear regression using MATLAB® software. The optimization procedure requires an error function to evaluate the goodness of fit of the equation to experimental data. Apart from the coefficient of determination (R^2), the sum of the residual square errors (SSE) was also used to measure the goodness of fit.

2.4. Diffraction method and Rietveld refinements

XRPD data were collected at the ESRF ID22 beam line, Grenoble, using a fixed wavelength of 0.40003(1)Å. A series of XRPD patterns were measured through nine parallel scintillation counters behind Si (111) analyzer crystals in the 0.5–19.5 2θ range, in steps of 25°C as a function of temperature while the sample was heated from room temperature to 600°C in air with a heating rate of $0.083°C \cdot s^{-1}$.

Measurements of XRPD patterns by conventional radiation at room temperature of both unloaded and loaded/reloaded samples were performed on a Bruker AXS D8 Advance diffractometer equipped with Si(Li) solid state detector (Sol-X). The experimental conditions were the following: Cu $K\alpha_1,\alpha_2$ radiation (λ = 1.54178 Å), 2θ range 3-110°, step size 0.02°, time/step 12 s, scattering, divergence, and receiving slits 0.6, 0.6 and 0.1 mm, respectively.

Rietveld refinements were performed using the Larson and Von Dreele [137] GSAS with an EXPGUI graphical interface [138].

2.5. Thermal analysis

TG and DTA measurements of both the calcined and reloaded ZSM-5 samples were performed in air at up to 900°C using a Netzsch STA 409 PC LUXX® - simultaneous TG/DTA thermogravimetric analyzer operating at 5°C/min heating rate under 50 $ml \cdot min^{-1}$.

3. Results and discussion

The results obtained in this investigation are divided in four sections. Overall the sections provide an overview on the behaviour of the ZSM-5 used as the adsorbing medium of VOCs dissolved in water solution and their reuse after a regeneration treatment. As reported also in chapter 2, samples are characterized by adsorption isotherm and thermal analysis in order to verify the adsorption capability of ZSM-5. Then, the same samples are characterized by a structural point of view to better understand not only the adsorption mechanism but also the desorption process during the regeneration process. In particular, *in situ* HT synchrotron XRPD is used as a key to a continuous monitoring of selected pollutants desorption process as well as the structural modifications undergoing on ZSM-5 upon thermal treatment. Understanding the transient and dynamic features of desorption processes can contribute in the research on a possible reactivation of these materials to expand zeolites' capabilities in environmental applications. The first part of this dissertation is focused on the VOCs adsorption process at ambient conditions from aqueous solutions. The first section describes four systems based on the adsorption of single contaminants. Specifically, the systems analyzed are focus on the adsorption of 1,2-DCE, TOL, MTBE and CB. The results obtained and discussed in section I are used as a basis to move to a more realistic systems.

Therefore, in section II the binary mixture competition was evaluated. Firstly, adsorption equilibria of VOCs binary mixtures in aqueous solution on ZSM-5 were measured over a wide range of concentrations. In order to evaluate the influence of natural organic matter on the removal of contaminants from water, VOCs-humic acid monomers competition was evaluated. It is generally found that adsorption decreases with increasing ionization of the molecule as the pH increases above the point of zero charge (pzc) of the surface due to charge repulsion between the anion and the increasingly negatively charged surface, and to the reduced solvophobic effect of the anion relative to the molecule. Both CA and p-HBA are low molecular weight compounds secreted into soil by plant tissues and/or decay of plant residues, they are allelochemicals and play an important role in agricultural and ecological dynamics.

Section II reported the results obtained for the following systems: MTBE/1,2-DCE, MTBE/TOL, TOL/CB, TOL/CA as well as TOL/p-HBA binary mixtures. This section concludes the study on the adsorption process of VOCs from aqueous solution at ambient conditions.

The desorption process of single components as well as VOCs binary mixture are discussed in Section III. This section gives an overview of the ZSM-5 behaviour during the thermal treatment as well as clarifies the desorption dynamics of specific adsorbed organics inside the zeolite channels system.

Finally, two single component systems are tested after thermal regeneration in order to verify if ZSM-5 after regeneration can be reused to a new VOCs adsorption cycle. The results are reported in section IV.

The most part of the results discussed in the following sections were previously published or accepted by international scientific journal (*e.g.*, RSC Advances, Microporous and Mesoporous Materials, Catalysis Today and Minerals). Other results here reported are still to be submitted. In the sections' text, published results are rearranged and integrated with the data in preparation to give a more organic and completely discussion of the treated issues. In general the experimental techniques are not reported for each treated systems, but they are summarized in the chapter dedicated to them. In some cases more details are reported in the specific paragraph in order to better explain the results.

Results and discussion	
Section I	
Adsorption of VOCs from aqueous solution at ambient conditions	➢ Evidence of 1,2-DCE adsorption from aqueous solution in ZSM-5 ➢ Evidence of TOL adsorption from aqueous solution in ZSM-5 ➢ Evidence of MTBE adsorption from aqueous solution in ZSM-5 ➢ Evidence of CB adsorption from aqueous solution in ZSM-5
Section II	
Competitive behaviour of VOCs and humic acid monomers from binary aqueous mixtures in ZSM-5 at ambient conditions	
Competitive adsorption of VOCs from binary aqueous mixtures on zeolite ZSM-5	➢ ZSM-5 loaded with TOL/MTBE and 1,2-DCE/MTBE binary mixtures ➢ ZSM-5 loaded with TOL/CB binary mixtures
Competitive adsorption of VOCs and humic acid monomers	
Section III	
Study of the desorption process of VOCs confined into ZSM-5 through the in situ HT synchrotron XRPD	➢ Desorption process of 1,2-DCE induced by heating ➢ Desorption process of TOL induced by heating ➢ Desorption process of MTBE induced by heating ➢ Desorption process of 1,2-DCE/MTBE and TOL/MTBE binary mixtures induced by heating
Section IV	
Adsorption behaviour of regenerated ZSM-5	➢ Adsorption behaviour of regenerated ZSM-5 reloaded with 1,2-DCE and TOL

3. SECTION I:

Adsorption of VOCs from aqueous solution at ambient conditions

The ZSM-5 samples loaded with VOCs are initially characterized through the adsorption isotherm at room temperature (25°C). The concentration of contaminants in aqueous solution was obtained by gas chromatography and mass spectrometry. However, the adsorption data provide insufficient insight to the adsorption mechanisms and the choice between the adsorption model should be based on the knowledge of the adsorption process [125]. Consequently, to gain information on the ZSM-5 adsorption sites a structural investigation was performed in order to localize the VOCs molecules in the ZSM-5 framework. This investigation starts with the study of single component systems. Then, the results obtained for single components were used as a basis to study the adsorption process of binary mixtures of hydrocarbons. The study of binary mixture systems is treated in section II and III.

3.1 Evidence of 1,2-DCE adsorption from aqueous solution in ZSM-5

The presence of 1,2-DCE molecules inside the zeolite pores was revealed by unit cell parameters variations and structural deformations obtained from synchrotron X-ray structure analyses carried out using the Rietveld method on exhausted zeolite samples. Very interestingly, structure refinements demonstrated that these changes are strongly related to the complexation of the guest species with water molecules [8]. This results confirm the previous chromatographic study that was published by Pasti et al. (2012) [14].

As reported by Martucci et al. [8] the structure refinements by full profile Rietveld analysis was carried out using the GSAS [137] package and the EXPGUI graphical interface [138] starting from the atom site positions reported by Pasti et al. [14]. Extraframework site were located by difference Fourier map. The Bragg peak shape was modelled using a modified pseudo-Voigt function with 0.01% cut-off peak intensity. The instrumental background was empirically fitted using a Chebyschev polynomial of the first kind with 16 variable coefficients for room temperature and 24 variable coefficients for HT data set. The 2θ-zero shift, scale factor and unit-cell parameters were accurately refined. Moreover, the 2θ-zero shift and the reflection intensity were preliminary refined with Le Bail extraction method and then kept fixed at the mean value in all patterns of the data set. Soft constraints were imposed on Si-O and O-O framework distances (1.60 and 2.60 Å, respectively) and on C-C (1.34 Å), C-Cl (1.74 and 2.76 Å) and Cl-Cl (4.34 Å) 1,2-DCE

distances and the weight was gradually released after the initial stages of refinement, H-atoms were not considered in the structure refinement due to their low scattering factors. In the final cycles, all positional parameters, site occupancy, and isotropic atomic displacement parameters were refined.

After 1,2-DCE adsorption [9,15] the automatic indexing of the peaks as well as the β values confirmed the $P2_1/n$ monoclinic symmetry [14]. Lattice parameters and refinement details of ZSM-5-1,2-DCE-30 are reported in Table 1. The features of unloaded material [14] are also listed for comparison. The dimensions of the 10-membered rings (10MRs) together with their C.F.A. and their ellipticity are reported in Table 2.

Table 1. Lattice parameters and refinement details of unloaded ZSM-5 and after 1,2-DCE adsorption [8,14].

	ZSM-5	**ZSM-5-1,2-DCE**
Space group	$P2_1/n$	$P2_1/n$
***a* (Å)**	19.8999(5)	19.9052(3)
***b* (Å)**	20.1174(6)	20.1199(3)
***c* (Å)**	13.3892(4)	13.3909(2)
***β* (°)**	90.546(3)	90.578(1)
***V* (Å^3)**	5359.9(3)	5362.7(1)
Wavelength of incident radiation (Å)	1.54178	0.400031(1)
Refined pattern 2θ (°) range	3-110	0.7-25
R_{wp} (%)	9.12	17.2
R_p (%)	8.4	13.5
R_{F^2} (%)	9.1	8.50
No. of contributing reflections	14142	12252
N_{obs}	5601	7239
N_{var}	289	282

$R_p = \Sigma[Y_{io}-Y_{ic}]/\Sigma Y_{io}$; $R_{wp} = [\Sigma wi(Y_{io}-Y_{ic})^2/\Sigma wiY_{io}^2]^{0.5}$; $R_{F2} = \Sigma|F_o^2-F_c^2|/|F_o^2|$

Table 2. Dimensions (Å) of the apertures of unloads ZSM-5 and after 1,2-DCE adsorption.

SC-A	ZSM-5 [14]	ZSM-5-1,2-DCE [8]
O7-O1	7.98(1)	8.21(1)
O8-O2	8.08(1)	8.11(1)
O31-O37	8.20(1)	8.28(1)
O44-O46	8.19(1)	8.63(1)
O47-O48	7.93(1)	7.96(1)
C.F.A.	22.68	24.14
ε	1.03	1.08

SC-A	ZSM-5 [14]	ZSM-5-1,2-DCE [8]
O11_O5	8.23(1)	8.15(1)
O20_O18	8.21(1)	8.49(1)
O21_O22	8.04(1)	8.01(1)
O27_O33	8.03(1)	8.38(1)
O28_O34	8.07(1)	7.081(1)
C.F.A.	22.68	23.51
ε	1.02	1.08

ZZ-B	ZSM-5 [14]	ZSM-5-1,2-DCE [8]
O17-O18	7.81(1)	7.71(1)
O23-O25	8.20(1)	8.49(1)
O30-O5	8.31(1)	8.59(1)
O31-O4	7.91(1)	7.64(1)
O44-O43	8.13(1)	8.18(1)
C.F.A.	22.65	23.12
ε	1.06	1.12

ZZ-A	ZSM-5 [14]	ZSM-5-1,2-DCE [8]
O20-O15	7.95(1)	8.28(1)
O24-O26	7.84(1)	8.26(1)
O27-O2	7.85(1)	8.16(1)
O28-O1	7.90(1)	7.96(1)
O41-O46	8.22(1)	8.68(1)
C.F.A.	21.65	24.37
ε	1.04	1.09

Rietveld refinement has revealed that different 1,2-DCE molecules could be connected by means of hydrogen bonds through water to 1,2-DCE water complexes, thus influencing the 1,2-DCE trans-gauche conformational equilibrium [14]. A similar result has been recently

found in hydrophobic mordenite after 1,2-DCE adsorption [124]. As reported above, Rietveld structure refinement of ZSM-5-1,2-DCE using *in situ* synchrotron XRPD data was performed starting from the structural model reported at room temperature by Pasti et al. [14]. The difference Fourier map, generated using the GSAS package, confirmed the distribution of the 1,2-DCE molecules over the two crystallographic independent sites (DCE1= C1, C2, Cl1, Cl2 sites; DCE2= C3, C4, Cl3, Cl4 sites) (Figure 4 and Table 3) localized by Pasti et al. [14].

Table 3. Extraframework sites coordinates of ZSM-5-1,2-DCE at room temperature [8]

	ZSM-5-1,2-DCE				
	x/a	**y/b**	**z/c**	**Fraction**	**Uiso**
C1	0.772(1)	0.468(8)	0.060(5)	0.85(1)	0.11(2)
C11	0.686(1)	0.470(3)	0.069(2)	0.85(1)	0.11(2)
Cl2	0.893(1)	0.484(2)	-0.029(2)	0.85(1)	0.11(2)
C2	0.807(1)	0.487(8)	-0.020(5)	0.85(1)	0.11(2)
C3	0.748(8)	0.796(1)	0.170(2)	0.75(1)	0.15(2)
Cl3	0.739(2)	0.720(1)	0.115(2)	0.75(1)	0.15(2)
C4	0.747(9)	0.855(1)	0.121(2)	0.75(1)	0.15(2)
Cl4	0.75(3)	0.931(1)	0.177(2)	0.75(1)	0.15(2)
W	0.638(5)	0.319(4)	0.329(6)	0.77(5)	0.43(1)

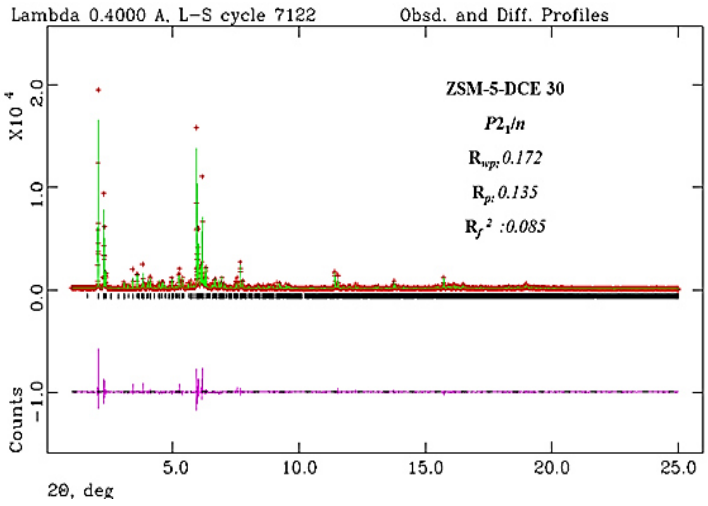

The 1,2-DCE1 site is located near SC-channels and 1,2-DCE2 site lied in the ZZ 10- ring channel, respectively [9,15]. As reported by Martucci et al. [8] the refined occupancies seem to indicate that 1,2-DCE molecules prefer to be hosted in the DCE1 site rather than in the DCE2 one (84% occupancy in DCE1 vs. 74% in DCE2) [56]. The location of co-adsorbed water molecules (W site, ~ 3.0 water/u.c, corresponding to ~ 1.5% in weight) was also confirmed. According to the starting model, all the 1,2-DCE molecules (~ 6.5 molecules/u.c., corresponding to ~ 9.5% in weight) assume a trans (anti)configuration and can interact with water thus forming 1,2-DCE -water molecule complexes (clusters or short chains) bridged via W to framework oxygen atoms (Figure 4).

Figure 4. Location of 1,2-DCE and water molecules in ZSM-5 along [100] and [010] directions [8].

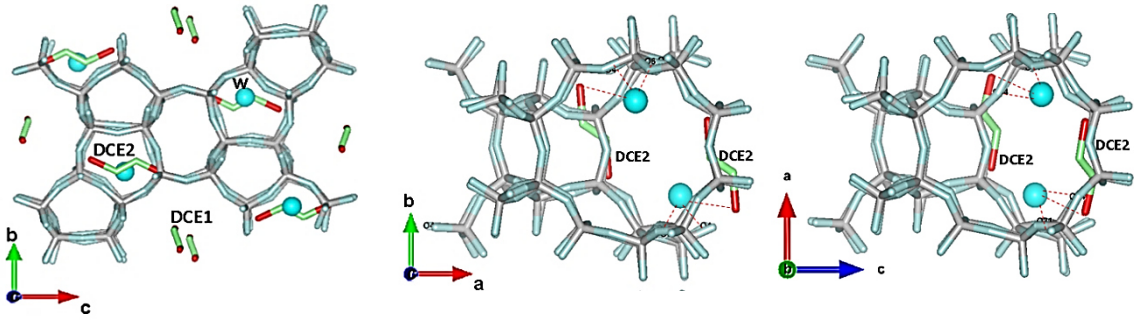

TG analysis was used to determine the amount of 1,2-DCE molecules embedded in the ZSM-5 framework. The TG curve (Figure 5) of the ZSM-5-1,2-DCE showed that, apart from the elimination of species (water and/or 1,2-DCE) weakly bonded to the surface (T < 100°C, weight loss 1.5%), a sudden change in its slope occurs at higher temperatures, which is reasonably due to the elimination of 1,2-DCE and/or H_2O molecules trapped within the zeolite pores.

Figure 5. TG, DTG and DTA curves in ZSM-5 loaded with 1,2-DCE [8].

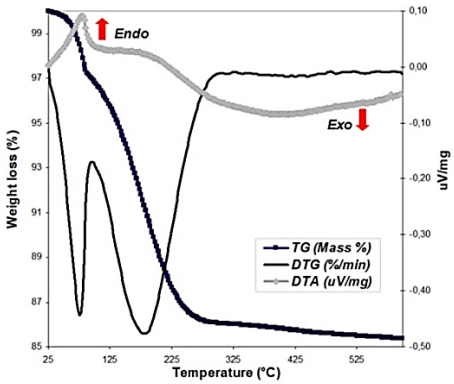

Total weight loss at 900°C is about 12.0% compared to 2.5% in the pristine sample [8,14]. This result is in very good agreement with the extraframework content given by the refined occupancies and with the saturation capacity determined by the adsorption isotherms [14].

3.2 Evidence of TOL adsorption from aqueous solution in ZSM-5

The adsorption of TOL in ZSM-5 from aqueous solution were investigated in order to obtain information on the kinetic and thermodynamics of the adsorption process [9].

The adsorption isotherm was determined using the batch method. Batch experiments were carried out in duplicate in 20 ml crimp top reaction glass flasks sealed with PTFE septa (Supelco, PA,USA). The flasks were filled in order to have minimum head space, a solid/solution 1:4 ($mg \cdot mL^{-1}$) ratio was employed. The solids were separated from the aqueous solution using centrifugation (14,000 rpm for 30 min) after equilibration, for 24 h at a temperature of 25.3 ± 0.5°C under stirring. TOL concentrations in solutions with zeolite were read before and after equilibration by HS-SPME-GC-FID in order to determine the adsorbed quantities (q) and the equilibrium concentrations (C_e). The equilibrium adsorption isotherm provides the relationship between the concentration of organic contaminant in solution and how much is adsorbed on the solid phase when the two-phase sys-tem is in equilibrium. The experimental data shows the Langmuirian shape and consequently the data were fitted to Langmuir and a bi-Langmuir models, which were employed to describe the adsorption of different organic compounds on ZSM-5 [139].
These two models are expressed by Equation 2 and Equation 3:

$$q = \frac{q_S b C_e}{1 + b C_e}$$

Equation 2 - Langmuir

$$q = \frac{q_{S1} b_1 C_e}{1 + b_1 C_e} + \frac{q_{S2} b_2 C_e}{1 + b_2 C_e}$$

Equation 3 - bi-Langmuir

where q_s is the saturation capacity of the adsorbent material, C_e the equilibrium concentration in the solution and b the binding constant, the subscripts refer to the type of adsorption sites. The estimated parameters from non-linear fitting are shown in Table 4.

Table 4. Langmuir isotherm parameters for the adsorption of TOL on ZSM-5 [9].

	B (L·mg^{-1})	q_S (mg·g^{-1})	R^2
Langmuir	3.17 (2.76, 3.59)	82 (77, 87)	0.9565
Bi-Langmuir	2.70 (2.27, 3.14) 3.36 (2.91, 3.80)	65 (61, 70) 26 (22, 30)	0.9865

The determination coefficients (R^2) of the Langmuir isotherm (0.9565) are not significantly different from the Langmuir isotherm (0.9865) obtained for adsorption data at 22.5°C. Since the difference in goodness of fitting parameters for the two isotherm models is not significant, the simplest model (*i.e.* Langmuir isotherm) can be employed to describe TOL adsorption in ZSM-5. Moreover, the monolayer adsorption capacity determined using the Langmuir isotherm is about 82 mg/g, which is in very good agreement with experimental value (81.6 mg/g). Finally, the equilibrium parameter R_L [140] was given byEquation 4:

$$R_L = \frac{1}{1 + bC_0}$$

Equation 4 - Equilibrium parameter

where C_0 is the initial concentration R_L values are in the 0.009–0.45 range, indicating that TOL adsorption onto ZMS-5 is favourable ($0 < R_L < 1$).

As for the adsorption kinetics, the effect of contact time on TOL adsorption in ZSM-5 was studied at different initial concentrations, as shown in Figure 6 a. The time to reach equilibrium was only 15 min. Adsorption is initially rapid, and then constant, possibly due to a greater abundance of adsorption sites available for adsorption during the initial stage. Various kinetic models have been suggested for describing adsorption processes. Amongst these, PFO and PSO are those commonly employed to investigate adsorption onto zeolites. These models are expressed in Equation 5 and Equation 6 as shown below:

$$q = q_e[1 - \exp(-k_1 t)]$$

Equation 5 - Kinetic model PFO

$$q = \frac{k_2 q_e^{\,2} t}{1 + k_2 q_e t}$$

Equation 6- Kinetic model PSO

where q is the amount of solute per unit mass of adsorbent at time t, q_e is the equilibrium value of q, k_1 and k_2 are the PFO and PSO rate constant, respectively. According to the theoretical analysis proposed by Azizian [141], PFO model better describes adsorption from a solution with a high initial solute concentration, while for initial solute concentrations which are not too high, a sorption PSO fit is generally better. It has also been demonstrated that for systems which are characterized using the PFO model, the observed rate constant is a linear function of the initial solute concentration; whereas the observed rate constant is a complex function of initial solute concentration for PSO kinetics systems. Table 5, reports correlation coefficients (R^2), kinetic parameters (k_1, k_2) and calculated $q_{e,cal}$ values obtained by non-linear regression.

Table 5. Kinetic parameters for the adsorption of TOL onto the ZSM-5 [9].

C_0 (mg·L^{-1})	$qe_{,exp}$ (mg·g^{-1})	Pseudo-first-order			Pseudo-second-order		
		k_1·(min^{-1})	$qe_{,cal}$ (mg·g^{-1})	R^2	k_2 (g·mg^{-1}·min^{-1})	$qe_{,cal}$ (mg·g^{-1})	R^2
16	31.3	9.48	32.1	0.8774	1.68	31.1	0.9934
24	43.9	5.123	43.8	0.8253	0.723	44.2	0.9705
32	57.4	3.821	56.1	0.7767	0.539	57.4	0.9121
45	62.8	2.891	64.1	0.6361	0.159	63.1	0.9233

R^2 comparison, obtained for PFO and PSO, suggests that TOL adsorption onto ZSM-5 takes place according to the pseudo-second-order kinetic model (Figure 6 b). Moreover, TOL uptake fit on ZSM-5 at 25°C for different initial TOL concentrations (Figure 6 a) in

an aqueous solution revealed that the PSO dependence rate constant on the equilibrium concentration follows a complex trend. Thus, the PSO model was confirmed [141,142].
In addition, the intraparticle diffusion model was applied in order to identify the adsorption steps (Equation 7):

$$q = k_{i,d} t^{1/2} + c_i$$

Equation 7 - Intrapaticle diffusion model

where k_i is the intraparticle diffusion rate constant and c_i is a constant for the *i*-th step. As shown in Figure 6 c, the two phase plot suggests that the adsorption process proceeds by surface adsorption and TOL intraparticle diffusion into the zeolite micropores for an initial TOL concentration of 45 mg·L^{-1}. By comparing the slopes of the two lines, it can be observed that $k_{i,1}$ is larger than $k_{i,2}$ (Table 6) for all the investigated concentrations, indicating that film diffusion is a more rapid process than intraparticle diffusion [143]. The intercept (c_i value) is significantly different from zero, confirming that the studied zeolites have a high level of initial adsorption.

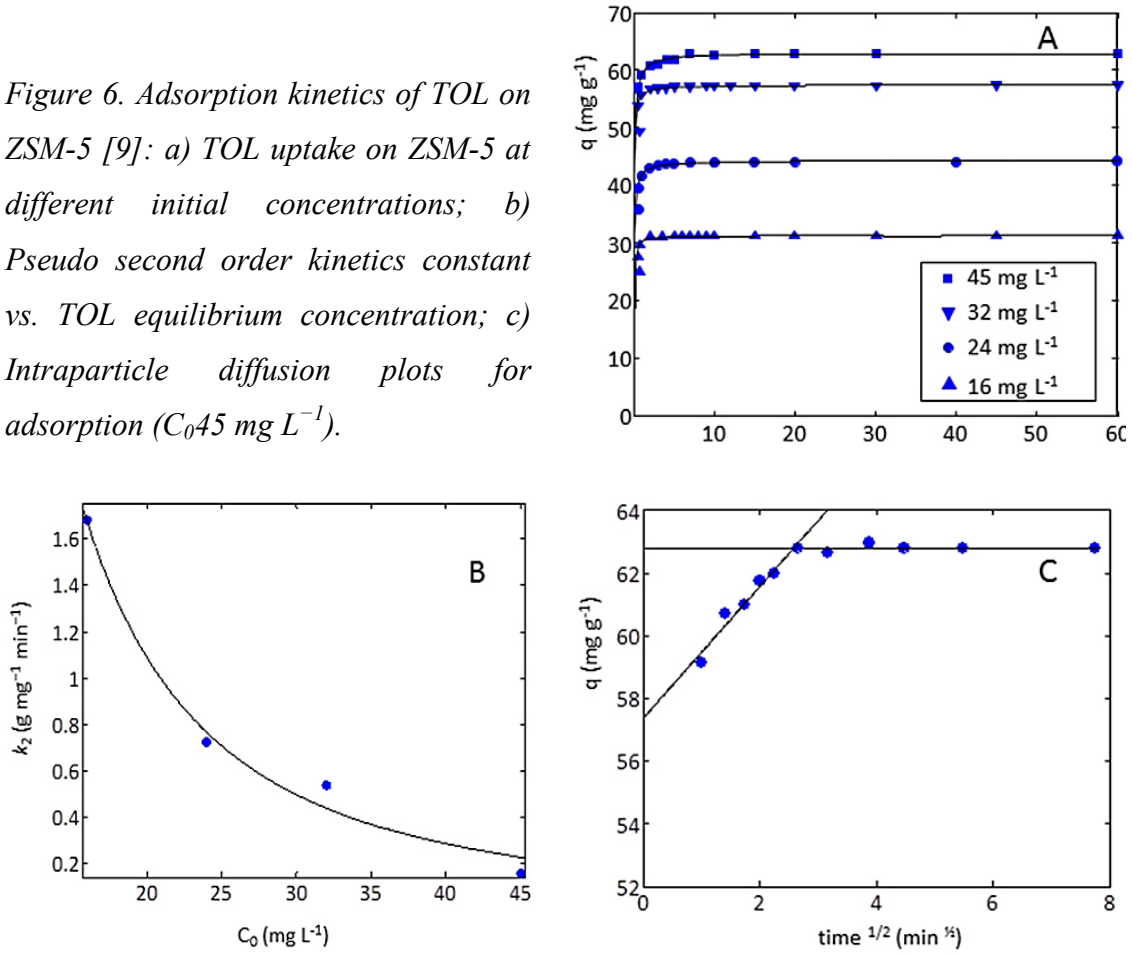

Figure 6. Adsorption kinetics of TOL on ZSM-5 [9]: a) TOL uptake on ZSM-5 at different initial concentrations; b) Pseudo second order kinetics constant vs. TOL equilibrium concentration; c) Intraparticle diffusion plots for adsorption ($C_0$45 mg L^{-1}).

Table 6. Intraparticle diffusion model parameters for the adsorption of TOL on ZSM-5 [9].

C_0 (mg·L^{-1})	$ki_{,1}$· (mg·g^{-1}·min$^{-1/2}$)	C_1 (mg·g^{-1})	R^2	$ki_{,2}$· (mg·g^{-1}·min$^{-1/2}$)	C_2 (mg·g^{-1})	R^2
16	0.54	28.8	0.9647	0.052	31.3	0.8553
24	1.01	41.2	0.8972	0.083	43.9	0.8676
32	1.62	53.1	0.9823	0.081	57.4	0.8662
45	2.11	57.3	0.9637	0.091	62.8	0.8755

Rietveld refinements were performed using the Larson and Von Dreele [137] GSAS with an EXPGUI graphical interface [138]. After TOL adsorption, the presence of peak doublets such as (i.e. 131 + 13-1 and 311 + 31-1, and 133 + 13-3 and 313 + 31-3) suggesting monoclinic symmetry. As a consequence, structure refinement of this sample (ZSM-5-TOL) was performed in the $P2_1/n$ space group starting from the framework atom site positions reported by Pasti et al [14] for the initial unloaded sample. The same space group was also reported for the same highly siliceous ZSM-5 zeolite used in this work by Ardit et al., Martucci et al., Pasti et al. and Rodeghero et al. [9–11,15,56,125,144].The refined β angle (90.545(1)°) confirms the assumption of the monoclinic symmetry after TOL adsorption (Table 7). Extra-framework sites were located by difference Fourier synthesis. H-atoms were not considered within the structure refinement due to their low scattering factors. Refined structural parameters for each data histogram were the follows: fractional coordinates and isotropic displacement factors for all atoms (one for each tetrahedral site and framework oxygen atom, one for each TOL molecule). TOL occupancy factors were refined in blocks, *e.g.* all the carbon atoms for each TOL molecule were constrained to have same value. The occupancy and isotropic displacement factors were varied in alternate cycles. Soft constraints were imposed on Si-O (1.60(1) Å), O-O (2.60(1) Å) and C-C (1.34 Å) distances and their weight was gradually released after the initial refinement stages. Lattice parameters and refinement details have been summarized in Table 7. The instrumental background was empirically fitted using a Chebyschev polynomial of the first kind with 16 variable coefficients for room temperature and 24 variable coefficients for HT data set. The 2θ-zero shift, scale factor and unit-cell parameters were accurately refined and the reflection intensity were was preliminary refined with Le Bail extraction method and then kept fixed at the mean value in all patterns of the data set. Peak intensity profiles (0.01% cut-off peak intensity) were modelled by

means of a pseudo-Voigt profile function using Gaussian U, V, and W coefficients, which is a Lorentzian particle-size broadening term. All positional parameters, site occupancy and isotropic atomic displacement parameters were refined in the final cycles.

Table 7. Lattice parameters and refinement details for ZSM-5-TOL at 30°C .The features of unloaded material are also listed for comparison [9], [14].

	ZSM-5	**ZSM-5-TOL 30**
Space group	$P2_1/n$	$P2_1/n$
***a* (Å)**	19.8999(5)	19.9062(1)
***b* (Å)**	20.1174(6)	20.1176(1)
***c* (Å)**	13.3892(4)	13.3926(1)
***β* (°)**	90.546(3)	90.5446(11)
***V* (Å^3)**	5359.9(3)	5363.01(12)
Wavelength (Å)	1.5417(1)	0.400031(1)
Refined 2θ (°) range	3-110	1-24.56
R_{wp} (%)	9.12	9.82
R_p (%)	8.4	10.54
Rf^2 (%)	9.1	8.7
Contributing reflections	14142	12055
N_{obs}	5601	7065
N_{var}	289	276

$R_p = \Sigma[Y_{io}-Y_{ic}]/\Sigma Y_{io}$; $R_{wp} = [\Sigma wi(Y_{io}-Y_{ic})^2/\Sigma wiY_{io}^2]^{0.5}$; $R_{F2} = \Sigma|F_o^2-F_c^2|/|F_o^2|$

The difference Fourier map indicated TOL molecules distribution over two crystallographic independent sites (TOL1 = C1, C2, C3, C4, C5,C6,C7 sites; TOL2 = C8, C9, C10, C11, C12, C13, C14 sites) (Table 8). TOL1 site is located close to the straight channel, while TOL2 molecules are located at the intersection between straight and sinusoidal channels (Figure 7) [10,56]. The final difference Fourier map showed two other peaks which were attributed to co-adsorbed water molecules (w1 and w2 sites, respectively).

Table 8. Atomic coordinates, thermal parameters and fraction of ZSM-5-TOL extraframework atoms [9].

	ZSM-5-TOL 30				
	x/a	**y/b**	**z/c**	**Uiso**	**Fraction**
			Site TOL 1		
C1	0.7491(36)	0.5795(28)	0.0559(75)	0.162(1)	0.86(1)
C2	0.3020(27)	0.4599(39)	-0.0152(83)	0.162(1)	0.86(1)
C3	0.8113(31)	0.5512(26)	0.0733(53)	0.162(1)	0.86(1)
C4	0.8270(23)	0.4906(22)	0.0315(41)	0.162(1)	0.86(1)
C5	0.7170(30)	0.4849(40)	-0.0412(70)	0.162(1)	0.86(1)
C6	0.2213(34)	0.5441(26)	0.0213(56)	0.162(1)	0.86(1)
C7	0.8884(28)	0.4625(46)	0.0496(41)	0.162(1)	0.86(1)
			Site TOL 2		
C8	0.2339(16)	0.1859(21)	0.8186(28)	0.219(2)	0.64(1)
C9	0.2339(16)	0.1270(21)	0.7645(28)	0.219(2)	0.64(1)
C10	0.2339(16)	0.1219(21)	0.9693(28)	0.219(2)	0.64(1)
C11	0.2339(16)	0.1829(21)	0.9209(28)	0.219(2)	0.64(1)
C12	0.2339(16)	0.0660(21)	0.9150(28)	0.219(2)	0.64(1)
C13	0.2339(16)	0.0660(21)	0.8131(28)	0.219(2)	0.64(1)
C14	0.2339(16)	0.0098(21)	0.7604(28)	0.219(2)	0.64(1)
			Water Sites		
w1	0.7218(2)	0.7066(3)	0.1683(4)	0.186(3)	0.85(3)
w2	0.4214(2)	0.4896(2)	-0.0282(4)	0.127(3)	0.55(3)

Figure 7. Location of TOL and water molecules in ZSM-5 along [100] and [001] directions. Observed (dotted upper line), calculated (solid upper line), and difference (solid lower line) powder diffraction pattern are also reported [9].

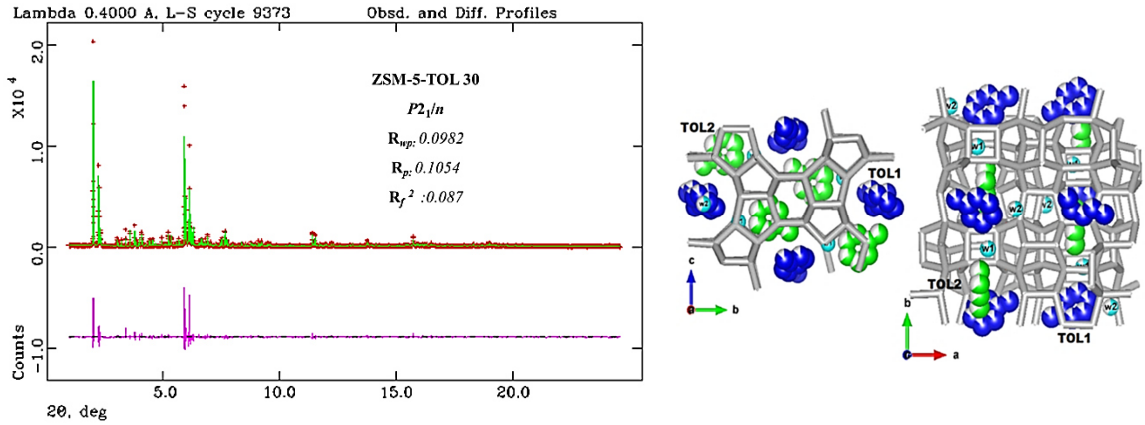

Both the TOL and water sites are partially occupied: TOL1 and TOL2 sites in 85% and 65% of cases, whereas w1 and w2 were occupied (Table 8) in 85% and 55% of cases, respectively. On the whole, 6 TOL molecules (which correspond to about 8.55% in weight) and approximately 2 water molecules (which correspond to approximately 2.0% in weight) were localized inside the ZSM-5 channel system. Therefore, structure refinement gave TOL content levels in very good agreement with the adsorption capacity (81.6 mg/g). The O atom refined distances for the water molecules from themselves (W2-W2 3.24(1) Å) and the TOL atoms (C1-w1 = 3.02(1) Å, C2-w2 = 2.46(1) Å, C5-w2 = 2.96 (1) Å, C11-w1 = 2.68(1) Å, C8-w1 = 2.34(1) Å, w1-C11 = 2.68(2) Å, w2-C5 = 2.96(3) Å) suggest the presence of water-TOL oligomers (TOL1-w1, TOL1-w2, TOL2-w1, TOL1-w2-w2) interacting with framework oxygens (C8-O18 = 3.15(4) Å, C9-O18 = 3.00(3) Å, C10-O17 = 3.04(4) Å, C10-O23 = 2.74(3) Å, C10-O43 = 2.67(3) Å). At the same time, TOL and w1 water molecules are connected to each other to form TOL1-w1-TOL2 molecular oligomer parallel to the *b* direction which are bonded to framework oxygen atoms. Water-organic complexes interacting with the framework were also detected by XRPD in ZSM-5 after 1,2-DCE [9,15] and MTBE [125] adsorption.

3.3 Evidence of MTBE adsorption from aqueous solution in ZSM-5

Removal of MTBE is particularly challenging because this compound is mobile and persistent in the environment due to its high water solubility, low Henry's law constant, small molecular size and resistance to biodegradation, particularly when considering the restrictive levels required for this contaminant. For these reasons MTBE adsorption from aqueous solution are also evaluated.

The aqueous phase MTBE concentrations in the $mg \cdot L^{-1}$ range is interesting because it represents the level of concern for natural and drinking water. Figure 8 shows MTBE adsorption isotherms on ZSM-5, obtained for dilute aqueous solutions at 25°C. The isotherm follows a linear trend. Similar trends have also been reported in the literature [145–147]. In this case the aqueous MTBE concentrations are included the $g \cdot L^{-1}$ range which is below the aqueous solubility (*i.e.* 50 gL^{-1}) and might be encountered in the event of spill. In particular, in Figure 8, it can be seen that the adsorption data on ZSM-5 follow a type I isotherm according to IUPAC classification [148]. A similar behaviour has been already observed for the adsorption of 1,2-DCE on ZSM-5 [14]. The type I isotherms are usually fitted by Langmuir, or heterogeneous extended Langmuir models [149] (Equation 8):

$$q_{e=} = \frac{q_s K c_e}{1 + K c_e}$$

Equation 8 - Heterogeneous extended Langmuir models

where q_s and b are the monolayer saturation capacities and the equilibrium constant respectively. In this model, the interaction between molecules in neighboring cages are considered negligible [150]. The data were also fitted using a bi-Langmuir isotherm type, which take into account of the presence of two adsorption sites characterized by different interaction energies (Equation 9):

$$q_{e=} \frac{q_{s,1} b_1 c_e}{1 + b_1 c_e} + \frac{q_{s,2} b_2 c_e}{1 + b_2 c_e}$$

Equation 9 - Adsorption sites characterized by different interaction energies

where b and qs have the same meaning as in the previous equation and the subscripts refer to sites 1 and 2, respectively. Figure 8 shows the agreement between experimental adsorption data of MTBE onto ZSM-5 and the Langmuir and bi-Langmuir adsorption

isotherm models. Non-linear fitting was employed to obtain the model parameters. The isotherm models are not significantly different in the low concentration range, they differ slightly solely in the high concentration range. Figure 8 lists the best adsorption isotherm parameters.

Figure 8. MTBE adsorption isotherms on ZSM-5 [125].

ZSM-5 MTBE

		R^2	SSE
Langmuir			
q_s	94	0.9946	155.8
b	0.498	0.9959	118.1
bi-Langmuir			
$q_{s.1}$	62		
b1	0.683		
$q_{s.2}$	32		
b2	0.234		

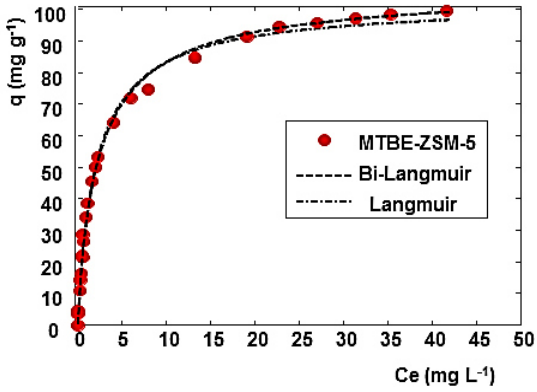

To statistically compare the two models, the ratio of the Fisher parameter was calculated from the sum of the squares of the residuals (Figure 8). As suggested by Gritti [151], one isotherm model would be statistically better than the other one if the ratio of their two Fisher parameters would exceed 3.47, given their degrees of freedom d_1 and d_2 (d_1 = 25-4 = 21, d_2 = 25-2 = 23) and a level of risk α of 0.05. Since the Fisher parameter was 3.35, the bi-Langmuir and the Langmuir adsorption models seem to be statistically equivalent. In such a case, the adsorption data provide insufficient insight to the adsorption mechanisms and the choice between the two adsorption models should be based on the knowledge of the adsorption process. Consequently, to gain information on the ZSM-5 adsorption sites a structural investigation was performed in order to localize the MTBE molecules in the ZSM-5 framework. Diffraction pattern shows that ZSM-5 maintains its crystallinity after MTBE adsorption and Rietveld refinement reveals that there are no evidences of changing in symmetry. In particular, the symmetry of loaded samples remains monoclinic $P2_1/n$ as in the starting material. The refined lattice parameters slight vary, and the unit cell volume remains substantially unchanged. Table 9 reports the refined lattice parameters of ZSM-5 loaded with the organic [56] and the unloaded sample for comparison [14]. Refinement details are also reported.

Table 9. Lattice parameters and refinement details for unloaded ZSM-5 and after MTBE adsorption [14,56].

	ZSM-5	**ZSM-5-MTBE**
Space group	$P2_1/n$	$P2_1/n$
***a* (Å)**	19.8999(5)	19.898(1)
***b* (Å)**	20.1174(6)	20.119(1)
***c* (Å)**	13.3892(4)	13.384(1)
***β* (°)**	90.546(3)	90.57(1)
***V* (Å^3)**	5359.9(3)	5358.1(1)
Wavelength (Å)	1.5417(1)	0.400031(1)
Refined 2θ (°) range	3-110	1-24
R_{wp} (%)	9.12	16.7
R_p (%)	8.4	13.12
R_{F^2} (%)	9.1	11.1
Contributing reflections	14142	11774
N_{obs}	5601	6357
N_{var}	289	364

$R_p = \Sigma[Y_{io}-Y_{ic}]/\Sigma Y_{io}$; $R_{wp} = [\Sigma wi(Y_{io}-Y_{ic})^2/\Sigma wiY_{io}^2]^{0.5}$; $R_{F2} = \Sigma|F_o^2-F_c^2|/|F_o^2|$

After MTBE adsorption, the structure refinement of ZSM-5 was carried out by using the same unloaded ZSM-5 sample as well as the same experimental conditions reported elsewhere. Our refinement allowed us to recognize two crystallographic independent extraframework sites. The first one, MTBE1 is located approximately at the intersection close to the SC channel (Figure 9 a and b); the second one, MTBE2 (Figure 9 a and b) is positioned in the ZZ channel. On the whole, 8 MTBE molecules (corresponding to roughly 11% w/w on dry zeolite base) were detected. In this system, additionally extraframework sites were detected and attributed to water molecules (about 1.5% w/w). According to ref. [9,15,126,152], the distances refined with the Rietveld method suggested the occurrence of MTBE-water oligomers (clusters or short chains) strongly interacting with the framework oxygens.

Figure 9. Observed, calculated, and difference synchrotron powder diffraction pattern, and MTBE sites fractional coordinates into ZSM-5 [56].

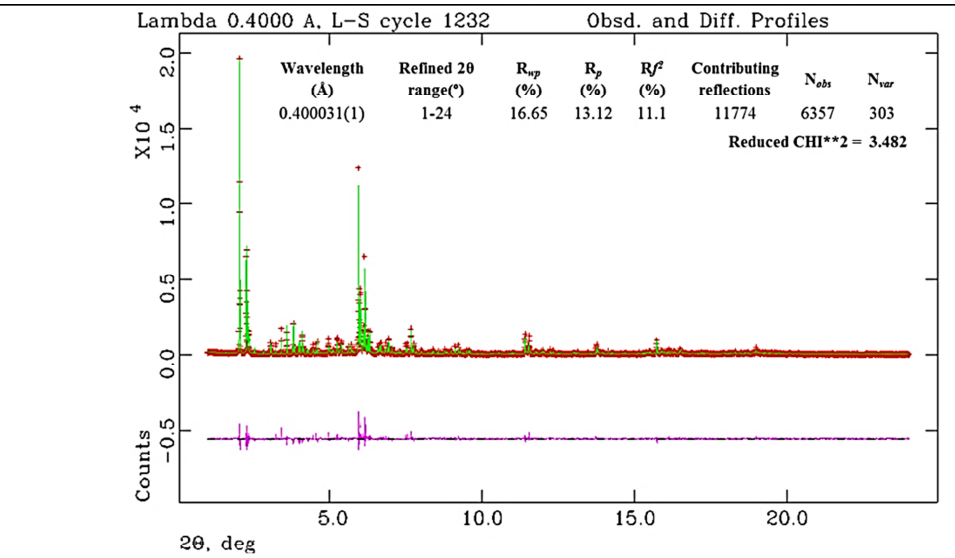

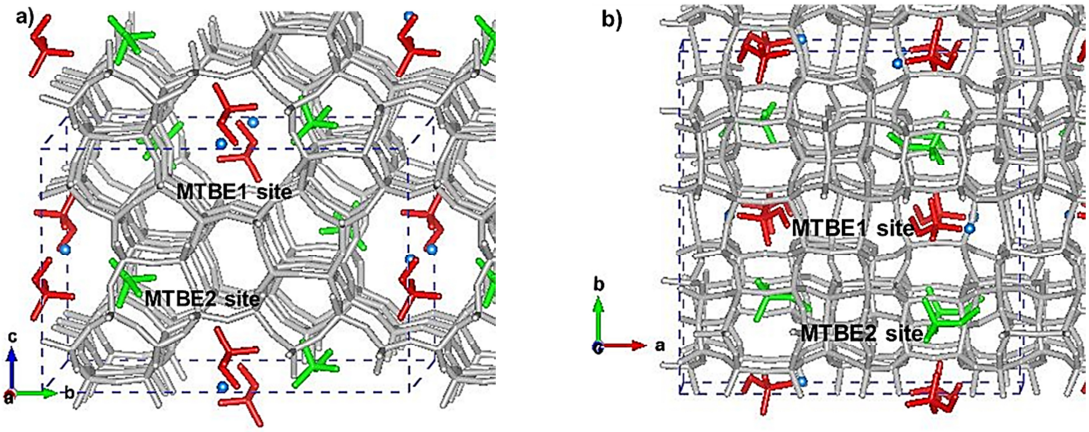

	x/a	y/b	z/c	Uiso	Fraction
			MTBE1 site		
C1M	0.7413 (1)	0.5649(1)	0.1387 (1)	0.195(23)	1.00(1)
C2M	0.7567(1)	0.4946 (1)	0.1307 (1)	0.195(23)	1.00(1)
C3M	0.1765 (1)	0.5163 (1)	-0.0915 (1)	0.195(23)	1.00(1)
C4-O	0.7051 (1)	0.4680(1)	0.0647 (1)	0.195(23)	1.00(1)
C5M	0.7473 (1)	0.4604 (1)	0.2250(1)	0.195(23)	1.00(1)
C6M	0.6839 (1)	0.5074 (1)	-0.0157(5)	0.195(23)	1.00(1)
			MTBE2 site		
C1aM	0.7425(1)	0.7197 (1)	0.0723(1)	0.123(4)	0.92(1)
C2aM	0.7471(1)	0.6937 (1)	0.1733 (1)	0.123(4)	0.92(1)
C3aM	0.7692(1)	0.6740 (1)	0.0002 (1)	0.123(4)	0.92(1)
C4aM	0.7734(1)	0.7850(1)	0.06569(1)	0.123(4)	0.92(1)
C5aO	0.6695(1)	0.7210(1)	0.0520(1)	0.123(4)	0.92(1)
C6aM	0.6211(1)	0.7564 (1)	0.1131 (1)	0.123(4)	0.92(1)

The amount of MTBE indicated by the refined occupancy are in agreement with the total weight loss obtained through thermal analysis (Figure 10).

Figure 10. TG, DTG and DTA curves in ZSM-5-MTBE in dry air atmosphere.

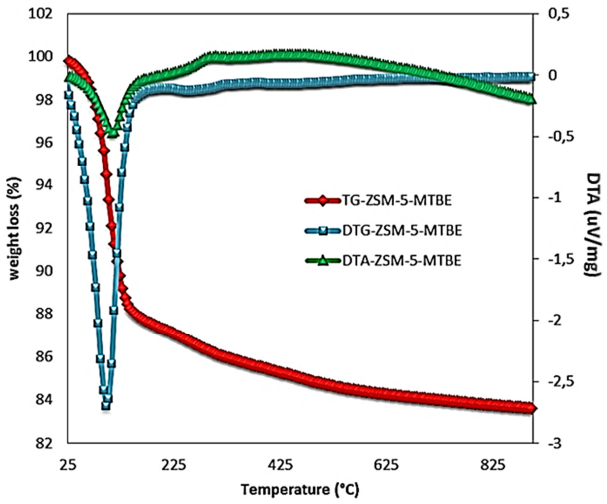

Moreover, the refined O-O distances that describe the 10MR channel indicate that, after MTBE adsorption, C.F.A. increase and the channel's apertures became more elliptical (Table 10).

Table 10. C.F.A. and ellipticity (ε) of unloaded ZSM-5 [14] and ZSM-5-MTBE systems [56].

SC-A	
ZSM-5	
ε	C.F.A.
1.03	22.68

SC-B	
ZSM-5	
ε	C.F.A.
1.02	22.68

ZZ-A	
ZSM-5	
ε	C.F.A.
1.04	21.65

ZZ-B	
ZSM-5	
ε	C.F.A.
1.06	22.65

SC-A	
ZSM-5-MTBE	
ε	C.F.A.
1.09	24

SC-B	
ZSM-5-MTBE	
ε	C.F.A.
1.06	23.67

ZZ-A	
ZSM-5-MTBE	
ε	C.F.A.
1.07	24.3

ZZ-B	
ZSM-5-MTBE	
ε	C.F.A.
1.1	22.91

3.4 Evidence of CB adsorption from aqueous solution in ZSM-5

The adsorption of another Cl-VOCs into ZSM-5 is also evaluated. In particular, CB molecules inside the zeolite pores was revealed by unit cell parameters variations and structural deformations obtained from X-ray structure analyses carried out using the Rietveld method. The results obtained by structural and thermal analysis are in good agreement with adsorption isotherms.

The adsorption isotherm was determined for the ZSM-5-CB at room temperature (20°C) using the batch method. As showed in Figure 11, CB is effectively absorbed by ZSM-5 in particular in the low concentration range.

Figure 11. Adsorption isotherm and adsorption kinetics of CB on ZSM-5.

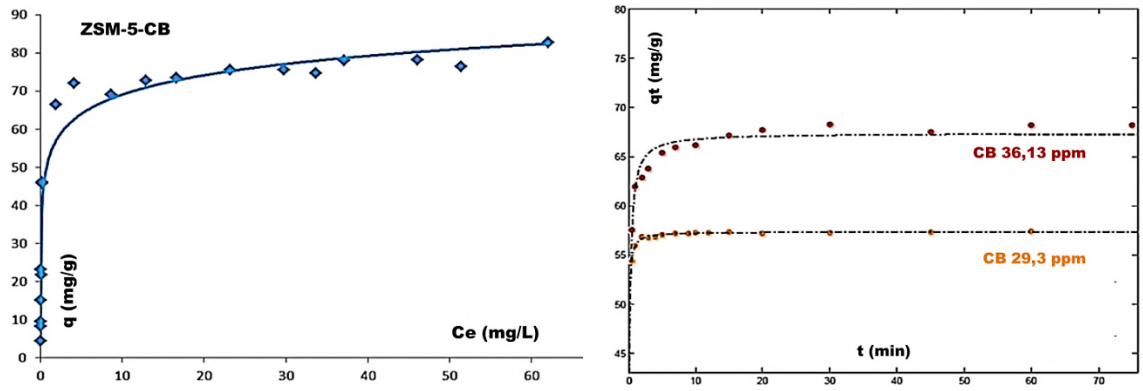

CB uptake fit on ZSM-5 for different initial CB concentrations (Figure 11) in an aqueous solution revealed that the adsorption processes is rapid and equilibrium is reached in about 30 min. The adsorbed amount of CB obtained with adsorption isotherm (Figure 11) resulted in very good agreement with the total weight loss (%) determined through thermal analysis (Figure 12).

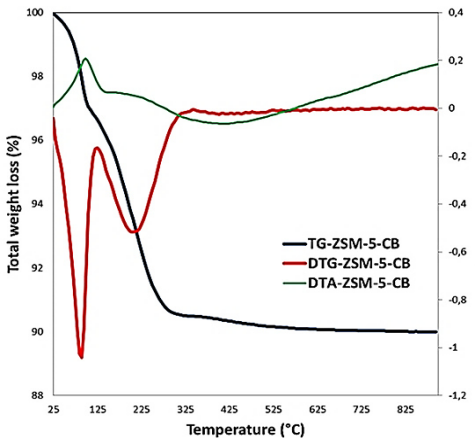

Figure 12. TG, DTG and DTA curves in ZSM-5-CB dry air atmosphere.

After CB adsorption, the evolution of the powder diffraction pattern indicates that ZSM-5 maintains its crystallinity and the monoclinic $P2_1/n$ symmetry after organics adsorption. In the following table the refined lattice parameters of starting material and of ZSM-5 loaded with CB are reported (Table 11).

Table 11. Lattice parameters and refinement details for ZSM-5 [14] before and after CB adsorption.

	ZSM-5	**ZSM-5-CB**
Space group	$P2_1/n$	$P2_1/n$
***a* (Å)**	19.8999(5)	19.8998(8)
***b* (Å)**	20.1174(6)	20.1117(7)
***c* (Å)**	13.3892(4)	13.3873(6)
***β* (°)**	90.546(3)	90.528(3)
***V* (Å^3)**	5359.9(3)	5357.6(4)
Wavelength (Å)	1.54178	1.54178
Refined 2θ (°) range	3-110	1-110
R_{wp} (%)	9.12	12.1
R_p (%)	8.4	9.4
R_F^2 (%)	9.1	6.3
Contributing reflections	14142	6742
N_{obs}	5601	11403
N_{var}	289	301

$R_p = \Sigma[Y_{io}-Y_{ic}]/\Sigma Y_{io}$; $R_{wp} = [\Sigma wi(Y_{io}-Y_{ic})^2/\Sigma wiY_{io}^2]^{0.5}$; $R_{F2} = \Sigma|F_o^2-F_c^2|/|F_o^2|$

The adsorbed organics molecules are detected through the Rietveld refinements starting by a model proposed by Nishi et al. [135]. Difference Fourier map indicate that CB molecules are distributed over two crystallographic independent sites (CB1 sites = C1, C2, C3, C4, C5, C6, Cl7; CB2 sites = C8, C9, C10, C11, C12, C13, Cl14) (Table 12 and Figure 13). CB1 site is located in the intersection between straight and sinusoidal channels and is occupied in the 99% of the cases, while CB2 (occupied in the 56 % of the cases) site is located in the sinusoidal channel.

Table 12. Coordinates of extraframework sites in ZSM-5 after CB adsorption.

	x/a	y/b	z/c	Fraction	Uiso
			CB1 site		
C1	0.7497(39)	0.5963(23)	0.0342(67)	0.99(2)	0.21(1)
C2	0.3025(34)	0.4451(36)	0.0132(50)	0.99(2)	0.21(1)
C3	0.8147(35)	0.5695(16)	0.0451(60)	0.99(2)	0.21(1)
C4	0.8214(29)	0.5011(16)	0.0510(29)	0.99(2)	0.21(1)
C5	0.7079(31)	0.4883(33)	-0.0076(58)	0.99(2)	0.21(1)
C6	0.2281(32)	0.5385(24)	-0.0088(54)	0.99(2)	0.21(1)
Cl7	0.8998(28)	0.4662(21)	0.0832(32)	0.99(2)	0.21(1)
			CB2 site		
C8	0.2142(19)	0.1496(35)	0.7506(44)	0.56(2)	0.38(1)
C9	0.2142(19)	0.0905(35)	0.6993(44)	0.56(2)	0.38(1)
C10	0.2142(19)	0.0904(35)	0.9044(44)	0.56(2)	0.38(1)
C11	0.2142(19)	0.1495(35)	0.8532(44)	0.56(2)	0.38(1)
C12	0.2142(19)	0.0313(35)	0.8531(44)	0.56(2)	0.38(1)
C13	0.2142(19)	0.0313(35)	0.7505(44)	0.56(2)	0.38(1)
Cl14	0.1806(19)	-0.0396(35)	0.6890(44)	0.56(2)	0.38(1)
			Water site		
w1	0.7208(35)	0.6866(41)	0.168(5)	1.0(8)	0.38(1)
w2	0.4002(50)	0.4818(34)	-0.029(6)	1.0 (9)	0.38(1)

Figure 13. Location of CB molecules in ZSM-5 channels system.

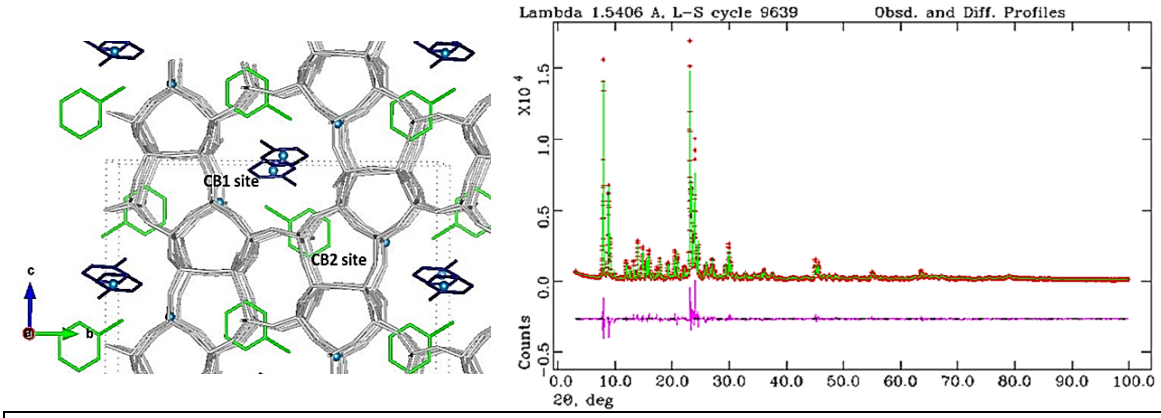

Interaction framework - host molecules – water

O31 – C7 = 2.63(1) W1 – C1 = 2.69

O41 – M5 = 2.84(1) W2 – M7 = 2.62

These results are in very good agreement with the total amount detected trough chromatographic analysis. Rietveld refinements also indicate the presence of co-adsorbed water molecules (~1.5%). In particular, based on the refined distances strong interactions between CB molecules hosted in both CB1 site and CB2 site, water molecules (W1 and W2) and framework oxygen atoms occur (Figure 13).

After organics adsorption, changes in both shape and channels dimensions are also detected. Specifically, the increase of both C.F.A. and ellipticity (ε) is observed (Table 13).

Table 13. C.F.A. and ellipticity (ε) of unloaded ZSM-5 [14] and ZSM-5-CB system.

SC-A	
ZSM-5-CB	
ε	C.F.A.
1.10	22.82

SC-B	
ZSM-5-CB	
ε	C.F.A.
1.03	23.49

ZZ-A	
ZSM-5-CB	
ε	C.F.A.
1.08	22.20

ZZ-B	
ZSM-5-CB	
ε	C.F.A.
1.04	24.38

SC-A	
ZSM-5[14]	
ε	C.F.A.
1.03	22.68

SC-B	
ZSM-5[14]	
ε	C.F.A.
1.02	22.68

ZZ-A	
ZSM-5[14]	
ε	C.F.A.
1.04	21.65

ZZ-B	
ZSM-5[14]	
ε	C.F.A.
1.06	22.65

3. SECTION II:

Competitive behaviour of VOCs and humic acid monomers from binary aqueous mixtures in ZSM-5 at ambient conditions

3.5. Competitive adsorption of VOCs from binary aqueous mixtures on zeolite ZSM-5

The adducts of zeolite and binary mixture of the selected VOCs are investigated by a structural approach in order to get a better understanding of the geometrical arrangement of adsorbed molecules as well as of their chemical environment in the zeolite pores to understand the functionality of the host–guest interactions between VOCs and zeolite. The insights gained from structural refining has been employed as input of the competitive adsorption modelling. The present combined approach of integrating structural information to thermodynamic equilibrium data is an excellent model system for realistically describing the adsorption process and helping in the interpretation of the adsorption mechanisms [56]. Adsorption equilibria of MTBE/TOL, and 1,2-DCE/MTBE binary mixtures in aqueous solution on ZSM-5 were measured over a wide range of concentrations.

In comparison with the single-component data, the loading of all of the three compounds was reduced in the presence of a second component in the mixture. The binary system was described by a competitive dual site Langmuir adsorption isotherm. The model was chosen on the basis of the results obtained from X-ray diffraction studies of the adsorbent material loaded with equimolar binary mixtures.

As a matter of fact, based on TOL, 1,2-DCE and MTBE fractional coordinates a competitive behaviour can be expected if these molecules are together present in the system. The short intermolecular distances [56] between the adsorption sites of MTBE, 1,2-DCE and TOL inside the zeolite framework clearly prevent the simultaneous occupancy of one site by more than one component, when these compounds are adsorbed from binary mixtures.

3.5.1 ZSM-5 loaded with TOL/MTBE and 1,2-DCE/MTBE binary mixtures

X-ray diffraction experiments were carried out at the high-resolution powder diffraction beamline ID22 of the ESRF (Grenoble, France) adopting the experimental conditions explained in the Experimental section in this work. X-ray diffraction studies were used to elucidate the detailed mechanism of 1,2-DCE/MTBE-water and TOL/MTBE-water adsorption on the zeolite. As for the ZSM-5 samples loaded with single contaminant, in 1,2-DCE/MTBE and TOL/MTBE loaded-ZSM-5 an automatic indexing of peaks revealed the presence of peak doublets (*i.e.*, 131 + 13-1, 311 + 31-1, 133 + 13-3, and 313 + 31-3) in the patterns indicating the monoclinic $P2_1/n$ symmetry. The crystal structure changes accompanying the mixture adsorption was investigated by Rietveld refinements using the EXPGUI interface, for General Structure Analysis System (GSAS) [138]. Initial fractional atomic coordinates for the framework atoms (space group $P2_1/n$) were based upon the model determined by Pasti et al. [14] for as synthesized ZSM-5. The peak profiles were modelled by a convolution of a double-exponential and a switch function with a pseudo-Voigt function; given the large number of structural parameters, the refinement was started by imposing severe constraints on the T-O bond distances. The weights constraints were progressively released in the last cycles. Furthermore, the displacement parameters for a given atom type (*i.e.*, Si and O sites) were constrained to be equal, thus limiting the number of refined atomic displacement parameters. The instrumental background was modelled by a Chebyshev polynomial with 16 coefficients.

Table 14. List details of the data collection and unit cell parameters of ZSM-5 unload [14] and loaded with single 1,2-DCE [8], TOL [9], MTBE molecules and binary mixtures of them [56].

	ZSM-5					
	Unloaded	**1,2-DCE**	**TOL**	**MTBE**	**MTBE 1,2-DCE**	**MTBE TOL**
Space group	$P2_1/n$	$P2_1/n$	$P2_1/n$	$P2_1/n$	$P2_1/n$	$P2_1/n$
***a* (Å)**	19.900(1)	19.905(1)	19.907(1)	19.898(1)	19.900(1)	19.895(1)
***b* (Å)**	20.117(1)	20.120(2)	20.118(1)	20.119(1)	20.116(1)	20.114(1)
***c* (Å)**	13.389(1)	13.391(1)	13.393(1)	13.384(1)	13.387(1)	13.383(1)
***β* (°)**	90.55(1)	90.58(1)	90.545(1)	90.57(1)	90.6(1)	90.59(1)
***V* (Å^3)**	5359.9(3)	5362.7(1)	5363.04(1)	5358.1(1)	5358.6(1)	5355.2(1)
Wavelength (Å)	1.54178	0.400031(1)	0.400031(1)	0.400031(1)	0.400031(1)	0.400031(1)
Refined 2θ(°) range	3-110	0.7-25	1-24.56	1-24	1-24	1-24
R_{wp} (%)	9.12	9.2	19.8	16.7	9.24	9.10
R_p (%)	8.4	8.5	14.54	13.12	7.61	8.25
R_f^2 (%)	9.1	7.50	8.7	11.1	8.8	9
Contributing reflections	14142	12252	12055	11774	11760	11783
N_{obs}	5601	7239	7065	6357	6357	6477
N_{var}	289	282	276	364	356	359

$R_p = \Sigma[Y_{io}-Y_{ic}]/\Sigma Y_{io}$; $R_{wp} = [\Sigma wi(Y_{io}-Y_{ic})^2/\Sigma wiY_{io}^2]^{0.5}$; $R_{F2} = \Sigma|F_o^2-F_c^2|/|F_o^2|$

After 1,2-DCE/MTBE and TOL/MTBE mixture adsorption, the ZSM-5 diffraction peak positions were found to be similar (Figure 14). Consequently, this finding could suggest that after adsorption unit-cell parameters were not remarkably modified (Table 14). In the low 2θ region (Figure 14) peak intensities (that are strongly dependent on the arrangement and occupancy of species in zeolite cavities) of the two patterns are different suggesting the entering of guest molecules in ZSM-5 channels.

Figure 14. ZSM-5 diffraction peak positions after binary mixtures (1,2-DCE/MTBE, TOL/MTBE) adsorption [56].

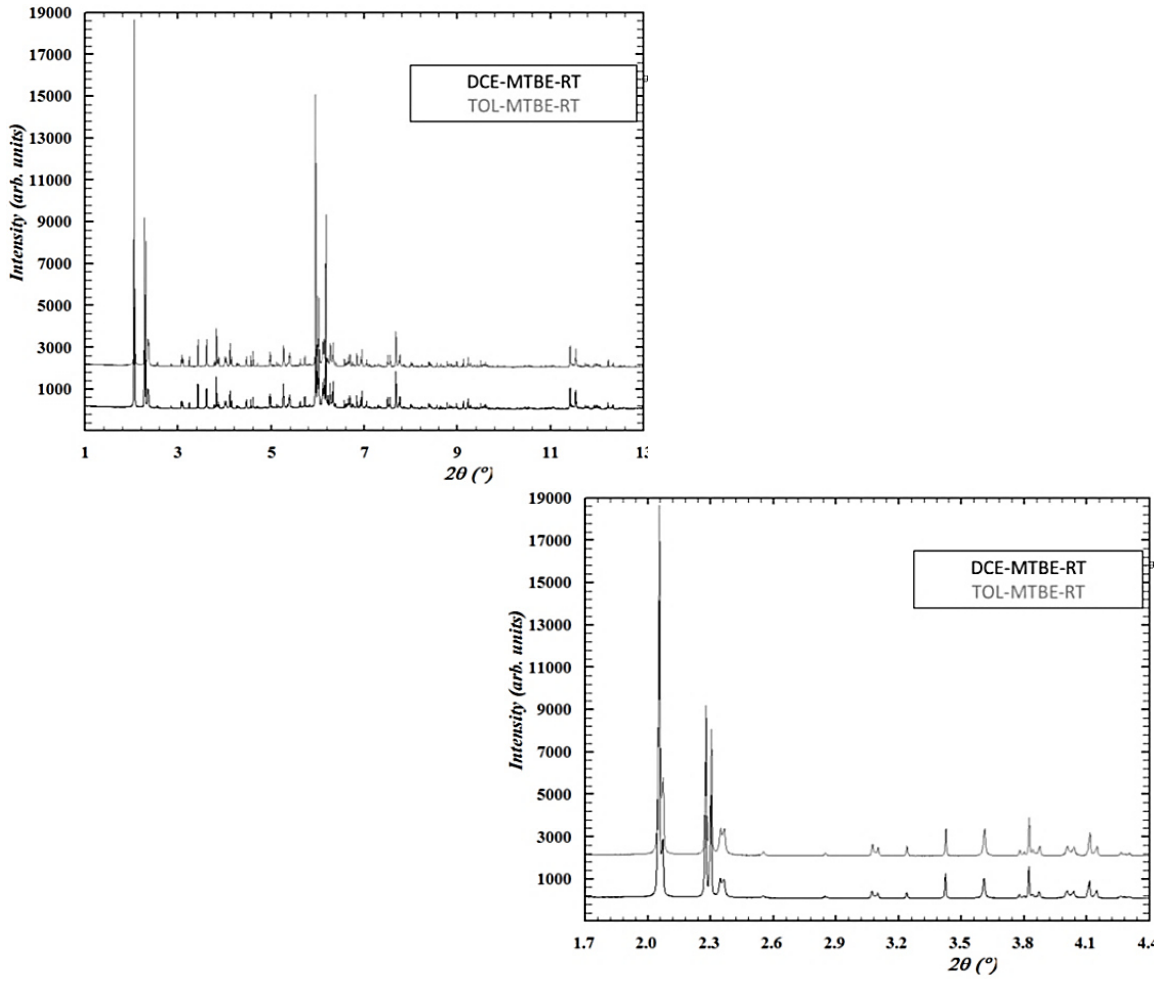

Iterating the Rietveld cycles (for both ZSM-5 1,2-DCE/MTBE and TOL/MTBE mixtures) and using the silica framework model without any inclusion of adsorbed guest molecules, the following residual values for fitting profiles with respect their correspondent diffraction patterns were obtained: R_{wp} = 23.96 and R_p = 18.35 for and R_{wp} = 23.45 and R_p = 19.57 for ZSM-5-MTBE/1,2-DCE and ZSM-5-TOL/MTBE, respectively. Therefore, difference Fourier maps calculated at this stage revealed the presence of residual electron density

residuals corresponding to the adsorbed organics, which had not yet been modelled. Considering the geometry of the 1,2-DCE, TOL and MTBE molecules, the maps suggested the presence of molecular species with different orientations in the channel systems. Incorporating these guest species into Rietveld refinements, the residual values in the Rietveld fit have been drastically decreased to R_{wp} = 9.24 and R_p = 7.61 and R_{wp} = 9.10 and R_p = 8.25 for ZSM-5-1,2-DCE/MTBE and ZSM-5-TOL/MTBE, respectively. The refined unit cell parameters for the ZSM-5-TOL/MTBE system are: a = 19.895(1); b = 20.114(1); c = 13.383(1) Å; β = 90.59(1)° and V = 5355.2(1) $Å^3$. In ZSM-5-1,2-DCE/MTBE mixture the unit cell parameters are the following: a = 19.900(1); b = 20.116(1); c = 13.387(1) Å; β = 90.6(1)° and V was 5358.6(1) $Å^3$ (Table 14). After TOL/MTBE and 1,2-DCE/MTBE mixture adsorption, Rietveld structure refinements provided information about the relative position of molecules inside the structure (Table 15). In ZSM-5-TOL/MTBE, TOL molecules are confined only in the TOL1 site (about 3.8 molecules, corresponding to approx. 5.3% on dry base), near the SC channel. Compared to ZSM-5-TOL system [9] (described in the previous section), the TOL2 site (located in the channels intersections or ZZ channel) is now empty (Figure 15 a and b). MTBE molecules are confined in MTBE2 site (ZZ channel) (roughly 3.4 MTBE molecules per unit cell, corresponding to approx. 4.5% on dry base). As far as it concerns the relative position of MTBE and 1,2-DCE molecules (ZSM-5-1,2-DCE/MTBE system), two independent extraframework sites are localised. MTBE (3.3 molecules p.u.c. corresponding to 4.5% in zeolite dw) is confined near the SC channel (MTBE1 site in Figure 15 a and b), whereas 1,2-DCE (2.7 molecules p.u.c. corresponding to 4.2% on dry base) is in the ZZ channel (1,2-DCE2 site). Difference Fourier maps calculated for both ZSM-5-1,2-DCE/MTBE and ZSM-5-TOL/MTBE revealed the occurrence of a low amount of co-adsorbed water in both the systems (about 4.0 molecule p.u.c. corresponding to approx. 1% w/w in zeolite). The refined distances between the framework oxygen, water oxygen atoms and organic molecules suggested the occurrence of water-MTBE and water-MTBE-1,2-DCE complexes interacting with the framework. The presence of organic–water complexes (clusters or short chains) stabilizing the guest structure within the zeolite host framework has also been recently observed in high-silica mordenite [124,126,152,153] as well as in Y zeolite after 1,2-DCE [14] and MTBE adsorption from aqueous solutions [125]. This finding could possibly explain the higher MTBE adsorption capacity (11% w/w found in ref. [154] and reconfirmed in ref. [125]), with respect to that observed from gas phase systems [155].

Table 15. Atomic coordinates of extraframework for both ZSM-5-MTBE/1,2-DCE and ZSM-5-MTBE/TOL [56]

.**ZSM-5-MTBE/1,2-DCE**

	x/a	y/b	z/c	Uiso	Fraction
			MTBE1 site		
C1	0.7392(4)	0.5740(2)	0.0598(1)	0.071(1)	0.81(1)
C2	0.7310(3)	0.5042(2)	0.0837(1)	0.071(1)	0.81(1)
C3	0.2188(3)	0.5365(3)	-0.035(8)	0.071(1)	0.81(1)
C4-O	0.6636(3)	0.4878(3)	0.0496(1)	0.071(1)	0.81(1)
C5	0.7303(6)	0.4931(5)	0.1907(1)	0.071(1)	0.81(1)
C6	0.6406(4)	0.5172(5)	-0.038(7)	0.071(1)	0.81(1)
			1,2-DCE2 site		
DCE-Cl	0.7455(20)	0.6895(7)	0.1577(18)	0.087(1)	0.68(1)
DCE-C1	0.7618(16)	0.7682(9)	0.1168(18)	0.087(1)	0.68(1)
DCE-C2	0.7418(16)	0.8225(7)	0.1657(14)	0.087(1)	0.68(1)
DCE-Cl2	0.7583(16)	0.9012(9)	0.1252(21)	0.087(1)	0.68(1)
			ZSM-5-MTBE/TOL		
	x/a	**y/b**	**z/c**	**Uiso**	**Fraction**
			TOL1 site		
M7	0.7776(1)	0.8978(1)	0.1843(5)	0.160(1)	0.94(1)
M1	0.2175(1)	0.0447(3)	0.6601(3)	0.160(1)	0.94(1)
M2	0.2175(1)	-0.0140(3)	0.6078(3)	0.160(1)	0.94(1)
M3	0.2175(1)	-0.0162(3)	0.8130(3)	0.160(1)	0.94(1)
M4	0.2175(1)	0.0447(3)	0.7631(3)	0.160(1)	0.94(1)
M5	0.2175(1)	-0.0744(3)	0.7632(2)	0.160(1)	0.94(1)
M6	0.2175(1)	-0.0744(3)	0.6578(3)	0.160(1)	0.94(1)
			MTBE2 site		
C1a	0.7434(2)	0.7227(2)	0.7227(3)	0.088(5)	0.84(10)
C2a	0.7227(3)	0.7057(6)	0.1696 (3)	0.088(5)	0.84(10)
C3a	0.7701(2)	0.6727(4)	-0.0002(3)	0.088(5)	0.84(10)
C4a	0.7696(3)	0.7696(2)	0.0437(8)	0.088(5)	0.84(10)
C5O	0.6698(3)	0.7186(1)	0.0512(1)	0.088(5)	0.84(10)
C6a	0.6221(1)	0.6221(2)	0.1129(2)	0.088(5)	0.84(10)

Figure 15. Modelled atoms of ZSM-5-1,2-DCE/MTBE and ZSM-5-TOL/MTBE. Sites in single component systems are also reported [56].

ZSM-5 loaded with binary mixtures

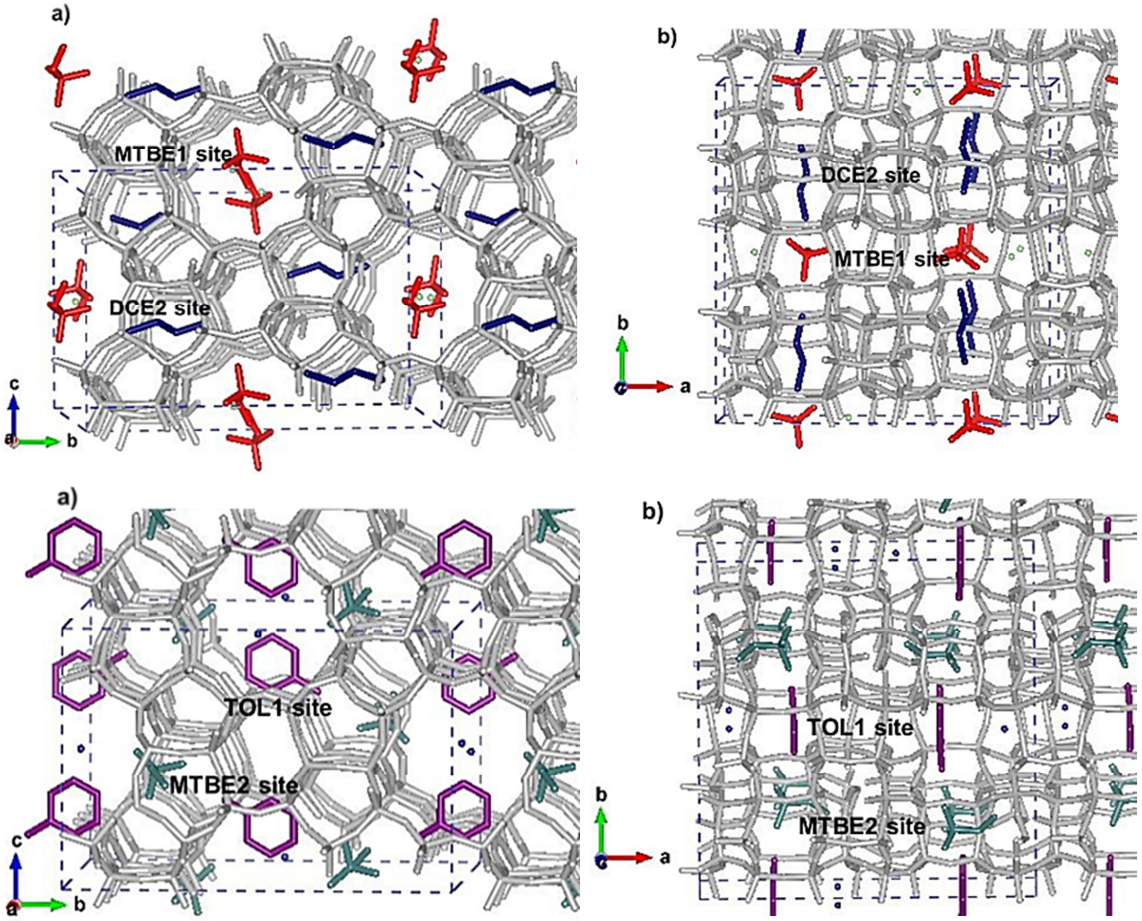

ZSM-5 loaded with single component

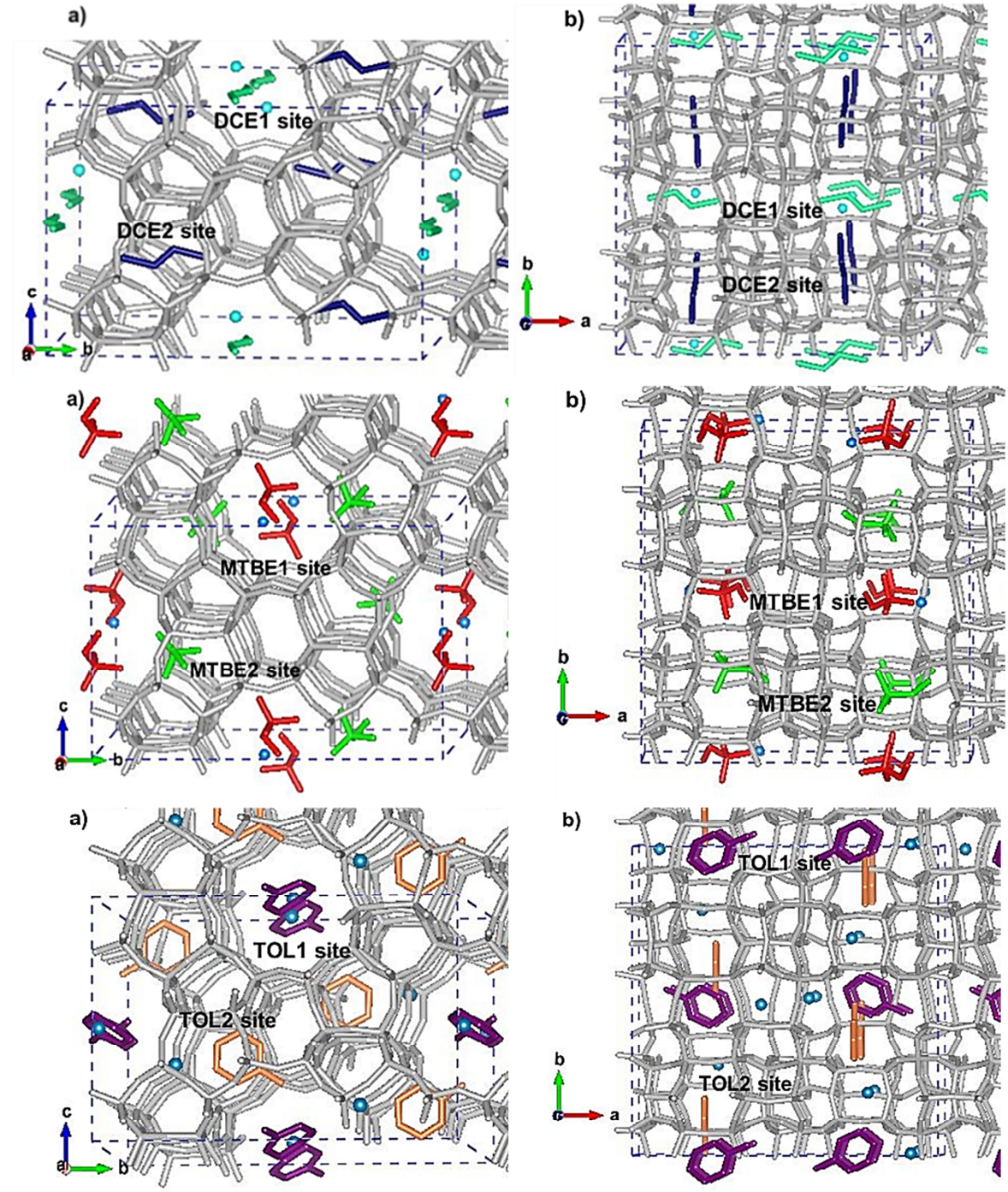

After loading, the changes in the framework geometry can be monitored by following both the 10-ring channels ellipticity (ε) and C.F.A. [56]. Table 16 reports the dimensions of both sinusoidal and straight channels, assuming a spherical shape with radius of 1.35 Å [156] for the framework oxygen atoms. The resulting apertures appear larger than those reported for the unloaded ZSM-5 but smaller than the maximum value diameter 7.6 Å) for an ideal circular 10-ring channel (C.F.A.= 24.5 $Å^2$). The overall effect of these variations accounts for the slight cell volume contraction observed with respect to the as-synthesized material.

Table 16. Dimensions of the apertures (Å) of ZSM-5 unload [14] and after adsorption of single and binary mixture of 1,2-DCE [9,56], TOL [10,56] and MTBE [56] molecules.

ZSM-5 SC-A	**ε**	**C.F.A.**	**ZSM-5 SC-B**	**ε**	**C.F.A.**
ZSM-5	1.03	22.68	ZSM-5	1.02	22.68
1,2-DCE	1.08	24.14	1,2-DCE	1.08	23.51
TOL	1.03	24.4	TOL	1.04	23.61
MTBE	1.09	24.0	MTBE	1.06	23.67
MTBE/1,2-DCE	1.07	24.16	MTBE/1,2-DCE	1.04	23.67
MTBE/TOL	1.09	24.06	MTBE/TOL	1.05	23.59
ZSM-5 ZZ-A	**ε**	**C.F.A.**	**ZSM-5 ZZ-B**	**ε**	**C.F.A.**
ZSM-5	1.04	21.65	ZSM-5	1.06	22.65
1,2-DCE	1.09	24.37	1,2-DCE	1.12	23.12
TOL	1.12	23.63	TOL	1.06	23.68
MTBE	1.07	24.3	MTBE	1.1	22.91
MTBE/1,2-DCE	1.05	24.28	MTBE/1,2-DCE	1.1	23.15
MTBE/TOL	1.06	24.35	MTBE/TOL	1.1	22.95

TG data confirmed this level of organics incorporation. The total weight loss at 900°C is approximatively 13% w/w, in very good agreement with the refined occupancies, as well as the adsorption data. Regarding the ZSM-5/TOL-MTBE system, Figure 16 reported the TG curve that shows a first weight loss below 100°C, which can be ascribed to the elimination of species weakly bonded (~ 3% w/w). Above this temperature, the slope suddenly changes most likely following the release of extraframework species (MTBE,

TOL and water molecules) (weight loss roughly 10.0% w/w on dry base). A similar trend was also observed for the ZSM-5-1,2-DCE/MTBE system.

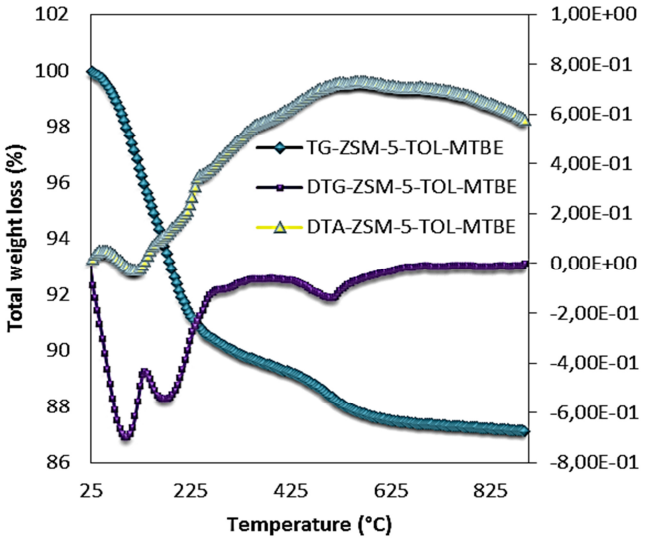

Figure 16. Thermal analysis of ZSM-5 loaded with TOL and MTBE in mixture.

Isotherm profiles from experiments with 1,2-DCE alone and with a 1,2-DCE/MTBE mixtures are shown in Figure 17 a. For competitive experiments, the 1,2-DCE isotherm in presence of MTBE is below than in the single component system (in at least a portion of the adsorption curve) indicating that MTBE and 1,2-DCE compete for the adsorption sites. Isotherms of 1,2-DCE alone and 1,2-DCE in presence of MTBE mainly diverge at the highest concentration range thus suggesting that the extent of competition can change with concentration. A similar trend was also observed for the adsorption of TOL and of TOL/MTBE mixtures (Figure 17 b), thus confirming the competitive nature of VOCs mixtures adsorption on zeolites. Many models have been proposed to describe competitive adsorption from liquid media [157–159] and, as mentioned in ref. [157], the selection of an isotherm model is usually based on literature data or intuition, or made through a trials and errors approach. In such cases, a model that better fits the experimental data would not adequately describe the actual physical behaviour of the adsorption system. The isotherm selected could lead to significant bias when employed in selected concentration ranges. Therefore, the choice of a model which not only accounts well for the experimental data in the considered cases but also has a physical meaning, is preferable.

Figure 17. Experimental uptake data of (a) 1,2-DCE/MTBE and (b) TOL/MTBE aqueous mixtures in ZSM-5 [56].

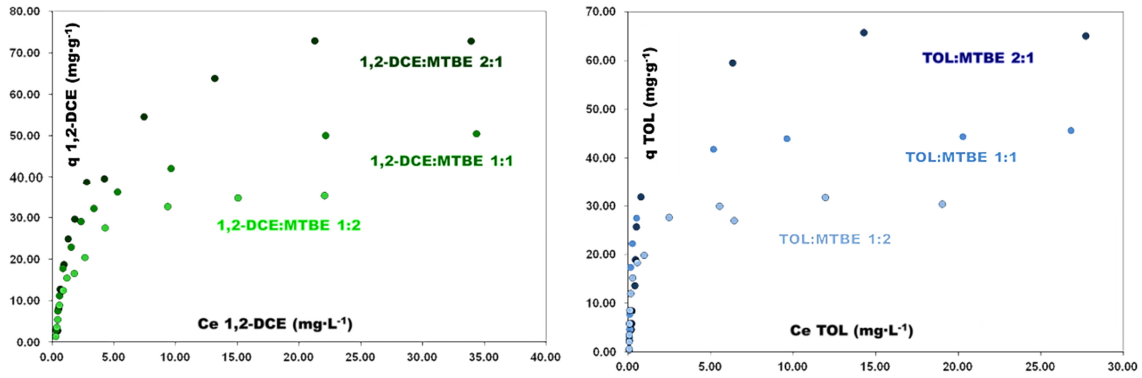

a) b)

The physical description of the adsorption systems derives from the structural refining investigation above reported. All of the three compounds are located into two different sites of the ZSM-5, these two sites cannot be simultaneously occupied by two different compounds and each site is available for a single molecule. On the basis of this information, the competitive CBLM [157] seems to be suitable for describing the adsorption of these mixtures. For each of the two compounds (i = 1, 2), the CBLM is given by Equation 10:

$$q_{e,i} = \frac{q_{s,a,i} K_{a,i} C_{e,i}}{1 + K_{a,1} C_{e,1} + K_{a,2} C_{e,2}} + \frac{q_{s,b,i} K_{b,i} C_{e,i}}{1 + K_{b,1} C_{e,1} + K_{b,2} C_{e,2}}, (i = 1,2)$$

Equation 10 - CBLM

where q_e (mg g^{-1}) is the amount of adsorbate per unit mass of adsorbent at the equilibrium with a solution of concentration C_e (mg L^{-1}), q_s (mg g^{-1}) the saturation capacity and K (L mg^{-1}) the equilibrium constant for the adsorption, the subscripts refer to sites a and b, and to compounds 1 and 2 of the binary mixture, respectively. However, the adsorption of these three compounds on this same zeolite was recently studied [9–11,15] and a Langmuir model was found satisfactory to fit the single-solute systems of all of the three compounds.

Based on the information afforded by single-component isotherms, the CLM isotherm (i = 1, 2) is given by Equation 11:

$$q_{e,i} = \frac{q_{s,i} K_i C_{e,i}}{1 + \sum K_i C_{e,i}}$$

Equation 11 - CLM

The CLM can, in fact, be applied to mixtures of components obeying Langmuir behaviour in single-solute system, and when the saturation capacities of the components are similar to each other. To account for differences in site availability for the components of the mixture, a modified model can be applied. In this latter model a number of sites with non-competitive adsorption was added and these additional sites are proportional to the difference between the maximum loadings of the two species [157]. The confidence limits, calculated at 95% of probability, of the saturation capacities obtained from the single component adsorption isotherms were 88–100 $mg \cdot g^{-1}$, 77–87 $mg \cdot g^{-1}$ and 113–27 $mg \cdot g^{-1}$ for MTBE, TOL and 1,2-DCE, respectively. These values correspond to 6.4–7.3, 5.4–6.1 and 7.3–8.3 molecules per unit cell. The differences in saturation capacities (molecules per unit cell) for both TOL/MTBE and MTBE/1,2-DCE mixtures were in the order of 10%, which can be considered acceptable for the applicability of CLM [160]. Both CLM and CBLM have been used to fit experimental adsorption data of organic species on microporous materials [161]. Another model often employed to describe adsorption from binary mixtures [162] is the IAST. However, it has been shown that IAST does not provide reliable results for the adsorption of alcohols from aqueous solution onto hydrophobic zeolites [162,163] probably due to strong solute–solvent interactions (hydrogen bonds). Deviations in IAST model can also be due to framework deformation upon adsorption [164–166] therefore, IAST seems to be not adequate to fit the data of the present work since the adsorption of the three selected compounds occurs with a slight cell volume modification as above mentioned. The adsorption of both the components of the aqueous binary mixtures on zeolite ZSM-5 at different concentrations have been determined. The effect of MTBE on the competitive adsorption of TOL and 1,2-DCE is also shown in Figure 18 a, that reports the adsorption selectivity (α) calculated as Equation 12:

$$\alpha_{TOL/MTBE} = \frac{x_{z,TOL}/x_{a,TOL}}{x_{z,TMTBE}/x_{a,MTBE}}$$

Equation 12 - Adsorption selectivity

where $\chi_{z,TOL}$ and $\chi_{z,TMTBE}$ are the adsorbed quantity per unit mass of adsorbent material, of TOL and MTBE onto ZSM-5 and $\chi_{a,TOL}$ and $\chi_{a,MTBE}$ are the concentration of TOL and MTBE in aqueous solution, respectively. Analogously, a similar relation can be obtained for the 1,2-DCE/MTBE adsorption system (Figure 18 b). The ZSM-5 selectivity towards TOL with respect to MTBE decreases with increasing MTBE concentration. Operation conditions in the lower concentration are selective to TOL which has a higher adsorption strength as determined in unary adsorption isotherm. On the contrary, the selectivity of ZSM-5 for 1,2-DCE slightly increases with increasing MTBE concentration, thus confirming that the saturation capacities and adsorption constants of these compound are similar (Figure 18).

Figure 18. ZSM-5 selectivity plot (a) TOL/MTBE system at equimolar condition (1:1) (b) 1,2-DCE/MTBE system at equimolar condition (1:1) [56].

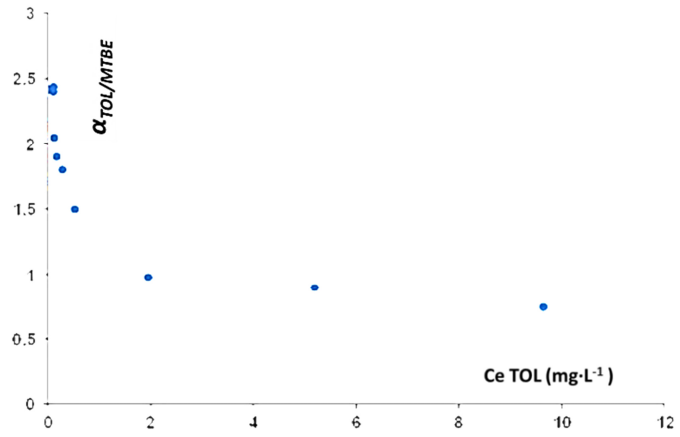

a)

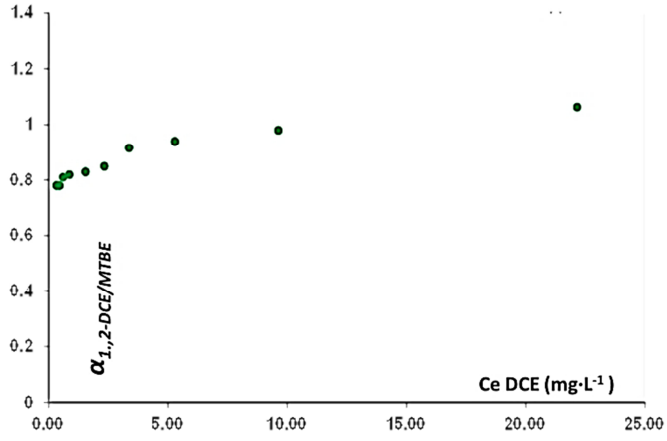

b)

Three dimensional plots of the adsorbed amount of MTBE and 1,2-DCE on the ZSM-5 zeolite from binary mixtures of TOL/MTBE and 1,2-DCE/MTBE, are shown in Figure 19. The contour surfaces are the competitive dual site Langmuir isotherms generated by non-linear fitting procedure. The results of estimated parameters for the CBLM and CLM are reported in Table 17. It can be seen that for binary mixtures, the determination coefficients of CBLM gave a better fit than CLM. *F* test was applied to the standard deviation of the residuals to examine if the difference of the two models was statistically significant, taking into account the different number of parameters in the fitting equations.

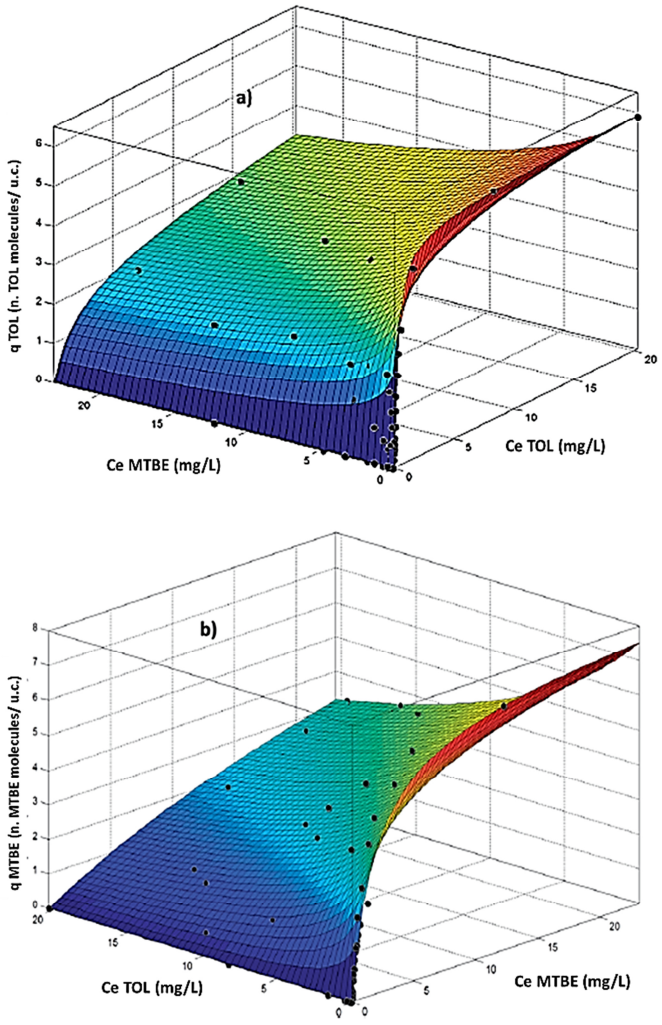

Figure 19. Surface fitting (a) number of TOL adsorbed molecules per ZSM-5 unit cell vs. the equilibrium concentrations of TOL and MTBE in aqueous solution, (b) number of MTBE adsorbed molecules per ZSM-5 unit cell vs. the equilibrium concentrations of TOL and MTBE in aqueous solution. The points represent the experimental data [56].

Table 17. Isotherm parameters for the adsorption of TOL/MTBE and 1,2-DCE/MTBE on ZSM-5 (25°C) [56].

				R^2	SSE
TOL/MTBE	TOL	Langmuir			
		q_s	83.7	0.9476	1559.8
		b	2.418		
		bi-Langmuir			
		$q_{s,A}$	48.2		
		b_1	0.683	0.9879	680.6
		$q_{s,B}$	37.1		
		b_2	0.234		
	MTBE	Langmuir			
		q_s	97.7		
		b	0.408	0.9374	1710.5
		bi-Langmuir			
		$q_{s,1}$	62		
		b_1	0.731	0.9821	728.3
		$q_{s,2}$	38		
		b_2	0.314		
1,2-DCE/MTBE	1,2-DCE	Langmuir			
		q_s	108	0.9146	2052.8
		b	0.219		
		bi-Langmuir			
		$q_{s,1}$	64		
		b_1	0.283	0.9759	908.7
		$q_{s,2}$	48		
		b_2	0.144		
	MTBE	Langmuir			
		q_s	96.8		
		b	0.427	0.8926	2870
		bi-Langmuir			
		$q_{s,1}$	62		
		b_1	0.661	0.9721	912.3
		$q_{s,2}$	34		
		b_2	0.247		

3.5.2. ZSM-5 loaded with TOL/CB binary mixture

Adsorption of TOL and CB mixture was also studied. Since these contaminants show very similar single-component adsorption isotherms, the competition between these two molecules seems particularly interesting.

Adsorption isotherms were collected on ZSM-5 after TOL and CB mixture adsorption (Figure 20). Data fitted by a competitive Langmuir isotherm clearly show strong similarities in both TOL and CB saturation capacity as well as affinity for ZSM-5.

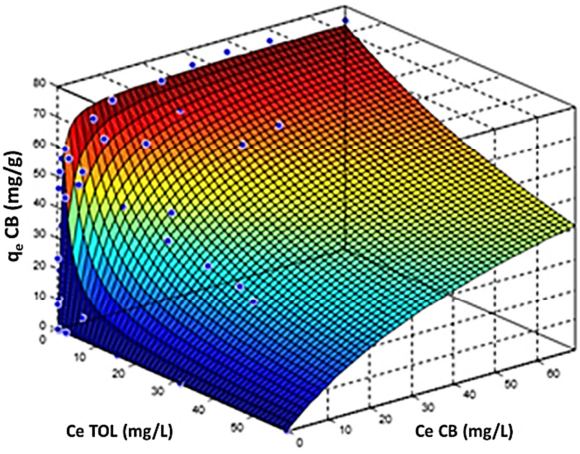

Figure 20. Amount of CB absorbed per unit weight of zeolite ZSM-5 vs. equilibrium concentrations of TOL and CB in aqueous solution.

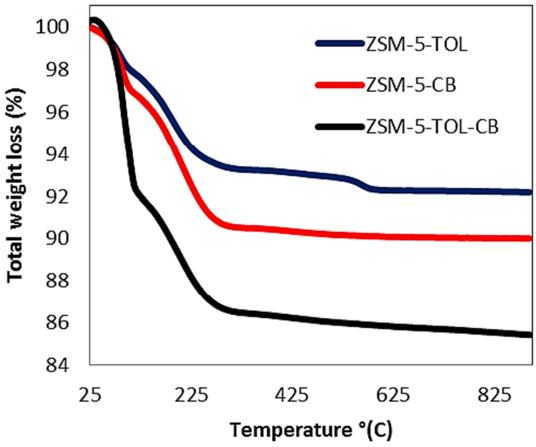

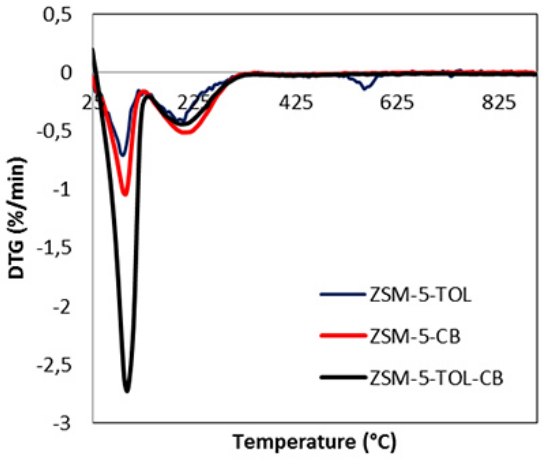

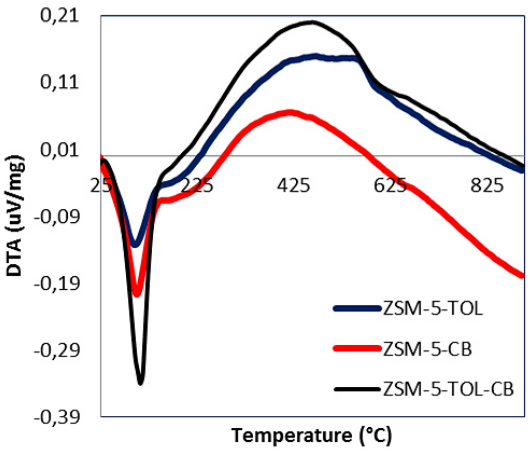

Figure 21. TG, DTG and DTA curves after adsorptions of TOL, CB and mixture of them in ZSM-5.

According to adsorption analysis, thermal measurements indicate that both TOL and CB are adsorbed in ZSM-5 in a comparable amount (Figure 21). The total weight loss obtained for ZSM-5 loaded with the mixture is about 13% in very good agreement with the results obtained through the adsorption analysis. As reported by DTA curves, the desorption of contaminants is an exothermic process (Figure 21).

After TOL/CB mixture adsorption, ZSM-5 maintains its crystallinity. In particular, in the diffraction pattern the variation of peaks intensity and position along the investigated 2θ range suggests changes in both lattice parameters and hosted extraframework species (Figure 22).

Figure 22. XRPD powder pattern diffraction of ZSM-5 loaded with TOL, CB and mixture of both organics. Unloaded ZSM-5 pattern (light blue line) are also reported for comparison.

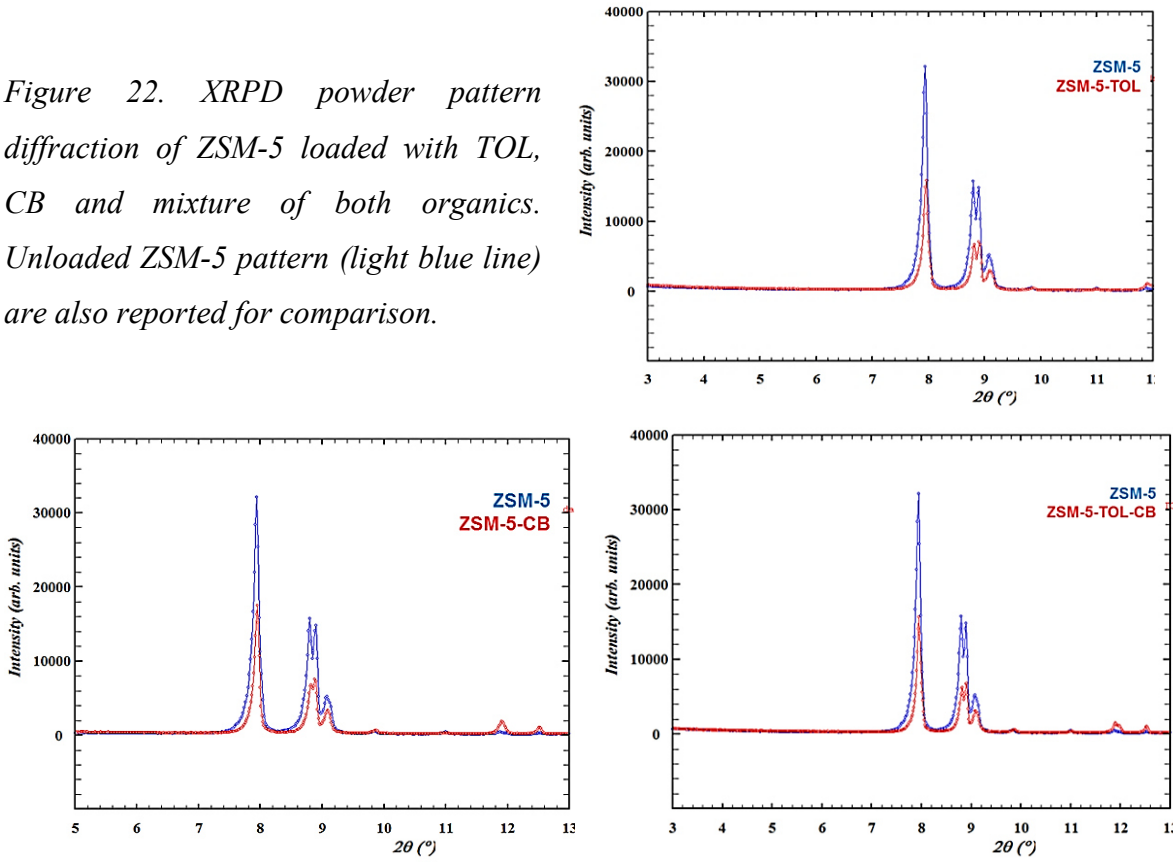

The adsorbed organics molecules are detected through the Rietveld refinements. In particular, difference Fourier map, generated using the GSAS package, indicated that TOL and CB molecules are distributed over two crystallographic independent sites (CB1 sites = C1, C2, C3, C4, C5, C6, Cl; TOL2 sites = C7, C8, C9, C10, C11, C12 C13) (Figure 23) CB1 site is located in the intersection between straight and sinusoidal channels, while TOL2 molecules are located in the sinusoidal channel. Rietveld refinements also indicate the presence of co-adsorbed water molecules (~1.5% w/w). In particular, on the basis of the refined distances a strong interaction of water-TOL and water-CB oligomers with the

framework oxygen atoms occurs (Figure 23). According to the adsorption isotherms, the refined occupancies confirm the strong and similar affinity of ZSM-5 for both TOL and CB. In general, the selectivity ratio CB/TOL for ZSM-5 zeolite is close to 1 and the refined occupancies indicate a slight preference for CB.

Figure 23. Extraframework coordinates of ZSM-5-CB/TOL. Lattice paramiters and refinement details are also reported.

	ZSM-5		
CB1 site	**x/a**	**y/b**	**z/c**
C1	0.751(5)	0.596 (2)	0.039(1)
C2	0.300(4)	0.444(3)	0.016(1)
C3	0.818(5)	0.570(1)	0.043(1)
C4	0.822(4)	0.501(1)	0.058(1)
C5	0.709(4)	0.489(3)	-0.004(1)
C6	0.227(4)	0.538(2)	-0.009(1)
Cl	0.901(3)	0.466(1)	0.085(5)
TOL2 site			
C7	0.213(2)	0.147(4)	0.747(5)
C8	0.213(2)	0.088(4)	0.696(5)
C9	0.213(2)	0.088(4)	0.901(5)
C10	0.213(2)	0.147(4)	0.850(5)
C11	0.213(2)	0.029(4)	0.850(5)
C12	0.213(2)	0.029(4)	0.748(5)
C13	0.213(2)	-0.029(4)	0.698(5)
Water sites			
W1	0.720(5)	0.686(5)	0.168(6)
W2	0.402(6)	0.482(5)	-0.026(10)

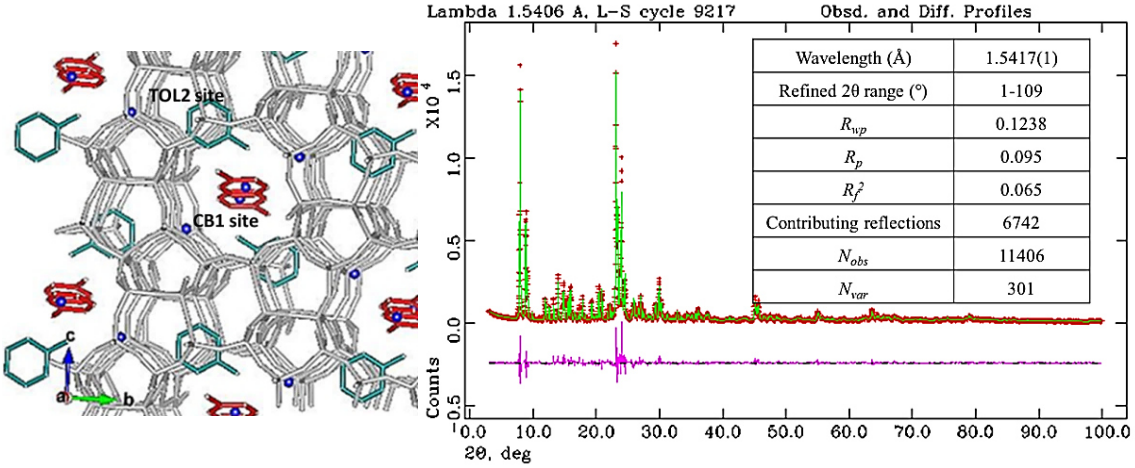

ZSM-5-TOL/CB monoclinic $P2_1/n$

a (Å)	**b (Å)**	**c (Å)**
19.902(1)	20.114(1)	13.388(1)
β (°) = 90.529(5)	**CB occupancy**	**TOL occupancy**
V (Å^3) = 5358.6(6)	98%	80%

Interaction framework - host molecules – water		
C7-O31 = 2.6	C1-W1 = 2.69	C2-W2 = 2.35
M1-O18 = 2.39		M2-O18 = 2.84

After organics adsorption, changes of the shape and dimensions of the channels also occurred. Specifically, an increase of both C.F.A. and ellipticity (ε) are observed (Table 18).

Table 18. Changes in C.F.A. and ellipticity (ε) in ZSM-5 before and after organics adsorption.

			ZSM-5		
SC-A	ε	C.F.A.	SC-B	ε	C.F.A.
ZSM-5	1.03	22.68	ZSM-5	1.02	22.68
TOL	1.05	23.68	TOL	1.052	23.64
CB	1.10	22.82	CB	1.03	23.49
CB/TOL	1.07	24.40	CB/TOL	1.04	23.62
ZZ-A	ε	C.F.A.	ZZ-B	ε	C.F.A.
ZSM-5	1.04	21.65	ZSM-5	1.06	22.65
TOL	1.03	24.13	TOL	1.08	23.15
CB	1.08	22.20	CB	1.04	24.38
CB/TOL	1.06	23.84	CB/TOL	1.12	23.63

3.6. Competitive adsorption of VOCs and humic acid monomers

The adsorption of CA and p-HBA on hydrophobic synthetic zeolites was also studied. The carboxylic acid and phenolic functional groups are abundant in natural organic matter and are present in the molecular structures of many natural and synthetic compounds released in water, including plant exudates, lignin derivatives and environmental contaminants. Silico aluminates are components of soil and zeolites have found application in the removal of organic contaminants from water [31]. The prior literature on adsorption of weak acids on siliceous materials is negligible. It is generally found that adsorption decreases with increasing ionization of the molecule as the pH increases above the point of zero charge (pzc) of the surface due to charge repulsion between the anion and the increasingly negatively charged surface, and to the reduced solvophobic effect of the anion relative to the molecule. Our study was undertaken to characterize the adsorption of selected monomers of humic acid by zeolites as part of a broader study on the adsorption of organic pollutants from dilute solution onto zeolites [9–11,15,56,123–125,153]. In order to evaluate the influence of natural organic matter on the removal of contaminants from water we studied sorption of CA and p-HBA to commercial zeolites. Both molecules are low molecular weight compounds secreted into soil by plant tissues and/or decay of plant residues, they are allelochemicals and play an important role in agricultural and ecological dynamics. Adsorption is favored by formation of H-bond between adsorbates and adsorbent and it occurs with the inclusion of water molecules. The adsorption experiments at different pH indicate that dissociation greatly affected the sorption due to electrostatic repulsion of anionic form of the adsorbates and the surface of the adsorbent. The effect of CA and p-HBA on the adsorption of TOL in zeolites was also investigated. Experimental results, reveal that both CA and p-HBA are highly adsorbed on zeolites. The host-guest-interactions were highlighted by Rietveld analysis, in agreement with Density Functional Theory calculations of the adduct stabilization energies. However, competitive adsorption of TOL and CA or p-HBA mixtures shows that aromatic hydrocarbons are preferentially adsorbed. The findings provide new understanding of the interactions between ionizable organic compounds and zeolites which have implications for fate of ionizable pollutants and in the removal of organic pollutants from water in presence of natural organic matter.

The adsorption of both CA and p-HBA on ZSM-5 has been investigated as a function of pH of the aqueous solution and in both the cases the adsorption capacity decreases as pH increases. The adsorption isotherms of CA on ZSM-5 at different pH are reported in Figure 24. Similar results were obtained for the p-HBA-ZSM-5 system.

Figure 24. a) CA Adsorption isotherms at different pH of the solution; b) Normalized saturation capacity of CA vs. pH.

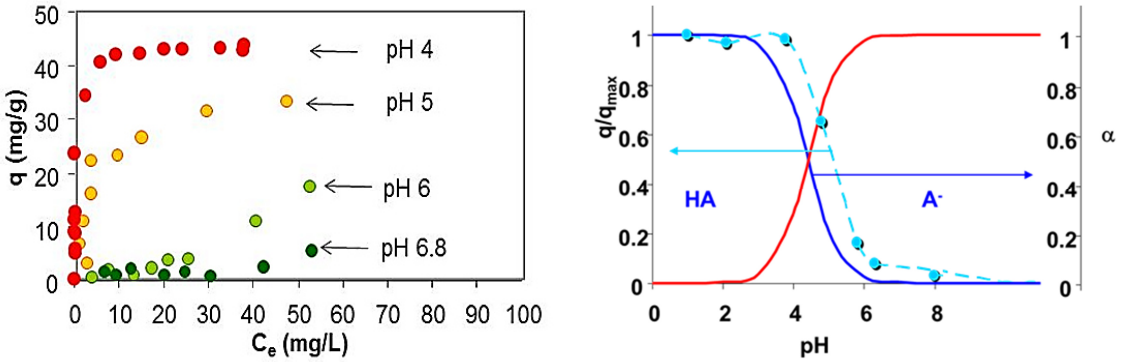

a) b)

The trend displayed in the saturation capacity (Figure 24 a) has conventional explanations. Sorption is greater at pH 4 due to the greater abundance of the neutral form and the lower negative charge of the surface compared to pH 7. According to adsorption isotherms, also thermogravimetric data, reported in Figure 25, confirms the adsorption of CA from acid solution (pH=4) and of p-HBA-ZSM-5 system.

Figure 25. Thermal results of a) ZSM-5-CA, ZSM-5, and b) of ZSM-5-p-HBA systems.

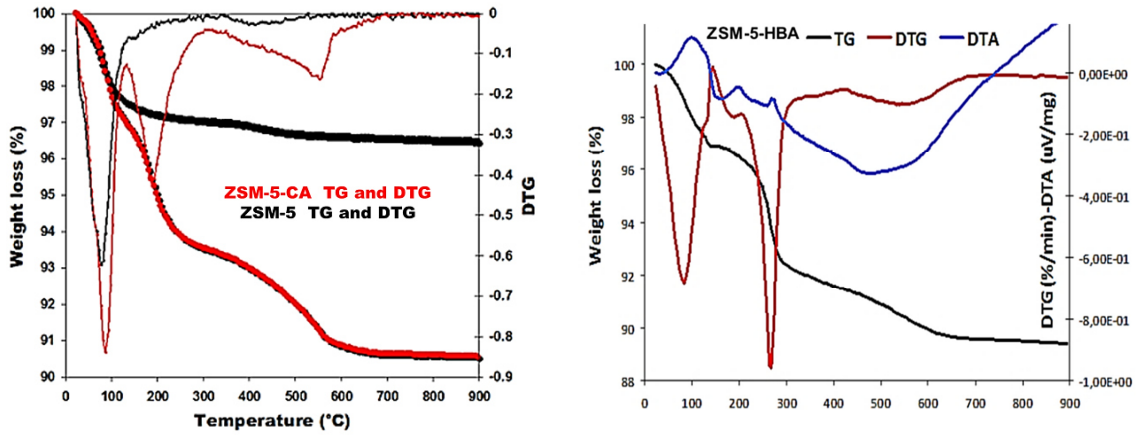

Rietveld refinements also revealed the incorporation of CA and p-HBA in the zeolites channel systems, consequently their adsorption capacities and/or adsorption kinetics could be reduced in the presence of these monomers. For this reason, the provided information about the position of molecules inside the ZSM-5 structure after adsorption (Figure 26) plays a key role.

Figure 26. a) Rietveld structure refinement of ZSM-5 saturated with CA and p-HBA b)

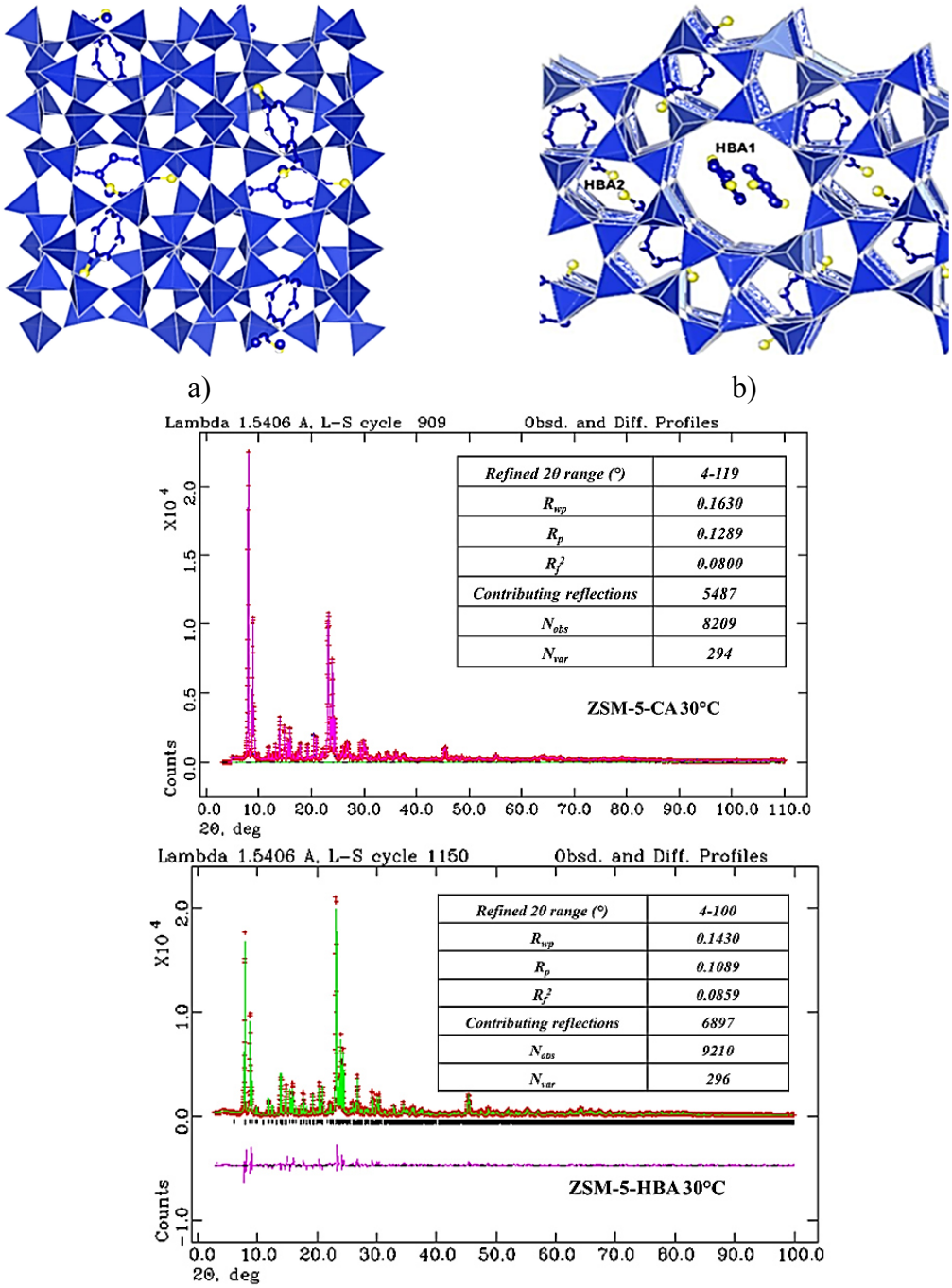

Rietveld refinements, revealed that p-HBA and CA occupied a similar site (in the intersection and sinusoidal channels) to that of VOCs, consequently they could reduce the hydrocarbons adsorption or competing for adsorption sites.

To better understand the VOCs and humic acid monomers competitive behaviour, a three dimensional plot of the adsorbed amount from dual component mixtures composed by VOCs and humic acid are elaborated (Figure 27). In particular, in the presence of TOL, the adsorbed CA was replaced, and the adsorption reached equilibrium in roughly 30 min. The replacement of adsorbed CA was also observed in the direct competitive adsorption experiments at pH 4.

In contrast, the TOL adsorption was slightly affected by the presence of CA (Figure 27).

A similar behaviour was also observed for TOL/p-HBA-ZSM-5 system.

Figure 27. Surface fitting of CA adsorbed quantity per unit mass of adsorbent vs. the equilibrium concentrations of TOL and CA in aqueous solution (pH=4).

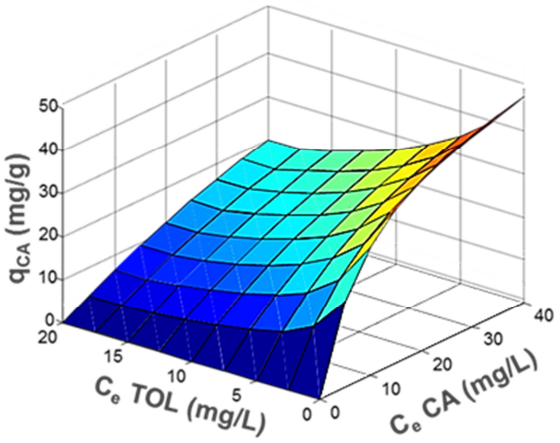

The higher selectivity of ZSM-5 for TOL with respect to CA and p-HBA was also observed in the competitive adsorption of TOL/p-HBA aqueous mixtures. This finding was confirmed by structural investigation of ZSM-5 loaded with single component solution of TOL, CA, p-HBA as well as from a binary mixtures of these chemicals. Strong similarities between the X-ray powder pattern of ZSM-5 after adsorption of the mixture and after only TOL adsorption, indicate that ZSM-5 adsorbs preferentially and selectively TOL, also in the presence of CA or p-HBA (Figure 28).

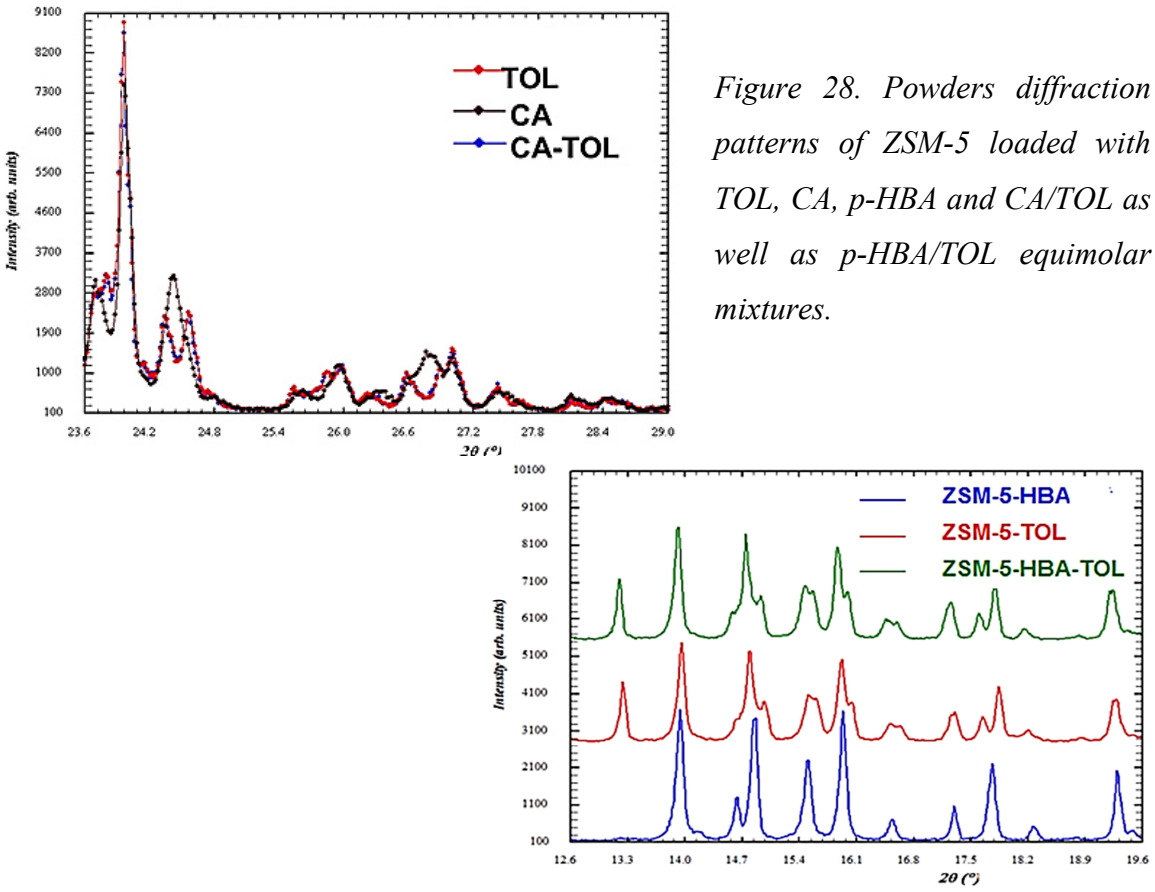

Figure 28. Powders diffraction patterns of ZSM-5 loaded with TOL, CA, p-HBA and CA/TOL as well as p-HBA/TOL equimolar mixtures.

As a matter of fact, ZSM-5 shows very favorable adsorption kinetics along with the highly irreversible adsorption of the selected emerging organic contaminants. In particular, the results highlight its strong VOCs adsorption selectivity also in presence of humic monomers. On the basis of these results, it is possible to conclude that zeolites may be suitable for integration into drinking water and wastewater treatment systems and in environmental remediation projects concerned with removal of emerging organic contaminants.

SECTION III:

Study of the desorption process of VOCs confined into ZSM-5 through the *in situ* HT synchrotron XRPD

3.7. Desorption process of 1,2-DCE induced by heating

The desorption behaviour of ZSM-5 loaded with 1,2-DCE was studied using the *in situ* synchrotron XRPD technique in the temperature range 30–600°C. Rietveld refinements allowed us to monitor the 1,2-DCE desorption process as well as the structural modifications undergoing on ZSM-5 upon a temperature-programmed thermal treatment. In particular, the *in situ* HT synchrotron XRPD, is used as a key to continuous monitoring the 1,2-DCE desorption process as well as the structural modifications undergoing on ZSM-5 upon a temperature programmed thermal treatment. These information are essential to understand the transient and dynamic features of desorption processes to better design and optimize the regeneration treatment of hydrophobic zeolites [8].

The structural model obtained at ambient conditions was used for the HT pattern analysis by adopting the same structure refinement strategies (see chapter - Results and discussion- Section I, 3.1).Through the analysis of XRPD patterns, a gradual overlapping of groups of peaks (Figure 29) reveals that a monoclinic $P2_1/n$ to orthorhombic P*nma* phase transition occurs with a Tc close to 70 ± 5°C. Moreover also Rietveld refinement highlight that there are no evidence to support a change in symmetry on the powder patterns until 75°C. For this reason the orthorhombic *Pnma* space group was used in all the crystal structure refinements in the 75–600°C temperature range. In this temperature range no evidence was found to support another change in symmetry during the thermal treatment. As recently reported by Ardit et al. [144], the same phase transition occurs in the same as-synthesized material used in this work, as demonstrated by *in situ* synchrotron X-ray diffraction data. The authors highlighted the tricritical character of this transition from ferroelastic (monoclinic) to paraelastic (orthorhombic) phase in ZSM-5 [144]. The occurrence of this phase transition also confirms the well-known crucial influence of the Si/Al ratio [132–136,167,168] as well of the adsorbed extra-framework molecules [15, 124,132–136,169–174] on the monoclinic-orthorhombic phase transition undergone by this zeolite.

Figure 29. Plot of ZSM-5-1,2-DCE in the 1.9-2.4 (a) and 5.7-6.4 (b) 2θ(°) range within the 30–600°C temperature interval. Observed, calculated, and difference powder diffraction pattern of ZSM-5 at 75 and 600°C are also reported.

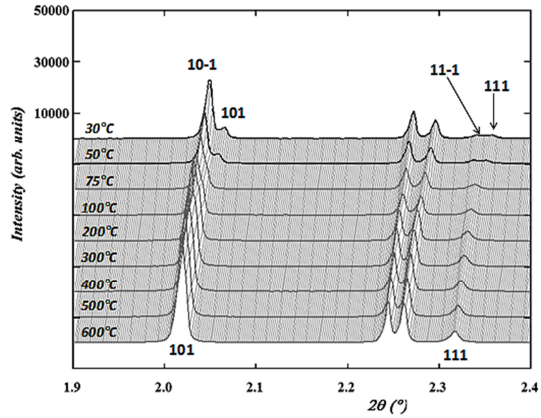

a)

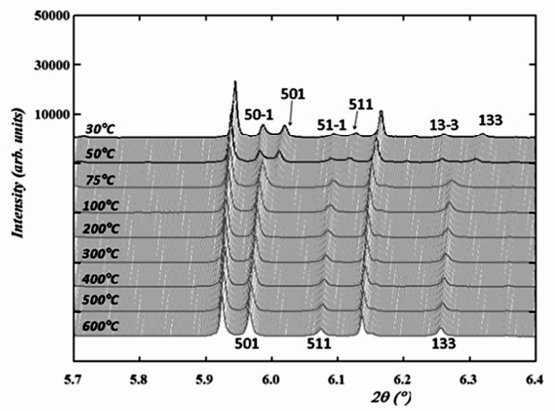

b)

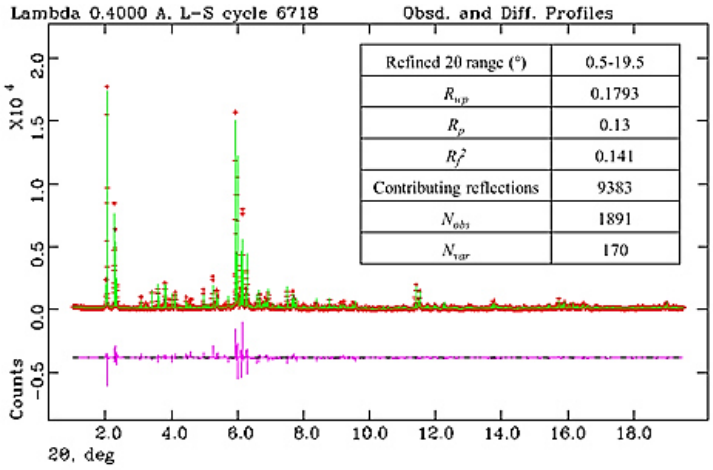

ZSM-5-1,2-DCE 75°C

ZSM-5-1,2-DCE 600°C

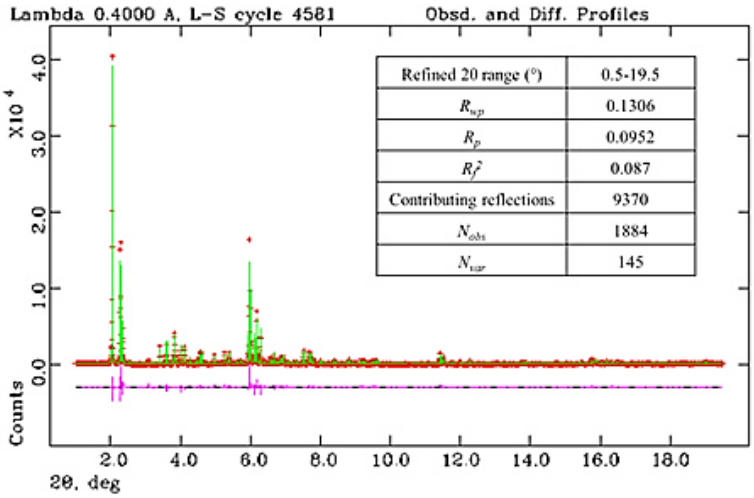

The complete set of lattice parameters of ZSM-5 at different temperatures is given in Table 19. To allow a better comparison between them, we report normalized values of cell parameters defined as $V(T)/V_0$, $a(T)/a_0$, $b(T)/b_0$, and $c(T)/c_0$, being the reference values those obtained in the refinement of the first orthorhombic pattern recorded at T = 30°C.

Table 19. Lattice parameters of ZSM-5-1,2-DCE in the temperature range 30-600°C.

ZSM-5-1,2-DCE [8]					
T(°C)	**a(Å)**	**b(Å)**	**c(Å)**	**V(Å3)**	**β(°)**
30	19.9052(3)	20.1199(3)	13.3909(2)	5362.65(1)	90.58(1)
40	19.9080(3)	20.1218(3)	13.3938(2)	5365.10(1)	90.54(1)
50	19.9118(3)	20.1213(3)	13.3962(2)	5367.36(1)	90.50(1)
60	19.9164(3)	20.1241(3)	13.4006(2)	5370.79(1)	90.43(1)
75	19.9336(3)	20.1129(3)	13.4077(9)	5375.46(1)	90
100	19.9378(6)	20.1067(5)	13.4076(6)	5374.90(1)	90
125	19.9394(5)	20.1024(5)	13.4066(2)	5373.99(2)	90
150	19.9392(4)	20.1022(4)	13.4054(2)	5373.15(2)	90
175	19.9373(5)	20.1031(5)	13.4042(3)	5373.30(2)	90
200	19.9348(4)	20.1054(4)	13.4034(3)	5372.05(2)	90
225	19.9339(4)	20.1040(4)	13.4024(3)	5371.04(2)	90
250	19.9331(4)	20.1014(4)	13.4014(3)	5369.72(2)	90
275	19.9321(4)	20.0978(4)	13.4004(3)	5368.10(2)	90
300	19.9311(4)	20.0942(3)	13.3996(2)	5366.51(2)	90
350	19.9290(4)	20.0886(3)	13.3980(2)	5363.84(2)	90
400	19.9274(4)	20.0832(2)	13.3969(2)	5361.53(2)	90
450	19.9254(3)	20.0785(3)	13.3956(2)	5359.20(2)	90
500	19.9229(3)	20.0743(3)	13.3941(2)	5356.83(2)	90
550	19.9203(4)	20.0708(4)	13.3924(2)	5354.51(2)	90
600	19.9175(4)	20.0675(4)	13.3906(2)	5352.14(2)	90

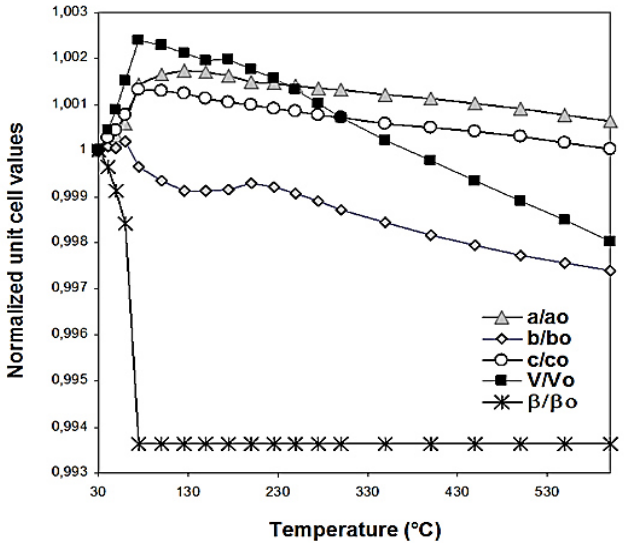

The slight increase of unit cell volume (ΔV~ 0.24%) up to 70°C can be reasonably related to the relaxation of the bonding interactions between the 1,2-DCE-water molecule complexes and framework oxygen atoms. The refined distances of the 1,2-DCE atoms from the O atoms in both framework and water molecules indicate that bonding between the water-1,2-DCE oligomer and the framework oxygen atoms breaks down during the first stage of temperature increase. As a consequence this attractive force, exerting a kind of negative pressure on the surrounding framework, disappears. The oxygen framework is thus free to relax and expand as demonstrated by the ellipticity decrease in the zeolite channel systems. The formation of more regular wide-open apertures upon heating is likely associated to the observed relative expansion of the framework thus explaining the evolution of the unit cell parameters and the positive cell volume expansion at low temperature. A similar framework expansion was also observed upon heating in B-ZSM-5 [173], as well as in other microporous materials such as wairakite [174], analcime [175], hydro-sodalite $Na_6[AlSiO_4]_6 \cdot 8H_2O$ [176] and silica sodalite [177].

The refined occupancies reported in Figure 30 showed that in this temperature range the 1,2-DCE1 site progressively decreases its occupancy and it is emptied at temperature (225°C) lower than that found for the organic hosted in 1,2-DCE2 site (350°C), which is forced into the sinusoidal channel. This is in agreement with the TG reported by Pasti et al. [14], according which the state of the 1,2-DCE-ZSM-5 system is altered in the temperature range ~ 150-350°C.

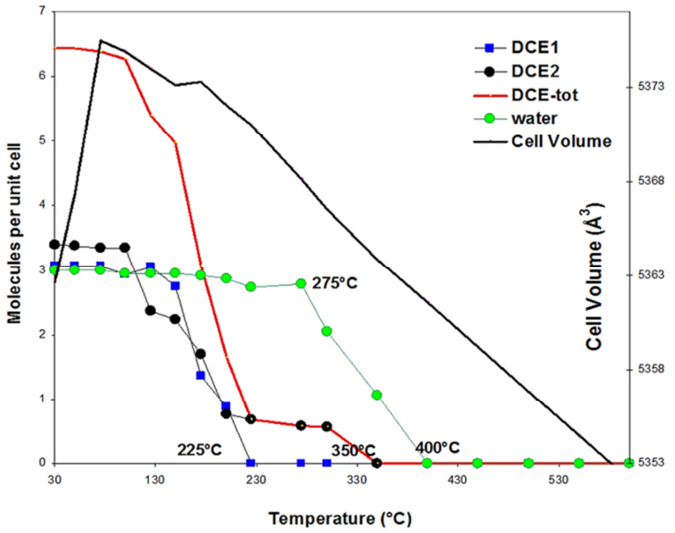

Figure 30. Variation of volume, 1,2-DCE and water molecules p.u.c as a function of temperature.

This finding indicated that 1,2-DCE molecules preferentially diffuse through the straight channel of orthorhombic ZSM-5. At 350°C all the Cl and C sites are emptied, thus confirming the completion of the thermal desorption of 1,2-DCE at this temperature. A similar behaviour was observed for site occupancy of water molecules. The parallelism in the decrease of 1,2-DCE and water occupancies with temperature increase, can be explained by the disassembly of water-1,2-DCE clusters caused by the 1,2-DCE thermal desorption. The serial structural refinements during the thermal ramp provide information on the way in which the occupancy of the extraframework sites affect the geometry of the framework. In Figure 31 a and b are reported the C.F.A. and the ellipticity of the 10 MR channels as a function of temperature. The opening of the zeolite framework pore system changes with temperature increase due the continuous structural changes associated with the heating process.

Figure 31. (a) C.F.A. and (b) ellipticity (ε) for the 10MR channels as a function of temperature.

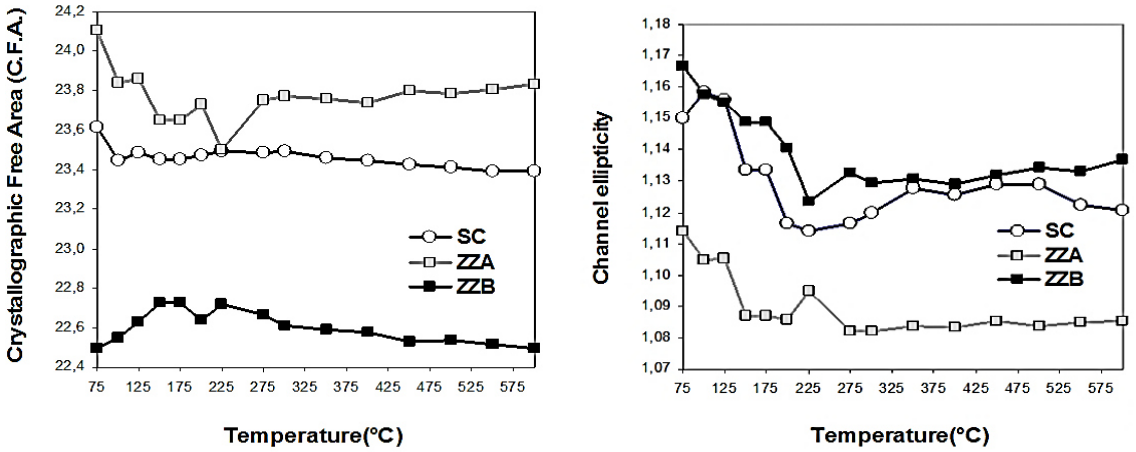

a) b)

Consequently, the C.F.A. depending on channel ellipticity also vary with temperature [8] (Figure 31 a). The channel ellipticity decrease with temperature increase reported in Figure 31 b is due to the framework flexibility of ZSM-5 [178–180]. In particular, the SC 10-ring channel become narrower and its ellipticity (defined as the ratio between the smaller (O-O) and larger (O-O) ‘‘free diameters’’ of the 10-rings) decreases. A similar contraction was also observed in the sinusoidal channels which become more regular: the resulting cumulative effect explains the unit-cell contraction registered upon heating. Once all 1,2-DCE and water molecules are completely decomposed, no further significant variations are registered in the dimension of the 10 MR channels. At temperature higher than 400°C, the host molecule desorption process is completed, therefore the unit cell contraction of ZSM-5 above this temperature can be described as a proper NTE process (Figure 30). This behaviour is similar to that observed in MFI-type materials synthesized in the presence of tetrapropylammonium as well in their calcined forms e.g. silicalite-1 [181] titanium silicalite-1 (TS-1) [182] and Fe-silicalite (Fe-MFI) [183]. In particular, in TS-1 and Fe-MFI a NTE was reported above the temperature which marks the end of the calcination process.

3.8. Desorption process of TOL induced by heating

In situ HT synchrotron XRPD was used in this study as a tool to understand the desorption process features of TOL adsorbed in organophilic ZSM-5 zeolite (SiO_2/Al_2O_3 ~ 280), as well as framework structural modifications upon thermal treatment from room temperature to 600°C. Rietveld refinements showed that TOL release starts in the 75 < T < 200°C temperature range. Furthermore, extraframework structural changes take place when TOL removal starts. Significant internal pressure is developed with the product diffusion causing a corresponding transient expansion in the 10-ring channels [9].

The evolution of the powder diffraction patterns as a function of temperature (Figure 32) indicated that ZSM-5 maintains its crystallinity up to the highest investigated temperature. In particular, Figure 32 shows the powder pattern evolution of the investigated ZSM-5-TOL sample when close to the monoclinic ($P2_1/n$) to orthorhombic ($P2_12_12_1$) phase transition at a Tc = 75°C ± 5 in the 1.7–4.7 (a) and 4.7–7.1(b) (°)2θ range.

Figure 32. Plot in situ XRPD patterns as a function of temperature for ZSM-5-TOL; refinements details are also reported for 75 and 400°C.

a)

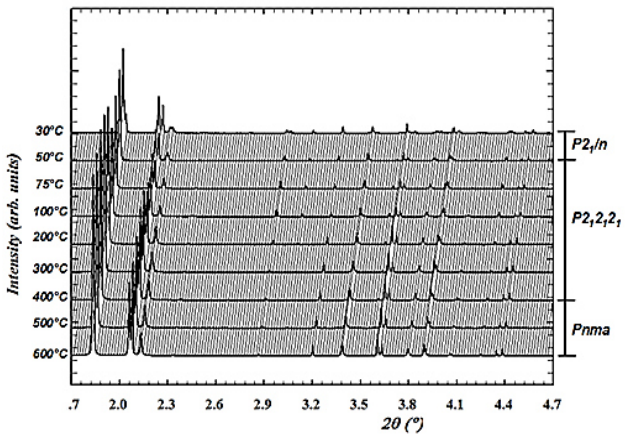

ZSM-5-TOL 75°C

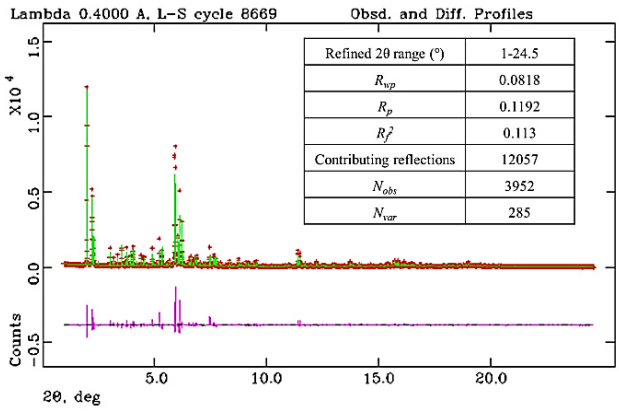

b)

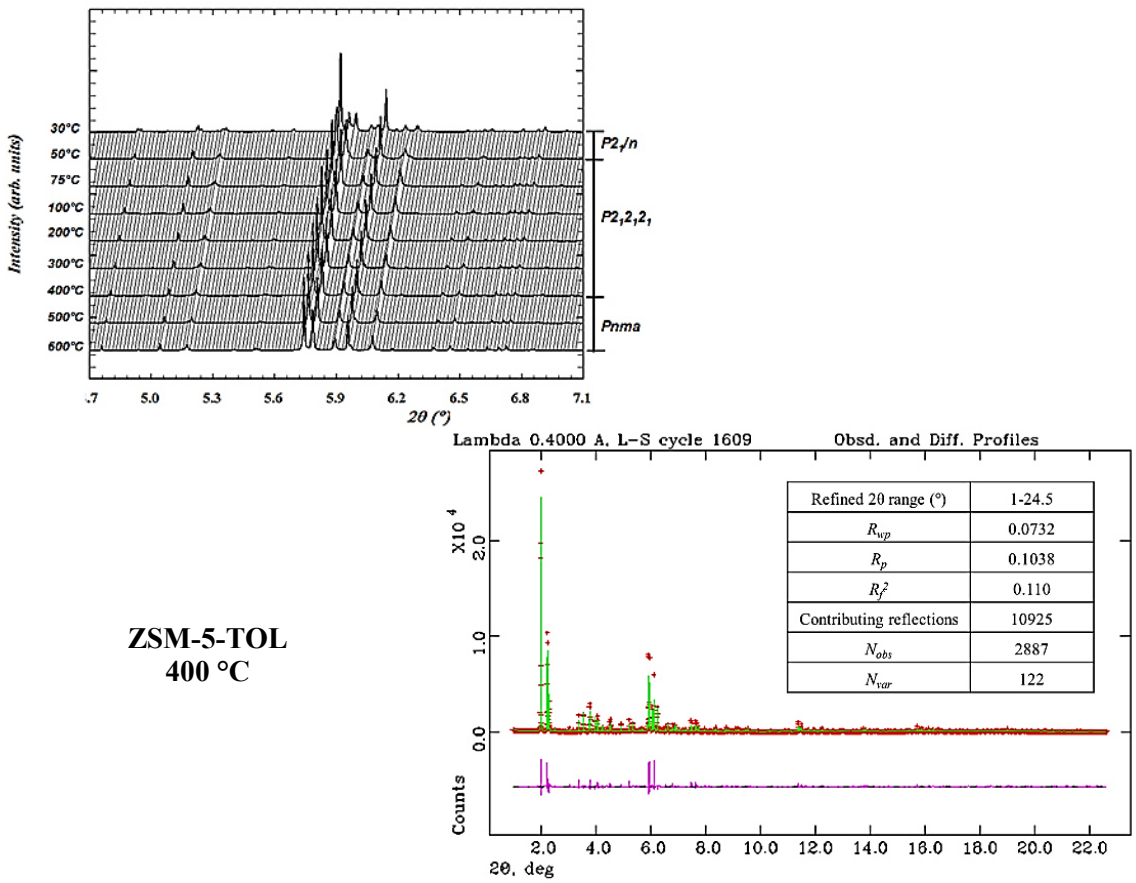

The symmetry change was marked by the gradual merging of several peaks doublet into single ones. The Rietveld refinement in the orthorhombic space group was carried out starting from the framework atomic coordinates reported by Nishi et al. [135]. The structural model obtained after the phase transition was then used for the ZSM-5 HT patterns, by adopting the same structure refinement strategies. After the desorption of the organic molecules (Tc close to 400 ±5°C), the slope variation of the unit cell volume suggested a new displacive phase transition from orthorhombic $P2_12_12_1$ to *Pnma*. As a consequence, all Rietveld refinements up to 400°C were performed in this latter space group, starting from the atomic model of Van Koningsveld et al [133]. Using this crystal structure model, based on the latter space group, appreciably improved the quality of the Rietveld refinement, as testified by the lower R_{wp} and R_p parameters. Cell parameter values defined as V(T)/ V_0, a(T)/ a_0, b(T)/ b_0, and c(T)/ c_0, are normalized compared to the reference values refined at T = 30°C. T-dependent variations in unit cell parameters in the 30–600°C T-range are reported in Figure 33 a.

Figure 33. a) Evolution of ZSM-5-TOL unit cell parameters, b) variation of TOL molecules p.u.c.; refinements details are also reported for 75 and 400°C.

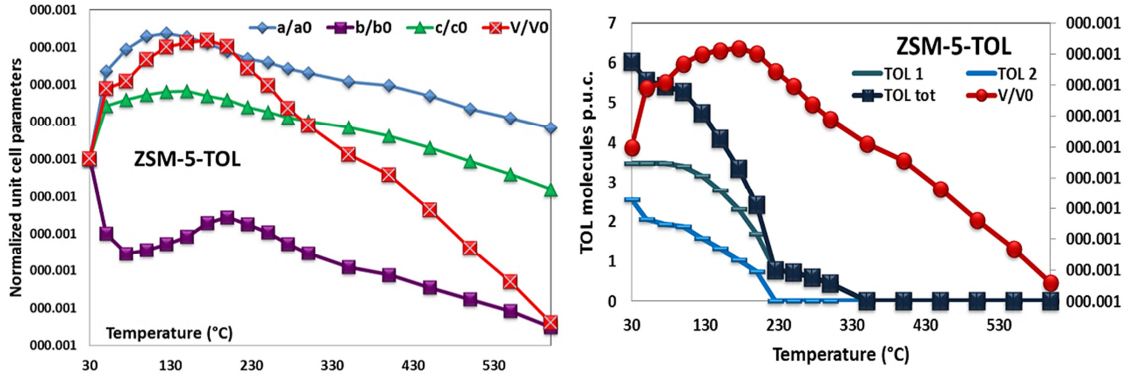

a) b)

In situ synchrotron XRPD data revealed a rapid increase in cell volume (Figure 33 a) in the 30 < T < 75°C T range. The linear expansion coefficients along *a*, *b* and *c* directions were α_a = 3.269 × 10^{-5}, α_b= -2.810 × 10^{-5} and α_c= 1,771 × 10^{-5}, respectively. The volume thermal expansion coefficient is α_V= 2.325 × 10^{-5}. 131 and 13–1 peak overlapping is still incomplete at 50°C, and broadening in the 2θ region is observed in the ZSM-5 pattern. This suggests that conversion to the orthorhombic symmetry is still occurring. Complete overlapping for this group of peaks is reached at about 70 ± 5°C(Tc), as a result of a complete monoclinic $P2_1/n$ to orthorhombic $P2_12_12_1$ phase transition. The latter space group was also adopted in the single-crystal XRD study by Nishi et al. [135] for an all silica MFI material which was highly-loaded with TOL. Nishi et al. [135] reported three kinds of TOL molecules in the unit cell: two of these were located at the intersection of between the straight sinusoidal channels, the third one in the sinusoidal channel. Our Rietveld refinement highlighted that $P2_1/n \rightarrow P2_12_12_1$ phase transition is accompanied by clear discontinuity in V(T)/V_0, a(T)/a_0,b(T)/b_0, and c(T)/c_0 curves (Figure 33 a). Initial cell expansion occurred even if TOL desorption only partially occurred, as demonstrated by the evolution of TOL content as a function of temperature (Figure 33 b). Table 20 lists the details of the data collection and the refined unit cell parameters at the temperatures in which phase transitions occurred.

Table 20. Lattice parameters and refinement details for ZSM-5-TOL at 30, 75, 400 and 600°C, respectively.

	ZSM-5–TOL [9] (*Wavelength (Å) 0.400031)*			
	30°C	**75°C**	**400°C**	**600°C**
Space group	$P2_1/n$	$P2_12_12_1$	*Pnma*	*Pnma*
***a* (Å)**	19.906(1)	19.935(1)	19.926(1)	19.914(1)
***b* (Å)**	20.118(1)	20.092(1)	20.086(1)	20.072(1)
***c* (Å)**	13.393(1)	13.403(1)	13.397(1)	13.387(1)
***β* (°)**	90.545(1)	90	90	90
***V* (Å^3)**	5363.01(2)	5368.62(1)	5361.85(1)	5351.21(1)
Refined 2θ (°) range	1-24.56	1-24.56	1-24.56	1-24.56
R_{wp} (%)	9.82	8.18	7.32	7.28
R_p (%)	10.54	11.92	10.38	10.21
Rf^2 (%)	8.7	11.33	11.09	11.11
Contributing reflections	12055	12057	10925	10682
N_{obs}	7065	3952	2887	2708
N_{var}	276	285	122	122

$R_p = \Sigma[Y_{io}-Y_{ic}]/\Sigma Y_{io}$; $R_{wp} = [\Sigma wi(Y_{io}-Y_{ic})^2/\Sigma wiY_{io}^2]^{0.5}$; $R_{F2} = \Sigma|F_o^2-F_c^2|/|F_o^2|$

After phase transition, TOL molecules remained confined near the straight channel (TOL1 site) as well as at the intersection between straight and sinusoidal channels (TOL2 site) (Figure 34 a and b; Table 21).

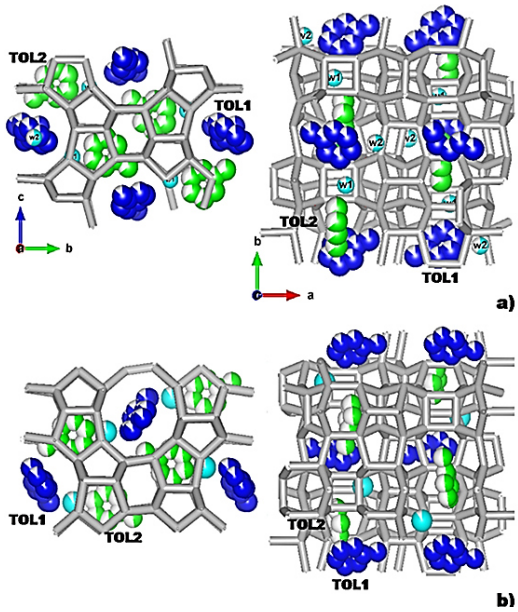

Figure 34. Location of TOL and water molecules in ZSM-5 along [100] and [001] directions, respectively, before (30°C) (a) and after (75°C) (b) the monoclinic to orthorhombic phase transition.

Difference Fourier maps also showed the occurrence of a clear weak maximum which is attributed to co-adsorbed water hosted in a fully occupied site (site W in Table 21).

Table 21. Atomic coordinates, thermal parameters, and fraction of ZSM-5-TOL extraframework atoms at 75°C [9].

ZSM-5-TOL 75°C

	x/a	y/b	z/c	Uiso	Fraction
			TOL1 Site		
C4	-0.0054(22)	0.8282(19)	0.2181(30)	0.127(1)	0.872(6)
C3	-0.0351(18)	0.7812(25)	0.2803(22)	0.127(1)	0.872(6)
C1	-0.0195(22)	0.7136(23)	0.2705(32)	0.127(1)	0.872(6)
C2	0.0159(26)	0.6913(19)	0.1874(41)	0.127(1)	0.872(6)
C5	0.0473(15)	0.7388(25)	0.1269(24)	0.127(1)	0.872(6)
C6	0.0296(20)	0.8061(23)	0.1347(25)	0.127(1)	0.872(6)
C7	-0.0188(28)	0.9012(20)	0.2322(51)	0.127(1)	0.872(6)
			TOL2 Site		
C13	-0.1075(18)	0.7480(56)	-0.0663(27)	0.106(1)	0.484(7)
C12	-0.1581(29)	0.7716(42)	-0.0051(25)	0.106(1)	0.484(7)
C10	-0.2243(23)	0.7635(48)	-0.0336(39)	0.106(1)	0.484(7)
C11	-0.2395(22)	0.7450(55)	-0.1313(45)	0.106(1)	0.484(7)
C8	-0.1883(35)	0.7228(35)	-0.1933(29)	0.106(1)	0.484(7)
C9	-0.1223(28)	0.7320(46)	-0.1647(26)	0.106(1)	0.484(7)
C14	-0.0366(21)	0.7545(104)	-0.0341(52)	0.106(1)	0.484(7)
			W Site		
W	0.153(4)	0.6713(20)	0.097(5)	0.161(1)	1.002(1)

At the same time, the simultaneous presence of small diffused maxima indicates that a few other water molecules are spread over a number of low occupied positions, which remained unlocalized by Rietveld structure refinement. The refined distances of TOL and water molecules oligomers (W-C5 = 2.55 Å; W-C11 = 2.76 Å) confirm their interaction with framework oxygens (W-O27 = 2.60 Å; W-O28 = 2.61 Å; C12-O44 = 2.80 Å). The refined occupancies indicate that TOL desorption starts from the TOL2 site. This process is accompanied by an increase in the opening of the zeolite framework pore system and, consequently, of the C.F.A. (Figure 35).

Figure 35. Evolution of C.F.A. (a) and ellipticity (ε) (b) as a function of temperature.

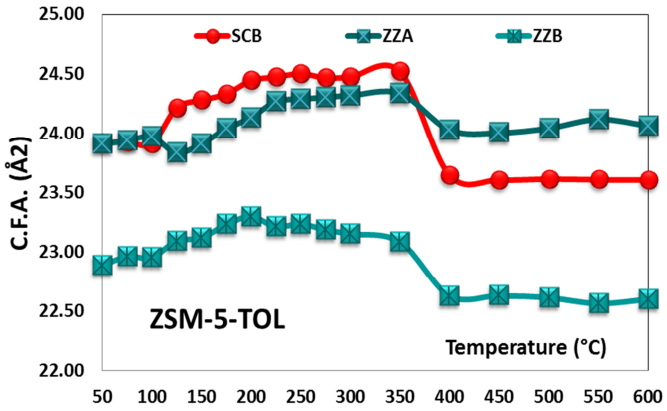

a)

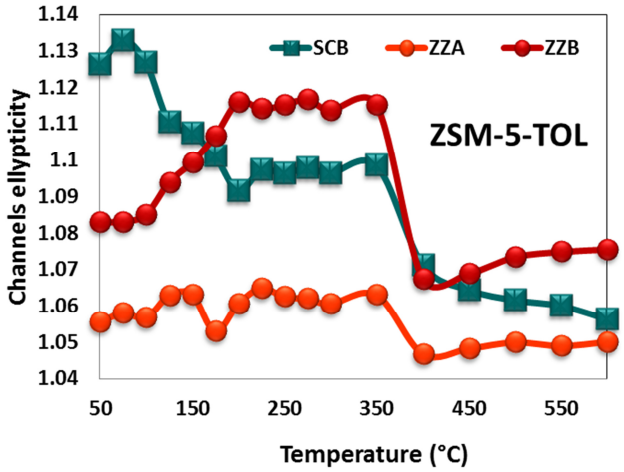

b)

This result also justifies the volume expansion in this stage of the experiment (Figure 35 a). The same cell volume increase was also reported on the same ZSM-5 sample after 1,2-DCE adsorption upon heating at Tc close to 70 ± 5°C [8]. Structure refinements of the occupancies show that the TOL removal starts in the 75 < T < 200°C temperature range.

The linear expansion coefficients along *a, b* and *c* directions at 200°C is $\alpha_a = -1.846 \times 10^{-7}$, $\alpha_b = 3.922 \times 10^{-6}$ and $\alpha_c = -5.969 \times 10^{-9}$, respectively. TOL1 content was reduced by about 50% as indicated by the decrease in TOL molecules per unit cell *vs.* temperature (Figure 33 b). At the same time, the TOL2 molecules are almost completely desorbed.

A T- dependent distortion mechanism in the framework takes place in correspondence with guest organic molecule release. Adsorbate diffusion led to significant internal pressure and caused a corresponding transient expansion ($\alpha_V = 3{,}740 \times 10^{-6}$) in the 10-ring channels. This trend suddenly changes between 200 and 400°C as a result of structural modifications induced by complete TOL removal, in good agreement with the evolution of refined organic occupancy fractions (Figure 33 b). In this T range, all the cell parameters decrease, the linear expansion coefficients along *a, b* and *c* directions at 400°C being $\alpha_a = -2.267 \times 10^{-6}$, $\alpha_b = -3.916 \times 10^{-6}$ and $\alpha_c = -2.443 \times 10^{-6}$. The negative volume expansion associated with organics removal is $\alpha_V = -8.620 \times 10^{-6}$. Geometrical features of pore openings indicate that the straight channel along the *b* axis is the more viable direction for TOL decomposition product. The unit cell parameter variations and the change in the cell volume slope *vs.* T dependence suggested a new displacive phase transition from orthorhombic $P2_12_12_1$ to *Pnma* at around 400°C. The quality of the Rietveld refinement based on this crystal structure model was appreciably better, as testified by lower R_{wp} and R_p parameters reported in Table 20.

The structure maintained this symmetry up to the highest investigated temperatures. The axial and volume thermal expansion coefficients in the 400– 600°C T-range are $\alpha_a = -2.896 \times 10^{-6}$, $\alpha_b = -3.512 \times 10^{-6}$ and $\alpha_c = -3.534 \times 10^{-6}$, $\alpha_V = -9.941 \times 10^{-6}$, respectively. Volume contraction in this T-range is true NTE since it occurs without any mass loss. This mechanism, which has been clearly documented in MFI-materials such as ZSM-5-loaded with 1,2-DCE [8], silicalite-1 [181], titanium silicalite-1 (TS-1) [182], Fe-silicalite (Fe-MFI), TS-1 and Fe-MFI [183], as well as in other microporous materials [112,175,180] and zeolites (*e.g.* zeolite omega [184], B-levyne [185] all silica sodalite [186] and all silica-faujasite [177]), can also be explained by relaxation in the framework distortions induced by water molecules passing through the zeolite tetrahedral rings during the preceding dehydration stage (*e.g.* analcime [186]).When all the volatile species have been desorbed, the non-equilibrium framework distortions are relaxed and the window apertures progressively decrease and become more circular, as demonstrated by the evolution in ellipticity values reported in Figure 35 b.

3.9. Desorption process of MTBE induced by heating

The temperature-induced desorption of MTBE from aqueous solutions onto hydrophobic ZSM-5 was studied by *in situ* HT synchrotron XRPD and chromatographic techniques. This kind of information is crucial for designing and optimizing the regeneration treatment of such zeolite. The evolution of the structural features monitored by full profile Rietveld refinements revealed that a monoclinic ($P2_1/n$) to orthorhombic (*Pnma*) phase transition occurred at about 100°C. MTBE desorption process caused a remarkable change in the unit cell parameters. Complete MTBE desorption was achieved upon heating at about 250°C. Rietveld analysis demonstrated that the desorption process occurred without any significant zeolite crystallinity loss, but with slight deformations in the channel apertures.

According to Martucci et al. [11,125] and as discussed in Section I above, MTBE molecules are hosted in two crystallographically independent sites: MTBE1 near the intersections of sinusoidal and straight 10MR channels (C1a, C2a, C3a, C4a, C5a, O1a sites) and MTBE2 in the sinusoidal 10MR channel (C1b, C2b, C3b, C4b, C5b, O1b sites), respectively. To summarize what has already been reported, on the whole, 8 MTBE molecules and about 2 water molecules were detected. Rietveld structure refinement confirmed the occurrence of MTBE-water complexes interacting with the framework stabilizing the guest structure within the zeolite host framework.

The automatic indexing of the peaks, carried out by the HighScore Plus v.3.0 software, revealed the gradual overlapping of groups of peaks (*i.e.* 131 + 13-1 and 311 + 31-1 in the first angular range, and 133 + 13-3 and 313 + 31-3 in the second range) attesting the monoclinic to orthorhombic phase transition, with a Tc close to 100 ± 5°C. Figure 36 shows the evolution of the investigated ZSM-5 sample close to the expected transition temperature, Tc, in the 3.70–4.30 (Figure 36 a) and 5.60– 6.50 (°)2θ (Figure 36 b). Therefore, recent works [9,10,144] reported this phenomena both in the unloaded ZSM-5 as well as in the same samples after organics adsorption. The evolution of refined unit cell parameters in as a function of temperature is illustrated in Figure 36.

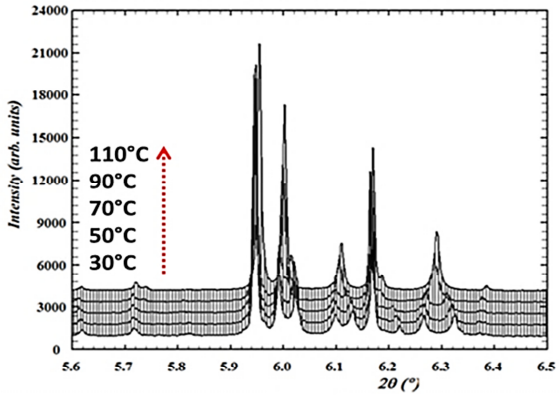

Figure 36. Evolution of ZSM-5-MTBE patterns close to the expected transition temperature [11]

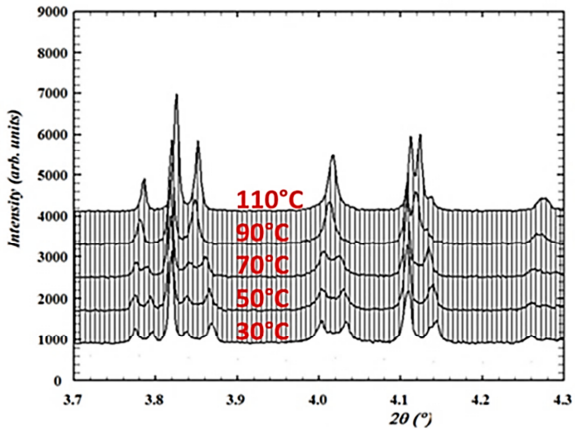

The general trend shows an initial increase of all the lattice parameters except for the *b* parameter (see Table 22). In particular, unit cell volume increase until about 125 ± 5°C then it remains about constant in the range between 125 - 200 ± 5°C and starts to decrease after 200 ± 5°C. A similar behaviour was also observed during the desorption process of 1,2-DCE [8] and TOL [9].

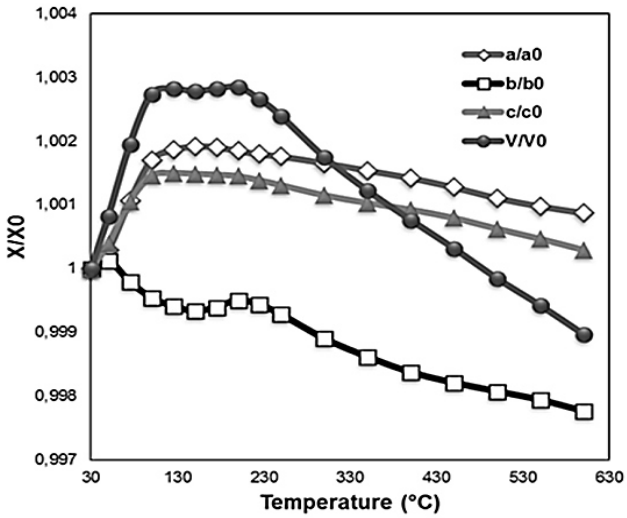

Figure 37. Evolution of ZSM-5-MTBE unit cell parameters. [11].

Table 22. Refined unit cell parameters as a function of temperature [11].

ZSM-5-MTBE					
T(°C)	**a (Å)**	**b(Å)**	**c(Å)**	**V (Å^3)**	**β (°)**
30	19.8984(2)	20.1191(1)	13.3844(1)	5358.02(1)	90.5741
40	19.9013(2)	20.1206(1)	13.3869(1)	5360.23(1)	90.5410
50	19.9042(2)	20.1217(1)	13.3896(1)	5362.39(1)	90.5013
60	19.9071(2)	20.1221(1)	13.3923(1)	5364.41(1)	90.4524
75	19.9194(2)	20.1150(1)	13.3985(1)	5368.45(1)	90.1744
80	19.9199(2)	20.1170(1)	13.4001(1)	5369.75(1)	90.1883
90	19.9250(2)	20.1126(1)	13.4017(1)	5370.62(1)	90.0492
100	19.9321(1)	20.1099(1)	13.4039(1)	5372.71(7)	90
125	19.9354(1)	20.1073(1)	13.4044(1)	5373.13(7)	90
150	19.9365(1)	20.1057(1)	13.4043(1)	5372.93(7)	90
175	19.9363(1)	20.1069(1)	13.4041(1)	5373.13(7)	90
200	19.9351(1)	20.1092(1)	13.4038(1)	5373.29(7)	90
225	19.9341(1)	20.1077(1)	13.4029(1)	5372.27(7)	90
250	19.9333(1)	20.1046(1)	13.4019(1)	5370.84(7)	90
300	19.9313(1)	20.0971(1)	13.3998(1)	5367.41(7)	90
350	19.9290(1)	20.0913(1)	13.3982(1)	5364.59(7)	90
400	19.9266(1)	20.0864(1)	13.3968(1)	5362.11(7)	90
450	19.9237(1)	20.0831(1)	13.3950(1)	5359.73(7)	90
500	19.9204(1)	20.0804(1)	13.3927(1)	5357.20(7)	90
550	19.9178(1)	20.0777(1)	13.3906(1)	5354.93(7)	90
600	19.9157(1)	20.0741(1)	13.3883(1)	5352.51(7)	90

As reported by Pasti et al. [14], Martucci et al. [8] and Rodeghero et al. [9] this behaviour is related to the relaxation of the bonding interactions between water-organics oligomers interacting with framework. The relaxation of the MTBE-framework oxygens refined distances clearly indicates that during the heating, this attractive force exerting a negative pressure is released and the framework is free to relax and expand. The process is also correlated to the MTBE desorption process which starts at 100°C and is complete at ~300°C. Figure 38 shows both the evolution of MTBE molecules p.u.c. and the unit cell volume as a function of temperature.

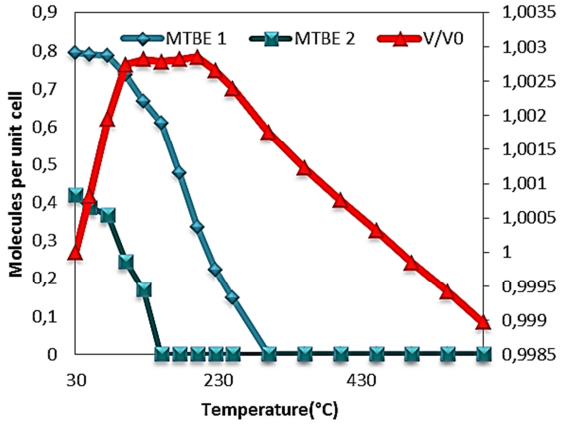

Figure 38. Evolution of MTBE molecules and unit cell volume as a function of temperature. Observed and Difference profiles after MTBE desorption are reported [11].

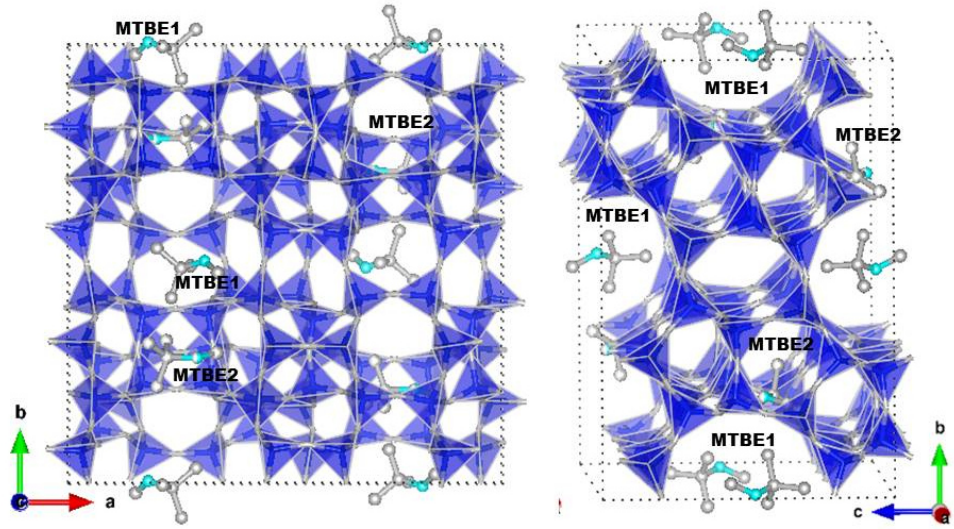

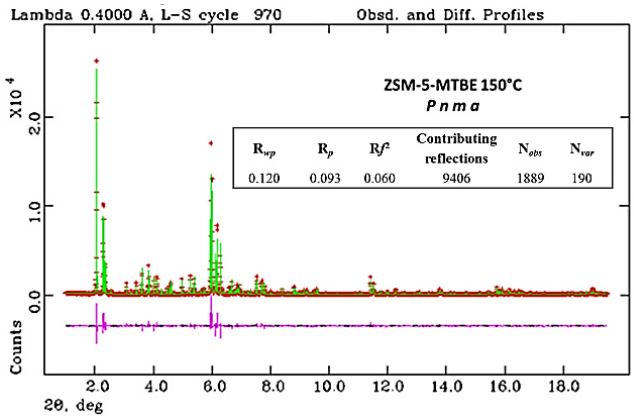

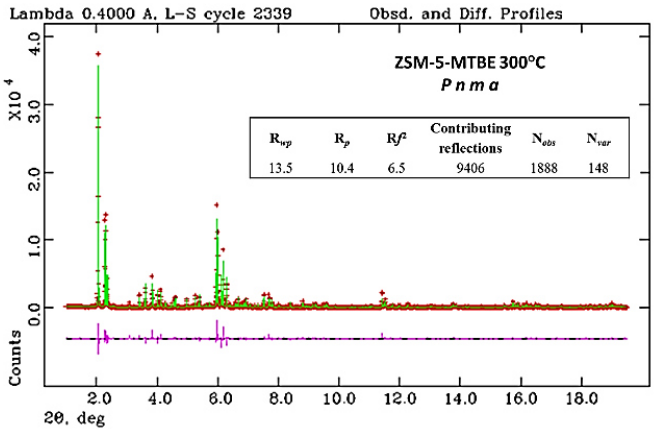

After the full organics desorption a contraction of the unit cell volume is observed until 600°C. This phenomena is explained as a NTE already observed not only in MFI-type materials [144,182–184,187], but also in other microporous materials [173,177,179,180,184,186,188–191], thus attesting the framework distortions relaxation induced by host molecules which diffuse through the zeolite channels during the heating process. The desorption process occurred without any significant zeolite crystal. Above 300°C the channels ellipticity decreases and wide-open apertures regularize. This process is accompanied by variations in the opening of the zeolite framework pore system and consequently, in the C.F.A. (Figure 39).

Figure 39. C.F.A. and ellipticity (ε) of the 10-ring channels as a function of temperature [11].

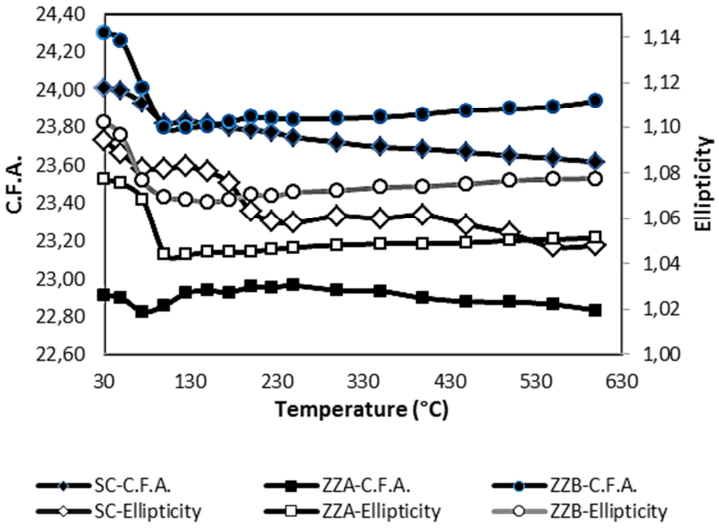

To sum up, the evolution of the structural features monitored by full profile Rietveld refinements revealed that a monoclinic ($P2_1/n$) to orthorhombic (*Pnma*) phase transition occurred at about 100°C. Complete MTBE desorption was achieved upon heating at about 300°C. Notwithstanding the change in the unit-cell parameters, Rietveld refinement demonstrated that the desorption process occurred without any significant zeolite crystallinity loss, but with slight deformations in the channel apertures.

3.10. Desorption process of 1,2-DCE/MTBE and TOL/MTBE binary mixtures induced by heating

In situ HT synchrotron XRPD was used in this study as a tool to understand the adsorption/desorption process features of MTBE/TOL and 1,2-DCE/MTBE binary mixtures adsorbed in organophilic ZSM-5 zeolite (SiO_2/Al_2O_3 ~280), as well as framework structural modifications upon thermal treatment from room temperature to 600°C. The binary system was described by a competitive dual site Langmuir adsorption isotherm. The results achieved from the series of time-resolved Rietveld refinements allowed to highlight the out-of-equilibrium effects which govern desorption of ZSM-5 powders in dynamic conditions. The decomposition of TOL and MTBE in both systems starts at about 100°C and continuously proceeds up to ~250°C. As far as concerns 1,2-DCE molecules, they are completely released from the cavities at ~350°C. Significant internal pressure is developed with the composition product diffusion, causing a corresponding transient distortion in the 10-ring channels. Above 400°C, the unit-cell volume contraction without any mass loss gives rise to a negative thermal expansion (NTE) process. The results clearly demonstrated that ZSM-5 regeneration is effective when it is thermally treated at about 350°C. Above this temperature, when all the organic have been desorbed, non-equilibrium distortions in the framework are relaxed and channel apertures become more circular, thus demonstrating the efficiency of thermal regeneration under mild conditions [192].

The results of our Rietveld refinement of ZSM-5-MTBE/TOL and ZSM-5-MTBE/1,2-DCE crystal structures at room temperature are in close agreement to what recently reported by Pasti et al. [56]. The parameters of the $P2_1/n$ cell at room temperature are a = 19.900(1) Å, b = 20.116(1) Å, c = 13.387(1) Å, β = 90.6(1), V=5358.6(1) $Å^3$ in ZSM-5-MTBE/1,2-DCE and a = 19.895(1) Å, b = 20.114(1) Å, c = 13.383(1) Å, β = 90.59°(1),V = 5355.2(1) $Å^3$ in ZSM-5-MTBE/TOL, respectively. The extraframework refined occupancies confirmed that the organics (~ 3.8 TOL and 3.4 MTBE molecules per unit cell in ZSM-5-MTBE/TOL; ~ 3 MTBE and 2.5 1,2-DCE in ZSM-5-MTBE/1,2-DCE per unit cell) interact with co-adsorbed water molecules thus forming organic–water complexes (clusters or short chains) interacting with the framework oxygens. A careful examination of the unit cell parameters plotted in Figure 40 as normalized values, $a(T)/a_0$, $b(T)/b_0$, $c(T)/c_0$, and $V(T)/V_0$ with a_0, b_0, c_0, and V_0 revealed that after heating up to 100ºC a slight increase in the unit-cell volume is observed in both samples.

Figure 40. Evolution of unit cell parameter for both binary mixtures (MTBE/1,2-DCE, MTBE/TOL) during in situ XRPD. Refinement details of the phase transition temperature are also reported.

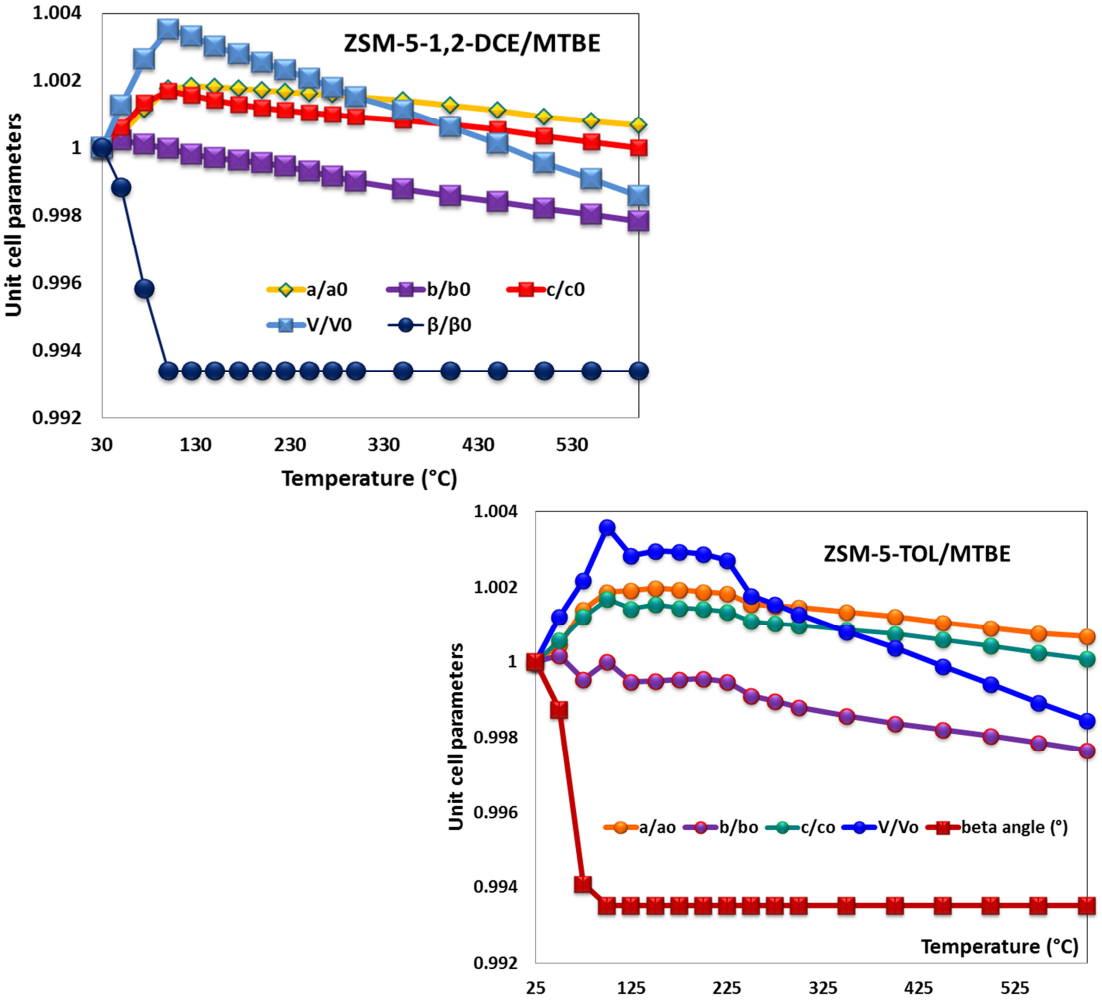

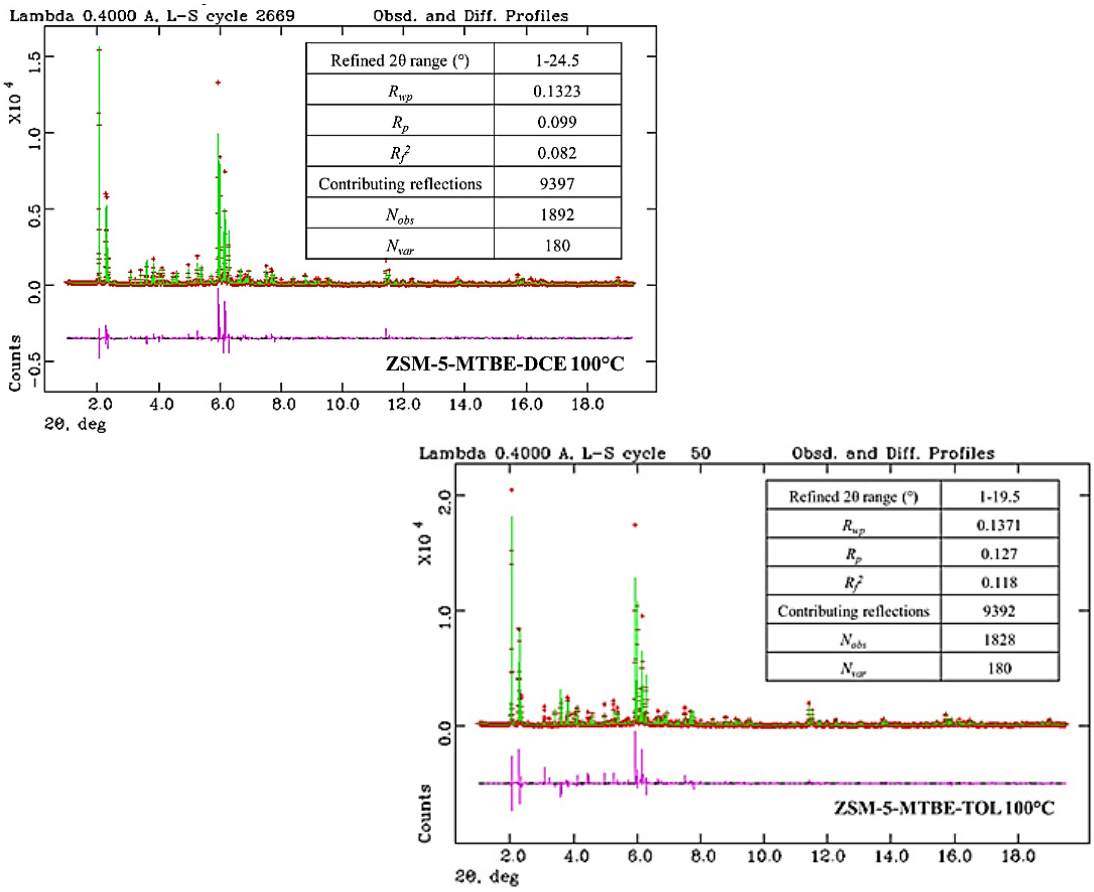

At the same time no changes are observed in extraframework site occupancies (Figure 41), indicating that this transient framework expansion is related to the release of the oligomers-framework oxygens interactions. The weakening of hydrogen bonding network is well known in the zeolite frameworks during the initial heating stages (*e.g.* in hydro-sodalite [176], in analcime [175], in wairakite [174], in silica sodalite [177], cavansite [193]; in ZSM-5-TOL [9], 1,2-DCE and MTBE-loaded [9,11], and in the same as-synthesized-high silica-ZSM-5 [144] used in this dissertation) and it was recently explained by Martucci et al. [8] as a "pore-mouth-breathing motion". This breathing is associated by a transient slight opening and regularization of the apertures, which is followed by a contraction.

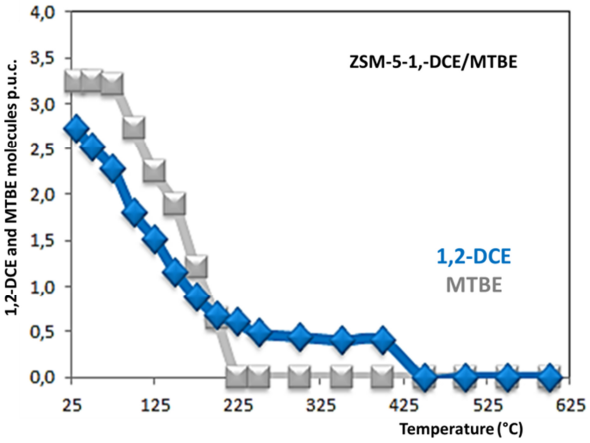

Figure 41. Desorption of host molecules as a function of temperature in ZSM-5-1,2-DCE/MTBE, and ZSM-5-TOL/MTBE, respectively; refinement details of the empty systems are also reported.

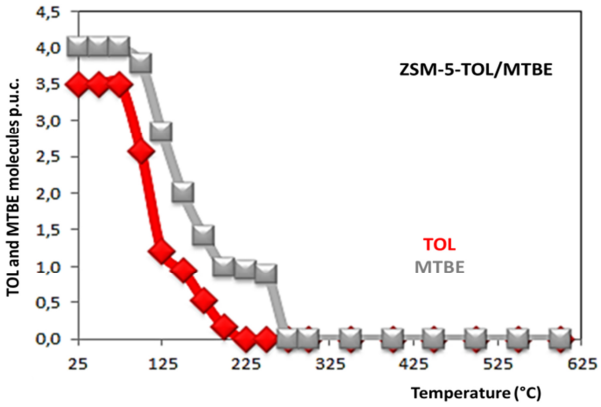

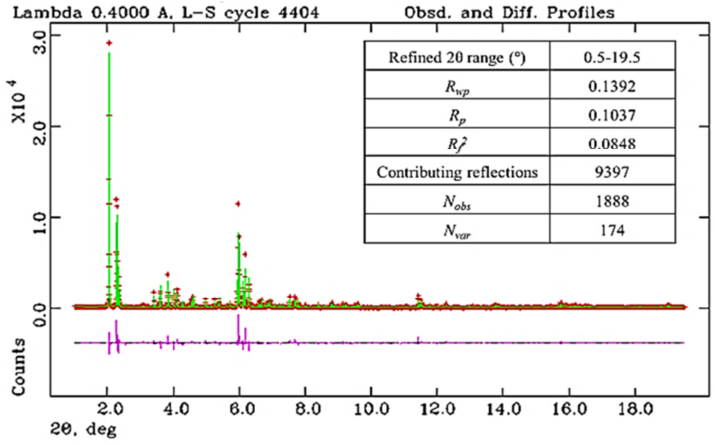

ZSM-5-1,2-DCE/MTBE

400°C

ZSM-5-TOL/MTBE

400°C

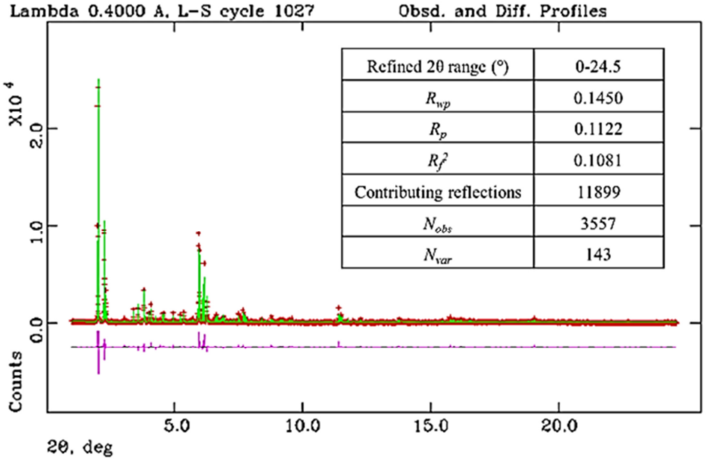

Upon 100°C the gradual overlapping of groups of peaks (Figure 42) reveals the monoclinic $P2_1/n$ to orthorhombic *Pnma* phase transition which was already recently observed in the same unloaded ZSM-5 before [144] and after loading with TOL [9], MTBE [11] and 1,2-DCE [8].

Figure 42. Evolution of powder diffraction patterns of ZSM-5-1,2-DCE/MTBE (a) and ZSM-5-TOL/MTBE (b) respectively, in the 25-100°C temperature range.

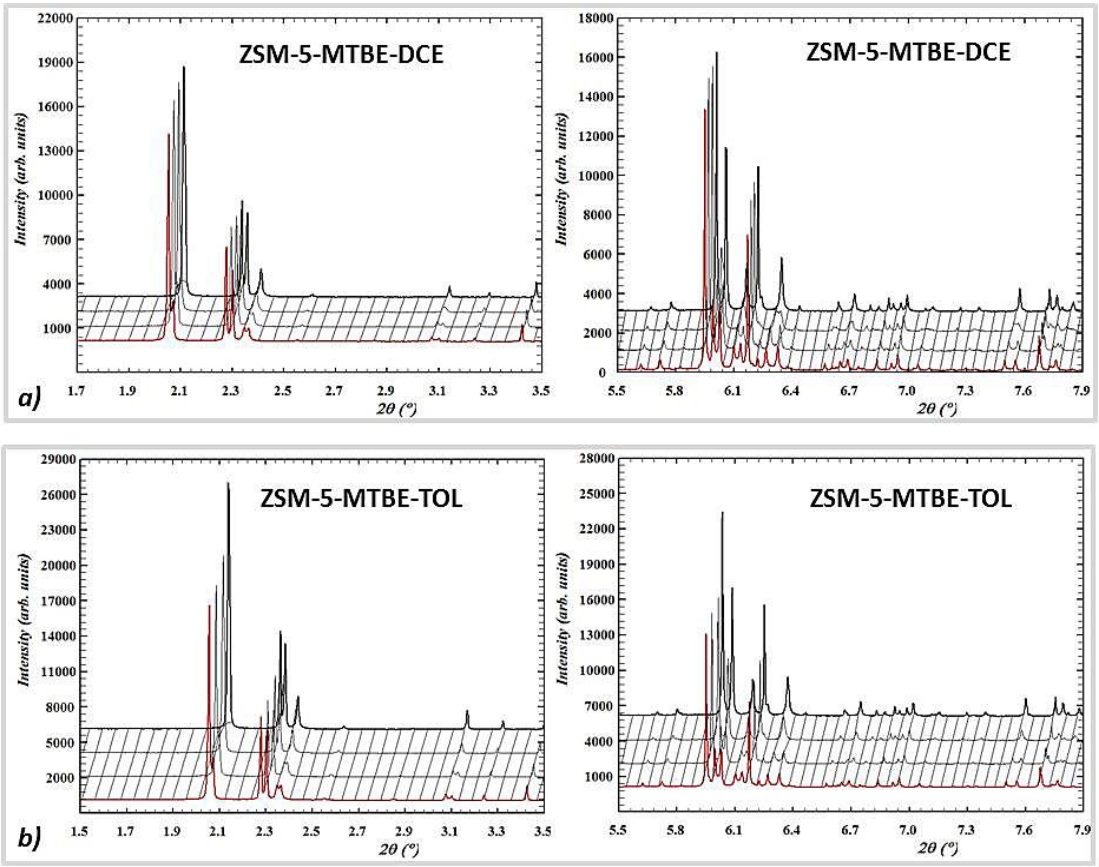

After the phase transition, the unit cell volume decreases and the desorption of the host organic molecules occurs (Figure 40 and Figure 41). Further insights on the sequence of the organics molecules release can be gained following the refined occupancies of the TOL, 1,2-DCE and MTBE sites as a function of temperature plotted in Figure 41. The desorption of TOL and MTBE in both systems starts at about 100°C and continuously proceeds up to ~250°C, then these sites are completely emptied. The onset of 1,2-DCE loss from the 1,2-DCE site also occurs at ~100°C and this site is fully emptied above 350°C. These results revealed that multi-component desorption cannot be predicted from the single component behaviour because it is strongly related to the distribution of host molecules in the zeolite channel systems. The evolution of refined occupancies versus

temperature suggested that species hosted in the ZZ or at the channel intersections, move more slowly than those adsorbed in or near SC, in very good agreement with the experimental adsorption enthalpy data reported below.

As far as concerns water molecules, they are completely released from the cavities at ~ 500°C. Thus, based on the extraframework site occupancy refinements, the T-dependent distortion mechanism in the framework takes place in correspondence with guest organic molecule release. Table 23 reports the C.F.A. of both ZZ and SC channels, as well as the ellipticity of the apertures at temperature, respectively.

Table 23. C.F.A. of both ZZ and SC channels, and ellipticity (ε) of the apertures at 30, 100 and 400 °C, respectively.

ZSM-5 SC-A	**ε**	**C.F.A.**	**ZSM-5 ZZ-A**	**ε**	**C.F.A.**
ZSM-5 [14]	1.03	22.68	ZSM-5 [14]	1.04	21.65
MTBE/1,2-DCE 30°C [56]	1.07	24.16	MTBE/1,2-DCE 30°C [56]	1.05	24.28
MTBE/1,2-DCE 100°C	1.09	23.84	MTBE/1,2-DCE 100°C	1.04	24.06
MTBE/1,2-DCE 400°C	1.08	23.72	MTBE/1,2-DCE 400°C	1.04	24.13
MTBE/TOL 30°C [56]	1.09	24.06	MTBE/TOL 30°C [56]	1.06	24.35
MTBE/TOL 100°C	1.05	23.88	MTBE/TOL 100°C	1.01	23.99
MTBE/TOL 400°C	0.94	23.72	MTBE/TOL 400°C	1	24.10
ZSM-5 SC-B	**ε**	**C.F.A.**	**ZSM-5 ZZ-B**	**ε**	**C.F.A.**
ZSM-5 [14]	1.02	22.68	ZSM-5 [14]	1.06	22.65
MTBE/1,2-DCE 30°C [56]	1.04	23.67	MTBE/1,2-DCE 30°C [56]	1,10	23.15
MTBE/TOL 30°C [56]	1.05	23.59	MTBE/1,2-DCE 100°C	1.07	22.92
			MTBE/1,2-DCE 400°C	1.07	22.81
			MTBE/TOL [56]	1,1	22.95
			MTBE/TOL 100°C	0.93	24.08
			MTBE/TOL 400°C	1.08	24.23

The C.F.A. values smaller than the maximum value (diameter 7.6 Å) for an ideal circular 10-ring channel (C.F.A.= 24.5 $Å^2$) accounts for the cell volume contraction observed upon heating. Above 500°C, the unit-cell volume contraction continues until the end of the heat treatment also without any mass loss giving rise to a NTE process. As already explained in the previous paragraphs, this phenomenon is due to the relaxation during the framework

distortions induced by extraframework molecules diffusing through the framework in the desorbing stage.

The adsorption of TOL on ZSM-5 was investigated at different temperatures. The TOL adsorption isotherms in the low concentration range at four different temperatures (from 5 to 22.5°C) are reported in Figure 43 a. It is seen that the adsorbed quantity is directly proportional to the solution concentration and the proportionality constant is the adsorption constant of TOL from aqueous solutions.

Figure 43. Adsorption isotherms in the low concentration range at four different temperatures (from 5 to 22.5 °C), for TOL (a), MTBE (b) and DCE (c), respectively.

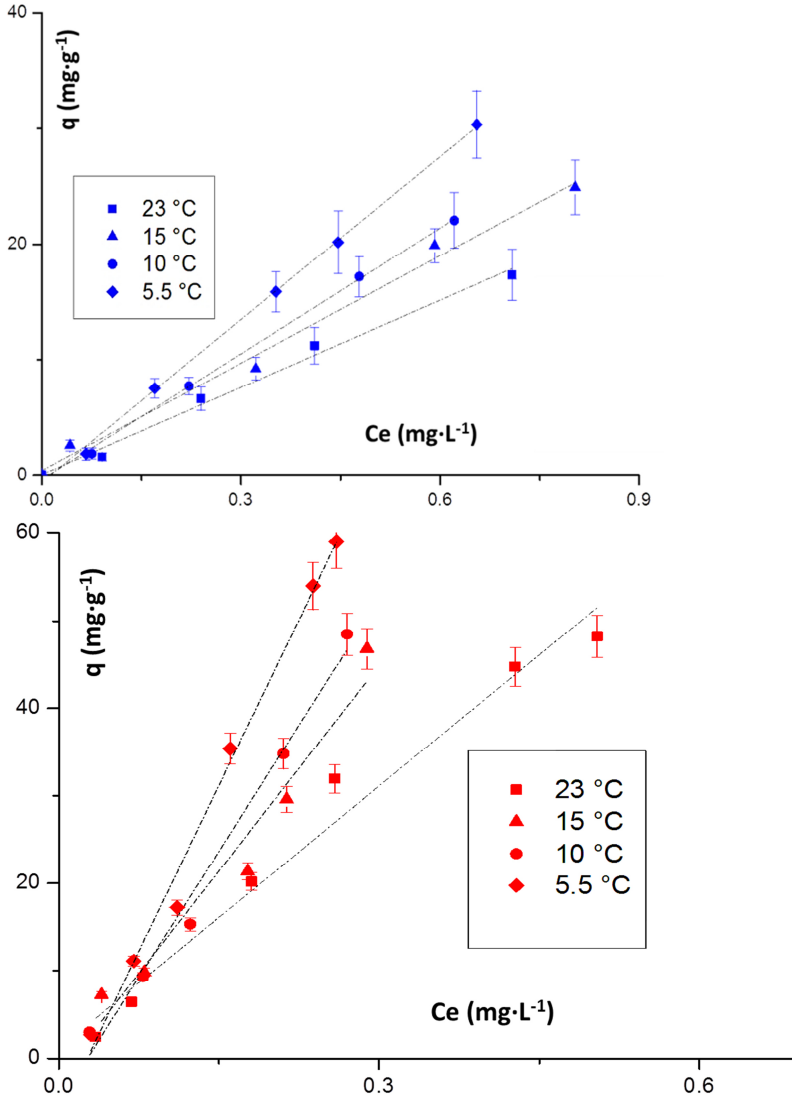

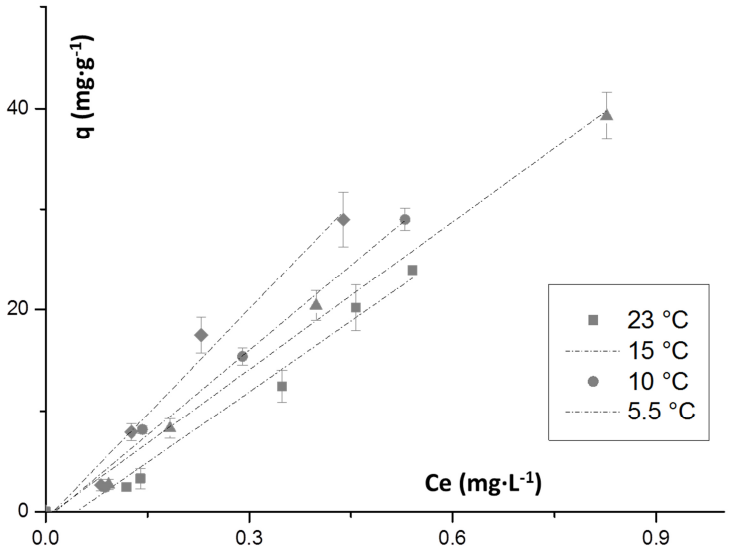

c)

Similar linear behaviour has been observed for the adsorption of diluted aqueous solution of MTBE and 1,2-DCE (Figure 43 b and c respectively). The adsorption constant values differ from those measured from gas phase mixture since the measure value takes into account of the interactions in the solution phase and in the adsorbed phase. Additionally, since K_{ads} from aqueous solution at a range of temperatures are available, we can calculate the enthalpy change associated with transfer of TOL to zeolites from aqueous solutions. According to the van't Hoff equation (Equation 13):

$$ln\left(\frac{K_{ads,2}}{K_{ads,1}}\right) = -\frac{\Delta H}{R}\left(\frac{1}{T_2} - \frac{1}{T_1}\right)$$

Equation 13 - van't Hoff equation

where $K_{ads,2}$ and $K_{ads,1}$ are the equilibrium constants at temperatures T_2 and T_1, respectively, ΔH is the enthalpy change for the process and R is the universal gas constant. The Van't Hoff plot for the ZSM-5-TOL system is shown in Figure 44 a, and by multiplying the slope of the Van't Hoff plot and the gas constant, a ΔH value of -42 kJ mol^{-1} for TOL was obtained (Table 24).

Figure 44. The Van't Hoff plot for the ZSM-5 after TOL (a), MTBE (b) and DCE (c) adsorption, respectively.

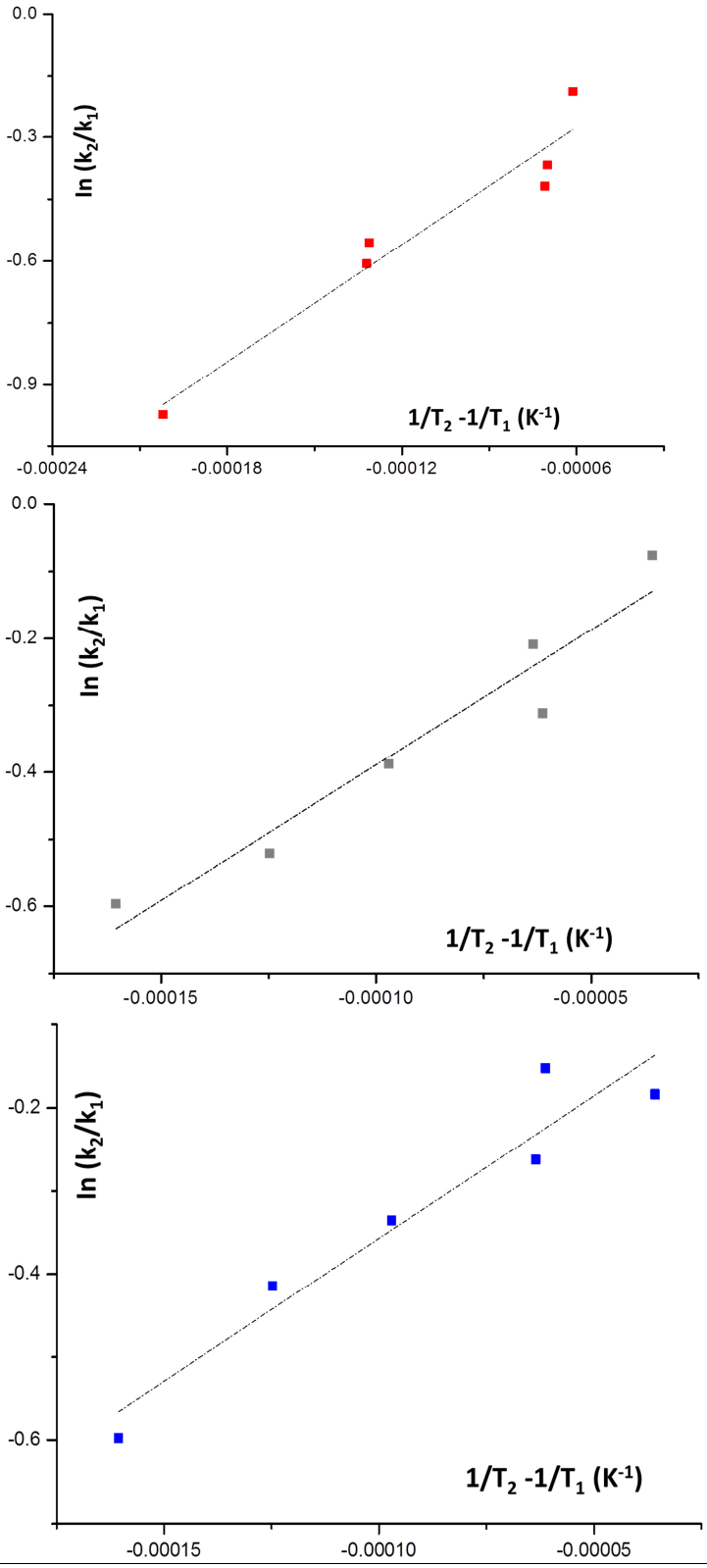

Table 24. ΔH value for ZSM-5 after TOL, MTBE and 1,2-DCE adsorption, respectively.

	MW	Water solubility (g/L)	log Kow	Tb (°C)	ΔH vaporization (kJ mol^{-1})	ΔH mixing (kJ mol^{-1})	ΔH Solvation (kJ mol^{-1})
TOL	92.14	0.52	2.77	110.6	37.3	10.58 0.75 1.8	-32.40
MTBE	88.15	48	1.2	55.2	30	-16.65 -17	-48.70
1,2-DCE	98.95	8.6	1.79	83.5	35.15 35	2.40 (3)	-32.75- 27.9

Analogously, the enthalpy change for 1,2-DCE and MTBE were calculated and the data are reported in Table 25. The adsorption of all of the three investigated compounds on ZSM-5 is exothermic. Therefore, the adsorption constant decreases with the increasing of system temperature.

Table 25. Enthalpy change for ZSM-5 after TOL, MTBE and 1,2-DCE adsorption, respectively.

	ΔH adsorption (g-s) (kJ mol^{-1})	ΔH adsorption (acq sol - s) (kJ mol^{-1})	ΔH adsorption Calc. (kJ mol^{-1})	KH (g-s)	ΔS adsorption (J mol^{-1} K^{-1})
TOL	84.1 100-80 83 86	-42	-78	14.4 mmol g-1 mbar 0.89 10^5 2.35 × 10^6	-140 125
MTBE	90	-38	-84	2 10^-3	
1,2-DCE	50-53	-27	-57	1/0.292	

To compare the experimental data of adsorption enthalpy to that obtained in gas phase system a thermodynamic cycle was considered. The cycle includes: a) removal of the organic compound from the aqueous solution, 2) vaporization of the organic compound, and 3) adsorption of the organic compound in gas phase into the zeolite pores. The enthalpy change corresponding to the immersion of the zeolite into water was neglected

since it is of the order of few mJ·mol^{-1} as reported in [194]. Therefore, the adsorption process of the organic from aqueous solution can be divided up as follow (Equation 14):

$$\Delta H_{ads,g} = \Delta H_{ads,aq} + \Delta H_{mix} + \Delta H_{vap}$$

Equation 14 - Enthalpy calculated from the aqueous adsorption isotherms

where $\Delta H_{ads,aq}$ is the enthalpy calculated from the aqueous adsorption isotherms, ΔH_{mix} is the partial molar heat of mixing, and ΔH_{vap} is the heat of vaporization. The enthalpies data available from literature are reported in Table 25. By substituting the data of Table 24 and Table 25 into Equation 14 the calculated adsorption enthalpy from gas phase into ZSM-5 were comparable to those experimentally obtained in previous works [194]. Additionally, the process entropy change (ΔS) can be calculated for each temperature by (Equation 15):

$$\ln K_{ads,aq} = \Delta H_{ads,aq} - T\Delta S_{ads,aq}$$

Equation 15 - Process entropy change

The values obtained are -82 and -72.4 and -57 J mol^{-1} K^{-1} for TOL, MTBE and 1,2-DCE respectively. The negative ΔS indicates that the degrees of freedom decrease during the adsorption process. By comparing the adsorption enthalpy of the three investigated compounds the more strongly adsorbed species is TOL. This finding seems to be in contrast to the order of the sequence of the organics molecules release observed by XRPD Rietveld analysis. In fact, TOL is released at lower temperature than 1,2-DCE possibly indicating a lower energy binding. However, this apparent data mismatch is not unusual for MFI zeolite. In fact, it has already reported a similar behaviour for the hexane isomers in MFI zeolite, also in this case the more strongly adsorbed species nC6 is more mobile in the structure with respect to the less strongly adsorbed species 2-methylpentane. This result confirms that the opposite order between strength of the adsorption interactions and mobility is mainly due to configurational entropy effects of the molecules inside the framework. This hypothesis is further confirmed by comparing the release of 1,2-DCE from MFI [8] in which it can be seen that the mobility of 1,2-DCE in the straight channel is higher than that close to the intersection. Figure 45 shows the discrete numerically differentiation of the data of Figure 41, which can be qualitatively employed to enhance differences in the thermal desorption process.

Figure 45. Temperature programmed desorption spectra and the DTG peaks of ZSM-5-MTBE-TOL and ZSM-5-MTBE-DCE.

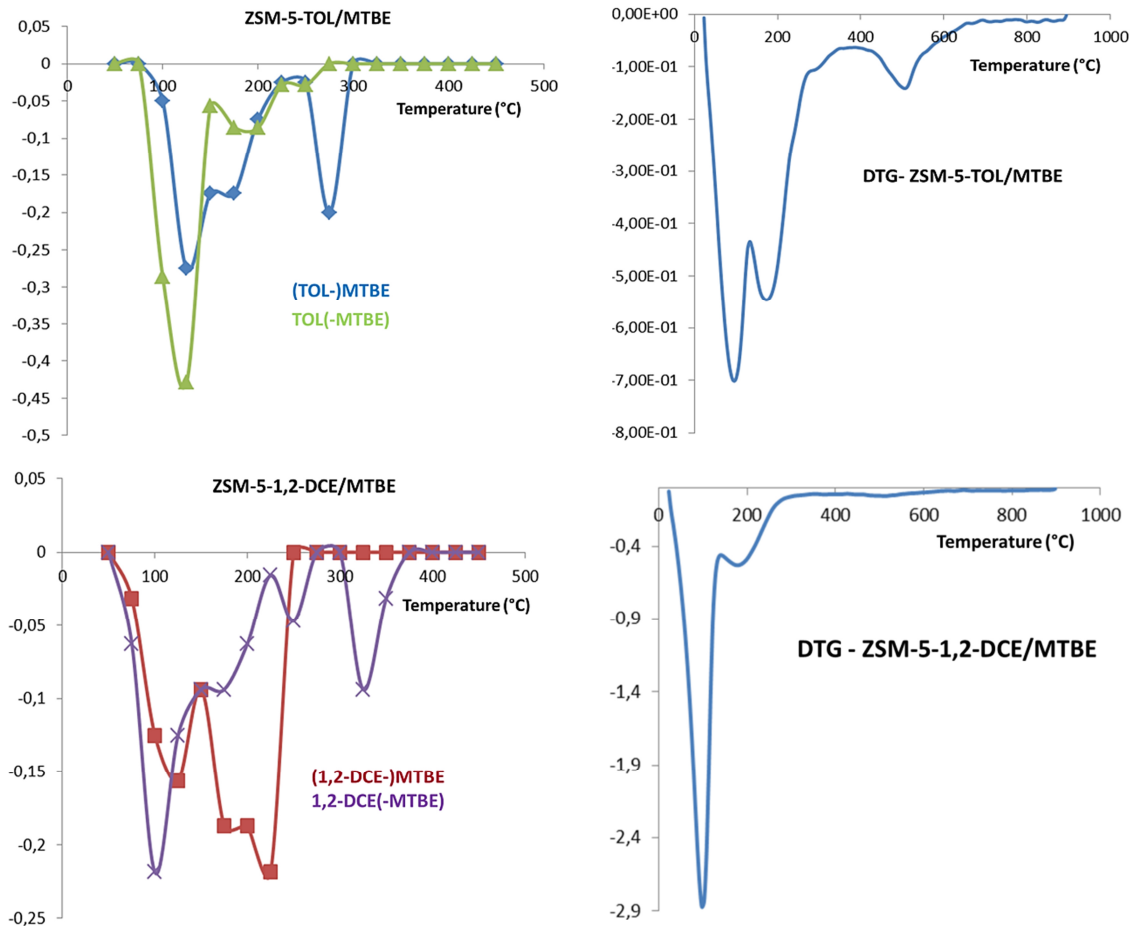

Figure 45 shows that in general two peaks are present and the second one located at higher temperature is more pronounced for compound principally adsorbed in the site close to the intersection. This behaviour is similar to those observed in thermal programmed desorption experiments of aromatic compounds from ZSM-5 [195]. It has been reported that for n-hexane and TOL the two sites inside the ZSM-5 framework, exhibit enthalpy variations that are very close, therefore the interaction energies are very similar. This finding is consistent with earlier interpretation of adsorbed molecules at high coverage reported by Sastre et al. [196] and Corma et al. [197] and also with our previous results in which a single site Langmuir model was found to be able to describe the adsorption isotherm of the single compounds located in two different sites. On the contrary, it was found that the entropy variations are very different, as revealed from studies on the transport process of the desorbed molecules within the zeolites during the desorption process. Strong

similarities between the desorption profiles observed in temperature programmed desorption spectrum and the DTG peaks reported in Figure 45 confirmed this hypothesis.

Therefore, a detailed study of the real evolution of the ZSM-5-loaded structure during the heating is presented, including a detailed analysis of the entropy variations during the temperature-induced-desorption process. The physical description allowed us to continuously monitor the kinetics and dynamic behaviour of this adsorbent medium during thermal regeneration. The evolution of refined occupancies as a function of temperature suggested that the kinetics of host MTBE molecules desorption is different in the TOL/MTBE and 1,2-DCE/MTBE mixtures, due to the different location of MTBE inside the ZSM-5 structure when adsorbed from the two binary solutions [56]. The hypothesis was confirmed by the negative ΔS values indicates that the degrees of freedom decrease during the adsorption process. The information obtained from structural refinement was employed for interpretation of competitive adsorption data. To the best of our knowledge this is one of first works showing the correlation between microscopic XRPD molecular information and macroscopic adsorption experimental data for binary mixtures.

SECTION IV:

Adsorption behaviour of regenerated ZSM-5

As reported by several recent scientific works [48,199–201] exhausted zeolites can be easily thermally regenerated after organics adsorption at low cost without changing their initial adsorption properties. The results reported in the previous section about the behaviour of ZSM-5 during the thermal treatment highlight that ZSM-5 can be regenerated without crystallinity loss or strong deformation of channels shape and dimension. In this section the adsorption capacity of ZSM-5 after regeneration process is tested in order to verify that the reactivated material can be reused to remove emerging organic contaminants from wastewater.

3.11. Adsorption behaviour of regenerated ZSM-5 reloaded with 1,2-DCE and TOL

The regeneration of ZSM-5 loaded with 1,2-DCE was conducted by HT calcination using the TG/DTA thermogravimetric analyzer operating at 5°C/min heating rate from room temperature to 600°C for completely burning off the organics. After regeneration, the XRPD pattern (ZSM-5-r) was collected and then indexed on a monoclinic unit cell that is consistent with that also observed for the unloaded material. According to Leardini et al. [48] the splitting of (131) and (133) peaks reveals the reversibility of the orthorhombic P*nma* to monoclinic P$2_1/n$ to phase transition. Figure 46 shows that after regeneration the diffraction peaks are very sharp, indicating that ZSM-5 retain its original crystallinity upon heating [8].

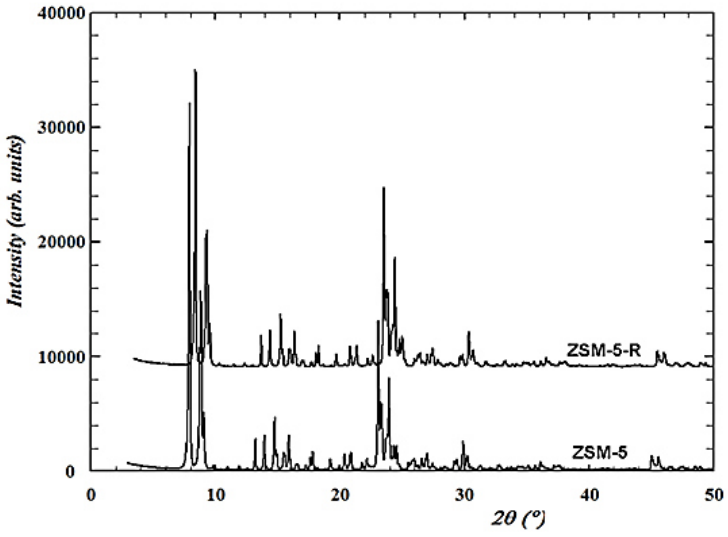

Figure 46. Powder diffraction patterns of ZSM-5 (unloaded) and ZSM-5-R (regenerated), respectively (the stacked plots have been shifted for easy comparison) [8].

Moreover, XRPD analysis demonstrates that the regenerated and reloaded zeolite perfectly regains the unit-cell parameters of fresh material (Table 26).

Table 26. Regenerated and 1,2-DCE reloaded ZSM-5 lattice parameters. Lattice parameters of unload ZSM-5 and after the first cycle of 1,2-DCE adsorption are also reported to comparison [8].

	ZSM-5			
	Unloaded [14]	1,2-DCE [8]	Regenerated [8]	Regenerated and Reloaded [8]
Space group	$P2_1/n$	$P2_1/n$	$P2_1/n$	$P2_1/n$
***a* (Å)**	19.8999(5)	19.9052(3)	19.8935(5)	19.8954(5)
***b* (Å)**	20.1174(6)	20.1199(3)	20.1165(5)	20.1177(5)
***c* (Å)**	13.3892(4)	13.3909(2)	13.3818(4)	13.3835(4)
***β* (°)**	90.546(3)	90.578(1)	90.559(2)	90.565(1)
***V* (Å^3)**	5359.9(3)	5362.7(1)	5354.9(2)	5356.5(1)

The regeneration/adsorption process also occurs without any significant deformations in the channel apertures (

Table 27). The refined atomic fractional coordinates obtained by the Rietveld method indicates minor differences in both the 1,2-DCE location (Figure 47 a and b).

Table 27 Dimensions (Å) of the apertures of unload ZSM-5, after thermal regeneration, after 1,2-DCE adsorption and for regenerated and reloaded sample.

	ZSM-5			
SC-A	Unloaded [14]	Regenerated [8]	Loaded [8]	Regenerated and reloaded [8]
O7-O1	7.98(1)	7.96(1)	8.21(1)	8.40(1)
O8-O2	8.08(1)	8.00(1)	8.11(1)	7.97(1)
O31-O37	8.20(1)	8.00(1)	8.28(1)	8.01(1)
O44-O46	8.19(1)	8.28(1)	8.63(1)	8.72(1)
O47-O48	7.93(1)	7.80(1)	7.96(1)	7.95(1)
C.F.A.	22.68	22.16	24.14	23.88
ε	1.03	1.06	1.08	1.10

	ZSM-5			
SC-A	Unloaded [14]	Regenerated [8]	Loaded [8]	Regenerated and reloaded [8]
O11_O5	8.23(1)	8.19(1)	8.15(1)	8.19(1)
O20_O18	8.21(1)	8.19(1)	8.49(1)	8.33(1)
O21_O22	8.04(1)	8.02(1)	8.01(1)	7.98(1)
O27_O33	8.03(1)	7.95(1)	8.38(1)	8.31(1)
O28_O34	8.07(1)	7.86(1)	7.081(1)	8.00(1)
C.F.A.	22.68	22.45	23.51	23.47
ε	1.02	1.04	1.08	1.04

	ZSM-5			
ZZ-B	Unloaded [14]	Regenerated [8]	Loaded [8]	Regenerated and reloaded [8]
O17-O18	7.81(1)	7.59(1)	7.71(1)	7.59(1)
O23-O25	8.20(1)	8.11(1)	8.49(1)	8.54(1)
O30-O5	8.31(1)	8.26(1)	8.59(1)	8.31(1)
O31-O4	7.91(1)	7.63(1)	7.64(1)	7.69(1)
O44-O43	8.13(1)	8.07(1)	8.18(1)	8.29(1)
C.F.A.	22.65	21.51	23.12	22.80
ε	1.06	1.08	1.12	1.12

	ZSM-5			
ZZ-A	Unloaded [14]	Regenerated [8]	Loaded [8]	Regenerated and reloaded [8]
O20-O15	7.95(1)	7.90(1)	8.28(1)	8.38(1)
O24-O26	7.84(1)	7.77(1)	8.26(1)	8.24(1)
O27-O2	7.85(1)	7.89(1)	8.16(1)	7.95(1)
O28-O1	7.90(1)	7.83(1)	7.96(1)	8.13(1)
O41-O46	8.22(1)	8.29(1)	8.68(1)	8.57(1)
C.F.A.	21.65	21.54	24.37	24.24
ε	1.04	1.06	1.09	1.08

Figure 47. Location of 1,2-DCE and water molecules in ZSM-5 at 30°C (a) and after regeneration and reloaded with 1,2-DCE (b), respectively [8]; refinement details of regenerated and regenerated-reloaded ZSM-5 are also reported.

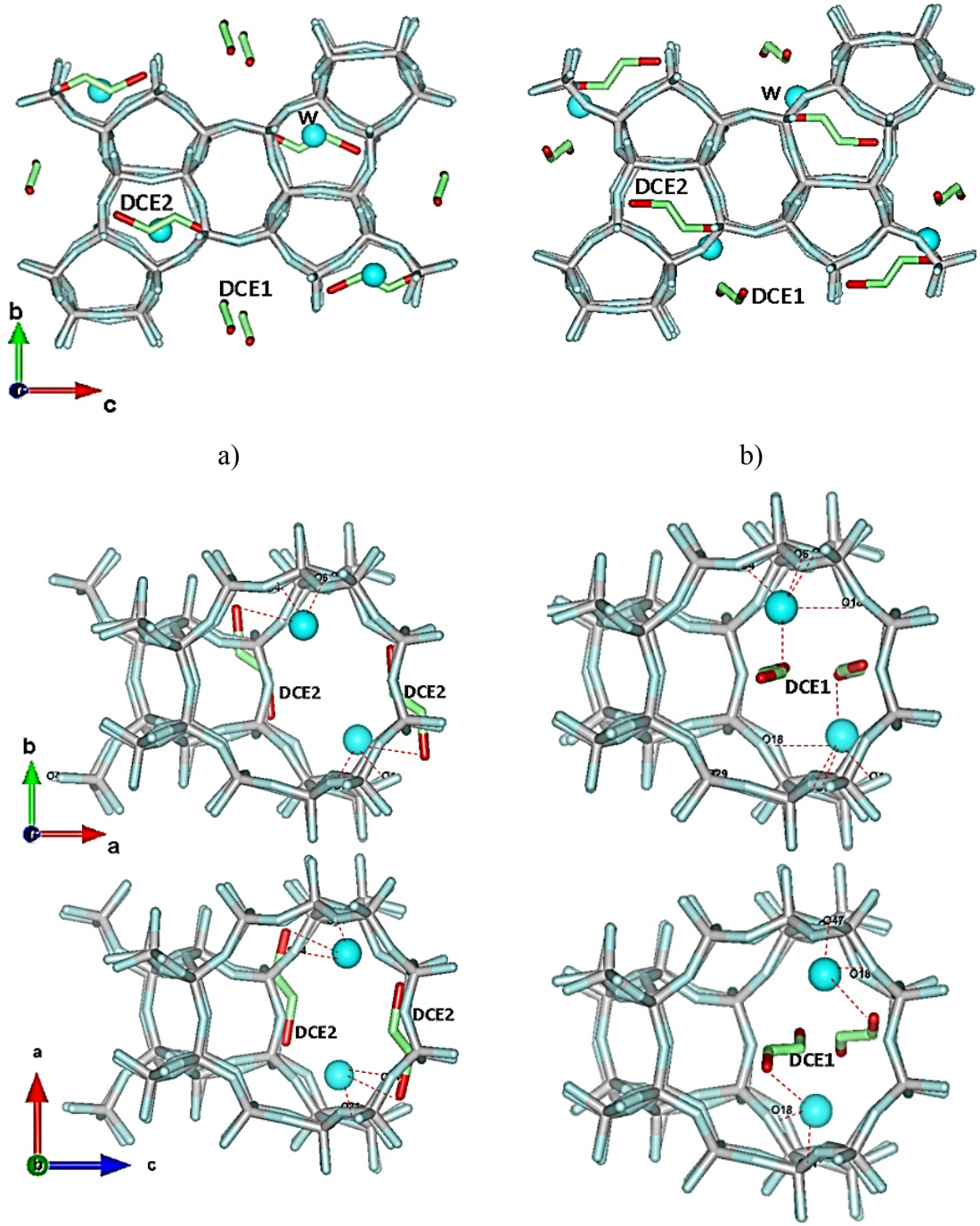

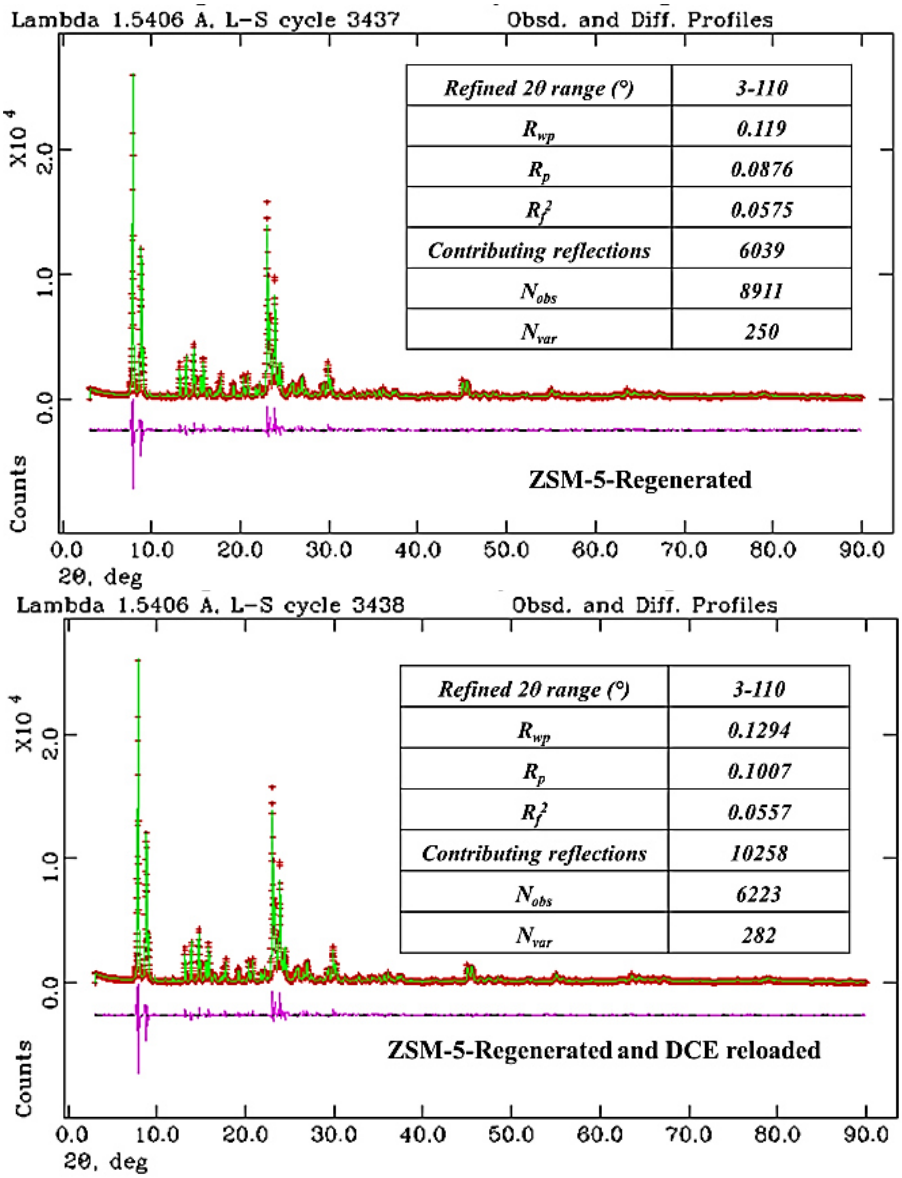

On the basis of the occupancies (Table 28), Rietveld refinements of ZSM-5 regenerated and reloaded (Figure 47) indicate that the organic content remains substantially unchanged thus confirming that, after regeneration, ZSM-5 is able to re-adsorb 1,2-DCE in amounts comparable to that adsorbed in the first cycle [8]. The occurrence of 1,2-DCE-water molecule complexes (clusters or short chains) bridged via W to framework oxygen atoms (Figure 47) was also confirmed. On the whole, ~ 6.6/p.u.c. 1,2-DCE molecules (corresponding to ~ 10.3% in weight) and ~ 5H_2O/p.u.c, (corresponding to ~ 1.5% in weight) were re-adsorbed in the channels systems, in very good agreement with the weight loss reported on the basis of thermal analysis (Figure 48).

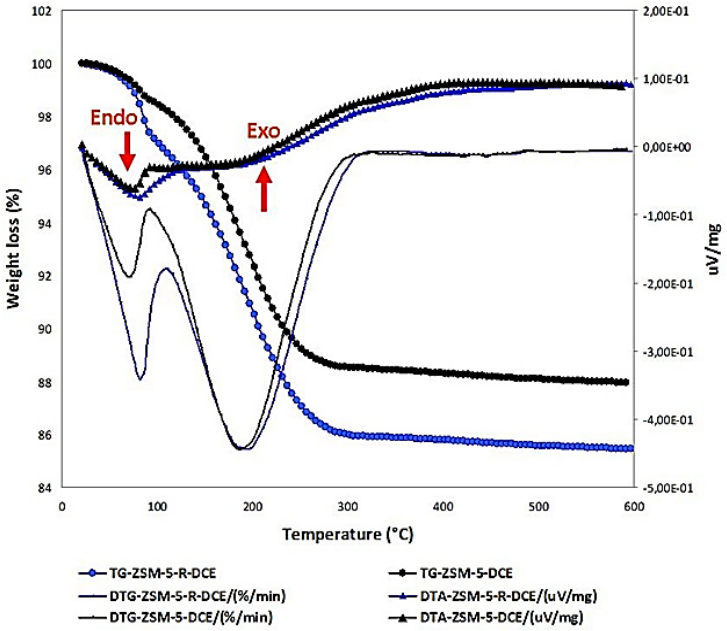

Figure 48. TG, DTG, and DTA curves in ZSM-5-1,2-DCE and ZSM-5-R-1,2-DCE dry air atmosphere [8].

Table 28. Extraframework coordinates of ZSM-5 after 1,2-DCE adsorption and after regeneration and reload with 1,2-DCE [8].

	ZSM-5-1,2-DCE-30				ZSM-5 REGENERATED AND 1,2-DCE RELOADED				
	x/a	y/b	z/c	Fraction		x/a	y/b	z/c	Fraction
1,2-DCE 1 sites									
C1	0.772(1)	0.468(8)	0.060(5)	0.85(1)	C1	0.782(3)	0.427(11)	0.101(1)	0.73(1)
C11	0.686(1)	0.470(3)	0.069(2)	0.85(1)	C11	0.697(1)	0.423(4)	0.079(5)	0.73(1)
Cl2	0.893(1)	0.484(2)	-0.029(2)	0.85(1)	Cl2	0.825(3)	0.466(11)	0.050(1)	0.73(1)
C2	0.807(1)	0.487(8)	-0.020(5)	0.85(1)	C2	0.908(1)	0.477(3)	0.081(3)	0.73(1)
1,2-DCE 2 sites									
C3	0.748(8)	0.796(1)	0.170(2)	0,76(1)	C3	0.736(11)	0.803(4)	0.111(2)	0.77(1)
Cl3	0.739(2)	0.720(1)	0.115(2)	0,76(1)	Cl3	0.707(3)	0.722(2)	0.107(3)	0.77(1)
C4	0.747(9)	0.855(1)	0.121(2)	0,76(1)	C4	0.739(11)	0.840(4)	0.195(4)	0.77(1)
Cl4	0.75(3)	0.931(1)	0.177(2)	0,76(1)	Cl4	0.770(3)	0.922(2)	0.195(3)	0.77(1)
W sites									
W	0.638(5)	0.319(4)	0.329(6)	0.77(5)	W	0.821(5)	0.913(5)	0.283(6)	0.75(2)

These results are in good agreement with the adsorption isotherms. Figure 49 shows the comparison of the adsorption performance of fresh and regenerated zeolite. The regenerated sample from air calcination produced slightly higher adsorption in the low concentration range than the fresh one as shown in the inset of Figure 49. Possibly, this is due to the decomposition of the low amount of NH_4 in the starting material. This result perfectly agrees with the weight loss estimated on the basis of thermal analyses (weight loss ~ 14.5%) reported in Figure 48, which is slightly higher than that observed in ZSM-5-1,2-DCE (12.0% in weight).

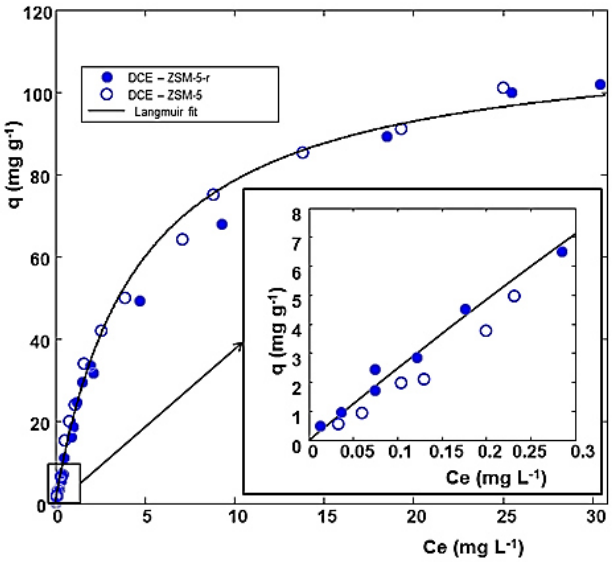

Figure 49. Adsorption isotherms of 1,2-DCE on fresh (ZSM-5) and thermally regenerated (ZSM-5-r) zeolites. The data obtained on the low concentration range are enlarged in the inset [8].

The adsorption data were fitted by using a Langmuir equation (Equation 16, Table 29) and the parameters found for the adsorption of 1,2-DCE on regenerated material were not statistically different to those charactering the fresh material reported in Pasti et al. [14].

Table 29. Fitting Results of the adsorption data of 1,2-DCE on regenerated zeolite. The fitting parameters are reported together with the confidence limits calculated at 95% of probability [8].

Organic -Zeolite	**Equation 16 – Langmuir equation**	**Parameters**		R^2
1,2-DCE-ZSM-5-r	$q = \frac{q_s K_L C_e}{1 + K_L C_e}$	K_L (L mg^{-1})	q_s (mg g^{-1})	0.9925
		0.20	117	
		(0.17, 0.23)	(111, 123)	

ZSM-5 was also tested for TOL re-adsorption under a solution concentration enabling zeolite saturation. The adsorption/desorption cycle was repeated twice on the same material. Figure 50 b, reports the comparison of fresh and regenerated zeolite adsorption capacities. It is clearly shown that the saturation capacity of the regenerated sample after air calcination does not significantly differ from fresh material.

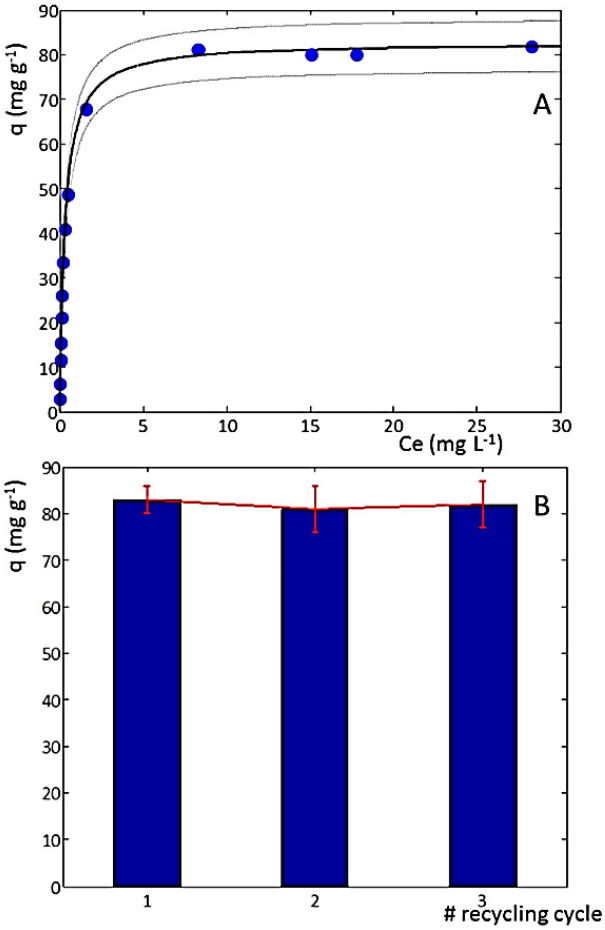

Figure 50 a) Isotherm for TOL adsorption onto ZSM-5; b) Pseudo second order kinetics constant vs. TOL saturation capacity on ZSM-5 after thermal regeneration [9].

Therefore, these results suggest that the regenerated ZSM-5 behaves as an adsorbent with undiminished adsorption capacity and opens up the possibility for a re-use of such material with clear benefits on the cost/performance ratio of the whole water treatment process. How many cycles the ZSM-5 can withstand towards organics adsorption will be matter of future investigation.

4.Concluding remarks

In this work, an exhaustive picture on the adsorption and desorption both as single component as well as binary mixture of VOCs within the ZSM-5 crystal lattice (*i.e.*, a microporous MFI material) have been provided by using the information gained from structural refinements as input of the isotherm modelling step in order to provide a physical description of the model. Four representative water contaminants, *i.e.*, 1,2-DCE, TOL, MTBE, and CB, have been selected among VOCs molecules as samples to be tested.

To start with, the adsorption from aqueous solutions of systems based on a single component as well as binary mixtures has been investigated by means of the batch adsorption method. Adsorption kinetics and adsorption isotherms provide an overview on the effectiveness of the VOCs adsorption within the ZSM-5 structure as well as an exhaustive picture on the VOCs dynamic adsorption.

Therefore, XRPD on the previously analyzed powders has been performed using both conventional and non-conventional X-ray radiations. These data, performed by means of the Rietveld method, corroborate those from adsorption techniques, and clearly reveal the incorporation of the investigated contaminants. In particular, structural refinements highlight that, in all the examined cases, organic molecules are adsorbed into two independent crystallographic sites. These sites are located at the intersection (*i.e.*, of straight and sinusoidal channels) and within the sinusoidal channel, namely site 1 and site 2, respectively. Besides, co-adsorbed water molecules are also detected. A small fraction of adsorbed water plays an important role in stabilizing the guest organic molecules within the zeolite host framework. The refined distances reveal strong interactions between organic compound–water molecule complexes (clusters or short chains) and the framework oxygen atoms. This evidence is also confirmed by the deformation of 10-ring tetrahedral channels opening after organics compound adsorption and explains the variation of lattice parameters.

All these findings indicate that ZSM-5 is a flexible material able to efficiently adsorb fuel-based compounds in its internal channels system. This adsorption can be conceived as an irreversible adsorption at ambient conditions. However, it is possible to induce the desorption of the adsorbed species, and completely regenerate the exhausted (*i.e.*, loaded with organic contaminants) ZSM-5, by heating. To achieve a complete understanding of the regeneration process, the desorption dynamics that occur during the thermal treatment have been investigated.

The *in situ* HT XRPD, performed at the beamline ID22 (ESRF Grenoble), has been used in order to continuously monitor the pollutants desorption process as well as the structural modifications which the ZSM-5 undergoes upon thermal treatment. The evolution of a series of diffraction patterns as function of temperature shows the occurrence of a phase transition in each loaded samples. In particular, it has been observed that the phase transition temperature is function of the involved contaminant species. In all the examined samples, Rietveld refinements indicate that the ZSM-5 phase transition occurs within the 75–100°C temperature range involving a symmetry change from monoclinic (space group $P2_1/n$) to orthorhombic (*Pnma* or $P2_12_12_1$ space group). After the adsorption of a single compound or binary mixtures, a careful inspection on the unit-cell parameters variation reveals that, up to 100ºC, the unit-cell volume slightly increases. At the same time, no changes are observed in the extraframework site occupancies indicating that this transient framework expansion is related to the release of the oligomers-framework oxygens interactions. It is well known that, during the initial heating stages, a weakening of hydrogen bonding network occurs in the zeolite frameworks, and it can be explained as a "pore-mouth-breathing" motion. This motion is accompanied by a transient opening and regularization of the zeolite channels, and afterward by a contraction. For temperatures higher than 100 °C, and after each phase transition, the unit-cell volume decreases and the hosted organic molecules start to desorb. The expulsion process is accompanied by a diffusion of the host molecules through the zeolite channels system. As a general trend, it has been observed that the site 1 (intersection site) is empty in the 250–300°C temperature range. Differently, the molecules confined at site 2 (sinusoidal channel) show a more scattered desorption process. Anyway, the maximum desorption temperature observed for site 2 is about 350°C. In the case of a site 2 desorption temperature higher than that of site 1, a blocking effect can be invoked. Specifically, the species hosted at the sinusoidal channel (site 2) move more slowly than those adsorbed at the intersection (site 1). When a multi-component system (binary mixtures) is involved, the desorption temperature of organic molecules for both sites 1 and 2 can be inferred from that of a zeolite which hosts a single component.

Once regenerated (thermally treated), some of the investigated zeolite samples (*i.e.*, those with 1,2-DCE and TOL as single components) are tested again in order to verify whether these reactivated materials can be reused to remove emerging organic contaminants from wastewater. With this purpose, the regenerated samples of ZSM-5 are subjected to new VOCs adsorption cycles. The regenerated ZSM-5 reloaded with 1,2-DCE

does not show any significant difference in the saturation capacity. Besides, the regenerated zeolite does not exhibit any crystallinity loss or deformations in the channel apertures, and possesses unit-cell parameters that can be almost overlapped with those of the fresh material. The refined occupancies obtained by the Rietveld method indicate that both location and content of 1,2-DCE molecules remain substantially unchanged. Hence, it is confirmed that, after regeneration, ZSM-5 is able to re-adsorb an amount of 1,2-DCE comparable to that previously adsorbed by the fresh material. The same behaviour has been also observed when the regenerated ZSM-5 was reloaded with TOL. These results highlight that ZSM-5 zeolite is a very promising adsorbent material with unchanged adsorption performances even after several adsorption/desorption cycles. The achieved deeper understanding of the adsorption/desorption behaviour of ZSM-5 is of great help in the optimization of water remediation technologies like PRBs using zeolites as "molecular sieve" adsorbing materials to remove fuels-based pollutants from water.

Additionally, the competitive aspect has been also evaluated. For example, the adsorption isotherms of CB and TOL as a single component in ZSM-5 show very similar trends. The evaluation of their competitive behaviour when adsorbed as binary mixture (CB/TOL) reveals a very similar competitive Langmuir isotherm, meaning that both TOL and CB have similar saturation capacity and affinity for the ZSM-5 zeolite. On the contrary, a different behaviour emerges whether the adsorption isotherms of single components differ one from each other. In the specific case of binary mixtures formed by MTBE/1,2-DCE and MTBE/TOL, it has been highlighted that, albeit both components are adsorbed, the loading of a second organic molecule tends to expel the first one adsorbed. Since the Rietveld structural investigation provides information on the relative position of molecules inside the ZSM-5 structure, the adsorption data of equimolar binary mixtures have been fitted to a Langmuir model based on the results obtained from these refinements. The short refined intermolecular distances among adsorption sites clearly prevents the simultaneous occupancy of one site by more than one component, when these compounds are adsorbed from binary mixtures. The complementary approach above described, *i.e.*, the integration of structural information with thermodynamic equilibrium data, allows to obtain an excellent model to realistically describe the adsorption process and it is helpful in interpreting the adsorption mechanisms.

Finally, adsorption studies of VOCs were also performed to provide insights on the zeolite selectivity during removal processes. A competitive behaviour was observed when the mixture involves VOCs and humic monomers, *e.g.*, CA and p-HBA. Rietveld

refinements indicate that humic monomers and VOCs occupy a similar position. Consequently, the VOCs adsorption capacities and/or adsorption kinetics could be reduced in the presence of these monomers. However, as demonstrated by adsorption isotherms, ZSM-5 zeolite adsorbs preferentially and selectively VOCs. For this reason, it can be assumed that ZSM-5 zeolite is suitable for the treatment of groundwater and wastewater also in presence of humic monomers.

In conclusion, in this dissertation the combination of *in situ* HT synchrotron XRPD and chromatographic techniques has been employed to explore the adsorption features of a ZSM-5 zeolite. In particular, it has been observed that this material is characterized by very favorable adsorption kinetics as well as a strong shape selectivity towards organic molecules. Moreover, this material can be efficiently regenerated at about 350°C without any significant difference in the saturation capacity and without any significant crystallinity loss. Furthermore, the absence of humic substances interference has been demonstrated.

References

[1] B. W. M. Raghav, S. Eden, K. Mitchell, "Contaminants of Emerging Concern in Water," *Publ. Water Resour. Res. Cent.*, pp. 1–12, 2013.

[2] C. Perego, R. Bagatin, M. Tagliabue, and R. Vignola, "Zeolites and related mesoporous materials for multi-talented environmental solutions," *Microporous Mesoporous Mater.*, vol. 166, pp. 37–49, 2013.

[3] A. J. D. P. Jones Lepp, T. D. A. Alvarez, C. R. Casey, "Monitoring of waterways for emerging contaminants using integrative sampling coupled with liquid chromatography-electrospray/mass spectrometry," 2004. [Online]. Available: https://cfpub.epa.gov/si/si_public_record_report.cfm?dirEntryId=75034.

[4] A. R. Gavaskar, B. C. Kim, S. H. Rosansky, S. K. Ong, K. Ave, and E. G. Marchand, "Crossflow Air Stripping and Catalytic Oxidation of Chlorinated Hydrocarbons from Groundwater," *Environ. Prog.*., vol. 14, no. 1, pp. 33–40, 1995.

[5] A. Dabrowski, "Adsorption - From theory to practice," *Adv. Colloid Interface Sci.*, vol. 93, no. 1–3, pp. 135–224, 2001.

[6] I. Ali, M. Asim, and T. A. Khan, "Low cost adsorbents for the removal of organic pollutants from wastewater," *J. Environ. Manage.*, vol. 113, pp. 170–183, 2012.

[7] E. Katsou, S. Malamis, M. Tzanoudaki, K. J. Haralambous, and M. Loizidou, "Regeneration of natural zeolite polluted by lead and zinc in wastewater treatment systems," *J. Hazard. Mater.*, vol. 189, no. 3, pp. 773–786, 2011.

[8] A. Martucci, E. Rodeghero, L. Pasti, V. Bosi, and G. Cruciani, "Adsorption of 1,2-dichloroethane on ZSM-5 and desorption dynamics by in situ synchrotron powder X-ray diffraction," *Microporous Mesoporous Mater.*, vol. 215, pp. 175–182, 2015.

[9] E. Rodeghero, A. Martucci, G. Cruciani, R. Bagatin, E. Sarti, V. Bosi, L. Pasti, "Kinetics and dynamic behaviour of toluene desorption from ZSM-5 using in situ high-temperature synchrotron powder X-ray diffraction and chromatographic techniques," *Catal. Today*, vol. 277, pp. 118–125, 2016.

[10] F. E. Ahmed, "Toxicology and human health effects following exposure to oxygenated or reformulated gasoline," *Toxicol. Lett.*, vol. 123, no. 2–3, pp. 89–113, 2001.

[11] E. Rodeghero, L. Pasti, E. Sarti, G. Cruciani, R. Bagatin, and A. Martucci, "Temperature-Induced Desorption of Methyl tert-Butyl Ether Confined on ZSM-5: An In Situ Synchrotron XRD Powder Diffraction Study," *Minerals*, vol. 7, no. 3, p. 34, 2017.

[12] S. J. Lawrence, D. Registry, and H. Services, "Description , Properties , and Degradation of Selected Volatile Organic Compounds Detected in Ground Water — A Review of Selected Literature," 2006.

[13] H. E. L. Brown, L. Theodore, *Chemistry: The central science*. Prentice Hall, 1988.

[14] L. Pasti, A. Martucci, M. Nassi, A. Cavazzini, A. Alberti, and R. Bagatin, "The role of water in DCE adsorption from aqueous solutions onto hydrophobic zeolites," *Microporous Mesoporous Mater.*, vol. 160, pp. 182–193, 2012.

[15] B. Huang, C. Lei, C. Wei, and G. Zeng, "Chlorinated volatile organic compounds (Cl-VOCs) in environment - sources, potential human health impacts, and current remediation technologies," *Environ. Int.*, vol. 71, pp. 118–138, 2014.

[16] P. I. Beamer, C. E. Luik, L. Abrell, S. Campos, M. E. Martínez, and A. E. Sáez, "Concentration of trichloroethylene in breast milk and household water from Nogales, Arizona," *Environ. Sci. Technol.*, vol. 46, no. 16, pp. 9055–9061, 2012.

[17] C. Lourencetti, J. O. Grimalt, E. Marco, P. Fernandez, L. Font-Ribera, C. M. Villanueva, M. Kogevinas, "Trihalomethanes in chlorine and bromine disinfected swimming pools: Air-water distributions and human exposure," *Environ. Int.*, vol. 45, no. 1, pp. 59–67, 2012.

[18] C. Y. Yang, Z. P. Xiao, S. C. Ho, T. N. Wu, and S. S. Tsai, "Association between trihalomethane concentrations in drinking water and adverse pregnancy outcome in Taiwan," *Environ. Res.*, vol. 104, no. 3, pp. 390–395, 2007.

[19] P. L. Zogorski, J. S. Carter, J. M. Ivahnenko, T. Lapham, W. W. Moran, M. J. Rowe, B. L. Toccalino, "Volatile organic compounds in the nation's ground water and drinking-water supply wells," US Geological Survey Circular, 1292, 101, 2006.

[20] J. A. Field and R. Sierra-Alvarez, "Biodegradability of chlorinated solvents and related chlorinated aliphatic compounds," *Rev. Environ. Sci. Biotechnol.*, vol. 3, no. 3, pp. 185–254, 2004.

[21] New York State Department of Health, "1,2-Dichloroethane (Water Source)," no. i.

Ambient Water Quality Value for Protection of Sources of Potable Water, pp. 1–12, 1998.

[22] New York State Department of Health, "Chlorobenzene (Water Source)," vol. 3. Ambient Water Quality Value for Protection of Sources of Potable Water, pp. 1–5, 1998.

[23] O. Charles, N. Adaku, I. Chemistry, P. Harcourt and P. M. B. Choba, "Polycyclic Aromatic Hydrocarbons (PAHs) and Benzene , Toluene , Ethylbenzene , and Xylene (BTEX) Contamination of Soils in Automobile Mechanic Workshops in Port-Harcourt Metropolis," *Forestry*, vol. 6, no. 9, pp. 242–246, 2010.

[24] J. P. Salanitro, P. B. Dorn, M. H. Huesemann, K. O. Moore, I. A. Rhodes, L. M. Rise Jackson, T. E. Vipond, M. M. Western, H. L. Wisniewski, "Crude oil hydrocarbon bioromediation and soil ecotoxicity assessment," *Environ. Sci. Technol.*, vol. 31, no. 6, pp. 1769–1776, 1997.

[25] E. Durmusoglu, F. Taspinar, and A. Karademir, "Health risk assessment of BTEX emissions in the landfill environment," *J. Hazard. Mater.*, vol. 176, no. 1–3, pp. 870–877, 2010.

[26] L. M. McKenzie, R. Z. Witter, L. S. Newman, and J. L. Adgate, "Human health risk assessment of air emissions from development of unconventional natural gas resources," *Sci. Total Environ.*, vol. 424, pp. 79–87, 2012.

[27] New York State Department of Health, "Benzene (Water Source)," Ambient Water Quality Value for Protection of Sources of Potable Water, 1998.

[28] New York State Department of Health, "Toluene (Water Source)." Ambient Water Quality Value for Protection of Sources of Potable Water, pp. 1–3, 1998.

[29] New York State Department of Health, "Xylene (o-, m-, p-) (Water Source)." Ambient Water Quality Value for Protection of Sources of Potable Water SUBSTANCES:, pp. 1–3, 1998.

[30] I. Reed, N. Reed, W. Beltran, L. Li, R. Encomienda, "Health assessment of toluene in California drinking water," *SciTech Connect*, 1989.

[31] P. K. Auerbach, S. M. Carrado, K. A. Dutta, *Handbook of layered materials*. CRC Press, 2004.

[32] New York State Department of Health, "Methyl tert-Butyl Ether (Water Source),"

no. April. Ambient Water Quality Value for Protection of Sources of Potable Water, pp. 1–7, 2000.

[33] V. K. Gupta, I. Ali, T. A. Saleh, A. Nayak and S. Agarwal, "Chemical treatment technologies for waste-water recycling—an overview," *RSC Adv.*, vol. 2, p. 6380, 2012.

[34] A. Martucci, I. Braschi, L. Marchese, and S. Quartieri, "Recent advances in clean-up strategies of waters polluted with sulfonamide antibiotics: a review of sorbents and related properties," *Mineral. Mag.*, vol. 78, no. 5, pp. 1115–1140, 2014.

[35] I. Oller, S. Malato, and J. A. Sánchez-Pérez, "Combination of Advanced Oxidation Processes and biological treatments for wastewater decontamination-A review," *Sci. Total Environ.*, vol. 409, no. 20, pp. 4141–4166, 2011.

[36] M. Perullini, M. Jobbágy, N. Mouso, F. Forchiassin and S. A. Bilmes, "Silica-alginate-fungi biocomposites for remediation of polluted water," *J. Mater. Chem.*, vol. 20, no. 31, p. 6479, 2010.

[37] B. P. Xin, C. H. Wu, C. H. Wu, and C. W. Lin, "Bioaugmented remediation of high concentration BTEX-contaminated groundwater by permeable reactive barrier with immobilized bead," *J. Hazard. Mater.*, vol. 244–245, pp. 765–772, 2013.

[38] J. Xu, G. P. Sheng, Y. Ma, L. F. Wang, and H. Q. Yu, "Roles of extracellular polymeric substances (EPS) in the migration and removal of sulfamethazine in activated sludge system," *Water Res.*, vol. 47, no. 14, pp. 5298–5306, 2013.

[39] L. Xu, J. Pan, J. Dai, X. Li, H. Hang, Z. Cao, Y. Yan, "Preparation of thermal-responsive magnetic molecularly imprinted polymers for selective removal of antibiotics from aqueous solution," *J. Hazard. Mater.*, vol. 233–234, pp. 48–56, 2012.

[40] W. Baran, E. Adamek, A. Sobczak, and A. Makowski, "Photocatalytic degradation of sulfa drugs with TiO2, Fe salts and TiO2/FeCl3 in aquatic environment-Kinetics and degradation pathway," *Appl. Catal. B Environ.*, vol. 90, no. 3–4, pp. 516–525, 2009.

[41] W. Baran, J. Sochacka, and W. Wardas, "Toxicity and biodegradability of sulfonamides and products of their photocatalytic degradation in aqueous solutions," *Chemosphere*, vol. 65, no. 8, pp. 1295–1299, 2006.

[42] E. Adamek, W. Baran, J. Ziemiańska, and A. Sobczak, "Effect of $FeCl_3$ on sulfonamide removal and reduction of antimicrobial activity of wastewater in a photocatalytic process with TiO_2," *Appl. Catal. B Environ.*, vol. 126, pp. 29–38, 2012.

[43] E. Adamek, W. Baran, and A. Sobczak, "Photocatalytic degradation of veterinary antibiotics: Biodegradability and antimicrobial activity of intermediates," *Process Saf. Environ. Prot.*, vol. 103, pp. 1–9, 2016.

[44] A. G. Trovó, R. F. P. Nogueira, A. Agüera, C. Sirtori, and A. R. Fernández-Alba, "Photodegradation of sulfamethoxazole in various aqueous media: Persistence, toxicity and photoproducts assessment," *Chemosphere*, vol. 77, no. 10, pp. 1292–1298, 2009.

[45] N. Nadarajah, J. Van Hamme, J. Pannu, A. Singh, and O. Ward, "Enhanced transformation of polycyclic aromatic hydrocarbons using a combined Fenton's reagent, microbial treatment and surfactants," *Appl. Microbiol. Biotechnol.*, vol. 59, no. 4–5, pp. 540–544, 2002.

[46] S. J. Park, T. I. Yoon, J. H. Bae, H. J. Seo and H. J. Park, "Biological treatment of wastewater containing dimethyl sulphoxide from the semi-conductor industry," *Process Biochem.*, vol. 36, no. 6, pp. 579–589, 2001.

[47] Y. U. Zeng, P. K. A. Hong and D. A. Wavrek, "Integrated Chemical-Biological Treatment of Benzo [*a*]pyrene," vol. 34, no. 5, pp. 854–862, 2000.

[48] L. Leardini, A. Martucci, I. Braschi, S. Blasioli, and S. Quartieri, "Regeneration of high-silica zeolites after sulfamethoxazole antibiotic adsorption: a combined *in situ* high-temperature synchrotron X-ray powder diffraction and thermal degradation study," *Mineral. Mag.*, vol. 78, no. 5, pp. 1141–1159, 2014.

[49] P. Misaelides, "Application of natural zeolites in environmental remediation: A short review," *Microporous Mesoporous Mater.*, vol. 144, no. 1–3, pp. 15–18, 2011.

[50] R. Vignola, R. Bagatin, A. De Folly D'Auris, C. Flego, M. Nalli, D. Ghisletti, R. Millini, R. Sisto, "Zeolites in a permeable reactive barrier (PRB): One year of field experience in a refinery groundwater-Part 1: The performances," *Chem. Eng. J.*, vol. 178, pp. 204–209, 2011.

[51] R. Vignola, R. Bagatin, A. De Folly D'Auris, E. Previde Massara, D. Ghisletti, R. Millini, R. Sisto, "Zeolites in a permeable reactive barrier (PRB): One-year of field

experience in a refinery groundwater. Part 2: Zeolite characterization," *Chem. Eng. J.*, vol. 178, pp. 210–216, 2011.

[52] H. Kayser, "Ueber die Verdichtung von Gasen an Oberflächen in ihrer Abhängigkeit von Druck und Temperatur," *Ann. Phys.*, vol. 250, no. 11, pp. 450–468, 1881.

[53] E. Worch, *Adsorption Technology in Water Treatment: Fundamentals, Processes, and Modeling*. 2012.

[54] R. Krishna and J. M. Van Baten, "Mutual slowing-down effects in mixture diffusion in zeolites," *J. Phys. Chem. C*, vol. 114, no. 30, pp. 13154–13156, 2010.

[55] R. Krishna and J. M. Van Baten, "Hydrogen bonding effects in adsorption of water-alcohol mixtures in zeolites and the consequences for the characteristics of the Maxwell-Stefan diffusivities," *Langmuir*, vol. 26, no. 13, pp. 10854–10867, 2010.

[56] L. Pasti, E. Rodeghero, E. Sarti, V. Bosi, A. Cavazzini, R. Bagatin and A. Martucci, "Competitive Adsorption of VOCs from binary aqueous mixtures on zeolite ZSM-5," *RSC Adv.*, vol. 6, pp. 54544–54552, 2016.

[57] S. H. Do, Y. J. Kwon, and S. H. Kong, "Feasibility study on an oxidant-injected permeable reactive barrier to treat BTEX contamination: Adsorptive and catalytic characteristics of waste-reclaimed adsorbent," *J. Hazard. Mater.*, vol. 191, no. 1–3, pp. 19–25, 2011.

[58] A. R. Gavaskar, "Design and construction techniques for permeable reactive barriers," *J. Hazard. Mater.*, vol. 68, no. 1–2, pp. 41–71, 1999.

[59] I. Snape, C. E. Morris, and C. M. Cole, "The use of permeable reactive barriers to control contaminant dispersal during site remediation in Antarctica," *Cold Reg. Sci. Technol.*, vol. 32, no. 2–3, pp. 157–174, 2001.

[60] E. Mena, C. Ruiz, J. Villaseñor, M. A. Rodrigo, and P. Cañizares, "Biological permeable reactive barriers coupled with electrokinetic soil flushing for the treatment of diesel-polluted clay soil," *J. Hazard. Mater.*, vol. 283, pp. 131–139, 2015.

[61] S. J. Liu, B. Jiang, G. Q. Huang, and X. G. Li, "Laboratory column study for remediation of MTBE-contaminated groundwater using a biological two-layer permeable barrier," *Water Res.*, vol. 40, no. 18, pp. 3401–3408, 2006.

[62] C. M. Kao, S. C. Chen, and J. K. Liu, "Development of a biobarrier for the

remediation of PCE-contaminated aquifer," *Chemosphere*, vol. 43, no. 8, pp. 1071–1078, 2001.

[63] C. M. Kao, S. C. Chen, J. Y. Wang, Y. L. Chen, and S. Z. Lee, "Remediation of PCE-contaminated aquifer by an in situ two-layer biobarrier: Laboratory batch and column studies," *Water Res.*, vol. 37, no. 1, pp. 27–38, 2003.

[64] M. Çakmakce, N. Kayaalp, and I. Koyuncu, "Desalination of produced water from oil production fields by membrane processes," *Desalination*, vol. 222, no. 1–3, pp. 176–186, 2008.

[65] B. van der Bruggen, M. Mänttäri and M. Nyström, "Drawbacks of applying nanofiltration and how to avoid them: A review," *Sep. Purif. Technol.*, vol. 63, no. 2, pp. 251–263, 2008.

[66] B. van der Bruggen and C. Vandecasteele, "Removal of pollutants from surface water and groundwater by nanofiltration: Overview of possible applications in the drinking water industry," *Environ. Pollut.*, vol. 122, no. 3, pp. 435–445, 2003.

[67] G. Crini, "Recent developments in polysaccharide-based materials used as adsorbents in wastewater treatment," *Prog. Polym. Sci.*, vol. 30, no. 1, pp. 38–70, 2005.

[68] S. M. Lee and D. Tiwari, "Organo and inorgano-organo-modified clays in the remediation of aqueous solutions: An overview," *Appl. Clay Sci.*, vol. 59–60, pp. 84–102, 2012.

[69] V. K. Gupta, "Application of low-cost adsorbents for dye removal - A review," *J. Environ. Manage.*, vol. 90, no. 8, pp. 2313–2342, 2009.

[70] P. J. M. Carrott and M. R. Carrott, "Lignin - from natural adsorbent to activated carbon: A review," *Bioresour. Technol.*, vol. 98, no. 12, pp. 2301–2312, 2007.

[71] C. Y. Yin, M. K. Aroua, and W. M. A. W. Daud, "Review of modifications of activated carbon for enhancing contaminant uptakes from aqueous solutions," *Sep. Purif. Technol.*, vol. 52, no. 3, pp. 403–415, 2007.

[72] A. Dabrowski, P. Podkoscielny, Z. Hubicki, and M. Barczak, "Adsorption of phenolic compounds by activated carbon - A critical review," *Chemosphere*, vol. 58, no. 8, pp. 1049–1070, 2005.

[73] N. A. Lotfi Monser, "SPTactcarbon-CuZn," *Sep. Purif. Technol.*, vol. 26, pp. 137–

146, 2002.

[74] M. Goyal, V. K. Rattan, R. C. Bansal, "Removal of copper from aqueous solutions by adsorption on activated carbons," *Colloid Surf. A.*, vol. 190, p. 229–238., 2001.

[75] Z. Jiang, Y. Liu, X. Sun, F. Tian, F. Sun, C. Liang, W. You, C. Han and C. Li, "Activated carbons chemically modified by concentrated H_2SO_4 for the adsorption of the pollutants from wastewater and the dibenzothiophene from fuel oils," *Langmuir*, vol. 19, no. 3, pp. 731–736, 2003.

[76] S. Iijima and T. Ichihashi, "Single-shell carbon nanotubes of 1-nm diameter," *Nature*, vol. 363, pp. 603–605, 1993.

[77] G. P. Rao, C. Lu, and F. Su, "Sorption of divalent metal ions from aqueous solution by carbon nanotubes: A review," *Sep. Purif. Technol.*, vol. 58, no. 1, pp. 224–231, 2007.

[78] T. W. Odom, J. L. Huang, P. Kim, and C. M. Lieber, "Atomic structure and electronic properties of single-walled carbon nanotubes," *Nature*, vol. 391, no. January, pp. 62–64, 1998.

[79] L. Dai, P. He, and S. Li, "Functionalized surfaces based on polymers and carbon nanotubes for some biomedical and optoelectronic applications," *Nanotechnology*, vol. 14, no. 10, pp. 1081–1097, 2003.

[80] A. C. Dillon, K. M. Jones, T. A. Bekkedahl, C. H. Kiang, D. S. Bethune and M. J. Heben, "Storage of hydrogen in single-walled carbon nanotubes," *Nature*, vol. 386. pp. 377–379, 1997.

[81] Q. H. Wang, A. A. Setlur, J. M. Lauerhaas, J. Y. Dai, E. W. Seelig, and R. P. H. Chang, "A nanotube-based field-emission flat panel display," *Appl. Phys. Lett.*, vol. 72, no. 22, pp. 2912–2913, 1998.

[82] H. D. Wagner, O. Lourie, Y. Feldman, and R. Tenne, "Stress-induced fragmentation of multiwall carbon nanotubes in a polymer matrix," *Appl. Phys. Lett.*, vol. 72, no. 2, pp. 188–190, 1998.

[83] A. M. Cassell, J. A. Raymakers, J. Kong, and H. Dai, "Large scale CVD synthesis of single-walled carbon nanotubes," *J. Phys. Chem. B*, vol. 103, no. 31, pp. 6484–6492, 1999.

[84] S. Agnihotri, M. J. Rood, and M. Rostam-Abadi, "Adsorption equilibrium of

organic vapors on single-walled carbon nanotubes," *Carbon N. Y.*, vol. 43, no. 11, pp. 2379–2388, 2005.

[85] P. A. Gauden, A. P. Terzyk, A. P. Rychlicki, G. Kowalczyk, P. Lota, K. Raymundo-Pinero, E. F. F. Béguin, "Thermodynamic properties of benzene adsorbed in activated carbons and multi-walled carbon nanotubes," *Chem. Phys. Lett.*, vol. 421, no. 4–6, pp. 409–414, 2006.

[86] X. Peng, Y. Li, Z. Luan, Z. Di, H. Wang, B. Tian, Z. Jan, "Adsorption of 1,2-dichlorobenzene from water to carbon nanotubes," *Chem. Phys. Lett.*, vol. 376, no. 1–2, pp. 154–158, 2003.

[87] M. Trojanowicz, "Analytical applications of carbon nanotubes: a review," *TrAC - Trends Anal. Chem.*, vol. 25, no. 5, pp. 480–489, 2006.

[88] P. J. Dorathi and P. Kandasamy, "Dechlorination of chlorophenols by zero valent iron impregnated silica," *J. Environ. Sci.*, vol. 24, no. 4, pp. 765–773, 2012.

[89] K. Choi and W. Lee, "Enhanced degradation of trichloroethylene in nano-scale zero-valent iron Fenton system with Cu(II)," *J. Hazard. Mater.*, vol. 211–212, no. March 2017, pp. 146–153, 2012.

[90] L. M. Kustov, E. D. Finashina, E. V. Shuvalova, O. P. Tkachenko, and O. A. Kirichenko, "Pd-Fe nanoparticles stabilized by chitosan derivatives for perchloroethene dechlorination," *Environ. Int.*, vol. 37, no. 6, pp. 1044–1052, 2011.

[91] C. Su, R. W. Puls, T. A. Krug, M. T. Watling, S. K. O'Hara, J. W. Quinn and N. E. Ruiz, "A two and half-year-performance evaluation of a field test on treatment of source zone tetrachloroethene and its chlorinated daughter products using emulsified zero valent iron nanoparticles," *Water Res.*, vol. 46, no. 16, pp. 5071–5084, 2012.

[92] W. Yin, J. Wu, P. Li, X. Wang, N. Zhu, P. Wu, and B. Yang, "Experimental study of zero-valent iron induced nitrobenzene reduction in groundwater: The effects of pH, iron dosage, oxygen and common dissolved anions," *Chem. Eng. J.*, vol. 184, no. December 2013, pp. 198–204, 2012.

[93] R. A. Crane and T. B. Scott, "Nanoscale zero-valent iron: Future prospects for an emerging water treatment technology," *J. Hazard. Mater.*, vol. 211–212, no. November, pp. 112–125, 2012.

[94] F. Fu, D. D. Dionysiou, and H. Liu, "The use of zero-valent iron for groundwater

remediation and wastewater treatment: A review," *J. Hazard. Mater.*, vol. 267, no. September, pp. 194–205, 2014.

[95] B. Dou, Q. Hu, J. Li, S. Qiao, and Z. Hao, "Adsorption performance of VOCs in ordered mesoporous silicas with different pore structures and surface chemistry," *J. Hazard. Mater.*, vol. 186, no. 2–3, pp. 1615–1624, 2011.

[96] V. R. Choudhary and K. Mantri, "Adsorption of aromatic hydrocarbons on highly siliceous MCM-41," *Langmuir*, vol. 16, no. 17, pp. 7031–7037, 2000.

[97] M. Hartmann and C. Bischof, "Mechanical Stability of Mesoporous Molecular Sieve MCM-48 Studied by Adsorption of Benzene, n-Heptane, and Cyclohexane," *J. Phys. Chem. B*, vol. 103, pp. 6230–6235, 1999.

[98] S. Z. Qiao, S. K. Bhatia, and D. Nicholson, "Study of Hexane Adsorption in Nanoporous MCM-41 Silica," *Langmuir*, vol. 20, no. 2, pp. 389–395, 2004.

[99] K. Kosuge, S. Kubo, N. Kikukawa, and M. Takemori, "Effect of Pore Structure in Mesoporous Silicas on VOC Dynamic Adsorption / Desorption Performance," *Langmuir*, vol. 23, no. C, pp. 3095–3102, 2007.

[100] A. Stein, B. J. Melde, and R. C. Schroden, "Hybrid Inorganic–Organic Mesoporous Silicates—Nanoscopic Reactors Coming of Age," *Adv. Mater.*, vol. 12, no. 19, pp. 1403–1419, 2000.

[101] H. Vinh-Thang, Q. Huang, M. Eić, D. Trong-On, and S. Kaliaguine, "Adsorption of C7 hydrocarbons on biporous SBA-15 mesoporous silica," *Langmuir*, vol. 21, no. 11, pp. 5094–5101, 2005.

[102] A.F. Cronsted, "Observation and description of an unknown kind of rock to be named zeolites," *R. Swedish Accademy Sci.*, vol. 17, pp. 120–130, 1756.

[103] M. Damour, "Description de la faujasite, nouvelle espèce minérale," *Ann. des Mincs*, vol. 4, pp. 395–399, 1842.

[104] H. Eichorn, "Ueber die Einwirkung verdunnter Salzlosungen auf Silicate," *Ann. Phys.*, vol. 105, p. 191, 1858.

[105] G. Friedel, "Sur quelques proprietes nouvelles des zeolithes," *Bull. la Soc. Fr. Mineral. Crystallogr.*, vol. 19, pp. 94–119, 1896.

[106] I. L. C. Buurmans, *Catalyst Particles for Fluid Catalytic Cracking Visualized at the Individual Particle Level by*, no. december. 2011.

[107] E. S. Weigel, O., "Adsorption of organic liquid vapors by chabazite," *Kristallogr*, vol. 61, pp. 125–154, 1925.

[108] A. F. Masters and T. Maschmeyer, "Zeolites - From curiosity to cornerstone," *Microporous Mesoporous Mater.*, vol. 142, no. 2–3, pp. 423–438, 2011.

[109] R. M. Barrer and P. J. Denny, "Hydrothermal chemistry of the silicates. Part IX. Nitrogenous aluminosilicates," *J. Chem. Soc.*, pp. 971–982, 1961.

[110] R. M. Barrer, "33. Synthesis of a zeolitic mineral with chabazite-like sorptive properties.," *J. Chem. Soc.*, pp. 127–132, 1942.

[111] M. H. Hey, "Studies on the zeolites part I: General review," *Mineral. Mag.*, vol. 22(131), pp. 422–437, 1930.

[112] G. Alberti, A. Armbruster, T. Artioli, G. Colella, C. Galli, E. Grice, J. D. Peacor, S. Quartieri, R. Rinaldi, M. Ross, R. A. Sheppard, E. Tillmanns, E. Vezzalini, "Recommended nomenclature for zeolite minerals: Report of the subcommittee on zeolites of the International Mineralogical Association, Commission on New Minerals and Mineral Names," *Can. Mineral.*, vol. 35, pp. 1571–1606, 1997.

[113] J. Smith, "International Mineralogical," in *International Mineralogical Association, Papers and Proceedings of the Third General Meeting, Mineralogical Society of America Special Paper Number One*, 1963, pp. 281–290.

[114] J. K. and C. Li, "A Study on the Hydrophobicity of Organosilane-Modified Zeolites" pp. 1–26, 2015.

[115] J. Xu, R. Pang, W. Yu, J. Huo, Q. Chen, *Chemistry of zeolites and related porous materials: synthesis and structure*. 2009.

[116] A. Corma, "State of the art and future challenges of zeolites as catalysts," *J. Catal.*, vol. 216, no. 1–2, pp. 298–312, 2003.

[117] "Zeolite Framework Types." [Online]. Available: http://europe.iza-structure.org/IZA-SC/ftc_table.php.

[118] P. Cappelletti, G. Rapisardo, B. De Gennaro, A. Colella, A. Langella, S. F. Graziano and M. De Gennaro, "Immobilization of Cs and Sr in aluminosilicate matrices derived from natural zeolites," *J. Nucl. Mater.*, vol. 414, no. 3, pp. 451–457, 2011.

[119] M. Kragović, A. Daković, Z. Sekulić, M. Trgo, M. Ugrina, J. Perić and G. D. Gatta, "Removal of lead from aqueous solutions by using the natural and Fe(III)-modified

zeolite," *Appl. Surf. Sci.*, vol. 258, no. 8, pp. 3667–3673, 2012.

[120] J. L. Ming, D. W., Boettinger, *Natural Zeolites: Occurrence, Properties, Applications*. 2001.

[121] R. S. Bowman, "Applications of surfactant-modified zeolites to environmental remediation," *Microporous Mesoporous Mater.*, vol. 61, no. 1–3, pp. 43–56, 2003.

[122] V. Sacchetto, C. Bisio, D. F. Olivas Olivera, G. Paul, G. Gatti, I. Braschi and L. Marchese, "Interactions of Toluene and n-Hexane on High Silica Zeolites: An Experimental and Computational Model Study," *J. Phys. Chem. C*, vol. 119, no. 44, pp. 24875–24886, 2015.

[123] A. Martucci, L. Pasti, N. Marchetti, A. Cavazzini, F. Dondi and A. Alberti, "Adsorption of pharmaceuticals from aqueous solutions on synthetic zeolites," *Microporous Mesoporous Mater.*, vol. 148, no. 1, pp. 174–183, 2012.

[124] A. Martucci, L. Pasti, M. Nassi, A. Alberti, R. Arletti, R. Bagatin, R. Vignola, R. Sticca, "Adsorption mechanism of 1,2-dichloroethane into an organophilic zeolite mordenite: A combined diffractometric and gas chromatographic study," *Microporous Mesoporous Mater.*, vol. 151, pp. 358–367, 2012.

[125] A. Martucci, I. Braschi, C. Bisio, E. Sarti, E. Rodeghero, R. Bagatin and L. Pasti, "Influence of water on the retention of methyl tertiary-butyl ether by high silica ZSM-5 and Y zeolites: a multidisciplinary study on the adsorption from liquid and gas phase," *RSC Adv.*, vol. 5, pp. 86997–87006, 2015.

[126] R. Arletti, A. Martucci, A. Alberti, L. Pasti, M. Nassi, and R. Bagatin, "Location of MTBE and toluene in the channel system of the zeolite mordenite: Adsorption and host-guest interactions," *J. Solid State Chem.*, vol. 194, pp. 135–142, 2012.

[127] L. Sumin, M. Youguang, S. Shuhua, and Z. Chunying, "The effect of hydrophobic modification of zeolites on Co2 absorption in different solvents," *Brazilian J. Chem. Eng.*, vol. 27, no. 2, pp. 327–338, 2010.

[128] P. A. Zapata, J. Faria, M. P. Ruiz, R. E. Jentoft, and D. E. Resasco, "Hydrophobic Zeolites for Biofuel Upgrading Reactions at the Liquid − Liquid Interface in Water / Oil Emulsions," *J. Am. Chem. Soc.*, vol. 134, p. 8570−8578, 2012.

[129] W. M. Bearlocher, Ch. Meier and D. H. Olson, "Atlas of Zeolite," 2001.

[130] P. B. Unit, T. Perbu, and N. Perbus, "Building scheme for MEL and MFI 1.,"

Channels, no. 2, pp. 3–6.

[131] F. T. Data, "Secondary building units: Channels," vol. 1, no. 22, pp. 212–213, 2012.

[132] H. van Koningsveld, J. C. Jansen, and H. van Bekkum, "The monoclinic framework structure of zeolite H-ZSM-5. Comparison with the orthorhombic framework of as-synthesized ZSM-5," *Zeolites*, vol. 10, no. 4, pp. 235–242, 1994.

[133] H. van Koningsveld, F. Tuinstra, J. C. Jansen, and H. van Bekkum, "On the preparation of a monoclinic (nearly) single crystal of zeolite HZSM-5," *Zeolites*, vol. 9, no. 3, pp. 253–256, 1989.

[134] H. van Koningsveld and J. Jansen, "Single Crystal Structure Analysis of Zeolite H-ZSM-5 Loaded with Naphthalene," *Microporous Mater.*, vol. 6, pp. 159–167, 1996.

[135] K. Nishi, A. Hidaka, and Y. Yokomori, "Structure of toluene6.4-ZSM-5 and the toluene disproportionation reaction on ZSM-5," *Acta Crystallogr. Sect. B Struct. Sci.*, vol. 61, no. 2, pp. 160–163, 2005.

[136] N. Kamiya, T. Oshiro, S. Tan, K. Nishi, and Y. Yokomori, "Adsorption process of phenol on silicalite-1 and crystal structure of phenol8.0-silicalite-1 using a single crystal X-ray diffraction method," *Microporous Mesoporous Mater.*, vol. 169, pp. 168–175, 2013.

[137] A. C. Larson and R. B. von Dreele, "General Structure Analysis System (GSAS)." Los Alamos National Laboratory Report LAUR, pp. 86–748, 2000.

[138] B. H. Toby, "EXPGUI , a graphical user interface for GSAS EXPGUI , a graphical user interface for GSAS," pp. 210–213, 2001.

[139] N. Hansen, R. Krishna, J. M. VanBaten, A. T. Bell, and F. J. Keil, "Analysis of diffusion limitation in the alkylation of benzene over H-ZSM-5 by combining quantum chemical calculations, molecular simulations, and a continuum approach," *J. Phys. Chem. C*, vol. 113, no. 1, pp. 235–246, 2009.

[140] W. J. Weber, "Adsorption processes," *Pure Appl. Chem.*, vol. 37, no. 3, pp. 375–392, 1974.

[141] S. Azizian, M. Haerifar, and H. Bashiri, "Adsorption of methyl violet onto granular activated carbon: Equilibrium, kinetics and modeling," *Chem. Eng. J.*, vol. 146, no. 1, pp. 36–41, 2009.

[142] W. Rudzinski and W. Plazinski, "Kinetics of solute adsorption at solid/solution

interfaces: A theoretical development of the empirical pseudo-first and pseudo-second order kinetic rate equations, based on applying the statistical rate theory of interfacial transport," *J. Phys. Chem. B*, vol. 110, no. 33, pp. 16514–16525, 2006.

[143] L. Ai, C. Zhang, F. Liao, Y. Wang, M. Li, L. Meng, and J. Jiang, "Removal of methylene blue from aqueous solution with magnetite loaded multi-wall carbon nanotube: Kinetic, isotherm and mechanism analysis," *J. Hazard. Mater.*, vol. 198, pp. 282–290, 2011.

[144] M. Ardit, A. Martucci, and G. Cruciani, "Monoclinic-Orthorhombic Phase Transition in ZSM-5 Zeolite: Spontaneous Strain Variation and Thermodynamic Properties," *J. Phys. Chem. C*, vol. 119, no. 13, pp. 7351–7359, 2015.

[145] Z. Guo, S. Zheng, Z. Zheng, F. Jiang, W. Hu, and L. Ni, "Selective adsorption of p-chloronitrobenzene from aqueous mixture of p-chloronitrobenzene and o-chloronitrobenzene using HZSM-5 zeolite," *Water Res.*, vol. 39, no. 6, pp. 1174–1182, 2005.

[146] J. Farrell, C. Manspeaker, and J. Luo, "Understanding competitive adsorption of water and trichloroethylene in a high-silica Y zeolite," *Microporous Mesoporous Mater.*, vol. 59, no. 2–3, pp. 205–214, 2003.

[147] S. Kleineidam, C. Schüth, and P. Grathwohl, "Solubility-normalized combined adsorption-partitioning sorption isotherms for organic pollutants," *Environ. Sci. Technol.*, vol. 36, no. 21, pp. 4689–4697, 2002.

[148] K. S. W. Sing, "Reporting physisorption data for gas/solid systems with special reference to the determination of surface area and porosity," *Pure Appl. Chem.*, vol. 54, no. 11, pp. 2201–2218, 1982.

[149] B. A. De Moor, M. F. Reyniers, O. C. Gobin, J. A. Lercher, and G. B. Marin, "Adsorption of C2-C8 n-alkanes in zeolites," *J. Phys. Chem. C*, vol. 115, no. 4, pp. 1204–1219, 2011.

[150] D. M. Ruthven, *Principles of adsorption and adsorption processes*. John Wiley & Sons, 1984.

[151] F. Gritti, W. Piatkowski, and G. Guiochon, "Comparison of the adsorption equilibrium of a few low-molecular mass compounds on a monolithic and a packed column in reversed-phase liquid chromatography," *J. Chromatogr. A*, vol. 978, no. 1–2, pp. 81–107, 2002.

[152] E. Güvenç and M. G. Ahunbay, "Adsorption of methyl tertiary butyl ether and trichloroethylene in MFI-type zeolites," *J. Phys. Chem. C*, vol. 116, no. 41, pp. 21836–21843, 2012.

[153] A. Martucci, L. Leardini, M. Nassi, E. Sarti, R. Bagatin, and L. Pasti, "Removal of emerging organic contaminants from aqueous systems: adsorption and location of methyl-tertiary-butyl-ether on synthetic ferrierite," *Mineral. Mag.*, vol. 78, no. 5, pp. 1161–1175, 2014.

[154] A. Erdem-Şenatalar, J. A. Bergendahl, A. Giaya and R. W. Thompson, "Adsorption of Methyl Tertiary Butyl Ether on Hydrophobic Molecular Sieves," *Environ. Eng. Sci.*, vol. 21, no. 6, pp. 722–729, 2004.

[155] M. Göktuğ Ahunbay, O. Karvan, and A. Erdem-Şenatalar, "MTBE adsorption and diffusion in silicalite-1," *Microporous Mesoporous Mater.*, vol. 115, no. 1–2, pp. 93–97, 2008.

[156] B. Y. R. D. Shannon, M. H. N. H. Baur, O. H. Gibbs, M. Eu and V. Cu, "Revised Effective Ionic Radii and Systematic Studies of Interatomie Distances in Halides and Chaleogenides Central Research and Development Department , Experimental Station , E . L Du Pont de Nemours The effective ionic radii of Shannon & Prewitt [Acta ," 1976.

[157] I. Quiñones and G. Guiochon, "Application of different isotherm models to the description of single-component and competitive adsorption data," *J. Chromatogr. A*, vol. 734, no. 1, pp. 83–96, 1996.

[158] J. Zhu, A. M. Katti, and G. Guiochon, "Comparison of various isotherm models for predicting competitive adsorption data," *J. Chromatogr. A*, vol. 552, no. C, pp. 71–89, 1991.

[159] W. Longlong, T. Xin, Z. Wei, Q. Dan, L. Qiang, J. Jin, L. Wangsuo, "The adsorption of water-soluble ionic liquids on graphene oxide of different oxygen content," *RSC Adv.*, vol. 4.102, pp. 58536–58545, 2014.

[160] J. S. Jain and V. L. Snoeyink, "Adsorption from bisolute systems on active carbon," *J. (Water Pollut. Control Fed.*, vol. 45, no. 12, pp. 2463–2479, 1973.

[161] D. G. Guiochon, G. Felinger, A. Shirazi, *Fundamentals of preparative and nonlinear chromatography*. Academic Press, 2006.

[162] R. Krishna, "Separating mixtures by exploiting molecular packing effects in microporous materials.," *Phys. Chem. Chem. Phys.*, vol. 17, no. 1, pp. 39–59, 2015.

[163] T. C. Bowen and L. M. Vane, "Ethanol, acetic acid, and water adsorption from binary and ternary liquid mixtures on high-silica zeolites," *Langmuir*, vol. 22, no. 8, pp. 3721–3727, 2006.

[164] Z. Li and S. Singh, "FTIR and ab initio investigations of the MTBE-water complex," *J. Phys. Chem. A*, vol. 112, no. 37, pp. 8593–8599, 2008.

[165] C. M. Simon, B. Smit, and M. Haranczyk, "PyIAST: Ideal adsorbed solution theory (IAST) Python package," *Comput. Phys. Commun.*, vol. 200, no. December, pp. 364–380, 2016.

[166] P. Bai, M. Tsapatsis, and J. I. Siepmann, "Multicomponent adsorption of alcohols onto silicalite-1 from aqueous solution: Isotherms, structural analysis, and assessment of ideal adsorbed solution theory," *Langmuir*, vol. 28, no. 44, pp. 15566–15576, 2012.

[167] G. T. Wu, E. L. Lawton, S. L. Olson, D. H. Rohrman, A. C. Kokotailo, "ZSM-5-type materials. Factors affecting crystal symmetry," *J. Phys. Chem.*, vol. 83(21), 1979.

[168] B. F. Mentzen, "Structural correlations between the framework symmetry of highly siliceous MFI zeolitic materials (silicalite, ZSM-5 for SiAl> 75) and the location or the geometry of sorbed molecules," *Mater. Res. Bull.*, vol. 27, no. 2, pp. 831–838, 1992.

[169] S. Fujiyama, N. Kamiya, K. Nishi, and Y. Yokomori, "Location of CO<inf>2</inf> on silicalite-1 zeolite using a single-crystal X-ray method," *Zeitschrift fur Krist.*, vol. 228, no. 4, 2013.

[170] H. Van Koningsveld, "Schemes for Building Zeolite Framework Models. Building scheme for AFI.," *Struct. Comm. Int. Zeolite Assoc.*, pp. 6–7.

[171] H. van Koningsveld, J. C. Jansen, and H. van Bekkum, "The location of p-dichlorobenzene in a single crystal of zeolite H-ZSM-5 at high sorbate loading," *Acta Crystallogr. Sect. B Struct. Sci.*, vol. 52, no. 1, pp. 140–144, 1996.

[172] H. Van Koningsveld, F. Tuinstra, H. Van Bekkum, and J. C. Jansen, "The location of p-xylene in a single crystal of zeolite H-ZSM-5 with a new, sorbate-induced,

orthorhombic framework symmetry," *Acta Crystallogr. Sect. B*, vol. 45, no. 4, pp. 423–431, 1989.

[173] L. Leardini, A. Martucci, and G. Cruciani, "The unusual thermal behaviour of boron-ZSM-5 probed by 'in situ' time-resolved synchrotron powder diffraction," *Microporous Mesoporous Mater.*, vol. 173, pp. 6–14, 2013.

[174] Y. V. Seryotkin, W. Joswig, V. V. Bakakin, I. A. Belitsky and B. A. Fursenko, "High-temperature crystal structure of wairakite," *Eur. J. Mineral.*, vol. 15, no. 3, pp. 475–484, 2003.

[175] G. Cruciani and A. Gualtieri, "Dehydration dynamics of analcime by in situ synchroton powder diffraction," *Am. Mineral.*, vol. 84, no. 1–2, pp. 112–119, 1999.

[176] J. Felsche and S. Luger, "Structural Collapse or Expansion of the Hydro-Sodalite Series $Na_8[AlSiO_4]_6(OH)_2 \cdot nH_2O$ and $Na_6[AlSiO_4]_6 \cdot nH_2O$ Upon Dehydratation," *Berichte der Bunsengesellschaft für Phys. Chemie*, vol. 90, no. 8, pp. 731–736, 1986.

[177] L. Leardini, A. Martucci, and G. Cruciani, "The unusual thermal expansion of pure silica sodalite probed by in situ time-resolved synchrotron powder diffraction," *Microporous Mesoporous Mater.*, vol. 151, pp. 163–171, 2012.

[178] M. Lassinantti Gualtieri, A. F. Gualtieri, and J. Hedlund, "The influence of heating rate on template removal in silicalite-1: An in situ HT-XRPD study," *Microporous Mesoporous Mater.*, vol. 89, no. 1–3, pp. 1–8, 2006.

[179] A. Alberti, "Phase transformations and structural modifications induced by heating in microporous materials," *Stud. Surf. Sci. Catal.*, vol. 155, pp. 19–43, 2005.

[180] A. Alberti and A. Martucci, "Reconstructive phase transitions in microporous materials: Rules and factors affecting them," *Microporous Mesoporous Mater.*, vol. 141, no. 1–3, pp. 192–198, 2011.

[181] D. S. Bhange and V. Ramaswamy, "High temperature thermal expansion behavior of silicalite-1 molecular sieve: in situ HTXRD study," *Microporous Mesoporous Mater.*, vol. 103, no. 1–3, pp. 235–242, 2007.

[182] D. S. Bhange and V. Ramaswamy, "Enhanced negative thermal expansion in MFI molecular sieves by varying framework composition," *Microporous Mesoporous Mater.*, vol. 130, no. 1–3, pp. 322–326, 2010.

[183] M. Milanesio, G. Artioli, A. F. Gualtieri, L. Palin, and C. Lamberti, "Template Burning inside TS-1 and Fe-MFI Molecular Sieves: An in Situ XRPD Study," *J. Am. Chem. Soc.*, vol. 125, no. 47, pp. 14549–14558, 2003.

[184] A. Martucci, M. de L. Guzman-Castillo, F. Di Renzo, F. Fajula, and A. Alberti, "Reversible channel deformation of zeolite omega during template degradation highlighted by in situ time-resolved synchrotron powder diffraction," *Microporous Mesoporous Mater.*, vol. 104, no. 1–3, pp. 257–268, 2007.

[185] L. Leardini, A. Martucci, A. Alberti, and G. Cruciani, "Template burning effects on stability and boron coordination in boron levyne studied by in situ time resolved synchrotron powder diffraction," *Microporous Mesoporous Mater.*, vol. 167, pp. 117–126, 2013.

[186] L. Leardini, S. Quartieri, G. Vezzalini, and R. Arletti, "Thermal behaviour of siliceous faujasite: Further structural interpretation of negative thermal expansion," *Microporous Mesoporous Mater.*, vol. 202, no. C, pp. 226–233, 2015.

[187] L. A. Villaescusa, P. Lightfoot, S. J. Teat, and R. E. Morris, "Variable-temperature microcrystal X-ray diffraction studies of negative thermal expansion in the pure silica zeolite IFR," *J. Am. Chem. Soc.*, vol. 123, no. 23, pp. 5453–5459, 2001.

[188] J. N. Grima, V. Zammit and R. Gatt, "Negative Thermal Expansion," *Xjenza – J. Malta Chamb. Sci.* -, vol. 11, pp. 17–29, 2006.

[189] I. Bull, P. Lightfoot, L. A. Villaescusa, L. M. Bull, R. K. Gover, J. S. Evans and R. E. Morris, "An X-ray Diffraction and MAS NMR Study of the Thermal Expansion Properties of Calcined Siliceous Ferrierite.pdf," no. 7, pp. 4342–4349, 2003.

[190] D. A. Woodcock, P. Lightfoot, P. A. Wright, L. A. Villaescusa, and M. A. Camblor, "Strong negative thermal expansion in the siliceous zeolites ITQ-1, ITQ-3 and SSZ-23," *J. Mater. Chem.*, vol. 9, no. 2, pp. 349–351, 1999.

[191] G. Cruciani, "Zeolites upon heating: Factors governing their thermal stability and structural changes," *J. Phys. Chem. Solids*, vol. 67, no. 9–10, pp. 1973–1994, 2006.

[192] E. Rodeghero, A. Martucci, G. Cruciani, E. Sarti, V. Bosi, R. Bagatin and L. Pasti, "Sorption and Desorption of methyl tert-butyl ether/toluene, and methyl tert-butyl ether/1,2 dichloroethane mixtures in high silica ZSM-5: study of temperature effect by a combined In Situ synchrotron X-ray powder diffraction and chromatographic techniques," *Prep.*

[193] A. Martucci, E. Rodeghero, and G. Cruciani, "Continuous dehydration of cavansite under dynamic conditions: an in situ synchrotron powder-diffraction study," *Eur. J. Mineral.*, vol. 28, no. 1, pp. 5–13, 2016.

[194] R. Krishna, "The Maxwell-Stefan description of mixture diffusion in nanoporous crystalline materials," *Microporous Mesoporous Mater.*, vol. 185, pp. 30–50, 2014.

[195] R. W. Rolando Roque Malherbea, "Study of Fourier transform infrared-temperature-programmed desorption of benzene, toluene and ethylbenzene from H-ZSM-5 and H-Beta zeolites," *Thermochim. Acta*, vol. 400, pp. 165–173, 2003.

[196] G. Sastre, N. Raj, C. R. A. Catlow, R. Roque-Malherbe, and A. Corma, "Selective Diffusion of C8 Aromatics in a 10 and 12 MR Zeolite. A Molecular Dynamics Study," *J. Phys. Chem. B*, vol. 102, no. 17, pp. 3198–3209, 1998.

[197] A. Corma, C. R. A. Catlow, and G. Sastre, "Diffusion of Linear and Branched C7 Paraffins in ITQ-1 Zeolite. A Molecular Dynamics Study," *J. Phys. Chem. B*, vol. 102, no. 37, pp. 7085–7090, 1998.

[198] I. Braschi, S. Blasioli, E. Buscaroli, D. Montecchio, and A. Martucci, "Physicochemical regeneration of high silica zeolite Y used to clean-up water polluted with sulfonamide antibiotics," *J. Environ. Sci. (China)*, vol. 43, pp. 302–312, 2016.

[199] E. Harlin, J. Makkonen, and M. Tiitta, "A method for the regeneration of zeolite catalysts," WO 2004080591 A1, 2004.

[200] R. Vignola, U. Cova, F. Fabiani, T. Sbardellati and R. Sisto, "Process for the regeneration of non-polar adsorbing zeolites used for the treatment of contaminated water," vol. WO, 2009.

Attachments

SECTION I:

Adsorption of VOCs from aqueous solution at ambient conditions

A-Evidence of 1,2-DCE adsorption from aqueous solution in ZSM-5

B-Evidence of TOL adsorption from aqueous solution in ZSM-5

C-Evidence of MTBE adsorption from aqueous solution

D- Evidence of CB adsorption from aqueous solution

Table 1-A 1. *Atomic coordinates and thermal parameters of framework after 1,2-DCE adsorption at 30°C [8].*

	ZSM-5-1,2-DCE-30			
	x/a	**y/b**	**z/c**	**Uiso**
T1	0.0548(3)	0.4203(3)	-0.3222(5)	0.0087(5)
T2	0.0316(4)	0.3162(4)	-0.1657(5)	0.0087(5)
T3	0.0608(3)	0.2809(3)	0.0541(5)	0.0087(5)
T4	0.0615(4)	0.1245(3)	0.0344(5)	0.0087(5)
T5	0.0271(3)	0.0775(4)	-0.1780(6)	0.0087(5)
T6	0.0564(4)	0.1967(3)	-0.3138(6)	0.0087(5)
T7	-0.1720(3)	0.4255(3)	-0.3246(5)	0.0087(5)
T8	-0.1259(3)	0.3112(3)	-0.1776(5)	0.0087(5)
T9	-0.1752(3)	0.2700(4)	0.0333(6)	0.0087(5)
T10	-0.1780(3)	0.1160(4)	0.0293(6)	0.0087(5)
T11	-0.1308(3)	0.0686(4)	-0.1793(6)	0.0087(5)
T12	-0.1650(3)	0.1844(4)	-0.3143(6)	0.0087(5)
T13	0.4415(3)	0.4291(3)	-0.3378(5)	0.0087(5)
T14	0.4730(3)	0.3124(4)	-0.1884(5)	0.0087(5)
T15	0.4387(4)	0.2779(3)	0.0279(5)	0.0087(5)
T16	0.4357(4)	0.1256(4)	0.0324(5)	0.0087(5)
T17	0.4750(3)	0.0713(3)	-0.1810(6)	0.0087(5)
T18	0.4367(4)	0.1862(3)	-0.3148(6)	0.0087(5)
T19	0.6723(3)	0.4222(3)	-0.3156(5)	0.0087(5)
T20	0.6325(3)	0.3107(4)	-0.1680(5)	0.0087(5)
T21	0.6678(3)	0.2715(4)	0.0444(6)	0.0087(5)
T22	0.6687(3)	0.1180(4)	0.0333(6)	0.0087(5)
T23	0.6316(4)	0.0714(4)	-0.1856(6)	0.0087(5)
T24	0.6810(3)	0.1929(4)	-0.2982(6)	0.0087(5)
O1	0.0659(5)	0.3772(5)	-0.2229(8)	0.0110(1)
O2	0.0632(6)	0.3128(6)	-0.0553(5)	0.0110(1)
O3	0.0473(6)	0.2027(3)	0.0439(3)	0.0110(1)
O4	0.0665(5)	0.1038(8)	-0.0809(6)	0.0110(1)
O5	0.0445(6)	0.1231(4)	-0.2724(7)	0.0110(1)
O6	0.0471(7)	0.2887(5)	-0.2245(9)	0.0110(1)

O7	-0.1601(6)	0.3703(5)	-0.2401(9)	0.0110(1)
O8	-0.1629(6)	0.3050(6)	-0.0724(7)	0.0110(1)
O9	-0.1565(7)	0.1927(3)	0.0253(2)	0.0110(1)
O10	-0.1719(5)	0.0834(7)	-0.0795(7)	0.0110(1)
O11	-0.1563(7)	0.1168(4)	-0.2671(9)	0.0110(1)
O12	-0.1337(7)	0.2432(5)	-0.2387(9)	0.0110(1)
O13	-0.0479(3)	0.3273(6)	-0.1595(8)	0.0110(1)
O14	-0.0522(3)	0.0800(7)	-0.1587(8)	0.0110(1)
O15	0.1222(4)	0.4188(6)	-0.3867(8)	0.0110(1)
O16	-0.0060(5)	0.3894(7)	-0.3867(9)	0.0110(1)
O17	-0.1342(4)	0.4040(7)	-0.4245(8)	0.0110(1)
O18	0.1308(4)	0.2022(7)	-0.3574(6)	0.0110(1)
O19	0.0029(5)	0.2116(6)	-0.4009(9)	0.0110(1)
O20	-0.1268(5)	0.1931(7)	-0.4188(7)	0.0110(1)
O21	0.0499(6)	0.0032(4)	-0.2042(8)	0.0110(1)
O22	-0.1423(6)	-0.0068(4)	-0.2145(8)	0.0110(1)
O23	-0.2509(3)	0.4316(6)	-0.3473(8)	0.0110(1)
O24	-0.2431(3)	0.2047(6)	-0.3329(9)	0.0110(1)
O25	-0.2527(3)	0.2780(8)	0.0618(9)	0.0110(1)
O26	-0.2541(3)	0.1108(7)	0.0667(8)	0.0110(1)
O27	0.4459(7)	0.3773(5)	-0.2472(8)	0.0110(1)
O28	0.4500 (8)	0.3173(5)	-0.0745(6)	0.0110(1)
O29	0.4293(6)	0.2001(3)	0.0066(9)	0.0110(1)
O30	0.4530(7)	0.0825(6)	-0.0675(7)	0.0110(1)
O31	0.4313(4)	0.1180(5)	-0.2535(9)	0.0110(1)
O32	0.4427(7)	0.2474(5)	-0.2386(10)	0.0110(1)
O33	0.6674(6)	0.3724(5)	-0.2226(8)	0.0110(1)
O34	0.6450(7)	0.3154(5)	-0.0498(5)	0.0110(1)
O35	0.6488(7)	0.1950(3)	0.0258(10)	0.0110(1)
O36	0.6582(7)	0.0838(7)	-0.0739(6)	0.0110(1)
O37	0.6722(6)	0.1177(4)	-0.2614(8)	0.0110(1)
O38	0.6441(8)	0.2427(5)	-0.2086(8)	0.0110(1)
O39	0.5534(3)	0.3113(9)	-0.1918(11)	0.0110(1)
O40	0.5531(3)	0.0887(5)	-0.1924(12)	0.0110(1)
O41	0.3703(4)	0.4225(6)	-0.3936(8)	0.0110(1)

O42	0.5007(5)	0.4151(6)	-0.4153(9)	0.0110(1)
O43	0.6303(4)	0.3931(6)	-0.4086(7)	0.0110(1)
O44	0.3708(5)	0.1950(6)	-0.3822(9)	0.0110(1)
O45	0.5020(5)	0.1846(6)	-0.3838(8)	0.0110(1)
O46	0.6314(4)	0.2069(7)	-0.3907(7)	0.0110(1)
O47	0.4625(6)	-0.0050(3)	-0.2101(8)	0.0110(1)
O48	0.6431(6)	-0.0050(3)	-0.2148(8)	0.0110(1)

Table 1-B 1. *Atomic coordinates and thermal parameters of ZSM-5-TOL framework atoms at 30°C [9].*

	ZSM-5-TOL 30			
	x/a	**y/b**	**z/c**	**Uiso**
T1	0.05446(27)	0.42113(27)	-0.3258(5)	0.0039(5)
T2	0.03203(29)	0.31505(30)	-0.1703(5)	0.0039(5)
T3	0.06232(29)	0.27937(28)	0.0481(5)	0.0039(5)
T4	0.06275(29)	0.12342(28)	0.0326(5)	0.0039(5)
T5	0.02723(25)	0.07685(33)	-0.1763(5)	0.0039(5)
T6	0.05683(29)	0.19469(28)	-0.3169(5)	0.0039(5)
T7	-0.17245(25)	0.42653(26)	-0.3214(5)	0.0039(5)
T8	-0.12565(28)	0.31186(28)	-0.1794(5)	0.0039(5)
T9	-0.17444(26)	0.27073(30)	0.0332(5)	0.0039(5)
T10	-0.17691(25)	0.11709(31)	0.0347(5)	0.0039(5)
T11	-0.12924(27)	0.07091(32)	-0.1734(5)	0.0039(5)
T12	-0.16479(27)	0.18911(29)	-0.3167(5)	0.0039(5)
T13	0.44402(29)	0.42853(27)	-0.3385(4)	0.0039(5)
T14	0.47345(27)	0.31093(34)	-0.1915(5)	0.0039(5)
T15	0.43874(29)	0.27958(27)	0.0281(5)	0.0039(5)
T16	0.43351(29)	0.12339(28)	0.0335(4)	0.0039(5)
T17	0.47441(27)	0.07222(30)	-0.1793(5)	0.0039(5)
T18	0.43871(30)	0.18592(25)	-0.3210(5)	0.0039(5)
T19	0.67059(25)	0.42386(28)	-0.3153(4)	0.0039(5)
T20	0.63214(27)	0.31113(31)	-0.1706(5)	0.0039(5)
T21	0.66945(27)	0.27262(31)	0.0450(5)	0.0039(5)
T22	0.67101(27)	0.11898(31)	0.0370(5)	0.0039(5)
T23	0.63197(29)	0.07370(30)	-0.1806(5)	0.0039(5)
T24	0.68095(27)	0.19403(31)	-0.3031(5)	0.0039(5)
O1	0.06247(41)	0.37775(38)	-0.2268(6)	0.0065(1)
O2	0.06513(43)	0.31050(42)	-0.0615(4)	0.0065(1)
O3	0.04938(44)	0.20146(24)	0.0388(10)	0.0065(1)
O4	0.06937(35)	0.10134(60)	-0.0813(4)	0.0065(1)
O5	0.04375(47)	0.12316(30)	-0.2697(6)	0.0065(1)
O6	0.04871(58)	0.24951(39)	-0.2320(7)	0.0065(1)

O7	-0.15686(50)	0.37557(42)	-0.2331(7)	0.0065(1)
O8	-0.16181(48)	0.30099(45)	-0.0751(5)	0.0065(1)
O9	-0.15629(51)	0.19365(26)	0.0326(9)	0.0065(1)
O10	-0.17032(33)	0.08620(55)	-0.0744(5)	0.0065(1)
O11	-0.15321(48)	0.12029(38)	-0.2600(7)	0.0065(1)
O12	-0.13737(55)	0.24831(44)	-0.2485(8)	0.0065(1)
O13	-0.04723(23)	0.32294(48)	-0.1611(9)	0.0065(1)
O14	-0.05092(21)	0.08091(47)	-0.1525(8)	0.0065(1)
O15	0.12282(30)	0.41857(41)	-0.3869(6)	0.0065(1)
O16	-0.00547(35)	0.39212(48)	-0.3923(7)	0.0065(1)
O17	-0.13483(32)	0.40321(48)	-0.4198(6)	0.0065(1)
O18	0.13109(27)	0.19783(55)	-0.3607(4)	0.0065(1)
O19	0.00392(32)	0.20770(44)	-0.4046(7)	0.0065(1)
O20	-0.12520(34)	0.18846(52)	-0.4195(5)	0.0065(1)
O21	0.04718(42)	0.00231(29)	-0.2033(6)	0.0065(1)
O22	-0.14266(48)	-0.00367(29)	-0.2084(6)	0.0065(1)
O23	-0.25150(19)	0.42873(53)	-0.3416(6)	0.0065(1)
O24	-0.24293(22)	0.19908(49)	-0.3387(7)	0.0065(1)
O25	-0.25148(21)	0.28053(56)	0.0613(7)	0.0065(1)
O26	-0.25265(19)	0.11066(55)	0.0718(6)	0.0065(1)
O27	0.45026(54)	0.37659(39)	-0.2490(6)	0.0065(1)
O28	0.44816(55)	0.31316(43)	-0.0789(5)	0.0065(1)
O29	0.42779(45)	0.20157(24)	0.0154(8)	0.0065(1)
O30	0.44603(54)	0.08736(51)	-0.0707(5)	0.0065(1)
O31	0.43719(40)	0.11814(35)	-0.2594(8)	0.0065(1)
O32	0.44257(49)	0.24728(39)	-0.2458(9)	0.0065(1)
O33	0.66100(52)	0.37721(40)	-0.2202(6)	0.0065(1)
O34	0.64655(49)	0.31191(39)	-0.0532(4)	0.0065(1)
O35	0.65162(50)	0.19580(26)	0.0331(9)	0.0065(1)
O36	0.66175(48)	0.08765(56)	-0.0718(5)	0.0065(1)
O37	0.66717(48)	0.12172(35)	-0.2593(7)	0.0065(1)
O38	0.66830(57)	0.24805(43)	-0.2183(6)	0.0065(1)
O39	0.55346(22)	0.30639(70)	-0.1914(9)	0.0065(1)
O40	0.55310(23)	0.08705(43)	-0.1811(9)	0.0065(1)
O41	0.37189(29)	0.42171(39)	-0.3903(7)	0.0065(1)

O42	0.50112(35)	0.41471(42)	-0.4183(7)	0.0065(1)
O43	0.63031(34)	0.39386(45)	-0.4083(5)	0.0065(1)
O44	0.37201(35)	0.19169(47)	-0.3873(7)	0.0065(1)
O45	0.50274(36)	0.18689(50)	-0.3915(7)	0.0065(1)
O46	0.63186(30)	0.20763(52)	-0.3955(5)	0.0065(1)
O47	0.46162(41)	-0.00406(25)	-0.2051(6)	0.0065(1)
O48	0.64637(49)	-0.00156(28)	-0.2104(6)	0.0065(1)

Table 1-C 1. *Fractional atomic coordinates of ZSM-5 loaded with MTBE at 30°C [56].*

	ZSM-5-MTBE 30			
	x/a	**y/b**	**z/c**	**Uiso**
T1	0.05422(24)	0.42299(20)	-0.32853(38)	0.0042(9)
T2	0.03289(24)	0.31648(24)	-0.16757(38)	0.0042(9)
T3	0.06535(21)	0.28079(22)	0.04463(42)	0.0042(9)
T4	0.06465(25)	0.12496(22)	0.03471(35)	0.0042(9)
T5	0.02811(23)	0.07270(24)	-0.17287(40)	0.0042(9)
T6	0.05738(21)	0.19424(23)	-0.30775(32)	0.0042(9)
T7	-0.17116(22)	0.42583(22)	-0.32245(39)	0.0042(9)
T8	-0.12479(24)	0.31179(24)	-0.17574(39)	0.0042(9)
T9	-0.17543(24)	0.26949(24)	0.03311(42)	0.0042(9)
T10	-0.17825(23)	0.11428(23)	0.03045(44)	0.0042(9)
T11	-0.12891(24)	0.06690(25)	-0.17525(45)	0.0042(9)
T12	-0.16457(24)	0.18877(23)	-0.30996(35)	0.0042(9)
T13	0.44273(23)	0.42431(22)	-0.33351(34)	0.0042(9)
T14	0.47104(18)	0.31072(23)	-0.18160(33)	0.0042(9)
T15	0.43780(15)	0.27990(21)	0.03490(24)	0.0042(9)
T16	0.43301(25)	0.12309(21)	0.03032(36)	0.0042(9)
T17	0.47292(24)	0.07354(23)	-0.18408(42)	0.0042(9)
T18	0.44110(22)	0.18896(21)	-0.31945(37)	0.0042(9)
T19	0.67263(21)	0.42165(23)	-0.31214(36)	0.0042(9)
T20	0.63190(22)	0.31124(25)	-0.16729(33)	0.0042(9)
T21	0.66960(23)	0.27186(26)	0.04872(40)	0.0042(9)
T22	0.67089(24)	0.11689(25)	0.03547(42)	0.0042(9)
T23	0.63030(25)	0.07300(27)	-0.18315(42)	0.0042(9)
T24	0.67949(26)	0.19301(25)	-0.30059(32)	0.0042(9)
O1	0.06146(38)	0.37608(32)	-0.23321(54)	0.0065(18)
O2	0.06726(31)	0.31902(29)	-0.05965(31)	0.0065(18)
O3	0.05498(38)	0.20338(18)	0.02473(74)	0.0065(18)
O4	0.06844(32)	0.09249(41)	-0.07377(35)	0.0065(18)
O5	0.04798(39)	0.12189(24)	-0.26137(47)	0.0065(18)
O6	0.05047(35)	0.24791(29)	-0.22068(44)	0.0065(18)
O7	-0.15563(43)	0.37305(34)	-0.23642(59)	0.0065(18)

O8	-0.16183(39)	0.30522(37)	-0.07123(52)	0.0065(18)
O9	-0.16226(52)	0.19167(19)	0.02132(75)	0.0065(18)
O10	-0.17055(29)	0.07977(38)	-0.07604(41)	0.0065(18)
O11	-0.15305(43)	0.11786(29)	-0.25968(57)	0.0065(18)
O12	-0.13460(40)	0.24524(34)	-0.23883(63)	0.0065(18)
O13	-0.04637(20)	0.32394(34)	-0.15701(68)	0.0065(18)
O14	-0.05068(19)	0.07744(42)	-0.15319(75)	0.0065(18)
O15	0.12231(27)	0.42139(32)	-0.39012(50)	0.0065(18)
O16	-0.00610(31)	0.39730(35)	-0.39772(64)	0.0065(18)
O17	-0.13576(28)	0.40270(40)	-0.42322(52)	0.0065(18)
O18	0.12970(22)	0.20008(44)	-0.35745(36)	0.0065(18)
O19	0.00057(26)	0.20709(33)	-0.39040(42)	0.0065(18)
O20	-0.12807(24)	0.19087(45)	-0.41556(42)	0.0065(18)
O21	0.04688(41)	-0.00138(21)	-0.20486(40)	0.0065(18)
O22	-0.14151(37)	-0.00732(23)	-0.21337(53)	0.0065(18)
O23	-0.25028(17)	0.43040(38)	-0.34101(49)	0.0065(18)
O24	-0.24293(21)	0.20141(35)	-0.32639(24)	0.0065(18)
O25	-0.25142(18)	0.28204(53)	0.06530(54)	0.0065(18)
O26	-0.25308(18)	0.10506(50)	0.06956(52)	0.0065(18)
O27	0.44229(37)	0.37445(29)	-0.24093(46)	0.0065(18)
O28	0.45256(29)	0.31606(26)	-0.06799(25)	0.0065(18)
O29	0.43035(40)	0.20195(17)	0.01880(42)	0.0065(18)
O30	0.44315(49)	0.09043(38)	-0.07694(45)	0.0065(18)
O31	0.43670(39)	0.11796(22)	-0.26704(59)	0.0065(18)
O32	0.44854(34)	0.24521(28)	-0.23598(42)	0.0065(18)
O33	0.66735(28)	0.37392(35)	-0.21734(50)	0.0065(18)
O34	0.64609(41)	0.31062(27)	-0.04980(28)	0.0065(18)
O35	0.65421(49)	0.19438(21)	0.03639(79)	0.0065(18)
O36	0.66041(43)	0.08847(49)	-0.07489(39)	0.0065(18)
O37	0.66624(43)	0.11901(27)	-0.26347(52)	0.0065(18)
O38	0.66036(41)	0.24441(33)	-0.21484(38)	0.0065(18)
O39	0.55290(16)	0.31543(44)	-0.18834(62)	0.0065(18)
O40	0.55165(21)	0.08823(35)	-0.18408(87)	0.0065(18)
O41	0.37281(25)	0.41915(38)	-0.39216(48)	0.0065(18)
O42	0.50237(30)	0.40541(40)	-0.40683(50)	0.0065(18)

O43	0.63233(29)	0.39012(36)	-0.40436(43)	0.0065(18)
O44	0.37444(27)	0.20140(39)	-0.38382(62)	0.0065(18)
O45	0.50498(26)	0.19123(36)	-0.39040(48)	0.0065(18)
O46	0.63497(18)	0.20763(40)	-0.39774(31)	0.0065(18)
O47	0.46054(32)	-0.00312(17)	-0.20787(47)	0.0065(18)
O48	0.64278(38)	-0.00319(23)	-0.20991(57)	0.0065(18)

Table 1-D 1. *Fractional atomic coordinates of ZSM-5 loaded with CB at 30°C.*

	ZSM-5-CB 30				
	x/a	**y/b**	**z/c**	**Uiso**	**Fraction**
T1	0.05411(33)	0.42329(37)	-0.3309(6)	0.0055(1)	1
T2	0.03247(38)	0.31542(37)	-0.1725(6)	0.0055(1)	1
T3	0.06486(37)	0.28047(34)	0.0417(7)	0.0055(1)	1
T4	0.06466(35)	0.12454(34)	0.0324(6)	0.0055(1)	1
T5	0.02879(33)	0.07299(41)	-0.1764(6)	0.0055(1)	1
T6	0.05825(39)	0.19297(36)	-0.3127(6)	0.0055(1)	1
T7	-0.17187(33)	0.42631(32)	-0.3255(6)	0.0055(1)	1
T8	-0.12534(35)	0.31053(35)	-0.1820(6)	0.0055(1)	1
T9	-0.17528(34)	0.26986(35)	0.0291(6)	0.0055(1)	1
T10	-0.17811(33)	0.11401(34)	0.0295(7)	0.0055(1)	1
T11	-0.12856(34)	0.06647(39)	-0.1778(6)	0.0055(1)	1
T12	-0.16465(35)	0.18652(36)	-0.3158(6)	0.0055(1)	1
T13	0.44347(35)	0.42485(40)	-0.3354(6)	0.0055(1)	1
T14	0.47403(34)	0.31018(40)	-0.1883(6)	0.0055(1)	1
T15	0.43884(38)	0.27995(34)	0.0335(7)	0.0055(1)	1
T16	0.43200(35)	0.12268(35)	0.0296(5)	0.0055(1)	1
T17	0.47247(35)	0.07387(42)	-0.1864(6)	0.0055(1)	1
T18	0.44087(38)	0.18747(35)	-0.3240(7)	0.0055(1)	1
T19	0.67219(32)	0.42139(35)	-0.3149(5)	0.0055(1)	1
T20	0.63303(35)	0.30943(39)	-0.1714(6)	0.0055(1)	1
T21	0.67096(36)	0.27240(36)	0.0459(6)	0.0055(1)	1
T22	0.67162(35)	0.11686(36)	0.0328(6)	0.0055(1)	1
T23	0.63045(36)	0.07308(40)	-0.1869(6)	0.0055(1)	1
T24	0.68038(38)	0.19211(38)	-0.3067(6)	0.0055(1)	1
O1	0.06155(58)	0.37551(49)	-0.2366(9)	0.002(2)	1
O2	0.06619(57)	0.31686(60)	-0.0641(6)	0.002(2)	1
O3	0.05335(60)	0.20287(28)	0.0253(14)	0.002(2)	1
O4	0.06860(47)	0.09400(80)	-0.0774(7)	0.002(2)	1
O5	0.04914(62)	0.12080(36)	-0.2661(9)	0.002(2)	1
O6	0.05034(74)	0.24713(46)	-0.2266(8)	0.002(2)	1
O7	-0.15630(64)	0.37181(50)	-0.2420(9)	0.002(2)	1

O8	-0.16230(63)	0.30309(58)	-0.0775(7)	0.002(2)	1
O9	-0.16351(72)	0.19170(28)	0.0215(13)	0.002(2)	1
O10	-0.16894(44)	0.08022(65)	-0.0775(6)	0.002(2)	1
O11	-0.15438(61)	0.11621(42)	-0.2627(9)	0.002(2)	1
O12	-0.13549(67)	0.24401(50)	-0.2456(10)	0.002(2)	1
O13	-0.04693(30)	0.32262(57)	-0.1633(12)	0.002(2)	1
O14	-0.05015(27)	0.07828(61)	-0.1579(11)	0.002(2)	1
O15	0.12152(37)	0.42109(51)	-0.3944(8)	0.002(2)	1
O16	-0.00745(42)	0.39922(75)	-0.3988(10)	0.002(2)	1
O17	-0.13676(39)	0.40565(60)	-0.4275(8)	0.002(2)	1
O18	0.13097(37)	0.19873(69)	-0.3610(5)	0.002(2)	1
O19	0.00239(43)	0.20503(62)	-0.3968(9)	0.002(2)	1
O20	-0.12628(46)	0.18679(66)	-0.4196(7)	0.002(2)	1
O21	0.04753(60)	-0.00143(36)	-0.2057(6)	0.002(2)	1
O22	-0.14036(53)	-0.00826(34)	-0.2129(8)	0.002(2)	1
O23	-0.25093(25)	0.43138(56)	-0.3434(7)	0.002(2)	1
O24	-0.24259(30)	0.19905(62)	-0.3359(10)	0.002(2)	1
O25	-0.25053(29)	0.28435(71)	0.0624(9)	0.002(2)	1
O26	-0.25297(26)	0.10271(69)	0.0669(8)	0.002(2)	1
O27	0.44480(64)	0.37397(44)	-0.2442(9)	0.002(2)	1
O28	0.45081(70)	0.31078(62)	-0.0747(6)	0.002(2)	1
O29	0.42827(61)	0.20173(30)	0.0244(13)	0.002(2)	1
O30	0.44376(69)	0.09359(77)	-0.0796(7)	0.002(2)	1
O31	0.43603(56)	0.11698(38)	-0.2706(9)	0.002(2)	1
O32	0.44657(66)	0.24457(45)	-0.2416(10)	0.002(2)	1
O33	0.66715(53)	0.37286(50)	-0.2210(7)	0.002(2)	1
O34	0.64700(63)	0.30918(50)	-0.0540(5)	0.002(2)	1
O35	0.65689(70)	0.19465(30)	0.0363(12)	0.002(2)	1
O36	0.66027(64)	0.09058(78)	-0.0789(6)	0.002(2)	1
O37	0.66611(62)	0.11823(41)	-0.2688(8)	0.002(2)	1
O38	0.66355(77)	0.24350(50)	-0.2196(8)	0.002(2)	1
O39	0.55404(30)	0.31134(82)	-0.1922(11)	0.002(2)	1
O40	0.55152(30)	0.08749(54)	-0.1885(12)	0.002(2)	1
O41	0.37328(36)	0.41896(58)	-0.3931(8)	0.002(2)	1
O42	0.50309(42)	0.40816(75)	-0.4100(9)	0.002(2)	1

O43	0.63261(41)	0.39036(56)	-0.4079(7)	0.002(2)	1
O44	0.37527(46)	0.19920(65)	-0.3907(9)	0.002(2)	1
O45	0.50557(44)	0.18950(70)	-0.3932(9)	0.002(2)	1
O46	0.63474(38)	0.20777(59)	-0.4020(7)	0.002(2)	1
O47	0.45890(52)	-0.00290(35)	-0.2069(8)	0.002(2)	1
O48	0.64363(55)	-0.00335(35)	-0.2107(9)	0.002(2)	1

SECTION II:

Competitive behaviour of VOCs and humic acid monomers from binary aqueous mixtures in ZSM-5 at ambient condition

E-ZSM-5 loaded with TOL/MTBE and 1,2-DCE/MTBE binary mixtures

F- ZSM-5 loaded with TOL/CB binary mixture

G- Competitive adsorption of VOCs and humic monomers

Table 2-E 1. *Fractional atomic coordinates of ZSM-5 loaded with 1,2-DCE and MTBE in mixture at 30°C [56].*

ZSM-5-1,2-DCE/MTBE 30				
x/a	**y/b**	**z/c**	**Uiso**	**Fraction**
T1	0.05462(19)	0.42182(19)	-0.32417(32)	0.006(7)
T2	0.03358(21)	0.31680(21)	-0.16631(32)	0.006(7)
T3	0.06290(21)	0.27997(19)	0.05014(34)	0.006(7)
T4	0.06256(20)	0.12432(18)	0.03536(32)	0.006(7)
T5	0.02814(18)	0.07568(22)	-0.17463(33)	0.006(7)
T6	0.05838(21)	0.19612(19)	-0.31093(35)	0.006(1)
T7	-0.17182(17)	0.42669(18)	-0.32289(33)	0.006(1)
T8	-0.12432(19)	0.31186(19)	-0.17895(32)	0.006(1)
T9	-0.17488(18)	0.27098(20)	0.03161(34)	0.006(1)
T10	-0.17767(17)	0.11601(20)	0.03348(38)	0.006(1)
T11	-0.12918(19)	0.06854(22)	-0.17399(36)	0.006(1)
T12	-0.16394(19)	0.18849(19)	-0.31393(34)	0.006(1)
T13	0.44311(20)	0.42731(20)	-0.33397(33)	0.006(1)
T14	0.47426(19)	0.31154(23)	-0.18726(34)	0.006(1)
T15	0.43981(21)	0.27906(18)	0.03298(35)	0.006(1)
T16	0.43396(21)	0.12298(19)	0.03431(30)	0.006(1)
T17	0.47423(19)	0.07325(21)	-0.18088(35)	0.006(1)
T18	0.43869(20)	0.18764(18)	-0.31803(40)	0.006(1)
T19	0.67165(17)	0.42225(19)	-0.31369(31)	0.006(1)
T20	0.63285(18)	0.31079(21)	-0.16849(32)	0.006(1)
T21	0.66961(19)	0.27306(21)	0.04659(33)	0.006(1)
T22	0.67028(18)	0.11838(20)	0.03575(35)	0.006(1)
T23	0.63168(20)	0.07382(22)	-0.18358(33)	0.006(1)
T24	0.68193(19)	0.19456(21)	-0.30117(34)	0.006(1)
O1	0.06357(30)	0.37897(27)	-0.22484(44)	0,012(1)
O2	0.06548(32)	0.31485(35)	-0.05671(29)	0,012(1)
O3	0.04929(32)	0.20250(15)	0.03525(73)	0,012(1)
O4	0.06832(26)	0.09826(44)	-0.07677(36)	0,012(1)
O5	0.04586(34)	0.12422(20)	-0.26487(45)	0,012(1)
O6	0.05209(42)	0.25037(26)	-0.22484(49)	0,012(1)

O7	-0.15505(36)	0.37405(29)	-0.23727(52)	0,012(1)
O8	-0.16146(37)	0.30364(32)	-0.07484(39)	0,012(1)
O9	-0.16003(42)	0.19320(17)	0.02626(69)	0,012(1)
O10	-0.16907(24)	0.08228(38)	-0.07342(37)	0,012(1)
O11	-0.15419(34)	0.11894(25)	-0.25855(49)	0,012(1)
O12	-0.13503(37)	0.24645(30)	-0.24445(57)	0,012(1)
O13	-0.04598(17)	0.32356(31)	-0.15952(70)	0,012(1)
O14	-0.05059(14)	0.07861(34)	-0.15426(59)	0,012(1)
O15	0.12190(21)	0.41832(30)	-0.38771(41)	0,012(1)
O16	-0.00646(24)	0.39279(36)	-0.38878(50)	0,012(1)
O17	-0.13482(23)	0.40570(33)	-0.42320(44)	0,012(1)
O18	0.13177(19)	0.19907(38)	-0.35761(30)	0,012(1)
O19	0.00393(23)	0.21012(30)	-0.39649(53)	0,012(1)
O20	-0.12433(25)	0.18774(37)	-0.41682(36)	0,012(1)
O21	0.04921(34)	0.00192(20)	-0.20446(37)	0,012(1)
O22	-0.14259(33)	-0.00573(20)	-0.21046(43)	0,012(1)
O23	-0.25099(13)	0.42853(36)	-0.34221(44)	0,012(1)
O24	-0.24183(16)	0.20094(32)	-0.33578(56)	0,012(1)
O25	-0.25135(15)	0.28285(43)	0.06134(48)	0,012(1)
O26	-0.25339(13)	0.10761(42)	0.06945(46)	0,012(1)
O27	0.44857(37)	0.37736(26)	-0.24185(47)	0,012(1)
O28	0.45227(40)	0.31265(31)	-0.07304(36)	0,012(1)
O29	0.42720(32)	0.20132(16)	0.01904(62)	0,012(1)
O30	0.44949(40)	0.08892(38)	-0.07047(40)	0,012(1)
O31	0.43466(27)	0.11913(23)	-0.25858(57)	0,012(1)
O32	0.44255(32)	0.24795(27)	-0.24090(62)	0,012(1)
O33	0.66423(34)	0.37579(29)	-0.21788(41)	0,012(1)
O34	0.64481(33)	0.31237(28)	-0.05051(28)	0,012(1)
O35	0.65343(40)	0.19587(17)	0.03391(68)	0,012(1)
O36	0.65915(36)	0.08833(39)	-0.07342(32)	0,012(1)
O37	0.66883(30)	0.12111(24)	-0.26109(45)	0,012(1)
O38	0.66833(41)	0.24654(30)	-0.21375(44)	0,012(1)
O39	0.55429(16)	0.30793(47)	-0.19265(57)	0,012(1)
O40	0.55286(17)	0.08771(29)	-0.18824(66)	0,012(1)
O41	0.37183(19)	0.41868(32)	-0.38797(43)	0,012(1)

O42	0.50143(23)	0.41202(34)	-0.41144(51)	0,012(1)
O43	0.63065(23)	0.39101(30)	-0.40527(37)	0,012(1)
O44	0.37331(27)	0.19559(36)	-0.38694(53)	0,012(1)
O45	0.50399(26)	0.18802(38)	-0.38606(45)	0,012(1)
O46	0.63295(21)	0.20963(34)	-0.39318(38)	0,012(1)
O47	0.46035(30)	-0.00299(18)	-0.20561(40)	0,012(1)
O48	0.64615(33)	-0.00177(20)	-0.21152(44)	0,012(1)

Table 2-E 2. *Fractional atomic coordinates of ZSM-5 loaded with TOL and MTBE in mixture at 30°C [56].*

	ZSM-5-TOL/MTBE 30			
	x/a	**y/b**	**z/c**	**Uiso**
T1	0.05368(24)	0.42216(21)	-0.32790(39)	0,003(1)
T2	0.03334(26)	0.31657(25)	-0.16674(38)	0,003(1)
T3	0.06515(22)	0.28088(24)	0.04645(44)	0,003(1)
T4	0.06344(22)	0.12511(24)	0.03500(37)	0,003(1)
T5	0.02850(23)	0.07306(26)	-0.17391(39)	0,003(1)
T6	0.05741(21)	0.19488(25)	-0.30799(32)	0,003(1)
T7	-0.17122(23)	0.42565(22)	-0.32420(39)	0,003(1)
T8	-0.12417(25)	0.31132(25)	-0.17770(40)	0,003(1)
T9	-0.17593(24)	0.27046(25)	0.03146(40)	0,003(1)
T10	-0.17898(23)	0.11443(22)	0.03097(34)	0,003(1)
T11	-0.12905(24)	0.06660(24)	-0.17554(37)	0,003(1)
T12	-0.16406(24)	0.18832(24)	-0.31122(37)	0,003(1)
T13	0.44213(22)	0.42439(23)	-0.33275(35)	0,003(1)
T14	0.47133(18)	0.31004(24)	-0.18197(34)	0,003(1)
T15	0.43779(16)	0.27995(22)	0.03492(26)	0,003(1)
T16	0.43281(25)	0.12352(22)	0.03065(38)	0,003(1)
T17	0.47316(25)	0.07360(24)	-0.18441(40)	0,003(1)
T18	0.44054(23)	0.18840(22)	-0.31947(39)	0,003(1)
T19	0.67239(21)	0.42101(24)	-0.31272(38)	0,003(1)
T20	0.63199(23)	0.31032(25)	-0.16755(35)	0,003(1)
T21	0.66988(25)	0.27305(27)	0.04793(42)	0,003(1)
T22	0.67036(21)	0.11739(24)	0.03381(41)	0,003(1)
T23	0.63057(26)	0.07311(27)	-0.18546(37)	0,003(1)
T24	0.68043(26)	0.19322(25)	-0.30066(34)	0,003(1)
O1	0.06233(39)	0.37651(33)	-0.23136(56)	0,005(1)
O2	0.06708(33)	0.31866(31)	-0.05823(32)	0,005(1)
O3	0.05312(39)	0.20357(19)	0.02716(76)	0,005(1)
O4	0.06768(32)	0.09398(42)	-0.07435(36)	0,005(1)
O5	0.04793(41)	0.12223(24)	-0.26256(46)	0,005(1)
O6	0.05116(37)	0.24815(30)	-0.22018(45)	0,005(1)

O7	-0.15472(44)	0.37221(34)	-0.23950(55)	0,005(1)
O8	-0.16216(38)	0.30449(33)	-0.07408(50)	0,005(1)
O9	-0.16508(39)	0.19211(19)	0.02194(61)	0,005(1)
O10	-0.16901(29)	0.07971(39)	-0.07495(32)	0,005(1)
O11	-0.15393(43)	0.11758(28)	-0.25945(49)	0,005(1)
O12	-0.13280(37)	0.24465(33)	-0.24096(60)	0,005(1)
O13	-0.04599(21)	0.32405(35)	-0.15719(69)	0,005(1)
O14	-0.05049(19)	0.07672(42)	-0.15553(70)	0,005(1)
O15	0.12074(25)	0.41955(36)	-0.39180(52)	0,005(1)
O16	-0.00752(29)	0.39548(37)	-0.39430(65)	0,005(1)
O17	-0.13617(27)	0.40420(39)	-0.42600(48)	0,005(1)
O18	0.12970(22)	0.20031(46)	-0.35769(38)	0,005(1)
O19	0.00052(26)	0.20846(34)	-0.39002(43)	0,005(1)
O20	-0.12762(25)	0.18888(41)	-0.41676(42)	0,005(1)
O21	0.04865(37)	-0.00091(22)	-0.20480(42)	0,005(1)
O22	-0.14228(39)	-0.00759(21)	-0.21338(52)	0,005(1)
O23	-0.25055(17)	0.42913(40)	-0.34213(48)	0,005(1)
O24	-0.24219(20)	0.20229(33)	-0.32741(26)	0,005(1)
O25	-0.25141(20)	0.28532(44)	0.06417(56)	0,005(1)
O26	-0.25406(17)	0.10265(28)	0.06769(28)	0,005(1)
O27	0.44365(37)	0.37485(30)	-0.23985(47)	0,005(1)
O28	0.45393(29)	0.31534(27)	-0.06809(26)	0,005(1)
O29	0.42823(39)	0.20220(18)	0.01903(42)	0,005(1)
O30	0.44620(49)	0.09111(41)	-0.07592(48)	0,005(1)
O31	0.43502(33)	0.11779(24)	-0.26589(65)	0,005(1)
O32	0.44674(35)	0.24536(30)	-0.23680(43)	0,005(1)
O33	0.66694(29)	0.37309(31)	-0.21820(48)	0,005(1)
O34	0.64498(42)	0.31145(28)	-0.04993(29)	0,005(1)
O35	0.65645(37)	0.19527(21)	0.03533(82)	0,005(1)
O36	0.65889(37)	0.08964(51)	-0.07658(38)	0,005(1)
O37	0.66762(42)	0.11866(25)	-0.26535(54)	0,005(1)
O38	0.66190(39)	0.24345(31)	-0.21300(37)	0,005(1)
O39	0.55314(16)	0.31296(44)	-0.19040(63)	0,005(1)
O40	0.55188(21)	0.08805(37)	-0.18923(68)	0,005(1)
O41	0.37150(14)	0.41753(28)	-0.38924(29)	0,005(1)

O42	0.50130(21)	0.40645(41)	-0.40748(52)	0,005(1)
O43	0.63130(24)	0.39013(37)	-0.40462(44)	0,005(1)
O44	0.37512(27)	0.20059(40)	-0.38686(58)	0,005(1)
O45	0.50568(26)	0.18985(35)	-0.38797(50)	0,005(1)
O46	0.63524(18)	0.20879(40)	-0.39676(32)	0,005(1)
O47	0.46021(33)	-0.00329(17)	-0.20654(50)	0,005(1)
O48	0.64387(38)	-0.00331(22)	-0.20994(61)	0,005(1)

Table 2-F 1. *Fractional atomic coordinates and thermal parameters of ZSM-5-TOL/CB framework at 30°C.*

	ZSM-5-TOL/CB 30			
	x/a	**y/b**	**z/c**	**Uiso**
T1	0.05463(28)	0.42328(30)	-0.3317(5)	0.0060(1)
T2	0.03521(29)	0.31614(34)	-0.1729(6)	0.0060(1)
T3	0.06483(34)	0.28026(26)	0.0417(6)	0.0060(1)
T4	0.06411(29)	0.12445(25)	0.0324(5)	0.0060(1)
T5	0.02872(24)	0.07247(31)	-0.1765(6)	0.0060(1)
T6	0.06052(32)	0.19341(31)	-0.3116(6)	0.0060(1)
T7	-0.17119(26)	0.42653(26)	-0.3267(5)	0.0060(1)
T8	-0.12318(27)	0.30989(28)	-0.1850(5)	0.0060(1)
T9	-0.17453(28)	0.27041(28)	0.0263(6)	0.0060(1)
T10	-0.17760(26)	0.11475(26)	0.0305(7)	0.0060(1)
T11	-0.12873(26)	0.06629(37)	-0.1766(7)	0.0060(1)
T12	-0.16387(32)	0.18546(27)	-0.3172(6)	0.0060(1)
T13	0.44334(29)	0.42406(32)	-0.3334(6)	0.0060(1)
T14	0.47460(28)	0.30866(35)	-0.1885(6)	0.0060(1)
T15	0.44022(30)	0.28041(25)	0.0352(6)	0.0060(1)
T16	0.43234(30)	0.12358(27)	0.0302(5)	0.0060(1)
T17	0.47383(27)	0.07480(36)	-0.1862(6)	0.0060(1)
T18	0.43993(29)	0.18757(32)	-0.3241(7)	0.0060(1)
T19	0.67228(25)	0.42089(29)	-0.3153(5)	0.0060(1)
T20	0.63296(27)	0.30801(32)	-0.1735(5)	0.0060(1)
T21	0.67052(27)	0.27298(31)	0.0438(5)	0.0060(1)
T22	0.67137(28)	0.11764(29)	0.0318(6)	0.0060(1)
T23	0.63155(29)	0.07390(38)	-0.1879(5)	0.0060(1)
T24	0.68189(33)	0.19215(34)	-0.3076(6)	0.0060(1)
O1	0.06368(53)	0.37706(47)	-0.2358(8)	0.0070(1)
O2	0.06631(59)	0.31826(47)	-0.0628(6)	0.0070(1)
O3	0.05366(50)	0.20279(21)	0.0226(11)	0.0070(1)
O4	0.06786(46)	0.09234(66)	-0.0764(7)	0.0070(1)
O5	0.04977(59)	0.12152(34)	-0.2643(9)	0.0070(1)
O6	0.05575(64)	0.24816(43)	-0.2258(7)	0.0070(1)

O7	-0.15380(62)	0.37166(51)	-0.2445(9)	0.0070(1)
O8	-0.15958(67)	0.30294(56)	-0.0799(7)	0.0070(1)
O9	-0.16222(68)	0.19221(22)	0.0206(13)	0.0070(1)
O10	-0.16790(36)	0.07963(54)	-0.0752(6)	0.0070(1)
O11	-0.15549(53)	0.11614(43)	-0.2606(8)	0.0070(1)
O12	-0.13466(62)	0.24368(51)	-0.2486(11)	0.0070(1)
O13	-0.04462(24)	0.32114(47)	-0.1674(13)	0.0070(1)
O14	-0.05024(20)	0.07783(55)	-0.1588(11)	0.0070(1)
O15	0.12153(31)	0.42135(40)	-0.3963(6)	0.0070(1)
O16	-0.00697(35)	0.39709(66)	-0.3977(9)	0.0070(1)
O17	-0.13578(33)	0.40772(47)	-0.4292(8)	0.0070(1)
O18	0.13273(28)	0.19686(60)	-0.3620(5)	0.0070(1)
O19	0.00383(35)	0.20697(53)	-0.3940(9)	0.0070(1)
O20	-0.12382(40)	0.18314(54)	-0.4197(6)	0.0070(1)
O21	0.04750(58)	-0.00184(29)	-0.2067(5)	0.0070(1)
O22	-0.14130(46)	-0.00837(35)	-0.2120(7)	0.0070(1)
O23	-0.25055(20)	0.42959(50)	-0.3436(7)	0.0070(1)
O24	-0.24148(28)	0.19872(54)	-0.3398(10)	0.0070(1)
O25	-0.25058(21)	0.28460(68)	0.0559(8)	0.0070(1)
O26	-0.25301(20)	0.10456(63)	0.0666(8)	0.0070(1)
O27	0.44563(61)	0.37368(38)	-0.2416(9)	0.0070(1)
O28	0.45480(58)	0.30922(55)	-0.0734(6)	0.0070(1)
O29	0.42595(48)	0.20257(24)	0.0276(11)	0.0070(1)
O30	0.44617(64)	0.09658(67)	-0.0796(7)	0.0070(1)
O31	0.43670(51)	0.11662(33)	-0.2714(9)	0.0070(1)
O32	0.44361(48)	0.24429(39)	-0.2411(10)	0.0070(1)
O33	0.66623(50)	0.37248(53)	-0.2215(7)	0.0070(1)
O34	0.64434(45)	0.30886(45)	-0.0555(5)	0.0070(1)
O35	0.65562(62)	0.19525(26)	0.0365(11)	0.0070(1)
O36	0.66111(60)	0.09194(66)	-0.0801(5)	0.0070(1)
O37	0.66772(49)	0.11821(42)	-0.2703(6)	0.0070(1)
O38	0.66688(75)	0.24309(54)	-0.2193(8)	0.0070(1)
O39	0.55441(24)	0.30743(76)	-0.1980(9)	0.0070(1)
O40	0.55274(24)	0.08827(45)	-0.1905(12)	0.0070(1)
O41	0.37280(27)	0.41758(55)	-0.3899(7)	0.0070(1)

O42	0.50249(33)	0.40696(66)	-0.4087(10)	0.0070(1)
O43	0.63224(33)	0.39017(42)	-0.4081(6)	0.0070(1)
O44	0.37438(41)	0.19795(59)	-0.3916(10)	0.0070(1)
O45	0.50500(40)	0.19137(62)	-0.3925(8)	0.0070(1)
O46	0.63445(34)	0.20861(48)	-0.4009(6)	0.0070(1)
O47	0.45970(43)	-0.00236(32)	-0.2032(6)	0.0070(1)
O48	0.64471(46)	-0.00279(36)	-0.2106(7)	0.0070(1)

Table 2-G 1. *Fractional atomic coordinates and thermal parameters of ZSM-5-p-HBA framework and extraframework at 30°C.*

	ZSM-5-p-HBA 30			
	x/a	**y/b**	**z/c**	**Uiso**
T1	0.4233(1)	1.0545(1)	0.4038(1)	0.0075(1)
T2	0.3036(1)	1.0313(1)	0.5435(1)	0.0075(1)
T3	0.2834(1)	1.0687(1)	0.7703(1)	0.0075(1)
T4	0.1251(1)	1.0676(1)	0.7691(1)	0.0075(1)
T5	0.0742(1)	1.0261(1)	0.5557(1)	0.0075(1)
T6	0.1801(1)	1.0561(1)	0.4037(1)	0.0075(1)
T7	0.4231(1)	0.8265(1)	0.4068(1)	0.0075(1)
T8	0.3028(1)	0.8716(1)	0.5442(1)	0.0075(1)
T9	0.2744(1)	0.8297(1)	0.7649(1)	0.0075(1)
T10	0.1194(1)	0.8291(1)	0.7675(1)	0.0075(1)
T11	0.0693(1)	0.8677(1)	0.5519(1)	0.0075(1)
T12	0.1803(1)	0.8232(1)	0.4105(1)	0.0075(1)
T13	0.9251(1)	1.0591(1)	0.5997(1)	0.0075(1)
T14	0.8064(1)	1.0301(1)	0.4556(1)	0.0075(1)
T15	0.7830(1)	1.0601(1)	0.2338(1)	0.0075(1)
T16	0.6240(1)	1.0621(1)	0.2320(1)	0.0075(1)
T17	0.5726(1)	1.0277(1)	0.4418(1)	0.0075(1)
T18	0.6812(1)	1.0592(1)	0.5956(1)	0.0075(1)
T19	0.9216(1)	0.8294(1)	0.5803(1)	0.0075(1)
T20	0.8038(1)	0.8714(1)	0.4409(1)	0.0075(1)
T21	0.7743(1)	0.8242(1)	0.2201(1)	0.0075(1)
T22	0.6196(1)	0.8228(1)	0.2233(1)	0.0075(1)
T23	0.5705(1)	0.8696(1)	0.4361(1)	0.0075(1)
T24	0.6814(1)	0.8313(1)	0.5797(1)	0.0075(1)
O1	0.3691(1)	1.0595(1)	0.4905(1)	0.0098(1)
O2	0.3005(1)	1.0592(1)	0.6550(1)	0.0098(1)
O3	0.2042(1)	1.0695(1)	0.7845(1)	0.0098(1)
O4	0.1082(1)	1.0557(1)	0.6540(1)	0.0098(1)
O5	0.1099(1)	1.0561(1)	0.4595(1)	0.0098(1)
O6	0.2394(1)	1.0557(1)	0.4831(1)	0.0098(1)

O7	0.3665(1)	0.8429(1)	0.4868(1)	0.0098(1)
O8	0.3003(1)	0.8406(1)	0.6535(1)	0.0098(1)
O9	0.1968(1)	0.8476(1)	0.7711(1)	0.0098(1)
O10	0.0933(1)	0.8352(1)	0.6549(1)	0.0098(1)
O11	0.1091(1)	0.8354(1)	0.4607(1)	0.0098(1)
O12	0.2369(1)	0.8498(1)	0.4847(1)	0.0098(1)
O13	0.3064(1)	0.9514(1)	0.5478(1)	0.0098(1)
O14	0.0825(1)	0.9465(1)	0.5553(1)	0.0098(1)
O15	0.4215(1)	1.1210(1)	0.3375(1)	0.0098(1)
O16	0.4064(1)	0.9914(1)	0.3345(1)	0.0098(1)
O17	0.4060(1)	0.8625(1)	0.3035(1)	0.0098(1)
O18	0.1845(1)	1.1218(1)	0.3368(1)	0.0098(1)
O19	0.1856(1)	0.9916(1)	0.3335(1)	0.0098(1)
O20	0.1852(1)	0.8624(1)	0.3075(1)	0.0098(1)
O21	-0.0030(1)	1.0450(1)	0.5537(1)	0.0098(1)
O22	-0.0086(1)	0.8546(1)	0.5372(1)	0.0098(1)
O23	0.4274(1)	0.7477(1)	0.3892(1)	0.0098(1)
O24	0.1910(1)	0.7454(1)	0.3908(1)	0.0098(1)
O25	0.2852(1)	0.7539(1)	0.7986(1)	0.0098(1)
O26	0.1087(1)	0.7540(1)	0.8056(1)	0.0098(1)
O27	0.8706(1)	1.0574(1)	0.5130(1)	0.0098(1)
O28	0.8023(1)	1.0648(1)	0.3487(1)	0.0098(1)
O29	0.7034(1)	1.0585(1)	0.2232(1)	0.0098(1)
O30	0.6031(1)	1.0651(1)	0.3468(1)	0.0098(1)
O31	0.6113(1)	1.0501(1)	0.5401(1)	0.0098(1)
O32	0.7408(1)	1.0468(1)	0.5185(1)	0.0098(1)
O33	0.8659(1)	0.8377(1)	0.4961(1)	0.0098(1)
O34	0.7995(1)	0.8441(1)	0.3292(1)	0.0098(1)
O35	0.6966(1)	0.8414(1)	0.2104(1)	0.0098(1)
O36	0.5982(1)	0.8344(1)	0.3371(1)	0.0098(1)
O37	0.6093(1)	0.8417(1)	0.5313(1)	0.0098(1)
O38	0.7369(1)	0.8524(1)	0.4998(1)	0.0098(1)
O39	0.8127(1)	0.9508(1)	0.4410(1)	0.0098(1)
O40	0.5808(1)	0.9486(1)	0.4276(1)	0.0098(1)
O41	0.9245(1)	1.1309(1)	0.6522(1)	0.0098(1)

O42	0.9080(1)	1.0027(1)	0.6808(1)	0.0098(1)
O43	0.9021(1)	0.8724(1)	0.6762(1)	0.0098(1)
O44	0.6855(1)	1.1335(1)	0.6388(1)	0.0098(1)
O45	0.6866(1)	1.0066(1)	0.6854(1)	0.0098(1)
O46	0.6882(1)	0.8763(1)	0.6769(1)	0.0098(1)
O47	0.4954(1)	1.0457(1)	0.4519(1)	0.0098(1)
O48	0.4929(1)	0.8535(1)	0.4477(1)	0.0098(1)

Extraframework sites ZSM-5-P-HBA 30

	x/a	**y/b**	**z/c**	**Uiso**	**Fraction**
			Site 1		
C1	0.0199(1)	0.7252(1)	0.1918(1)	0.0720(1)	1
C2	0.0677(1)	0.7664(1)	0.1477(1)	0.0720(1)	1
C3	0.0611(1)	0.8369(1)	0.1529(1)	0.0720(1)	1
C4	0.0088(1)	0.8648(1)	0.2084(1)	0.0720(1)	1
C5	-0.0382(1)	0.8234(1)	0.2539(1)	0.0720(1)	1
C6	-0.0332(1)	0.7537(1)	0.2442(1)	0.0720(1)	1
C7	0.0299(1)	0.6566(1)	0.1955(1)	0.0720(1)	1
C8	0.0744(1)	0.6254(1)	0.1315(1)	0.0720(1)	1
C9	0.0076(1)	0.9332(1)	0.2267(1)	0.0720(1)	1
			Site 2		
C10	-0.1060(1)	0.7792(1)	-0.0888(1)	0.0641(1)	0.658(1)
C11	-0.0944(1)	0.7556(1)	0.0074(1)	0.0641(1)	0.658(1)
C12	-0.1439(1)	0.7148(1)	0.0474(1)	0.0641(1)	0.658(1)
C13	-0.2071(1)	0.7092(1)	0.0124(1)	0.0641(1)	0.658(1)
C14	-0.2179(1)	0.7424(1)	-0.0857(1)	0.0641(1)	0.658(1)
C15	-0.1696(1)	0.7839(1)	-0.129731	0.0641(1)	0.658(1)
C16	0.4484(4)	0.6994(1)	0.1456(1)	0.0641(1)	0.658(1)
C17	0.4791(1)	0.7444(1)	0.2109(1)	0.0641(1)	0.658(1)
C18	0.7356(1)	0.6829(1)	0.0488(1)	0.0641(1)	0.658(1)

Table 2-G 2. *Fractional atomic coordinates and thermal parameters of ZSM-5-CA framework and extraframework sites at 30°C*

	ZSM-5-CA 30			
	x/a	**y/b**	**z/c**	**Uiso**
T1	0.424(3)	1.056(1)	0.407(2)	0.0049(1)
T2	0.308(4)	1.030(2)	0.551(9)	0.0049(1)
T3	0.282(7)	1.062(6)	0.775(7)	0.0049(1)
T4	0.124(1)	1.065(1)	0.775(4)	0.0049(1)
T5	0.073(5)	1.028(1)	0.564(6)	0.0049(1)
T6	0.184(3)	1.059(8)	0.415(2)	0.0049(1)
T7	0.424(3)	0.828(9)	0.423(3)	0.0049(1)
T8	0.307(5)	0.871(1)	0.558(2)	0.0049(1)
T9	0.273(2)	0.827(2)	0.778(7)	0.0049(1)
T10	0.119(4)	0.825(1)	0.777(7)	0.0049(1)
T11	0.072(5)	0.870(1)	0.565(8)	0.0049(1)
T12	0.185(3)	0.827(2)	0.423(2)	0.0049(1)
T13	0.924(3)	1.057(1)	0.593(2)	0.0049(1)
T14	0.808(4)	1.030(2)	0.449(9)	0.0049(1)
T15	0.782(7)	1.062(6)	0.225(7)	0.0049(1)
T16	0.624(1)	1.065(1)	0.225(4)	0.0049(1)
T17	0.573(5)	1.028(1)	0.436(6)	0.0049(1)
T18	0.684(3)	1.059(8)	0.585(2)	0.0049(1)
T19	0.924(3)	0.828(9)	0.577(3)	0.0049(1)
T20	0.807(5)	0.871(1)	0.442(2)	0.0049(1)
T21	0.773(2)	0.827(2)	0.222(7)	0.0049(1)
T22	0.619(4)	0.825(1)	0.223(7)	0.0049(1)
T23	0.572(5)	0.870(1)	0.435(8)	0.0049(1)
T24	0.685(3)	0.827(2)	0.577(2)	0.0049(1)
O1	0.371(6)	1.058(5)	0.495(8)	0.0121(1)
O2	0.306(2)	1.058(14)	0.662(2)	0.0121(1)
O3	0.203(1)	1.062(1)	0.778(2)	0.0121(1)
O4	0.100(7)	1.064(4)	0.662(2)	0.0121(1)
O5	0.114(4)	1.053(8)	0.470(3)	0.0121(1)
O6	0.242(7)	1.053(2)	0.494(3)	0.0121(1)

O7	0.372(7)	0.840(6)	0.510(7)	0.0121(1)
O8	0.300(6)	0.847(2)	0.670(8)	0.0121(1)
O9	0.196(3)	0.843(2)	0.784(3)	0.0121(1)
O10	0.094(8)	0.835(5)	0.665(6)	0.0121(1)
O11	0.115(7)	0.843(4)	0.475(7)	0.0121(1)
O12	0.244(8)	0.846(2)	0.496(2)	0.0121(1)
O13	0.311(2)	0.950(1)	0.554(3)	0.0121(1)
O14	0.082(3)	0.949(1)	0.575(2)	0.0121(1)
O15	0.422(8)	1.126(1)	0.348(3)	0.0121(1)
O16	0.406(3)	0.997(2)	0.332(5)	0.0121(1)
O17	0.400(1)	0.867(1)	0.326(4)	0.0121(1)
O18	0.189(1)	1.130(6)	0.360(2)	0.0121(1)
O19	0.190(1)	1.001(5)	0.335(2)	0.0121(1)
O20	0.191(4)	0.871(5)	0.324(7)	0.0121(1)
O21	-0.004(5)	1.045(1)	0.549(6)	0.0121(1)
O22	-0.005(6)	0.855(5)	0.544(7)	0.0121(1)
O23	0.429(7)	0.750(6)	0.398(4)	0.0121(1)
O24	0.188(8)	0.750(7)	0.395(2)	0.0121(1)
O25	0.286(2)	0.750(5)	0.798(2)	0.0121(1)
O26	0.107(6)	0.750(7)	0.811(2)	0.0121(1)
O27	0.871(6)	1.058(5)	0.505(3)	0.0121(1)
O28	0.806(2)	1.058(2)	0.338(2)	0.0121(1)
O29	0.703(1)	1.062(1)	0.222(3)	0.0121(1)
O30	0.600(7)	1.064(4)	0.338(2)	0.0121(1)
O31	0.614(4)	1.053(2)	0.530(3)	0.0121(1)
O32	0.742(7)	1.053(1)	0.506(3)	0.0121(1)
O33	0.872(7)	0.840(6)	0.490(7)	0.0121(1)
O34	0.800(6)	0.847(2)	0.330(8)	0.0121(1)
O35	0.696(3)	0.843(4)	0.216(3)	0.0121(1)
O36	0.594(8)	0.835(5)	0.335(6)	0.0121(1)
O37	0.615(7)	0.843(4)	0.525(7)	0.0121(1)
O38	0.744(8)	0.846(1)	0.503(2)	0.0121(1)
O39	0.811(3)	0.950(1)	0.446(3)	0.0121(1)
O40	0.582(3)	0.949(1)	0.425(2)	0.0121(1)
O41	0.922(8)	1.126(1)	0.652(4)	0.0121(1)

O42	0.906(3)	0.997(2)	0.668(3)	0.0121(1)
O43	0.900(1)	0.867(2)	0.674(4)	0.0121(1)
O44	0.689(1)	1.130(6)	0.640(2)	0.0121(1)
O45	0.690(1)	1.001(5)	0.665(2)	0.0121(1)
O46	0.691(4)	0.871(5)	0.676(7)	0.0121(1)
O47	0.496(5)	1.045(1)	0.451(9)	0.0121(1)
O48	0.495(6)	0.855(5)	0.456(7)	0.0121(1)

Extraframework sites ZSM-5-CA 30

	x/a	**y/b**	**z/c**	**Uiso**	**Fraction**
C1	-0.0031(1)	0.8150(1)	0.2296(1)	0.250(1)	0.693(1)
C2	0.0015(1)	0.7607(1)	0.2940(1)	0.250(1)	0.693(1)
C3	-0.0026(1)	0.6952(1)	0.2580(1)	0.250(1)	0.693(1)
C4	-0.0118(1)	0.6843(1)	0.1560(1)	0.250(1)	0.693(1)
C5	-0.0158(1)	0.7390(1)	0.0910(1)	0.250(1)	0.693(1)
C6	-0.0117(1)	0.8042(1)	0.1281(1)	0.250(1)	0.693(1)
C7	-0.0368(1)	0.7890(1)	-0.0036(1)	0.250(1)	0.693(1)
C8	0.3974(1)	0.7678(1)	0.0273(1)	0.250(1)	0.693(1)
C9	0.3669(1)	0.7694(1)	0.1211(1)	0.250(1)	0.693(1)
O1C	0.0070(1)	0.7721(1)	0.3949(1)	0.250(1)	0.693(1)
O2C	0.3112(1)	0.7133(1)	0.1337(1)	0.250(1)	0.693(1)
O3C	0.4096(1)	0.7689(1)	0.2170(1)	0.250(1)	0.693(1)
O4C	0.9910(1)	0.8651(1)	0.2582(1)	0.250(1)	0.693(1)

SECTION III:

Study of the desorption process of VOCs confined into ZSM-5 through the *in situ* HT synchrotron XRPD

H- Desorption process of 1,2-DCE induced by heating

I- Desorption process of TOL induced by heating

L- Desorption process of MTBE induced by heating

M- Desorption process of 1,2-DCE/MTBE and TOL/MTBE binary mixtures induced by heating

Table 3-H 1. *Fractional atomic coordinates and thermal parameters of ZSM-5-1,2-DCE framework at 75°C [8].*

	ZSM-5-1,2-DCE 75 [10]				
	x/a	**y/b**	**z/c**	**Uiso**	**Fraction**
T1	0.4210(9)	0.0552(9)	-0.3366(12)	0.124(1)	1
T2	0.3100(9)	0.0345(8)	-0.1864(12)	0.124(1)	1
T3	0.2809(8)	0.0606(9)	0.0199(12)	0.124(1)	1
T4	0.1175(8)	0.0540(9)	0.0298(13)	0.124(1)	1
T5	0.0743(9)	0.0309(8)	-0.1826(13)	0.124(1)	1
T6	0.1870(9)	0.0489(8)	-0.3260(12)	0.124(1)	1
T7	0.4268(10)	-0.1674(7)	-0.3203(13)	0.124(1)	1
T8	0.3111(9)	-0.1259(8)	-0.1853(12)	0.124(1)	1
T9	0.2728(8)	-0.1706(7)	0.0333(13)	0.124(1)	1
T10	0.1221(9)	-0.1857(8)	0.0381(12)	0.124(1)	1
T11	0.0736(10)	-0.1282(9)	-0.1914(13)	0.124(1)	1
T12	0.1909(10)	-0.1761(7)	-0.3316(12)	0.124(1)	1
O1	0.3741(11)	0.0435(15)	-0.2469(17)	0.0228(2)	1
O2	0.3092(14)	0.0562(13)	-0.0860(15)	0.0228(2)	1
O3	0.2020(10)	0.0537(14)	0.0186(16)	0.0228(2)	1
O4	0.0933(12)	0.0487(14)	-0.0844(16)	0.0228(2)	1
O5	0.1170(11)	0.0371(14)	-0.2802(17)	0.0228(2)	1
O6	0.2445(12)	0.0404(14)	-0.2399(17)	0.0228(2)	1
O7	0.3763(11)	-0.1627(14)	-0.2205(17)	0.0228(2)	1
O8	0.3038(16)	-0.1668(11)	-0.0789(15)	0.0228(2)	1
O9	0.1933(10)	-0.1472(11)	0.0371(17)	0.0228(2)	1
O10	0.1031(13)	-0.1556(13)	-0.0747(16)	0.0228(2)	1
O11	0.1267(11)	-0.1505(14)	-0.2822(18)	0.0228(2)	1
O12	0.2491(13)	-0.1649(13)	-0.2594(18)	0.0228(2)	1
O13	0.3091(14)	-0.0428(9)	-0.1761(17)	0.0228(2)	1
O14	0.0782(13)	-0.0458(10)	-0.1726(19)	0.0228(2)	1
O15	0.4168(13)	0.1360(11)	-0.3788(18)	0.0228(2)	1
O16	0.4063(13)	0.0133(11)	-0.4256(18)	0.0228(2)	1
O17	0.4096(14)	-0.1237(11)	-0.4278(18)	0.0228(2)	1
O18	0.1943(15)	0.1075(10)	-0.4063(16)	0.0228(2)	1

O19	0.2017(15)	-0.0129(11)	-0.3879(17)	0.0228(2)	1
O20	0.2028(16)	-0.1288(11)	-0.4202(17)	0.0228(2)	1
O21	0.0020(11)	0.0470(14)	-0.2132(17)	0.0228(2)	1
O22	0.0019(11)	-0.1488(14)	-0.2204(17)	0.0228(2)	1
O23	0.4299(20)	-0.250000	-0.3540(26)	0.0228(2)	1
O24	0.1962(21)	-0.250000	-0.3510(25)	0.0228(2)	1
O25	0.2834(19)	-0.250000	0.0520(25)	0.0228(2)	1
O26	0.1003(18)	-0.250000	0.0828(26)	0.0228(2)	1

Table 3-H 2. *Fractional atomic coordinates and thermal parameters of ZSM-5-1,2-DCE framework at 600°C [8].*

	ZSM-5-1,2-DCE 600				
	x/a	**y/b**	**z/c**	**Uiso**	**Fraction**
T1	0.4206(7)	0.0589(8)	-0.3292(11)	0.024(8)	1
T2	0.3083(8)	0.0301(6)	-0.1819(10)	0.024(8)	1
T3	0.2807(6)	0.0630(7)	0.0349(10)	0.024(8)	1
T4	0.1206(6)	0.0658(7)	0.0329(11)	0.024(8)	1
T5	0.0730(7)	0.0285(7)	-0.1832(11)	0.024(8)	1
T6	0.1874(8)	0.0553(7)	-0.3280(10)	0.024(8)	1
T7	0.4244(8)	-0.1739(7)	-0.3226(11)	0.024(8)	1
T8	0.3129(8)	-0.1293(6)	-0.1836(10)	0.024(8)	1
T9	0.2747(7)	-0.1714(6)	0.0273(10)	0.024(8)	1
T10	0.1204(7)	-0.1753(7)	0.0284(11)	0.024(8)	1
T11	0.0713(8)	-0.1331(7)	-0.1822(11)	0.024(8)	1
T12	0.1908(8)	-0.1697(6)	-0.3167(10)	0.024(8)	1
O1	0.3733(9)	0.0495(14)	-0.2353(14)	0.054(1)	1
O2	0.3059(12)	0.0670(10)	-0.0786(12)	0.054(1)	1
O3	0.2031(7)	0.0600(11)	0.0351(12)	0.054(1)	1
O4	0.0991(10)	0.0695(11)	-0.0866(12)	0.054(1)	1
O5	0.1196(9)	0.0599(13)	-0.2702(14)	0.054(1)	1
O6	0.2454(9)	0.0432(13)	-0.2475(15)	0.054(1)	1
O7	0.3754(10)	-0.1625(12)	-0.2332(15)	0.054(1)	1
O8	0.3038(12)	-0.1442(9)	-0.0733(12)	0.054(1)	1
O9	0.1968(8)	-0.1568(8)	0.0180(13)	0.054(1)	1
O10	0.0891(10)	-0.1647(10)	-0.0821(13)	0.054(1)	1
O11	0.1233(10)	-0.1559(12)	-0.2608(15)	0.054(1)	1
O12	0.2503(11)	-0.1555(13)	-0.2449(16)	0.054(1)	1
O13	0.3121(12)	-0.0502(7)	-0.1750(13)	0.054(1)	1
O14	0.0789(10)	-0.0538(8)	-0.1791(15)	0.054(1)	1
O15	0.4138(12)	0.1314(9)	-0.3857(16)	0.054(1)	1
O16	0.4047(11)	-0.0033(10)	-0.3992(15)	0.054(1)	1
O17	0.3998(11)	-0.1453(9)	-0.4296(15)	0.054(1)	1
O18	0.1979(13)	0.1218(9)	-0.3899(14)	0.054(1)	1

O19	0.1900(13)	-0.0062(9)	-0.3972(13)	0.054(1)	1
O20	0.1934(13)	-0.1326(8)	-0.4168(12)	0.054(1)	1
O21	0.0019(8)	0.0548(13)	-0.2019(14)	0.054(1)	1
O22	0.0037(9)	-0.1495(12)	-0.2035(15)	0.054(1)	1
O23	0.4185(17)	-0.250000	-0.3624(21)	0.054(1)	10
O24	0.2030(17)	-0.250000	-0.3344(19)	0.054(1)	10
O25	0.2815(14)	-0.250000	0.0539(20)	0.054(1)	10
O26	0.0967(16)	-0.250000	0.0681(22)	0.054(1)	10

Table 3-I 1. Atomic coordinates and thermal parameters of ZSM-5-TOL framework atoms at 75°C [9].

	ZSM-5-TOL 75			
	x/a	**y/b**	**z/c**	**Uiso**
T1	0.42335(12)	1.05723(18)	0.40607(30)	0.0058(5)
T2	0.30866(16)	1.02977(11)	0.55517(34)	0.0058(5)
T3	0.28147(11)	1.06068(24)	0.77610(34)	0.0058(5)
T4	0.12311(11)	1.06488(20)	0.77175(30)	0.0058(5)
T5	0.07104(13)	1.02821(12)	0.56127(30)	0.0058(5)
T6	0.18529(16)	1.06016(23)	0.42018(46)	0.0058(5)
T7	0.42257(13)	0.82800(14)	0.42384(38)	0.0058(5)
T8	0.30637(14)	0.87063(13)	0.56301(41)	0.0058(5)
T9	0.27087(12)	0.82772(14)	0.78099(38)	0.0058(5)
T10	0.11651(14)	0.82548(15)	0.77498(37)	0.0058(5)
T11	0.06895(16)	0.87064(13)	0.56260(37)	0.0058(5)
T12	0.18456(14)	0.82837(19)	0.42802(36)	0.0058(5)
T13	0.92276(13)	1.05695(17)	0.59106(20)	0.0058(5)
T14	0.80882(16)	1.02989(11)	0.44280(30)	0.0058(5)
T15	0.78208(11)	1.06161(25)	0.22097(24)	0.0058(5)
T16	0.62374(11)	1.06542(19)	0.22594(21)	0.0058(5)
T17	0.57135(13)	1.02788(12)	0.43774(29)	0.0058(5)
T18	0.68580(16)	1.05996(20)	0.57641(32)	0.0058(5)
T19	0.92277(13)	0.82705(14)	0.57737(41)	0.0058(5)
T20	0.80648(15)	0.87071(11)	0.43901(44)	0.0058(5)
T21	0.77051(12)	0.82904(13)	0.22079(41)	0.0058(5)
T22	0.61608(13)	0.82649(15)	0.22596(39)	0.0058(5)
T23	0.56862(16)	0.87030(13)	0.43894(40)	0.0058(5)
T24	0.68445(15)	0.82669(19)	0.57283(39)	0.0058(5)
O1	0.36857(16)	1.06028(23)	0.49188(39)	0.0132(1)
O2	0.31204(30)	1.05752(41)	0.66650(45)	0.0132(1)
O3	0.20230(9)	1.06053(29)	0.76940(48)	0.0132(1)
O4	0.09526(25)	1.06499(28)	0.66039(34)	0.0132(1)
O5	0.11298(14)	1.05486(24)	0.46843(38)	0.0132(1)
O6	0.23985(16)	1.05123(44)	0.50547(61)	0.0132(1)

O7	0.36821(23)	0.83572(22)	0.50968(56)	0.0132(1)
O8	0.30354(25)	0.84835(35)	0.67706(41)	0.0132(1)
O9	0.19339(11)	0.84497(28)	0.77939(68)	0.0132(1)
O10	0.08987(29)	0.83432(18)	0.66374(34)	0.0132(1)
O11	0.11231(17)	0.84165(31)	0.47287(35)	0.0132(1)
O12	0.23937(22)	0.84866(36)	0.50847(52)	0.0132(1)
O13	0.31426(35)	0.95006(9)	0.55649(66)	0.0132(1)
O14	0.08136(22)	0.94931(11)	0.57257(58)	0.0132(1)
O15	0.42469(19)	1.12686(26)	0.34774(45)	0.0132(1)
O16	0.40585(22)	0.99827(31)	0.33027(47)	0.0132(1)
O17	0.39899(27)	0.86792(30)	0.32704(57)	0.0132(1)
O18	0.19400(25)	1.13176(27)	0.36892(50)	0.0132(1)
O19	0.19425(33)	1.00278(32)	0.33854(69)	0.0132(1)
O20	0.19431(23)	0.87231(31)	0.32983(46)	0.0132(1)
O21	-0.00583(10)	1.04384(21)	0.54319(30)	0.0132(1)
O22	-0.00787(16)	0.85706(21)	0.54086(49)	0.0132(1)
O23	0.43144(22)	0.75057(17)	0.39722(27)	0.0132(1)
O24	0.19221(30)	0.75091(20)	0.40109(56)	0.0132(1)
O25	0.28052(27)	0.74922(14)	0.79843(50)	0.0132(1)
O26	0.10730(30)	0.74942(18)	0.80897(33)	0.0132(1)
O27	0.86861(15)	1.06208(14)	0.50456(25)	0.0132(1)
O28	0.81313(24)	1.05432(30)	0.32979(29)	0.0132(1)
O29	0.70296(9)	1.06195(31)	0.22863(48)	0.0132(1)
O30	0.59556(26)	1.06248(29)	0.33696(22)	0.0132(1)
O31	0.61310(14)	1.05690(19)	0.52912(28)	0.0132(1)
O32	0.73984(15)	1.05335(34)	0.48997(42)	0.0132(1)
O33	0.86870(25)	0.83572(21)	0.49133(63)	0.0132(1)
O34	0.80364(28)	0.84918(31)	0.32460(46)	0.0132(1)
O35	0.69300(10)	0.84591(25)	0.22386(74)	0.0132(1)
O36	0.58813(29)	0.83477(18)	0.33656(33)	0.0132(1)
O37	0.61241(18)	0.83984(31)	0.52709(35)	0.0132(1)
O38	0.73976(24)	0.84781(32)	0.49360(57)	0.0132(1)
O39	0.81389(33)	0.95017(8)	0.44685(59)	0.0132(1)
O40	0.58212(22)	0.94886(11)	0.43045(63)	0.0132(1)
O41	0.92407(23)	1.12534(28)	0.65261(44)	0.0132(1)

O42	0.90435(18)	0.99649(33)	0.66374(36)	0.0132(1)
O43	0.89889(28)	0.86618(31)	0.67466(62)	0.0132(1)
O44	0.69529(25)	1.12963(31)	0.63288(55)	0.0132(1)
O45	0.69464(31)	0.99989(35)	0.65364(45)	0.0132(1)
O46	0.69327(24)	0.86996(32)	0.67192(48)	0.0132(1)
O47	0.49441(10)	1.04353(20)	0.45472(33)	0.0132(1)
O48	0.49177(16)	0.85769(21)	0.46169(50)	0.0132(1)

Table 3-I 2. *Atomic coordinates and thermal parameters of ZSM-5-TOL framework atoms at 400°C [9].*

	ZSM-5-TOL 400			
	x/a	**y/b**	**z/c**	**Uiso**
T1	0.42223(25)	0.05680(27)	-0.3367(4)	0.0144(7)
T2	0.30981(31)	0.03016(27)	-0.1851(4)	0.0144(7)
T3	0.27946(27)	0.06115(27)	0.0330(4)	0.0144(7)
T4	0.12181(29)	0.06527(28)	0.0255(4)	0.0144(7)
T5	0.07016(28)	0.02836(28)	-0.1838(4)	0.0144(7)
T6	0.18818(26)	0.05923(30)	-0.3205(4)	0.0144(7)
T7	0.42318(28)	-0.17243(20)	-0.3227(4)	0.0144(7)
T8	0.30913(31)	-0.12914(28)	-0.1806(4)	0.0144(7)
T9	0.27290(32)	-0.17163(19)	0.0362(4)	0.0144(7)
T10	0.11827(32)	-0.17403(20)	0.0296(4)	0.0144(7)
T11	0.07029(28)	-0.12897(31)	-0.1819(5)	0.0144(7)
T12	0.18771(30)	-0.17205(20)	-0.3161(4)	0.0144(7)
O1	0.36968(33)	0.06094(48)	-0.24822(49)	0.0463(1)
O2	0.31521(30)	0.05529(46)	-0.07283(40)	0.0463(1)
O3	0.20095(22)	0.06090(37)	0.01705(55)	0.0463(1)
O4	0.09123(33)	0.06698(47)	-0.08474(51)	0.0463(1)
O5	0.11527(26)	0.05267(46)	-0.27452(52)	0.0463(1)
O6	0.24127(32)	0.05429(53)	-0.23266(57)	0.0463(1)
O7	0.37274(38)	-0.16185(44)	-0.23256(56)	0.0463(1)
O8	0.30677(38)	-0.15066(60)	-0.06648(35)	0.0463(1)
O9	0.19522(27)	-0.15521(53)	0.03146(69)	0.0463(1)
O10	0.09042(47)	-0.16603(34)	-0.08109(41)	0.0463(1)
O11	0.11650(33)	-0.15473(55)	-0.27055(49)	0.0463(1)
O12	0.24369(39)	-0.15421(54)	-0.23628(60)	0.0463(1)
O13	0.31381(61)	-0.04957(24)	-0.18804(84)	0.0463(1)
O14	0.07933(48)	-0.05021(25)	-0.16834(77)	0.0463(1)
O15	0.42167(38)	0.12557(27)	-0.39739(51)	0.0463(1)
O16	0.40381(38)	-0.00342(33)	-0.40939(64)	0.0463(1)
O17	0.39730(38)	-0.13363(33)	-0.41886(50)	0.0463(1)
O18	0.19465(43)	0.13017(30)	-0.37469(43)	0.0463(1)

O19	0.20002(47)	0.00069(32)	-0.39880(59)	0.0463(1)
O20	0.19895(42)	-0.12956(30)	-0.41506(46)	0.0463(1)
O21	-0.00565(22)	0.04441(39)	-0.20900(43)	0.0463(1)
O22	-0.00537(28)	-0.14524(58)	-0.20789(53)	0.0463(1)
O23	0.42737(74)	-0.25000	-0.35007(85)	0.0463(1)
O24	0.19124(65)	-0.25000	-0.34211(87)	4.62(18)
O25	0.28329(69)	-0.25000	0.05475(103)	4.62(18)
O26	0.10890(66)	-0.25000	0.06502(66)	4.62(18)

Table 3-L 1. *Framework atomic coordinates of ZSM-5-MTBE at 100°C [11].*

	ZSM-5-MTBE 100			
	x/a	**y/b**	**z/c**	**Uiso**
T1	0.22697(24)	-0.17189(16)	0.03435(32)	0.0081(7)
T2	-0.07688(20)	-0.05589(21)	0.33995(30)	0.0081(7)
T3	0.19088(24)	-0.12981(21)	-0.18254(33)	0.0081(7)
T4	0.07116(23)	0.12925(23)	0.31793(36)	0.0081(7)
T5	-0.07587(22)	0.17191(15)	0.32380(32)	0.0081(7)
T6	0.21965(20)	0.06216(21)	0.02932(29)	0.0081(7)
T7	0.12260(20)	-0.06602(21)	0.52457(32)	0.0081(7)
T8	-0.11859(24)	-0.17388(16)	0.47035(35)	0.0081(7)
T9	0.30902(24)	-0.03007(21)	0.31059(31)	0.0081(7)
T10	0.18619(21)	-0.05830(23)	0.17352(34)	0.0081(7)
T11	0.18755(24)	0.17202(16)	0.18192(33)	0.0081(7)
T12	0.07154(22)	-0.02829(22)	0.31571(32)	0.0081(7)
O1	-0.11000(48)	-0.250000	0.43509(48)	0.0163(1)
O2	0.11447(22)	-0.05243(32)	0.22289(36)	0.0163(1)
O3	0.19663(33)	0.12961(23)	0.08259(36)	0.0163(1)
O4	0.19159(50)	0.250000	0.15546(65)	0.0163(1)
O5	0.19252(33)	-0.12980(22)	0.12099(35)	0.0163(1)
O6	-0.00486(18)	-0.04360(31)	0.29420(35)	0.0163(1)
O7	0.21780(45)	-0.250000	0.05639(61)	0.0163(1)
O8	0.24141(26)	-0.05163(43)	0.25791(52)	0.0163(1)
O9	-0.00469(22)	0.14406(37)	0.29226(42)	0.0163(1)
O10	0.19538(36)	-0.00083(25)	0.09255(49)	0.0163(1)
O11	0.11676(26)	0.15599(42)	0.22954(39)	0.0163(1)
O12	-0.07808(27)	-0.12600(18)	0.39749(40)	0.0163(1)
O13	0.31188(29)	-0.05939(35)	0.42039(31)	0.0163(1)
O14	-0.12978(27)	-0.05781(34)	0.25214(39)	0.0163(1)
O15	0.30454(20)	-0.15453(36)	0.03169(55)	0.0163(1)
O16	0.09435(29)	-0.06679(30)	0.41359(30)	0.0163(1)
O17	-0.10124(31)	0.13341(23)	0.42042(38)	0.0163(1)
O18	0.19412(31)	-0.15396(35)	-0.06973(28)	0.0163(1)
O19	0.08153(33)	0.05044(18)	0.33099(58)	0.0163(1)

O20	-0.07044(48)	0.250000	0.34780(55)	0.0163(1)
O21	-0.12669(30)	0.16071(36)	0.23438(44)	0.0163(1)
O22	-0.09407(29)	0.00295(23)	0.41618(44)	0.0163(1)
O23	0.24436(31)	0.15376(43)	0.25959(49)	0.0163(1)
O24	0.09087(35)	0.16622(27)	0.41891(33)	0.0163(1)
O25	0.29847(16)	0.06129(31)	0.02097(50)	0.0163(1)
O26	0.31310(47)	0.04987(17)	0.31466(61)	0.0163(1)

Table 3-L 2. *Atomic coordinates and thermal parameters of ZSM-5-MTBE framework atoms at 400°C [11].*

	ZSM-5-MTBE 400			
	x/a	**y/b**	**z/c**	**Uiso**
T1	0.22798(26)	-0.17153(17)	0.03597(37)	0.0208(8)
T2	-0.07681(22)	-0.05705(23)	0.33738(33)	0.0208(8)
T3	0.19023(27)	-0.12897(24)	-0.18048(37)	0.0208(8)
T4	0.07105(26)	0.12979(26)	0.31797(41)	0.0208(8)
T5	-0.07622(25)	0.17196(17)	0.32202(36)	0.0208(8)
T6	0.21940(22)	0.06105(24)	0.03252(33)	0.0208(8)
T7	0.12273(22)	-0.06485(24)	0.52745(36)	0.0208(8)
T8	-0.11800(27)	-0.17376(18)	0.47001(40)	0.0208(8)
T9	0.31067(27)	-0.03041(23)	0.31324(35)	0.0208(8)
T10	0.18786(24)	-0.05953(26)	0.17800(37)	0.0208(8)
T11	0.18831(27)	0.17205(18)	0.18359(38)	0.0208(8)
T12	0.07146(25)	-0.02775(25)	0.31720(36)	0.0208(8)
O1	-0.11001(54)	-0.250000	0.43464(56)	0.0397(1)
O2	0.11585(25)	-0.05407(35)	0.22713(43)	0.0397(1)
O3	0.19726(38)	0.12912(26)	0.08485(41)	0.0397(1)
O4	0.19421(55)	0.250000	0.15730(77)	0.0397(1)
O5	0.19453(37)	-0.13087(25)	0.12500(38)	0.0397(1)
O6	-0.00462(21)	-0.04336(34)	0.29273(38)	0.0397(1)
O7	0.21906(52)	-0.250000	0.05436(74)	0.0397(1)
O8	0.24251(30)	-0.05303(49)	0.26337(56)	0.0397(1)
O9	-0.00487(24)	0.14430(42)	0.29099(48)	0.0397(1)
O10	0.19711(40)	-0.00147(28)	0.09812(54)	0.0397(1)
O11	0.11694(30)	0.15750(48)	0.23038(45)	0.0397(1)
O12	-0.07690(30)	-0.12646(21)	0.39669(44)	0.0397(1)
O13	0.31428(30)	-0.05681(41)	0.42501(36)	0.0397(1)
O14	-0.12895(31)	-0.06099(36)	0.24865(45)	0.0397(1)
O15	0.30543(22)	-0.15375(42)	0.03185(63)	0.0397(1)
O16	0.09210(31)	-0.06481(36)	0.41763(35)	0.0397(1)
O17	-0.10233(35)	0.13249(26)	0.41726(44)	0.0397(1)
O18	0.19394(34)	-0.15120(41)	-0.06672(32)	0.0397(1)

O19	0.08168(37)	0.05100(21)	0.32988(70)	0.0397(1)
O20	-0.07070(53)	0.250000	0.34789(61)	0.0397(1)
O21	-0.12658(35)	0.16215(38)	0.23144(52)	0.0397(1)
O22	-0.09580(33)	0.00210(27)	0.41172(51)	0.0397(1)
O23	0.24439(36)	0.15270(48)	0.26245(55)	0.0397(1)
O24	0.08968(40)	0.16642(31)	0.41954(36)	0.0397(1)
O25	0.29823(17)	0.06054(35)	0.02009(54)	0.0397(1)
O26	0.31568(52)	0.04935(19)	0.31283(70)	0.0397(1)

Table 3-M 1. *Atomic coordinates and thermal parameters of ZSM-5-1,2-DCE/MTBE framework atoms at 100°C [192].*

	ZSM-5-1,2-DCE/MTBE 100			
	x/a	**y/b**	**z/c**	**Uiso**
T1	0.22942(15)	-0.17171(10)	0.03328(33)	0.0057(1)
T2	-0.07683(12)	-0.05683(15)	0.34016(30)	0.0057(1)
T3	0.19206(19)	-0.12966(14)	-0.18388(43)	0.0057(1)
T4	0.06930(22)	0.12926(15)	0.31462(41)	0.0057(1)
T5	-0.07686(15)	0.17239(8)	0.32403(26)	0.0057(1)
T6	0.21882(11)	0.06120(23)	0.03019(33)	0.0057(1)
T7	0.12326(12)	-0.06539(16)	0.52499(28)	0.0057(1)
T8	-0.11635(18)	-0.17410(10)	0.47316(37)	0.0057(1)
T9	0.30993(19)	-0.02963(13)	0.31036(37)	0.0057(1)
T10	0.18702(18)	-0.05978(27)	0.17577(41)	0.0057(1)
T11	0.18611(18)	0.17233(10)	0.18123(44)	0.0057(1)
T12	0.07136(14)	-0.02824(13)	0.31446(31)	0.0057(1)
O1	-0.10758(44)	-0.250000	0.43824(53)	0.0134(23)
O2	0.11461(18)	-0.05548(31)	0.22355(39)	0.0134(23)
O3	0.19568(26)	0.12908(23)	0.08242(38)	0.0134(23)
O4	0.19271(48)	0.250000	0.15493(88)	0.0134(23)
O5	0.19596(36)	-0.13044(23)	0.12179(32)	0.0134(23)
O6	-0.00515(12)	-0.04357(24)	0.29366(21)	0.0134(23)
O7	0.21984(41)	-0.250000	0.05260(82)	0.0134(23)
O8	0.24120(20)	-0.05215(55)	0.26170(55)	0.0134(23)
O9	-0.00703(22)	0.14254(25)	0.28964(42)	0.0134(23)
O10	0.19602(33)	-0.00109(22)	0.09628(62)	0.0134(23)
O11	0.11432(25)	0.15819(38)	0.22682(35)	0.0134(23)
O12	-0.07639(19)	-0.12607(15)	0.39955(31)	0.0134(23)
O13	0.31394(25)	-0.05606(50)	0.42227(45)	0.0134(23)
O14	-0.13024(20)	-0.06043(26)	0.25263(45)	0.0134(23)
O15	0.30681(13)	-0.15478(35)	0.02856(67)	0.0134(23)
O16	0.09368(22)	-0.06469(36)	0.41473(33)	0.0134(23)
O17	-0.10215(24)	0.13308(17)	0.42030(36)	0.0134(23)
O18	0.19529(31)	-0.15186(44)	-0.06982(33)	0.0134(23)

O19	0.08181(22)	0.05065(12)	0.32544(81)	0.0134(23)
O20	-0.06867(33)	0.250000	0.34987(38)	0.0134(23)
O21	-0.12957(36)	0.16398(22)	0.23616(54)	0.0134(23)
O22	-0.09530(22)	0.00271(17)	0.41439(51)	0.0134(23)
O23	0.24159(34)	0.15239(48)	0.26067(64)	0.0134(23)
O24	0.08813(35)	0.16578(23)	0.41648(29)	0.0134(23)
O25	0.29772(10)	0.06098(19)	0.01977(39)	0.0134(23)
O26	0.31500(43)	0.05014(11)	0.30958(93)	0.0134(23)

Table 3-M 2. *Atomic coordinates and thermal parameters of ZSM-5- 1,2-DCE/MTBE framework atoms at 400°C [192].*

	ZSM-5-MTBE/1,2-DCE 400			
	x/a	**y/b**	**z/c**	**Uiso**
T1	0.22978(18)	-0.17163(12)	0.03411(43)	0.011(1)
T2	-0.07702(14)	-0.05680(18)	0.33855(40)	0.011(1)
T3	0.19190(25)	-0.12936(18)	-0.18252(55)	0.011(1)
T4	0.06882(27)	0.12915(18)	0.31460(52)	0.011(1)
T5	-0.07714(19)	0.17248(10)	0.32291(32)	0.011(1)
T6	0.21873(14)	0.06078(28)	0.03225(43)	0.011(1)
T7	0.12349(15)	-0.06557(20)	0.52606(37)	0.011(1)
T8	-0.11541(22)	-0.17422(13)	0.47299(47)	0.011(1)
T9	0.31090(23)	-0.02980(16)	0.31298(47)	0.011(1)
T10	0.18828(24)	-0.06036(33)	0.17926(50)	0.011(1)
T11	0.18630(23)	0.17237(13)	0.18285(57)	0.011(1)
T12	0.07136(17)	-0.02822(16)	0.31528(41)	0.011(1)
O1	-0.10600(57)	-0.250000	0.43758(69)	0.026(1)
O2	0.11535(24)	-0.05653(40)	0.22571(52)	0.026(1)
O3	0.19605(36)	0.12902(28)	0.08405(49)	0.026(1)
O4	0.19380(60)	0.250000	0.15660(112)	0.026(1)
O5	0.19785(44)	-0.13065(29)	0.12433(40)	0.026(1)
O6	-0.00513(16)	-0.04306(32)	0.29274(25)	0.026(1)
O7	0.21934(55)	-0.250000	0.05216(105)	0.026(1)
O8	0.24165(26)	-0.05321(67)	0.26663(61)	0.026(1)
O9	-0.00765(27)	0.14147(29)	0.28871(53)	0.026(1)
O10	0.19788(38)	-0.00106(27)	0.10081(76)	0.026(1)
O11	0.11397(30)	0.15890(49)	0.22737(45)	0.026(1)
O12	-0.07620(25)	-0.12560(19)	0.39914(38)	0.026(1)
O13	0.31615(26)	-0.05427(64)	0.42588(56)	0.026(1)
O14	-0.12985(28)	-0.06173(31)	0.25024(64)	0.026(1)
O15	0.30745(15)	-0.15572(47)	0.02782(84)	0.026(1)
O16	0.09223(24)	-0.06420(49)	0.41674(45)	0.026(1)
O17	-0.10314(32)	0.13357(21)	0.41928(46)	0.026(1)
O18	0.19479(40)	-0.15040(55)	-0.06787(43)	0.026(1)

O19	0.08237(28)	0.05068(14)	0.32529(106)	0.026(1)
O20	-0.06775(38)	0.250000	0.34874(46)	0.026(1)
O21	-0.12996(45)	0.16486(25)	0.23486(68)	0.026(1)
O22	-0.09659(28)	0.00315(22)	0.41152(70)	0.026(1)
O23	0.24113(42)	0.15189(57)	0.26316(81)	0.026(1)
O24	0.08668(42)	0.16583(31)	0.41685(37)	0.026(1)
O25	0.29748(12)	0.06120(23)	0.01815(46)	0.026(1)
O26	0.31596(51)	0.04996(15)	0.30903(115)	0.026(1)

Table 3-M 3. *Atomic coordinates and thermal parameters of ZSM-5-TOL/MTBE framework atoms at 100°C [192].*

	ZSM-5-TOL/MTBE 100			
	x/a	**y/b**	**z/c**	**Uiso**
T1	0.42292(15)	1.05584(19)	0.65872(30)	0.008(1)
T2	0.30906(23)	1.02941(17)	0.81051(38)	0.008(1)
T3	0.28085(15)	1.06120(23)	1.02926(33)	0.008(1)
T4	0.12314(15)	1.06622(18)	1.02371(31)	0.008(1)
T5	0.07109(18)	1.02800(16)	0.81627(34)	0.008(1)
T6	0.18643(21)	1.05933(27)	0.67594(43)	0.008(1)
T7	0.42373(19)	0.82793(11)	0.67678(30)	0.008(1)
T8	0.30848(22)	0.86967(18)	0.81709(45)	0.008(1)
T9	0.27166(21)	0.82824(12)	1.03538(34)	0.008(1)
T10	0.11770(24)	0.82562(12)	1.02979(39)	0.008(1)
T11	0.07097(25)	0.87096(18)	0.81857(44)	0.008(1)
T12	0.18670(20)	0.82761(12)	0.68105(45)	0.008(1)
O1	0.36920(24)	1.05822(34)	0.74597(44)	0.011(1)
O2	0.31448(26)	1.05638(51)	0.92194(45)	0.011(1)
O3	0.20206(12)	1.06104(24)	1.01718(40)	0.011(1)
O4	0.09298(24)	1.06770(35)	0.91389(36)	0.011(1)
O5	0.11412(21)	1.05269(35)	0.72351(41)	0.011(1)
O6	0.24062(23)	1.05308(58)	0.76213(59)	0.011(1)
O7	0.37326(37)	0.83812(36)	0.76719(51)	0.011(1)
O8	0.30432(35)	0.84735(45)	0.93095(36)	0.011(1)
O9	0.19434(19)	0.84573(34)	1.03308(70)	0.011(1)
O10	0.09069(41)	0.83274(22)	0.91859(28)	0.011(1)
O11	0.11630(30)	0.84465(44)	0.72928(38)	0.011(1)
O12	0.24413(37)	0.84430(53)	0.75895(71)	0.011(1)
O13	0.31232(56)	0.94947(14)	0.81080(93)	0.011(1)
O14	0.08210(28)	0.94958(14)	0.83272(82)	0.011(1)
O15	0.42346(21)	1.12584(13)	0.60134(19)	0.011(1)
O16	0.40499(25)	0.99716(18)	0.58262(53)	0.011(1)
O17	0.39687(24)	0.86677(19)	0.58104(37)	0.011(1)
O18	0.19330(43)	1.13039(23)	0.62246(36)	0.011(1)

O19	0.19716(37)	1.00125(23)	0.59580(64)	0.011(1)
O20	0.19661(30)	0.87108(22)	0.58249(39)	0.011(1)
O21	-0.00556(15)	1.04210(26)	0.79438(28)	0.011(1)
O22	-0.00516(26)	0.85684(33)	0.79320(45)	0.011(1)
O23	0.43003(44)	0.750000	0.65203(53)	0.011(1)
O24	0.18938(57)	0.750000	0.65303(88)	0.011(1)
O25	0.28104(44)	0.750000	1.05533(85)	0.011(1)
O26	0.10912(45)	0.750000	1.06618(55)	0.011(1)

Table 3-M 4. *Atomic coordinates and thermal parameters of ZSM-5-TOL/MTBE framework atoms at 400°C [192].*

	ZSM-5-MTBE/TOL 400			
	x/a	**y/b**	**z/c**	**Uiso**
T1	0.42296(16)	0.05672(18)	-0.33784(27)	0.017(6)
T2	0.31059(21)	0.03025(17)	-0.18568(29)	0.017(6)
T3	0.28068(16)	0.05987(19)	0.03265(26)	0.017(6)
T4	0.12323(16)	0.06535(18)	0.02603(28)	0.017(6)
T5	0.07091(18)	0.02768(18)	-0.18220(29)	0.017(6)
T6	0.18818(18)	0.06067(21)	-0.31934(30)	0.017(6)
T7	0.42349(19)	-0.17206(12)	-0.32111(27)	0.017(6)
T8	0.30948(21)	-0.12938(18)	-0.18001(32)	0.017(6)
T9	0.27127(20)	-0.17130(12)	0.03729(29)	0.017(6)
T10	0.11722(21)	-0.17423(13)	0.03166(33)	0.017(6)
T11	0.07106(20)	-0.12953(19)	-0.18048(34)	0.017(6)
T12	0.18795(20)	-0.17246(13)	-0.31639(32)	0.017(6)
O1	0.37019(23)	0.06115(28)	-0.24952(37)	0.042(1)
O2	0.31708(20)	0.05433(34)	-0.07283(30)	0.042(1)
O3	0.20212(13)	0.06045(25)	0.01537(37)	0.042(1)
O4	0.09043(21)	0.06658(29)	-0.08243(29)	0.042(1)
O5	0.11542(18)	0.05377(29)	-0.27269(34)	0.042(1)
O6	0.24169(22)	0.05504(39)	-0.23174(41)	0.042(1)
O7	0.37405(28)	-0.16263(30)	-0.22892(40)	0.042(1)
O8	0.30517(27)	-0.14961(33)	-0.06527(27)	0.042(1)
O9	0.19377(17)	-0.15331(35)	0.03428(51)	0.042(1)
O10	0.08960(31)	-0.16751(22)	-0.07952(30)	0.042(1)
O11	0.11691(24)	-0.15683(38)	-0.26876(36)	0.042(1)
O12	0.24474(29)	-0.15532(38)	-0.23722(47)	0.042(1)
O13	0.31414(43)	-0.04971(14)	-0.19007(58)	0.042(1)
O14	0.08259(27)	-0.05085(15)	-0.16695(60)	0.042(1)
O15	0.42467(21)	0.12643(18)	-0.39628(35)	0.042(1)
O16	0.40310(25)	-0.00197(22)	-0.41310(42)	0.042(1)
O17	0.39557(25)	-0.13259(21)	-0.41581(34)	0.042(1)
O18	0.19464(30)	0.13198(20)	-0.37249(29)	0.042(1)

O19	0.19980(30)	0.00251(22)	-0.39899(44)	0.042(1)
O20	0.19767(29)	-0.12798(20)	-0.41410(33)	0.042(1)
O21	-0.00538(15)	0.04133(25)	-0.20792(28)	0.042(1)
O22	-0.00504(20)	-0.14319(32)	-0.20770(38)	0.042(1)
O23	0.42965(42)	-0.250000	-0.34726(48)	0.042(1)
O24	0.19209(44)	-0.250000	-0.34554(63)	0.042(1)
O25	0.28030(44)	-0.250000	0.05342(64)	0.042(1)
O26	0.10954(46)	-0.250000	0.06845(47)	0.042(1)

SECTION IV:

Adsorption behaviour of regenerated ZSM-5

N- Adsorption behaviour of regenerated ZSM-5 reloaded with 1,2-DCE and TOL

Table 4-N 1. *Lattice parameters and Uiso of framework atoms after 1,2-DCE adsorption (ZSM-5-1,2-DCE-30), after thermal regeneration (ZSM-5-R) and for regenerated and reloaded ZSM-5(ZSM-5-R-1,2-DCE) [8].*

SAMPLES		x/a	y/b	z/c	Uiso
ZSM-5-1,2-DCE-30	**T1**	0.0548(3)	0.4203(3)	-0.3222(5)	0.0087(5)
ZSM-5-R		0.0576(11)	0.4175(11)	-0.3153(17)	0.0027(9)
ZSM-5-R-1,2-DCE		0.0539(4)	0.4236(4)	-0.3289(6)	0.0019(3)
ZSM-5-1,2-DCE-30	**T2**	0.0316(4)	0.3162(4)	-0.1657(5)	0.0087(5)
ZSM-5-R		0.0323(10)	0.3117(13)	-0.1601(14)	0.0027(9)
ZSM-5-R-1,2-DCE		0.0332(4)	0.3162(4)	-0.1692(6)	0.0019(3)
ZSM-5-1,2-DCE-30	**T3**	0.0608(3)	0.2809(3)	0.0541(5)	0.0087(5)
ZSM-5-R		0.0598(10)	0.2771(11)	0.0513(15)	0.0027(9)
ZSM-5-R-1,2-DCE		0.0636(4)	0.2823(4)	0.0442(8)	0.0019(3)
ZSM-5-1,2-DCE-30	**T4**	0.0615(4)	0.1245(3)	0.0344(5)	0.0087(5)
ZSM-5-R		0.0610(10)	0.1214(12)	0.0318(17)	0.0027(9)
ZSM-5-R-1,2-DCE		0.0643(4)	0.1263(4)	0.0333(5)	0.0019(3)
ZSM-5-1,2-DCE-30	**T5**	0.0271(3)	0.0775(4)	-0.1780(6)	0.0087(5)
ZSM-5-R		0.0310(11)	0.0708(11)	-0.1814(16)	0.0027(9)
ZSM-5-R-1,2-DCE		0.02781(34)	0.0732(4)	-0.1742(6)	0.0019(3)
ZSM-5-1,2-DCE-30	**T6**	0.0564(4)	0.1967(3)	-0.3138(6)	0.0087(5)
ZSM-5-R		0.0544(10)	0.1923(12)	-0.3129(15)	0.0027(9)
ZSM-5-R-1,2-DCE		0.0582(4)	0.1939(4)	-0.3083(6)	0.0019(3)

ZSM-5-1,2-DCE-30	**T7**	-0.1720(3)	0.4255(3)	-0.3246(5)	0.0087(5)
ZSM-5-R		-0.1748(11)	0.4248(11)	-0.3278(16)	0.0027(9)
ZSM-5-R-1,2-DCE		-0.17206(34)	0.42672(33)	-0.3263(6)	0.0019(3)
ZSM-5-1,2-DCE-30	**T8**	-0.1259(3)	0.3112(3)	-0.1776(5)	0.0087(5)
ZSM-5-R		-0.1262(10)	0.3125(12)	-0.1773(14)	0.0027(9)
ZSM-5-R-1,2-DCE		-0.1251(4)	0.3110(4)	-0.1807(6)	0.0019(3)
ZSM-5-1,2-DCE-30	**T9**	-0.1752(3)	0.2700(4)	0.0333(6)	0.0087(5)
ZSM-5-R		-0.1752(11)	0.2793(11)	0.0413(15)	0.0027(9)
ZSM-5-R-1,2-DCE		-0.17594(34)	0.2682(4)	0.0284(6)	0.0019(3)
ZSM-5-1,2-DCE-30	**T10**	-0.1780(3)	0.1160(4)	0.0293(6)	0.0087(5)
ZSM-5-R		-0.1783(11)	0.1215(11)	0.0460(16)	0.0027(9)
ZSM-5-R-1,2-DCE		-0.17920(33)	0.1128(4)	0.0274(7)	0.0019(3)
ZSM-5-1,2-DCE-30	**T11**	-0.1308(3)	0.0686(4)	-0.1793(6)	0.0087(5)
ZSM-5-R		-0.1286(10)	0.0737(11)	-0.1683(15)	0.0027(9)
ZSM-5-R-1,2-DCE		-0.1291(4)	0.0653(4)	-0.1774(7)	0.0019(3)
ZSM-5-1,2-DCE-30	**T12**	-0.1650(3)	0.1844(4)	-0.3143(6)	0.0087(5)
ZSM-5-R		-0.1684(10)	0.1873(11)	-0.3170(15)	0.0027(9)
ZSM-5-R-1,2-DCE		-0.1639(4)	0.1866(4)	-0.3145(7)	0.0019(3)
ZSM-5-1,2-DCE-30	**T13**	0.4415(3)	0.4291(3)	-0.3378(5)	0.0087(5)
ZSM-5-R		0.4423(11)	0.4262(11)	-0.3264(17)	0.0027(9)
ZSM-5-R-1,2-DCE		0.4420(4)	0.4246(4)	-0.3352(6)	0.0019(3)
ZSM-5-1,2-DCE-30	**T14**	0.4730(3)	0.3124(4)	-0.1884(5)	0.0087(5)
ZSM-5-R		0.4685(9)	0.3102(12)	-0.1867(15)	0.0027(9)
ZSM-5-R-1,2-DCE		0.4735(4)	0.3115(4)	-0.1870(6)	0.0019(3)
ZSM-5-1,2-DCE-30	**T15**	0.4387(4)	0.2779(3)	0.0279(5)	0.0087(5)
ZSM-5-R		0.4359(10)	0.2770(12)	0.0311(15)	0.0027(9)
ZSM-5-R-1,2-DCE		0.4398(4)	0.2791(4)	0.0339(7)	0.0019(3)

ZSM-5-1,2-DCE-30		0.4357(4)	0.1256(4)	0.0324(5)	0.0087(5)
ZSM-5-R	**T16**	0.4344(11)	0.1200(12)	0.0278(15)	0.0027(9)
ZSM-5-R-1,2-DCE		0.4322(4)	0.1218(4)	0.0287(5)	0.0019(3)
ZSM-5-1,2-DCE-30		0.4750(3)	0.0713(3)	-0.1810(6)	0.0087(5)
ZSM-5-R	**T17**	0.4689(10)	0.0650(11)	-0.1910(16)	0.0027(9)
ZSM-5-R-1,2-DCE		0.4723(4)	0.0734(4)	-0.1882(6)	0.0019(3)
ZSM-5-1,2-DCE-30		0.4367(4)	0.1862(3)	-0.3148(6)	0.0087(5)
ZSM-5-R	**T18**	0.4389(11)	0.1834(11)	-0.3223(16)	0.0027(9)
ZSM-5-R-1,2-DCE		0.4388(4)	0.1881(4)	-0.3204(7)	0.0019(3)
ZSM-5-1,2-DCE-30		0.6723(3)	0.4222(3)	-0.3156(5)	0.0087(5)
ZSM-5-R	**T19**	0.6682(11)	0.4249(11)	-0.3184(16)	0.0027(9)
ZSM-5-R-1,2-DCE		0.67207(32)	0.4206(4)	-0.3127(5)	0.0019(3)
ZSM-5-1,2-DCE-30		0.6325(3)	0.3107(4)	-0.1680(5)	0.0087(5)
ZSM-5-R	**T20**	0.6302(9)	0.3157(12)	-0.1666(15)	0.0027(9)
ZSM-5-R-1,2-DCE		0.6324(4)	0.3098(4)	-0.1696(6)	0.0019(3)
ZSM-5-1,2-DCE-30		0.6678(3)	0.2715(4)	0.0444(6)	0.0087(5)
ZSM-5-R	**T21**	0.6724(10)	0.2784(11)	0.0550(15)	0.0027(9)
ZSM-5-R-1,2-DCE		0.6682(4)	0.2712(4)	0.0480(6)	0.0019(3)
ZSM-5-1,2-DCE-30		0.6687(3)	0.1180(4)	0.0333(6)	0.0087(5)
ZSM-5-R	**T22**	0.6739(12)	0.1206(12)	0.0466(15)	0.0027(9)
ZSM-5-R-1,2-DCE		0.6691(4)	0.1160(4)	0.0337(6)	0.0019(3)
ZSM-5-1,2-DCE-30		0.6316(4)	0.0714(4)	-0.1856(6)	0.0087(5)
ZSM-5-R	**T23**	0.6314(10)	0.0715(12)	-0.1810(16)	0.0027(9)
ZSM-5-R-1,2-DCE		0.6295(4)	0.0732(4)	-0.1876(6)	0.0019(3)
ZSM-5-1,2-DCE-30	**T24**	0.6810(3)	0.1929(4)	-0.2982(6)	0.0087(5)
ZSM-5-R		0.6789(10)	0.1929(11)	-0.3082(14)	0.0027(9)

ZSM-5-R-1,2-DCE		0.6806(4)	0.1921(4)	-0.3043(6)	0.0019(3)
ZSM-5-1,2-DCE-30		0.0659(5)	0.3772(5)	-0.2229(8)	0.0109(1)
ZSM-5-R	**O1**	0.0626(18)	0.3765(16)	-0.2140(23)	0.0084(2)
ZSM-5-R-1,2-DCE		0.0643(6)	0.3743(5)	-0.2363(9)	0.0042(5)
ZSM-5-1,2-DCE-30		0.0632(6)	0.3128(6)	-0.0553(5)	0.0109(1)
ZSM-5-R	**O2**	0.0694(16)	0.3126(19)	-0.0551(16)	0.0084(2)
ZSM-5-R-1,2-DCE		0.0659(6)	0.3214(6)	-0.0598(6)	0.0042(5)
ZSM-5-1,2-DCE-30		0.0473(6)	0.2027(3)	0.0439(3)	0.0109(1)
ZSM-5-R	**O3**	0.0490(17)	0.2009(11)	0.0271(28)	0.0084(2)
ZSM-5-R-1,2-DCE		0.0520(7)	0.20476(34)	0.0236(15)	0.0042(5)
ZSM-5-1,2-DCE-30		0.0665(5)	0.1038(8)	-0.0809(6)	0.0109(1)
ZSM-5-R	**O4**	0.0695(17)	0.0956(19)	-0.0827(18)	0.0084(2)
ZSM-5-R-1,2-DCE		0.0694(5)	0.0944(9)	-0.0761(8)	0.0042(5)
ZSM-5-1,2-DCE-30		0.0445(6)	0.1231(4)	-0.2724(7)	0.0109(1)
ZSM-5-R	**O5**	0.0465(20)	0.1191(14)	-0.2696(24)	0.0084(2)
ZSM-5-R-1,2-DCE		0.0468(7)	0.1205(4)	-0.2657(10)	0.0042(5)
ZSM-5-1,2-DCE-30		0.0471(7)	0.2887(5)	-0.2245(9)	0.0109(1)
ZSM-5-R	**O6**	0.0521(21)	0.2465(16)	-0.2240(24)	0.0084(2)
ZSM-5-R-1,2-DCE		0.0514(8)	0.2460(5)	-0.2185(8)	0.0042(5)
ZSM-5-1,2-DCE-30		-0.1601(6)	0.3703(5)	-0.2401(9)	0.0109(1)
ZSM-5-R	**O7**	-0.1560(21)	0.3779(17)	-0.2334(24)	0.0084(2)
ZSM-5-R-1,2-DCE		-0.1574(7)	0.3712(5)	-0.2431(10)	0.0042(5)
ZSM-5-1,2-DCE-30		-0.1629(6)	0.3050(6)	-0.0724(7)	0.0109(1)
ZSM-5-R	**O8**	-0.1637(17)	0.3093(20)	-0.0697(16)	0.0084(2)
ZSM-5-R-1,2-DCE		-0.1627(7)	0.3048(6)	-0.0759(8)	0.0042(5)

ZSM-5-1,2-DCE-30		-0.1565(7)	0.1927(3)	0.0253(2)	0.0109(1)
ZSM-5-R	**O9**	-0.1639(17)	0.2004(11)	0.0437(26)	0.0084(2)
ZSM-5-R-1,2-DCE		-0.1620(8)	0.19022(34)	0.0166(14)	0.0042(5)
ZSM-5-1,2-DCE-30		-0.1719(5)	0.0834(7)	-0.0795(7)	0.0109(1)
ZSM-5-R	**O10**	-0.1648(18)	0.0926(20)	-0.0647(19)	0.0084(2)
ZSM-5-R-1,2-DCE		-0.1725(5)	0.0769(7)	-0.0788(8)	0.0042(5)
ZSM-5-1,2-DCE-30		-0.1563(7)	0.1168(4)	-0.2671(9)	0.0109(1)
ZSM-5-R	**O11**	-0.1521(20)	0.1194(15)	-0.2609(24)	0.0084(2)
ZSM-5-R-1,2-DCE		-0.1543(7)	0.1154(5)	-0.2631(10)	0.0042(5)
ZSM-5-1,2-DCE-30		-0.1337(7)	0.2432(5)	-0.2387(9)	0.0109(1)
ZSM-5-R	**O12**	-0.1466(22)	0.2489(17)	-0.2453(28)	0.0084(2)
ZSM-5-R-1,2-DCE		-0.1340(8)	0.2433(5)	-0.2427(11)	0.0042(5)
ZSM-5-1,2-DCE-30		-0.0479(3)	0.3273(6)	-0.1595(8)	0.0109(1)
ZSM-5-R	**O13**	-0.0472(9)	0.3191(23)	-0.1539(26)	0.0084(2)
ZSM-5-R-1,2-DCE		-0.04663(35)	0.3247(6)	-0.1622(13)	0.0042(5)
ZSM-5-1,2-DCE-30		-0.0522(3)	0.0800(7)	-0.1587(8)	0.0109(1)
ZSM-5-R	**O14**	-0.0479(10)	0.0779(22)	-0.1575(27)	0.0084(2)
ZSM-5-R-1,2-DCE		-0.05115(32)	0.0785(7)	-0.1532(11)	0.0042(5)
ZSM-5-1,2-DCE-30		0.1222(4)	0.4188(6)	-0.3867(8)	0.0109(1)
ZSM-5-R	**O15**	0.1298(14)	0.4155(19)	-0.3680(25)	0.0084(2)
ZSM-5-R-1,2-DCE		0.1212(5)	0.4253(6)	-0.3935(9)	0.0042(5)
ZSM-5-1,2-DCE-30		-0.0060(5)	0.3894(7)	-0.3867(9)	0.0109(1)
ZSM-5-R	**O16**	-0.0023(16)	0.3974(21)	-0.3947(26)	0.0084(2)
ZSM-5-R-1,2-DCE		-0.0078(5)	0.3985(8)	-0.3966(10)	0.0042(5)

ZSM-5-1,2-DCE-30		-0.1342(4)	0.4040(7)	-0.4245(8)	0.0109(1)
ZSM-5-R	**O17**	-0.1386(14)	0.3987(21)	-0.4275(24)	0.0084(2)
ZSM-5-R-1,2-DCE		-0.1376(5)	0.4055(7)	-0.4291(8)	0.0042(5)
ZSM-5-1,2-DCE-30		0.1308(4)	0.2022(7)	-0.3574(6)	0.0109(1)
ZSM-5-R	**O18**	0.1275(13)	0.1873(19)	-0.3605(24)	0.0084(2)
ZSM-5-R-1,2-DCE		0.1316(4)	0.1986(8)	-0.3561(6)	0.0042(5)
ZSM-5-1,2-DCE-30		0.0029(5)	0.2116(6)	-0.4009(9)	0.0109(1)
ZSM-5-R	**O19**	-0.0053(15)	0.2022(21)	-0.3925(23)	0.0084(2)
ZSM-5-R-1,2-DCE		0.0026(5)	0.2092(7)	-0.3925(10)	0.0042(5)
ZSM-5-1,2-DCE-30		-0.1268(5)	0.1931(7)	-0.4188(7)	0.0109(1)
ZSM-5-R	**O20**	-0.1313(14)	0.1938(21)	-0.4222(20)	0.0084(2)
ZSM-5-R-1,2-DCE		-0.1259(5)	0.1878(8)	-0.4193(8)	0.0042(5)
ZSM-5-1,2-DCE-30		0.0499(6)	0.0032(4)	-0.2042(8)	0.0109(1)
ZSM-5-R	**O21**	0.0514(20)	-0.0008(11)	-0.2182(26)	0.0084(2)
ZSM-5-R-1,2-DCE		0.0465(7)	-0.0014(4)	-0.2052(7)	0.0042(5)
ZSM-5-1,2-DCE-30		-0.1423(6)	-0.0068(4)	-0.2145(8)	0.0109(1)
ZSM-5-R	**O22**	-0.1485(21)	-0.0001(11)	-0.2009(26)	0.0084(2)
ZSM-5-R-1,2-DCE		-0.1383(6)	-0.0096(4)	-0.2155(9)	0.0042(5)
ZSM-5-1,2-DCE-30		-0.2509(3)	0.4316(6)	-0.3473(8)	0.0109(1)
ZSM-5-R	**O23**	-0.2539(10)	0.4186(20)	-0.3444(27)	0.0084(2)
ZSM-5-R-1,2-DCE		-0.25148(31)	0.4334(6)	-0.3439(8)	0.0042(5)
ZSM-5-1,2-DCE-30		-0.2431(3)	0.2047(6)	-0.3329(9)	0.0109(1)
ZSM-5-R	**O24**	-0.2467(9)	0.1901(20)	-0.3511(20)	0.0084(2)
ZSM-5-R-1,2-DCE		-0.24217(33)	0.2007(7)	-0.3344(11)	0.0042(5)
ZSM-5-1,2-DCE-30		-0.2527(3)	0.2780(8)	0.0618(9)	0.0109(1)
ZSM-5-R	**O25**	-0.2504(10)	0.2975(16)	0.0776(22)	0.0084(2)
ZSM-5-R-1,2-DCE		-0.25221(34)	0.2803(8)	0.0609(10)	0.0042(5)

ZSM-5-1,2-DCE-30		-0.2541(3)	0.1108(7)	0.0667(8)	0.0109(1)
ZSM-5-R	**O26**	-0.2515(11)	0.1039(17)	0.0828(24)	0.0084(2)
ZSM-5-R-1,2-DCE		-0.25435(30)	0.1046(8)	0.0674(8)	0.0042(5)
ZSM-5-1,2-DCE-30		0.4459(7)	0.3773(5)	-0.2472(8)	0.0109(1)
ZSM-5-R	**O27**	0.4406(20)	0.3767(15)	-0.2346(25)	0.0084(2)
ZSM-5-R-1,2-DCE		0.4410(7)	0.3743(5)	-0.2427(10)	0.0042(5)
ZSM-5-1,2-DCE-30		0.4500 (8)	0.3173(5)	-0.0745(6)	0.0109(1)
ZSM-5-R	**O28**	0.4409(18)	0.3141(18)	-0.0746(16)	0.0084(2)
ZSM-5-R-1,2-DCE		0.4538(7)	0.3139(6)	-0.0714(6)	0.0042(5)
ZSM-5-1,2-DCE-30		0.4293(6)	0.2001(3)	0.0066(9)	0.0109(1)
ZSM-5-R	**O29**	0.4303(17)	0.1995(12)	0.0094(27)	0.0084(2)
ZSM-5-R-1,2-DCE		0.4285(7)	0.2010(4)	0.0184(14)	0.0042(5)
ZSM-5-1,2-DCE-30		0.4530(7)	0.0825(6)	-0.0675(7)	0.0109(1)
ZSM-5-R	**O30**	0.4424(19)	0.0866(20)	-0.0821(19)	0.0084(2)
ZSM-5-R-1,2-DCE		0.4450(8)	0.0893(9)	-0.0787(8)	0.0042(5)
ZSM-5-1,2-DCE-30		0.4313(4)	0.1180(5)	-0.2535(9)	0.0109(1)
ZSM-5-R	**O31**	0.4314(17)	0.1139(15)	-0.2650(26)	0.0084(2)
ZSM-5-R-1,2-DCE		0.4315(6)	0.1169(4)	-0.2685(11)	0.0042(5)
ZSM-5-1,2-DCE-30		0.4427(7)	0.2474(5)	-0.2386(10)	0.0109(1)
ZSM-5-R	**O32**	0.4388(20)	0.2459(16)	-0.2453(26)	0.0084(2)
ZSM-5-R-1,2-DCE		0.4453(7)	0.2445(5)	-0.2364(10)	0.0042(5)
ZSM-5-1,2-DCE-30		0.6674(6)	0.3724(5)	-0.2226(8)	0.0109(1)
ZSM-5-R	**O33**	0.6545(21)	0.3848(15)	-0.2165(22)	0.0084(2)
ZSM-5-R-1,2-DCE		0.6699(6)	0.3725(6)	-0.2174(8)	0.0042(5)

ZSM-5-1,2-DCE-30		0.6450(7)	0.3154(5)	-0.0498(5)	0.0109(1)
ZSM-5-R	**O34**	0.6531(18)	0.3154(18)	-0.0503(16)	0.0084(2)
ZSM-5-R-1,2-DCE		0.6432(7)	0.3092(6)	-0.0508(5)	0.0042(5)
ZSM-5-1,2-DCE-30		0.6488(7)	0.1950(3)	0.0258(10)	0.0109(1)
ZSM-5-R	**O35**	0.6624(17)	0.2000(11)	0.0423(27)	0.0084(2)
ZSM-5-R-1,2-DCE		0.6511(8)	0.1935(4)	0.0393(14)	0.0042(5)
ZSM-5-1,2-DCE-30		0.6582(7)	0.0838(7)	-0.0739(6)	0.0109(1)
ZSM-5-R	**O36**	0.6560(20)	0.0947(20)	-0.0683(19)	0.0084(2)
ZSM-5-R-1,2-DCE		0.6584(7)	0.0900(9)	-0.0784(6)	0.0042(5)
ZSM-5-1,2-DCE-30		0.6722(6)	0.1177(4)	-0.2614(8)	0.0109(1)
ZSM-5-R	**O37**	0.6636(20)	0.1201(15)	-0.2649(25)	0.0084(2)
ZSM-5-R-1,2-DCE		0.6681(7)	0.1172(4)	-0.2687(9)	0.0042(5)
ZSM-5-1,2-DCE-30		0.6441(8)	0.2427(5)	-0.2086(8)	0.0109(1)
ZSM-5-R	**O38**	0.6646(20)	0.2528(17)	-0.2275(25)	0.0084(2)
ZSM-5-R-1,2-DCE		0.6627(8)	0.2429(5)	-0.2162(9)	0.0042(5)
ZSM-5-1,2-DCE-30		0.5534(3)	0.3113(9)	-0.1918(11)	0.0109(1)
ZSM-5-R	**O39**	0.5490(9)	0.3130(24)	-0.1771(29)	0.0084(2)
ZSM-5-R-1,2-DCE		0.5537(4)	0.3140(9)	-0.1958(11)	0.0042(5)
ZSM-5-1,2-DCE-30		0.5531(3)	0.0887(5)	-0.1924(12)	0.0109(1)
ZSM-5-R	**O40**	0.5497(9)	0.0721(21)	-0.1934(30)	0.0084(2)
ZSM-5-R-1,2-DCE		0.5509(4)	0.0902(6)	-0.1931(13)	0.0042(5)
ZSM-5-1,2-DCE-30		0.3703(4)	0.4225(6)	-0.3936(8)	0.0109(1)
ZSM-5-R	**O41**	0.3677(14)	0.4175(18)	-0.3734(26)	0.0084(2)
ZSM-5-R-1,2-DCE		0.3718(4)	0.4209(7)	-0.3944(9)	0.0042(5)

ZSM-5-1,2-DCE-30		0.5007(5)	0.4151(6)	-0.4153(9)	0.0109(1)
ZSM-5-R	**O42**	0.4973(15)	0.4075(20)	-0.4082(27)	0.0084(2)
ZSM-5-R-1,2-DCE		0.5020(5)	0.4057(9)	-0.4089(10)	0.0042(5)
ZSM-5-1,2-DCE-30		0.6303(4)	0.3931(6)	-0.4086(7)	0.0109(1)
ZSM-5-R	**O43**	0.6317(14)	0.3962(20)	-0.4164(23)	0.0084(2)
ZSM-5-R-1,2-DCE		0.6320(5)	0.3875(7)	-0.4044(8)	0.0042(5)
ZSM-5-1,2-DCE-30		0.3708(5)	0.1950(6)	-0.3822(9)	0.0109(1)
ZSM-5-R	**O44**	0.3713(14)	0.1765(16)	-0.3872(24)	0.0084(2)
ZSM-5-R-1,2-DCE		0.3734(6)	0.2018(7)	-0.3879(10)	0.0042(5)
ZSM-5-1,2-DCE-30		0.5020(5)	0.1846(6)	-0.3838(8)	0.0109(1)
ZSM-5-R	**O45**	0.5041(14)	0.1842(18)	-0.3891(24)	0.0084(2)
ZSM-5-R-1,2-DCE		0.5042(5)	0.1887(8)	-0.3889(10)	0.0042(5)
ZSM-5-1,2-DCE-30		0.6314(4)	0.2069(7)	-0.3907(7)	0.0109(1)
ZSM-5-R	**O46**	0.6329(13)	0.2108(19)	-0.4027(21)	0.0084(2)
ZSM-5-R-1,2-DCE		0.6342(4)	0.2077(7)	-0.3996(8)	0.0042(5)
ZSM-5-1,2-DCE-30		0.4625(6) -	0.0050(3)	-0.2101(8)	0.0109(1)
ZSM-5-R	**O47**	0.4504(20)	-0.0077(10)	-0.2287(25)	0.0084(2)
ZSM-5-R-1,2-DCE		0.4614(6)	-0.0036(4)	-0.2134(9)	0.0042(5)
ZSM-5-1,2-DCE-30		0.6431(6) -	0.0050(3)	-0.2148(8)	0.0109(1)
ZSM-5-R	**O48**	0.6572(21)	-0.0017(11)	-0.2092(28)	0.0084(2)
ZSM-5-R-1,2-DCE		0.6414(6)	-0.0039(4)	-0.2111(10)	0.0042(5)